ASD-TDR-63-132

ELECTRON BEAM WELDING OF AEROSPACE MATERIALS

TECHNICAL DOCUMENTARY REPORT NO. ASD-TDR-63-132

February 1963

DIRECTORATE OF MATERIALS AND PROCESSES
AERONAUTICAL SYSTEMS DIVISION
AIR FORCE SYSTEMS COMMAND
WRIGHT-PATTERSON AIR FORCE BASE, OHIO

Project 7351, Task 735102

(PREPARED UNDER CONTRACT NO. AF33(657)-7763
BY HAMILTON STANDARD, A DIVISION OF THE UNITED AIRCRAFT CORPORATION,
WINDSOR LOCKS, CONNECTICUT; WILLIAM I. KERN AND LAWRENCE E. LUBIN, AUTHORS)

NOTICES

When Government drawings, specifications, or other data are used for any purpose other than in connection with a definitely related Government procurement operation, the United States Government thereby incurs no responsibility nor any obligation whatsoever; and the fact that the Government may have formulated, furnished, or in any way supplied the said drawings, specifications, or other data, is not to be regarded by implication or otherwise as in any manner licensing the holder or any other person or corporation, or conveying any rights or permission to manufacture, use, or sell any patented invention that may in any way be related thereto.

Qualified requesters may obtain copies of this report from the Armed Services Technical Information Agency, (ASTIA), Arlington Hall Station, Arlington 12 Virginia.

This report has been released to the Office of Technical Services, U.S. Department of Commerce, Washington 25, D.C., for sale to the general public.

Copies of this report should not be returned to the Aeronautical Systems Division unless return is required by security considerations, contractual obligations, or notice on a specific document.

ASD–TDR–63–132

ELECTRON BEAM WELDING OF AEROSPACE MATERIALS

TECHNICAL DOCUMENTARY REPORT NO. ASD-TDR-63-132

February 1963

DIRECTORATE OF MATERIALS AND PROCESSES
AERONAUTICAL SYSTEMS DIVISION
AIR FORCE SYSTEMS COMMAND
WRIGHT–PATTERSON AIR FORCE BASE, OHIO

Project 7351, Task 735102

(PREPARED UNDER CONTRACT NO. AF33(657)–7763
BY HAMILTON STANDARD, A DIVISION OF THE UNITED AIRCRAFT CORPORATION,
WINDSOR LOCKS, CONNECTICUT; WILLIAM I. KERN AND LAWRENCE E. LUBIN, AUTHORS)

FOREWORD

This report was prepared by the Electron Beam Department and the Materials Engineering Department of the Hamilton Standard Division of the United Aircraft Corporation, Windsor Locks, Connecticut. This contract was initiated 1 January, 1962 under United States Air Force Contract No. AF 33(657)-7763, Task No. 735102. The work was administered under the direction of Aeronautical Systems Division, Air Force Systems Command, United States Air Force, Wright-Patterson Air Force Base, Ohio, with Mr. R. E. Bowman acting as project engineer.

The work reported herein was performed under the supervision of Mr. J. W. Meier. This work was terminated 31 December, 1962.

Acknowledgement is made of the valuable assistance of Electron Beam Laboratory and Materials Laboratory personnel, especially Messrs. H. Charland, M. Millen, W. F. Kearns, M. Mooney, W. H. Colman, and H. R. Ohlheiser.

ABSTRACT

High-voltage electron beam welding techniques capable of producing butt welds of optimum strength and ductility were developed for B120VCA titanium, D6AC steel, molybdenum-0.5% titanium to tungsten, and beryllium. Welds were produced in material thicknesses of 0.125 inch for the B120VCA titanium; 0.290 inch and 0.090 inch for the D6AC steel; 0.100 inch, 0.050 inch, and 0.005 inch for the molybdenum-0.5% titanium welded to tungsten; and 0.040 inch for the beryllium. The effects of thermal treatments (aging and heat treating) were investigated in the B120VCA and D6AC by welding and testing a variety of weld/thermal treatment combinations.

A comprehensive preliminary welding phase was conducted during which the effects of various welding conditions on weld-zone characteristics were evaluated by visual, radiographic or dye penetrant, and metallographic inspection. Welds were evaluated for extent of fusion, grain size, cracking, porosity, and other pertinent effects.

Butt welds of each material thickness, joint combination, and thermal treatment (where applicable) were evaluated for mechanical properties. Weld tensile properties were determined at room temperature for all conditions, at temperatures to 2200 F for molybdenum to tungsten, and at temperatures to 1000 F for beryllium. Weld transverse bend ductilities were determined by bend testing at temperatures to 1000 F. The internal-notch tensile properties (G_c^*) of B120VCA titanium and D6AC steel were determined at room temperature. Room-temperature impact tests were performed on 0.290-inch D6AC.

Results of the metallographic and mechanical property investigations of the electron beam welds were compared with base-metal properties and with published data for other joining techniques.

PUBLICATION REVIEW

This report has been reviewed and is approved.

FOR THE COMMANDER

I. PERLMUTTER
Chief, Physical Metallurgy Branch
Metals and Ceramics Laboratory
Directorate of Materials and Processes

TABLE OF CONTENTS

TABLE OF CONTENTS (Continued)

LIST OF FIGURES

LIST OF FIGURES (Continued)

LIST OF FIGURES (Continued)

LIST OF FIGURES (Continued)

LIST OF FIGURES (Continued)

LIST OF FIGURES (Continued)

LIST OF FIGURES (Continued)

LIST OF TABLES

LIST OF TABLES (Continued)

SUMMARY

Techniques were developed for the production of high quality electron beam welds in several representative aerospace materials; specifically butt welding techniques were developed for 0.125-inch B120VCA titanium, 0.290- and 0.090-inch D6AC low alloy steel, 0.100-, 0.050-, and 0.005-inch molybdenum-0.5% titanium to tungsten, and 0.040-inch beryllium. The B120VCA titanium and D6AC steel were welded in a variety of heat-treated conditions.

Optimum welding techniques were developed through an evaluation of the effects of welding parameters upon the weld-zone characteristics of a series of trial welds. Specific welding conditions evaluated included: accelerating voltage, to 150,000 volts; beam current, to 21 milliamperes; welding speed, to 120 inches per minute; beam diameter, 0.010 to 0.025 inch; 60-cycle beam oscillation, to amplitudes of $\pm$ 0.200 inch; and beam pulsing techniques, 10 to 3,000 cycles per second with beam on-times of 0.05 to 10 milliseconds. Trial welds were evaluated by visual, radiographic, dye penetrant, and metallographic techniques.

Final welds were produced in each material thickness, heat treatment (where applicable), and joint combination using the best weld settings developed during the trial-weld phase of the program.

Highest-quality welds in B120VCA titanium were produced using a slightly defocused beam that was oscillated in the direction of welding. The 0.090-inch D6AC steel was also welded with a defocused beam (0.015-inch diameter) in order to eliminate the weld bead irregularities which appear to be characteristic of electron beam welds in D6AC produced by the consumable electrode vacuum-cast process. Final weldments in 0.290-inch D6AC were produced using a two-pass technique, the second pass serving as a clean-up pass to smooth the irregular top bead.

For all thicknesses of the molybdenum-0.5% titanium welded to tungsten joint combination beam location relative to the joint centerline was the most important single parameter. Location of the beam up to 0.006 inch on the tungsten side of the joint produced welds with minimum fusion, recrystallization, and grain size. Optimum welds in beryllium were produced using moderately high-power densities together with slow welding speeds.

All final welds were inspected by radiographic and dye penetrant techniques. The tensile properties of the welds in all materials were determined at room temperature; at 1600 F, 1900 F, and 2200 F for the molybdenum-0.5% titanium welded to tungsten; and at 500 F and 1000 F for the beryllium. Weld ductility was determined by transverse bend testing at temperatures to 1000 F. Ductile-to-brittle transition temperatures were established from the bend-test results. Impact tests were performed upon 0.290-inch D6AC welds at room temperature.

Manuscript released by authors 23 January 1963 for publication as an ASD Technical Documentary Report.

SUMMARY (Continued)

The fracture-toughness properties of welds in B120VCA titanium and D6AC steel were determined using a recently developed internal-notch tensile testing technique. This technique, which utilizes a load-deflection curve of an internally notched specimen, was used to calculate G_c^* values.

For all materials, the electron beam welds exhibited depth-to-width ratios greater than and grain sizes less than those generally obtained in conventionally produced fusion welds in similar material thicknesses.

Electron beam welds in all materials possessed strength properties that were generally in excess of those exhibited by similar joints produced by conventional fusion welding techniques. Welds in heat-treated D6AC exhibited ultimate tensile strengths exceeding 95 percent of base-metal strength. The tensile strengths of the molybdenum-0.5% titanium to tungsten welds at 2200 F and of the beryllium welds at 1000 F were equivalent to base-metal strengths at similar temperatures. Relative tensile strengths of the molybdenum-0.5% titanium to tungsten and beryllium welds decreased with decreasing temperature, reaching at room temperature seventy percent of the molybdenum-0.5% titanium recrystallized base-metal strength and sixty-five percent of the beryllium base-metal strength, respectively.

As might be expected, the transverse bend ductility of the electron beam weldments was, in general, somewhat lower than that of the corresponding base metals. For beryllium, the ductile-to-brittle transition temperature was 640 F above the base-metal transition temperature. All thicknesses of the molybdenum-0.5% titanium welded to tungsten exhibited transition temperatures at least 225 F lower than electron beam weldments in equivalent thicknesses of tungsten welded to itself. Both the cold rolled and aged B120VCA base metal and the B120VCA electron beam welds in all aged conditions were able to withstand bend angles of only twenty degrees prior to failure, when tested at temperatures up to their respective aging temperatures. Electron beam welds in D6AC steel that were heat treated after welding exhibited a transition temperature approximately 30 F above the heat-treated base-metal transition temperature. When welded in the less ductile heat-treated condition, the resultant weld ductile-to-brittle transition temperature was approximately 80 F above the base-metal transition temperature.

The results of fracture-toughness testing of B120VCA titanium welds revealed that electron beam welds in all aging conditions of this titanium alloy exhibit fracture-toughness properties superior to those of the base metal in equivalent aged conditions.

The fracture-toughness and impact properties of D6AC steel tested in the as-welded condition were poor because of extremely hard and brittle untempered martensite present in the fusion zone. However, when heat treated or tempered subsequent to welding, the D6AC weldments retained up to seventy percent of the base-metal fracture toughness.

Analysis of tensile and fracture-toughness data for 0.290-inch D6AC indicated the presence of an inherent weld zone discontinuity resulting

SUMMARY (Continued)

from the extremely columnar grain solidification pattern of the fusion zone. This intergranular discontinuity, not detected by normal weldment inspection techniques, in combination with the brittle untempered martensite present in welds tested without post-welding thermal treatment, contributed to the low ductility and fracture-toughness exhibited by the 0.290-inch D6AC welds.

INTRODUCTION

The increased materials demand of aerospace technology has created new uses for a spectrum of materials. All-beta titaniums, high-strength tool steels, refractory metals, and beryllium are just four of the varied classes of materials currently in use. The production of reliable joints of adequate strength, and in many cases with a minimum of post-weld treatment, is a definite requirement for present and future production.

The high-voltage electron beam welding process, with its inherent minimal energy input to the workpiece and relatively narrow weld zones, offers a welding technique which shows promise of being able to satisfy the above mentioned reliability and minimum processing requirements. In the relatively few short years since its introduction as a joining technique, the electron beam process has demonstrated its ability to reliably join almost all metals and alloys known to modern-day technology. In addition, a wide variety of dissimilar metal joints (metallurgical compatability of the base materials being the limiting factor) and materials in various thermal treatments have been successfully welded. All of these advantages indicate increasing use of the electron beam welding process in aerospace technology.

The program reported herein was undertaken to investigate the application of electron beam welding as a joining technique for the following materials: B120VCA, an all-beta titanium alloy; D6AC, a low alloy high-strength steel; molybdenum-0.5% titanium to tungsten, a dissimilar refractory metal joint; and beryllium, a light structural metal. The objective was to develop techniques for producing butt weldments in these materials. For the B120VCA titanium and D6AC steel, a variety of thermal treatments were investigated.

CONCLUSIONS

Results of the electron beam welding program on aerospace materials lead to the following conclusions:

1. High quality butt welds can be produced in commercially available B120VCA titanium, D6AC low alloy steel, arc-cast molybdenum-0.5% titanium welded to pure tungsten, and QMV-grade beryllium. For all materials welded, relative grain size, fusion and heat-affected zone widths, and mechanical properties were generally superior to arc welds in similar materials and thicknesses.

2. With slight modification of existing welding equipment to control the exhausting of toxic vapors, beryllium can be reproducibly welded by high-voltage electron beam techniques:

   a. Highest quality welds in beryllium are associated with welding performed using a moderately high power density and slow welding speed.

   b. Beryllium welds produced during this program exhibited strengths equivalent to base metal at 1000 F. Relative tensile strength decreased with decreasing testing temperature, reaching sixty-five percent of base-metal strength at room temperature. The tensile and bend ductilities of these welds were lower than those associated with base metal.

   c. Based on metallographic studies, improvement in weldment mechanical properties can be expected with further optimization of weld-zone microstructure.

3. The joint combination of molybdenum-0.5% titanium welded to tungsten readily lends itself to fabrication by high-voltage electron beam techniques:

   a. Welds with minimum fusion and recrystallized zones and relatively fine grain size are produced in molybdenum-0.5% titanium welded to tungsten when the beam is located up to 0.006 inch on the tungsten side of the joint and welding is performed using a high power density beam and moderately fast welding speeds.

   b. In the temperature range of 1600 to 1900 F, the tensile strengths exhibited by joints produced in molybdenum-0.5% titanium welded to tungsten by electron beam techniques exceeded joint strengths of electron beam welds in either tungsten or molybdenum-0.5% titanium welded to themselves. At 2200 F, the molybdenum-0.5% titanium welded to tungsten possessed tensile strength equivalent to molybdenum-0.5% titanium base-metal strength.

CONCLUSIONS (Continued)

c. The transverse bend ductility of electron beam welded molybdenum-0.5% titanium to tungsten falls into the range of values established for electron beam welds in each respective thickness of molybdenum-0.5% titanium and tungsten.

4. The susceptibility of the B120VCA titanium to weld-bead surface undercutting made it necessary to modify welding techniques in order to produce smooth, non-undercut welds:

   a. Optimum weld-bead surface quality was obtained when welding was performed using a slightly defocused beam that was oscillated longitudinally with respect to the welded joint.

   b. Electron beam welds in B120VCA retained seventy-percent of base-metal tensile strength; however, the base-metal strength level tested (in excess of 220,000 psi) was higher than generally utilized for this alloy.

   c. Fracture-toughness properties of electron beam welds in all aging conditions of B120VCA were generally superior to those of the base metal in equivalent aged conditions.

   d. The high strength level of the B120VCA base metal used in the program contributed to the poor transverse bend ductility in both base metal and electron beam welds.

5. As with the B120VCA titanium, modified welding techniques were required to produce smooth continuous weld beads in D6AC steel:

   a. Weld-bead quality was dependent upon welding with a slightly defocused beam.

   b. The combination of the extremely high hardenability of the D6AC steel and the rapid quench rates associated with electron beam welding creates a solidification mechanism which produces a brittle martensite in the fusion zone. Immediate tempering is required to prevent cracking and improve mechanical properties.

   c. The room-temperature tensile strength of electron beam welds in both thicknesses of D6AC steel exceeds ninety-percent of base-metal strength when welded in the heat-treated condition.

   d. Weldments in D6AC steel that were given an immediate post-welding temper exhibited the highest tensile ductility, retaining sixty-percent of heat-treated base-metal ductility. Fracture-toughness results indicated higher toughness for weldments with post-welding thermal treatment.

CONCLUSIONS (Continued)

6. Considerable improvement in strength and ductility of electron beam welds in B120VCA titanium and D6AC steel can be achieved using welding parameters which produce deep narrow weld zones of minimum energy input. The surface irregularities that characterize B120VCA and D6AC welds produced under such conditions can be eliminated by using a second clean-up pass, or filler metal of base-metal composition.

RECOMMENDATIONS

The following recommendations are based on the results of the program:

1. Further work with beryllium should be conducted to develop optimum high-power-density electron beam welding techniques which produce random, fine-grained weld zone microstructures. Investigation should be conducted to determine if any relationship exists among chamber pressure, input power density, and weld quality.

2. The successful welding techniques developed in the present program for welding molybdenum-0.5% titanium to tungsten should be evaluated as production techniques through the welding of prototype parts. The prototypes should represent a variety of configurations and should be evaluated by techniques pertinent to the end use of the parts.

3. To provide further improvement in the strength and ductility of electron beam weldments in B120VCA titanium and D6AC steel, high-power-density electron beam welding techniques should be developed using filler metal of base-metal composition as a means of eliminating undercutting and other surface discontinuities associated with the deep, narrow weld zones with minimum fusion and heat effect in these materials.

4. The use of preheating and an immediate post-weld thermal treatment should be investigated for D6AC steel. Evaluation should be concentrated on obtaining weld zone microstructures free from any brittle untempered martensite.

5. Further work should be conducted on the high-voltage electron beam welding of B120VCA titanium in an optimum aged condition. The proper aging treatment should be selected through a comprehensive tensile and fracture-toughness testing program designed to determine the optimum combination of strength and toughness for a given strength level.

Description of Tests

Material

All material used throughout the welding program was representative of commercially available B120VCA titanium, D6AC steel, molybdenum-0.5% titanium, pure tungsten, and beryllium. A complete list of the material used in the program is found in Table 1.

B120VCA titanium was received in the solution-treated condition. Two plate thicknesses were obtained to be used for the various processing and aging combinations. 0.125-inch plate solution treated after fabrication was aged by normal procedures, and 0.250-inch solution-treated plate was cold rolled to a cross-section of 0.125 inch to investigate the weldability of B120VCA plate aged to the high strengths obtainable in the cold-worked condition. Cold rolling to a reduction of 50% was performed using 21 reduction passes.

D6AC steel, produced as consumable electrode vacuum-cast material, was obtained in the annealed condition. Both the 0.320-inch and 0.110-inch thick plate were received in the as-rolled condition and consequently plate surfaces were characterized by hot-rolling scale and decarburization to a thickness of 0.015 inch. Surface grinding of all D6AC steel was required to produce plate suitable for welding and testing. Final D6AC plate thicknesses used in the program were 0.290 inch and 0.090 inch.

Molybdenum-0.5% titanium (Mo-0.5% Ti) and pure tungsten in sheet thickness of 0.100 inch, 0.050 inch and 0.005 inch were transferred to the program from a previous welding program conducted under ASD sponsorship.* Additional Mo-0.5% Ti and pure tungsten sheet 0.050-inch thick were obtained to supplement the material available. All of the Mo-0.5% Ti was arc-cast material; the pure tungsten was produced by powder metallurgy techniques.

QMV grade beryllium in a sheet thickness of 0.040 inch was supplied by the Air Force. This sheet was produced in an early phase of the Air Force sheet rolling program and may not be representative of that produced in the later phases. A complete description of the materials appears in Results of Tests, Base Metal.

Machining

Standard machining procedures were used for the cutting, grinding, milling, drilling and polishing of both the B120VCA titanium and the D6AC steel.

The hot-rolling scale and decarburization present on both thicknesses of D6AC steel were removed through a series of grinding operations. Initially, both faces of the plates were rough ground to a predetermined depth using a Blanchard grinder. Final finishing operations were performed on a standard surface grinder. All surface grinding was performed in a direction parallel to the sheet rolling direction. Figure 1 illustrates the 0.300-inch (nominal)

*AF 33(616)-7439, Task No. 73516

Description of Tests (Continued)

D6AC plate in both the as-received and surface ground condition.

Spark-erosion techniques were used for the machining of the internal-notch configuration into the B120VCA titanium and both thicknesses of the D6AC steel. In all cases, highest quality cuts were obtained using graphite electrodes and employing slow feeds and a two-ampere discharge current. Due to the inherent brittleness of both the Mo-0.5% Ti and tungsten, specialized and carefully controlled machining procedures were required. Techniques developed at Hamilton Standard during a previous Mo-0.5% Ti and tungsten welding investigation were used throughout the present program. These machining procedures are discussed in detail in the summary technical report for that program.[1]

Machining of beryllium was performed on a subcontract basis due to the toxicity of the material and the lack of established facilities and procedures required to safely perform machining operations at Hamilton Standard.

Machined surfaces on all Mo-0.5% Ti, tungsten, and beryllium specimens subjected to mechanical testing were polished to minimize machining defects which could propagate premature failure. For Mo-0.5% Ti and tungsten, machined surfaces were chemically polished by a five-minute immersion in a solution of 67% lactic acid, 22% HNO_3, and 11% HF followed by a water rinse. The beryllium machined surfaces were chemically polished by five-minute immersion in a solution of 2% HF, 40% HNO_3, and 58% H_2O followed by a water rinse. (All percentages volume percent.) After machining, all specimens intended for final welding or for mechanical testing were inspected for cracks and laminations.

Thermal Treatments

The aging treatments used in the subject program for both the solution treated and the solution treated and 50% cold-rolled B120VCA titanium base metal and weldments were based on highest consistently attainable tensile strength values of 0.125-inch thick specimens.

The aging response of the 0.125-inch solution-treated B120VCA titanium was determined at a temperature of 900 F and at aging times of 12 to 96 hours. The results of this evaluation are shown in Figure 2. The material exhibited an excellent aging response as indicated by the maximum tensile strength obtained (226,000 psi). Based on the strength values shown in Figure 2, the optimum aging treatment for the 0.125-inch solution-treated B120VCA titanium was chosen as 72 hours at 900 F.

The aging response of the 0.125-inch thick solution treated 50% cold-rolled (received as 0.250-inch solution-treated plate) B120VCA titanium was determined at a temperature of 800 F and at aging times of 4 to 20 hours. The results of this evaluation are shown in Figure 3. The material exhibited a good aging response as indicated by the maximum tensile strength obtained (250,000 psi) for a 16 hour aging treatment. The 12 hour aging treatment produced a slightly lower tensile strength (244,000 psi) than the 16 hour

aging treatment, but the elongation values were slightly higher and there was a greater spread between tensile-strength values and yield-strength (0.2% offset) values. Therefore, the optimum aging treatment for the 0.125-inch solution treated and 50% cold-rolled B120VCA titanium was chosen as 12 hours at 800 F.

Severe surface contamination on a trial lot of the solution-treated B120VCA titanium appeared after aging at 900 F for 72 hours in air. Therefore, all 72 hour aging treatments at 900 F were performed in an argon atmosphere. Aging at 900 F for 72 hours in argon produced only minor surface contamination which was equivalent to that resulting from the 800 F - 12 hour - air atmosphere aging treatment.

The surface contamination resulting from both titanium aging treatments was easily removed by the following cleaning procedure:

A. Rinse specimens in warm (110 F) solution of one (1) part HF, 10 parts HNO_3, and 20 parts H_2O up to five minutes.

B. Water rinse.

C. Rinse off scale in hot (150 F) 30% aqueous solution of H_2SO_4 up to five minutes.

D. Water rinse and air dry.

All B120VCA titanium specimens were cleaned as above prior to aging.

In order to produce optimum properties at a strength level of approximately 240,000 psi (Rockwell C50 hardness) the following heat treatment was chosen for both thicknesses of D6AC low alloy steel base metal and weldments:

A. Copper plate for surface protection.

B.* Fixture to prevent distortion.

C. Austenitize at 1600 F for one (1) hour, or one hour per inch of thickness, in endothermic atmosphere.

D. Oil quench (120 - 140 F oil, severely agitated)

E. Air cool to room temperature.

* Fixture at this step if not done prior to hardening

F. Double temper at 700 F, four (4) hours each, with intermittent and final air cool to room temperature.

G. Remove fixtures.

H. Strip copper plate.

Description of Tests (Continued)

The endothermic atmosphere was used to prevent surface decarburization. The generated gas, which contained CH_4, CO, H_2, and N_2, was adjusted to neutrality toward the D6AC by controlling the dew point. A protective thickness of electroplated copper was applied to the D6AC as an additional guard against surface decarburization.

Distortion of the 0.090-inch D6AC was minimized by fixturing prior to hardening or prior to tempering depending on the size of the load.

Base-metal Evaluation

All material used in the program was visually inspected in the as-received condition. Particular emphasis was placed upon the inspection of the tungsten, Mo-0.5% Ti, and beryllium sheet for cracks, laminations, and general surface quality.

Samples extracted from each material thickness were subjected to chemical analysis. Metallic alloying elements and impurities were determined by spectrographic analysis, oxygen and hydrogen contents were determined by vacuum fusion analysis, and the nitrogen content was determined by the Kjeldahl method. Carbon analyses for the tungsten and molybdenum-0.5% titanium were supplied by the material vendors. The beryllium was not analyzed; however, an analysis was supplied by the sheet fabricator.

Thorough metallographic evaluation was performed on all material thicknesses in the as-received condition. Additional evaluation was performed on B120VCA titanium and D6AC steel after heat treatment, and tungsten and Mo-0.5% Ti after recrystallization. The evaluation included hardness testing and metallographic examination for the presence of inclusions (such as carbides, nitrides, and oxides), laminations, and other defects that would inhibit weldability.

All specimens for metallographic examination were mounted in bakelite and prepared for examination by standard grinding and polishing techniques. Microstructures were revealed by etching using the etchants and etching procedures listed in Table 2.

Diamond - pyramid hardness values were determined on a Zwick Microhardness Testing Machine. All microhardness determinations were made using a 200-gram load.

Room-temperature tensile tests were performed on all materials in all thicknesses and heat treatments (where applicable). In addition, tensile tests were performed on the 0.050-inch Mo-0.5% Ti at 1600 F, 1900 F, and 2200 F; on the 0.050-inch tungsten at 2200 F, and 2500 F, 2800 F; and on the 0.040-inch beryllium at 1000 F. The specimens used for both room and elevated-temperature tensile testing are shown in Figures 4 through 7.

During the room-temperature tensile testing of tungsten, Mo-0.5% Ti, and beryllium, the fixture shown in Figure 8 was employed. The fixture was equipped with a rigid, removable member which isolated all stresses from the

tensile specimen during test setup. This minimized premature brittle failures induced by specimen mishandling. The fixture also provided a more positive method of gripping the specimens during application of the tensile load.

Elevated-temperature tensile testing of beryllium was performed in a stagnant air atmosphere using a standard ceramic muffle type tensile testing furnace. The beryllium tensile specimen was contained within the furnace in a protective tube-pull rod assembly shown in Figure 9. This protective tube served to confine all beryllium particles that were produced during failure of the specimen.

Elevated-temperature tensile tests of both tungsten and Mo-0.5% Ti were conducted in a Marshall 3000 F tensile testing furnace at a vacuum of approximately 1×10^{-4} millimeters of mercury. Figure 10 illustrates the furnace and control console in operating position. The specimen pull-rod and gripping assembly for the high temperature tests is shown in Figure 11. The grips, either tungsten or Mo-0.5% Ti bar, depending on the testing temperature, were threaded into Inconel X pull rods, which operated in cooler regions of the furnace. The tensile specimens were held in the grips with tungsten pins. To minimize stresses, and thus eliminate specimen failure during setup, a close-fitting, smooth walled tube was placed in the furnace prior to specimen-pull rod insertion. This tube guided the assembled pull rod and gripping unit into position and also protected the furnace heating elements from damage during setup. Temperature measurements were made at the specimen surface with a platinum/platinum - 10% rhodium thermocouple. All specimens were stabilized at temperature for five minutes prior to testing. The short time at temperature was justified because of the long heat up times (approximately one hour) and the relatively thin specimen cross-section.

Transverse bend-ductility tests were conducted at room temperature on all materials in all thicknesses and heat treatments (where applicable). Figures 12 through 15 illustrate the bend-test specimen configuration. All specimens were bent about an axis parallel to the material surface but perpendicular to the sheet rolling direction. As the 0.050-inch tungsten, 0.040-inch beryllium, all aged titanium, 0.290-inch annealed D6AC, and all heat treated D6AC were brittle at room temperature, their ductile-to-brittle transition temperatures were determined by bend testing at temperatures to 1000 F.

The elevated-temperature and room-temperature bend tests were conducted using the setup illustrated in Figure 16. The figure shows the ambient box and heating coils used for obtaining elevated temperatures. During the test, spans of 2 inches for B120VCA and 0.090-inch D6AC, 4.5 inches for the 0.290-inch D6AC, and 1 1/4 inches for Mo-0.5% Ti, tungsten, and beryllium were maintained between specimen supporting shoulders. Bend radii employed for the various material thicknesses are listed in Table 3. The rate of deflection used for all bend testing was 0.5 inch per minute. At elevated temperatures the specimen temperature was continuously monitored with a thermocouple placed in direct contact with the specimen. All specimens were

bent until failure occurred or the limit of the fixture was reached.

Subsequent to bend testing, the specimens were visually examined to determine the degree of ductility exhibited in the failure. Angle of bend at failure was defined as the angle through which the specimen was bent, from the horizontal plane, at the onset of failure. To serve as a standard for the comparison of weld and base-metal properties, the ductile-to-brittle transition temperature was arbitrarily defined as the temperature at which a bend angle of 30 degrees was achieved before initiation of failure.

Internal-notch fracture toughness ("G_c") tests were conducted at room temperature on D6AC steel and B120VCA titanium in all thicknesses and heat treatments. A detailed description of the procedures and theory entailed in this highly specialized testing is presented in Appendix A.

Figures 17 and 18 illustrate a typical center-notch "G_c" specimen. Figure 19 illustrates a "G_c" specimen in place in a standard Tinius Olsen 60,000-pound Universal Tensile Machine prior to testing. The special "G_c" self-aligning clamping fixtures are shown in Figure 20.

Prior to testing, both tips of the central notch in the "G_c" specimen were fatigue cracked using a Krouse Plate Cyclic Bending Machine shown in Figure 21. The apparent surface-crack lengths at each notch tip were inspected to ensure the existence of a "through" crack.

The specimen was bolted finger-tight in the self-aligning fixture and preloaded to 2000 pounds. After readjusting the specimen for good alignment, the specimen bolts were tightened with a wrench, and the apparent tip-crack lengths recorded. A specially built, medium-magnification, 2-inch gauge length, extensometer was clamped in place and the specimen tested at a constant strain rate of 0.1-inch per minute to failure.

After failure, all fracture surfaces were evaluated for type of failure, percent (%) shear, extent of "wing" cracks, and any abnormalities.

An autographic plot of load vs. strain was used to calculate the crack length at the initiation of fast fracture, the net section stress, and the fracture toughness.

Impact tests were performed at room temperature on all heat treatments of 0.290-inch D6AC. The substandard size specimen used for impact testing is shown in Figures 22 and 23. Testing was performed on a standard pendulum-type impact testing machine.

Welding Equipment

All welding was performed on a Hamilton-Zeiss high-voltage, high power-density electron beam welding machine. The Hamilton-Zeiss equipment, Figure 24, is rated at three kilowatts, with accelerating potentials to 150,000 volts and beam currents to 20 milliamperes. Beam spot size can be controlled by electromagnetic focusing to a diameter of less than 0.010-inch.

Description of Tests (Continued)

A schematic of the electron gun is shown in Figure 25. The electrons are formed and accelerated and the initial focus is determined by the triode-type electron gun in the upper portion of the schematic. The triode gun design permits regulation of the beam current independent of accelerating potential. Thus, beam current can be continuously varied from zero to 20 milliamperes at any accelerating potential. The grid also permits pulsing of the beam by cyclic variation of the grid voltage.

The optical system, apparent in the center of the column, is designed so that weld location can be precisely controlled by viewing the workpiece coaxially with the electron beam at magnfications of 20 or 40 power. The optics not only permit exact location of beam impact point, but also permit viewing of the joint during welding. Optical viewing was invaluable during the preliminary phases of this program to observe the phenomena occurring during and immediately subsequent to the welding operation; and, of course, the optics were used continually for precise location of the beam at the desired location.

The electromagnetic beam deflection system permits oscillation of the electron beam in a wide variety of modes. Excitation of the deflection coils with an AC electrical signal induces beam oscillation at corresponding frequencies and wave shapes to a maximum amplitude of $\pm$ 0.25 inch. The utilization of beam oscillation provides wide control of heat distribution to the workpiece.

Specific welding condition ranges available for the Hamilton-Zeiss 3 KW welding machine are summarized as follows:

Accelerating Voltage	0 to 150,000 volts
Beam Current	0 to 20 milliamperes
Maximum Beam Power	3 kilowatts
Welding Speed	0 to 120 inches per minute
Beam Oscillation Amplitude	0 to 0.250 inch
Beam Pulsing Rate	0.1 to 3000 cps
Beam Pulse on Times	0.05 to 10 milliseconds

Trial Welding

A comprehensive trial-welding program was conducted on each material thickness, heat treatment (where applicable), and joint combination to establish the best welding techniques. The primary purpose of trial welding was to establish welding parameters for each material thickness, heat-treat variation, and joint combination that gave butt welds of optimum appearance, strength, and ductility.

Approximate welding conditions required for each material thickness, heat-treat variation, and joint combination were established by making weld passes at a variety of settings in solid blocks of material. Parameters studied included accelerating voltage, beam current, welding speed, beam oscillating conditions, location of beam focal point in relation to work-piece surface, and location of beam in relation to joint centerline for the

tungsten-to-Mo-0.5% Ti weldments (tungsten/Mo-0.5% Ti).

Experience has shown that under identical welding conditions, weld zone characteristics developed in solid material closely approximate those developed in actual butt welds. Therefore, analysis of a cross-section of a weld pass in solid material provided a rapid method of determining the range of settings required for an actual butt weld.

Trial butt welding was performed on the specimens illustrated in Figures 26 and 27. To provide good fit-up, the mating edges of specimen pairs were finish ground to approximately 32 RMS with sharp, non-broken edges. Before welding, all specimens were degreased in hot trichloroethylene and then chemically cleaned. The cleaning solutions used for all materials welded are listed in Table 4. A typical butt-welding fixture is illustrated in Figure 28. The pieces for welding were butted together and held in place by hold-down straps.

Butt welds at a variety of settings were produced in all material thicknesses, heat-treat variations, and material combinations. Table 5 lists the ranges of settings used for each joint type. Throughout the trial welding phase of the program, feedback from previous trial-weld evaluation was utilized for selection of trial-weld settings.

Trial-Weld Evaluation

The purpose of trial-weld evaluation was to determine, by various weld evaluation procedures, which combination of welding-machine settings produced the weld-zone characteristics that would promote optimum overall weld appearance, weld strength, and ductility. The best settings established in trial welding would then be used for producing welds for final testing.

The evaluation procedure was conducted in three general phases: (1) Visual inspection, (2) metallographic evaluation, and (3) fluorescent penetrant, magnetic particle, and radiographic inspection. Welds which were unacceptable with regard to visual inspection were either rejected immediately or were metallographically evaluated for microstructure characteristics. Naturally, all welds that were visually acceptable were also subjected to metallographic evaluation. Radiographic and fluorescent penetrant inspections were applied only to trial welds associated with welding conditions being considered for final welding.

Visual inspection of the welds was performed on all specimens. In fact, in many cases, the workpiece itself was observed during and immediately after welding through the welding-machine optical viewing system. All welds were visually inspected for undercutting, cracking, extreme bead roughness, and similar surface effects.

Metallographic examination of the welds was performed on specimens mounted and suitably prepared for metallographic evaluation following the same procedures used for the base metal. For butt welds in all materials,

cross-sections of the welds taken normal to the welding direction were examined. Trial weldments in the 0.005-inch tungsten/Mo-0.5% Ti were evaluated by micro-examination of the weld beads. Previous experience has shown that examination of weld beads, rather then weld cross-sections, of relatively thin joints yields more meaningful results.

Weld microstructures were evaluated for overall weld quality and soundness. Particular emphasis was placed on determining the degree of penetration, extent of fusion and heat-affected zones, grain size, and grain solidification pattern. The weld zones were also examined for micro-cracking and microporosity. Examination was conducted both before and after etching. The same etchants used for base-metal evaluation were used during the trial-weld evaluation phase of the program.

Fluorescent penetrant, magnetic particle, and radiographic inspection techniques were used on welds produced by the potential final weld settings. Because of the narrowness of electron beam welds, careful radiographic inspection techniques, including radiographing the weld at a 30 degree angle across the seam, were required.

The selection of final weld settings was guided by the results obtained during trial-weld evaluation.

Final Welding

The best welding techniques established in trial welding were used to produce butt weldments for mechanical property evaluation in the following material conditions:

I. B120VCA Titanium

a. 0.125-inch solution treated - aged 72 hours at 900 F - welded
b. 0.125-inch solution treated - welded - aged 72 hours at 900 F
c. 0.125-inch solution treated - cold rolled 50% - aged 12 hours at 800 F - welded

II. D6AC Steel

a. 0.290- and 0.090-inch - annealed - heat treated - welded
b. 0.290- and 0.090-inch - annealed - heat treated - welded - stress relieved
c. 0.290- and 0.090-inch - annealed - welded - heat treated

III. Molybdenum-0.5% Titanium Welded to Tungsten

a. 0.005-inch Mo-0.5% Ti welded to 0.005-inch tungsten
b. 0.050-inch Mo-0.5% Ti welded to 0.050-inch tungsten
c. 0.100-inch Mo-0.5% Ti welded to 0.100-inch tungsten

IV. Beryllium

a. 0.040-inch beryllium

Description of Tests (Continued)

The final-weld specimen configurations are illustrated in Figures 29 through 38. The specimens were manufactured so that the edges for welding were perpendicular to the rolling direction. All specimens were cleaned and fixtured by the same techniques used in trial welding. Butt welding was performed perpendicular to the sheet rolling direction. The final weld settings used for each material thickness, heat treat-variation and joint combination are listed in Table 6.

In order to protect final weldments against pick up of contaminents from the welding fixture, the slot in the welding fixture shown in Figure 28 was always lined with strips of material corresponding to the base material being welded. This procedure was especially important when welding titanium and the refractory metals, materials that are sensitive to contamination by foreign atoms.

Representative final weldments in the several materials are shown in Figures 29 through 38.

Final Weld Evaluation

All final weld specimens were visually examined for undercutting, weld cracking, and degree of penetration. Fluorescent penetrant, magnetic particle, and radiographic inspection techniques were used on all specimens for the detection of cracks and porosity. Representative final weld specimens from each material thickness, heat-treat variation, and joint combination were inspected by metallographic techniques for extent of fusion and heat-affected zones, grain size, and grain solidification pattern. Microhardness values were determined in weld-zone cross-sections by testing techniques similar to those used on base metal. Microhardness surveys were made across representative final weldments in all material thickness and thermal treatment combinations.

The tensile properties of electron beam weldments were evaluated at room temperature for all processing and aging variations of B120VCA titanium, all material thicknesses and heat treatments of D6AC steel, 0.040-inch beryllium, and on 0.050-inch tungsten/Mo-0.5% Ti. In addition, tensile properties of 0.040-inch beryllium and 0.050-inch tungsten/Mo-0.5% Ti were evaluated at elevated temperatures. Elevated-temperature tensile tests were performed on specimens of 0.050-inch tungsten/Mo-0.5% Ti at 1600 F, 1900 F, and 2200 F and on specimens of 0.040-inch beryllium at 500 F and 1000 F. Specimens and testing procedures were similar to those used for base-metal tensile property evaluation. All tests were performed on weldments in the as-welded condition; that is, the original weld-bead surface was intact with no machining clean-up. Specimens were either tested as-welded, heat treated, or stress relieved, depending upon the condition to be tested. After fracture, all specimens were examined for origin (weld or base metal) of failure.

The transverse bend-ductility and ductile-to-brittle transition temperatures were determined for electron beam weldments in all processing and aging variations of B120VCA titanium, all heat-treat variations of the

0.090-inch D6AC steel, all thicknesses of tungsten/Mo-0.5% Ti, and 0.040-inch beryllium. The specimens and testing procedures were similar to those used on the base metal.

During all bend testing, the face of the weld (beam impingement side) was placed in tension. As with the base metal, the specimens were visually inspected after test to determine the angle at failure. The location of failure, relative to the joint centerline, was also noted.

The fracture toughness of weldments in all processing and aging variations of B120VCA and all heat-treat variations of the 0.090-inch D6AC steel was determined at room temperature. Specimens and testing procedures were similar to those used for base-metal fracture toughness property evaluation. All weldments were tested with the original weld bead intact. Emphasis was placed on the careful placement of the center notch within the fusion zone. Figure 39 illustrates a fracture-toughness tensile specimen in a typical final weldment.

The room-temperature impact properties were determined for weldments in all conditions of 0.290-inch D6AC. Specimens and testing procedures similar to those used for base-metal evaluation were employed.

Results of Tests

Base-metal Evaluation Results

Results of chemical analyses of each material thickness appear in Table 7.

With the exception of the poor surface condition existing on the hot-rolled D6AC plate, visual examination of the as-received base metal failed to reveal any cracks, laminations or other defects.

Representative sections of all base metal in all conditions are illustrated in Figures 40 through 60. Metallographic examination of the as-received materials showed, in general, a lack of detectable inclusions with the exception of the 0.050-inch Mo-0.5% Ti base metal. Inclusions were revealed in 0.050-inch Mo-0.5% Ti after electropolishing. These inclusions are apparent in Figure 50.

Decarburization to a depth of 0.015-inch below the surface was found in both thicknesses of D6AC plate. Figure 61 shows a cross-section of D6AC both before and after removal of the decarburized surface layer. The results of hardness tests performed on all material thicknesses and conditions are listed in Table 8.

Base-metal tensile test results at both room and elevated temperatures (where applicable) are presented in Table 9. For reference, the variation of base-metal strength with temperature is shown in Figure 97 for 0.050-inch tungsten and Mo-0.5% Ti and in Figure 73 for 0.040-inch beryllium. Due to the extreme brittleness of the tungsten base metal, all of the tensile specimens tested at room temperature failed prematurely, with the failures occurring outside of the reduced gauge section.

The ductile-to-brittle transition temperatures determined for the various material thicknesses and heat treatments are listed in Table 10. In all cases, the ductile-to-brittle transition temperature was arbitrarily chosen to be that temperature at which a bend angle of 30 degrees was achieved before the onset of cracking.

The tensile and bend properties of the 0.050-inch Mo-0.5% Ti and tungsten base metal utilized during the welding investigation conducted under Air Force Contract Number AF 33(616)-7439 Task Number 735102 are presented in Table 11 along with the weldment mechanical property data. These strength and ductility properties are presented since mechanical property test data for the Mo-0.5% Ti and tungsten welded to themselves (under the above referenced contract) will be used as base-line data for the evaluation of Mo-0.5% Ti welded to tungsten.

The results of internal-notch tensile tests performed at room temperature on all processing and aging variations of B120VCA and on both thicknesses of D6AC in all heat treatments are listed in Table 12.

Results of Tests (Continued)

Room-temperature impact tests performed on heat treatment variations of D6AC are summarized in Table 13.

Beryllium Trial-weld Evaluation Results

Best results were obtained in electron beam welding of beryllium by using moderately high power densities and slow welding speeds. The resultant welds were sound, crack-free, and exhibited good joint strengths.

Photomicrographs showing weld cross-sections and microstructures for the 0.040-inch beryllium are presented in Figures 62 through 68. Figure 62 shows the effect of welding at a slow speed. Figure 63 represents a weld made at a relatively fast welding speed. Figures 64 and 65 illustrate the effects of welding at relatively fast speeds using longitudinal and circular beam oscillation. Figures 66 through 68 show the effect of beam defocus at slow welding speeds. Figure 67 illustrates the weld zone microstructure of the weld settings associated with the final weld settings.

Beryllium Final-weld Evaluation Results

Visual and dye penetrant inspection of the 0.040-inch beryllium final welds indicated that both the top and bottom weld beads were smooth, continuous, and crack-free.

Figures 69 through 72 show various examples of a final weldment in 0.040-inch beryllium. Figures 69 and 70 show the top and bottom weld beads respectively. Figure 71 shows a 70X magnification of the weld-zone cross-section. A 100X photomicrograph of the weld-zone microstructure is presented in Figure 72.

Results obtained from room and elevated-temperature tensile tests are presented in Table 14. Figure 73 illustrates the effect of increasing temperature upon the tensile strength of electron beam welded 0.040-inch beryllium. Base-metal results are also included on the plot.

The ductile-to-brittle transition temperature for weldments in 0.040-inch beryllium is listed in Table 15 along with the corresponding base-metal transition temperature. The change in transverse bend ductility with temperature for beryllium weldments is shown in Figure 74. For reference base-metal results are included on the same plot.

Molybdenum-0.5% Titanium to Tungsten Trial-weld Evaluation Results

All three thicknesses of the Mo-0.5% Ti/tungsten joint combination were as easily weldable as the individual base metals. No problems were encountered in producing sound, crack-free welds. Results of a previous electron beam welding program[1] indicated that maximum weld ductility and strength were dependent on limited fusion and recrystallized zones. Therefore, due to the difference in melting point of the two joint materials (approximately 1500 degrees F) the beam location relative to the joint center-

line was considered to be the most critical single parameter. Consequently, trial welding was concentrated on determining the effects of beam location on joint quality.

Photomicrographs showing weld cross-sections and microstructures in 0.100-inch and 0.050-inch Mo-0.5% Ti/tungsten trial butt welds are shown in Figures 75 through 81. In Figure 75 the effect of impinging the beam on the joint centerline is shown. Figure 76 illustrates the effect of moving the beam location to the Mo-0.5% Ti side of the joint. The welds shown in Figures 77 and 78 were produced by locating the beam on the tungsten side of the joint.

The 0.050-inch Mo-0.5% Ti/tungsten welds reacted to variations in beam location in a manner similar to the 0.100-inch welds. Figures 79 through 81 illustrate the effects of varied beam locations relative to the joint centerline for the 0.050-inch Mo-0.5% Ti/tungsten trial butt welds. The weld settings associated with Figures 78 and 81 were chosen for the final weld settings for 0.100-inch and 0.050-inch Mo-0.5% Ti/tungsten.

Weld beads from 0.005-inch Mo-0.5% Ti/tungsten welds are shown in Figures 82 through 84. The weld in Figure 82 was made with the beam located on the joint centerline. Figure 83 shows a weld produced with the beam located on the tungsten side of the joint. Figure 84 illustrates a weld made with a 0.005-inch joint overlap. The settings of Figure 84 were chosen for the final settings for 0.005-inch Mo-0.5% Ti/tungsten. Figure 85 is a schematic drawing of the modified joint design used for butt welding of the 0.005-inch Mo-0.5% Ti/tungsten.

Molybdenum-0.5% Titanium to Tungsten Final-weld Evaluation Results

Inspection of final welds by visual, radiographic and dye penetrant techniques indicated that the weld beads were smooth and continuous, no cracking was present, and only a minute amount of porosity occurred in the 0.100-inch and 0.050-inch welds.

Examples of the final welds in all three thicknesses of materials are shown in Figures 86 through 96. Top and bottom weld beads, 20X magnifications of weld-zone cross-sections, and 100X photomicrographs of the weld-zone microstructure are presented in these figures.

The results of room and elevated-temperature tensile tests on the 0.050-inch Mo-0.5% Ti/tungsten weldments are presented in Table 16. Figure 97 illustrates the variation of weld tensile strength with increasing temperature. Base-metal results are included on this plot for reference.

The ductile-to-brittle transition temperatures for weldments in all three thicknesses of Mo-0.5% Ti welded to tungsten are listed in Table 17. The changes in transverse ductility for the electron beam weldments are shown in Figures 98 through 100. For reference the base-metal results are shown on the same plots.

Results of Tests (Continued)

B120VCA Titanium Trial-weld Evaluation Results

Both the solution treated and aged and the cold rolled and aged B120VCA titanium were readily weldable by electron beam techniques. Sound welds were produced using a variety of welding conditions. Highest quality welds were associated with minimum fusion and heat-affected zones together with smooth, continuous weld beads. Due to the extreme fluidity of this titanium alloy, considerable development was required in order to determine weld settings which would produce weld beads with minimum, if any, undercutting. Acceptable weld beads were induced by welding with a slightly defocused beam oscillated in the direction of welding ("X" beam oscillation).

Early in the trial welding of B120VCA sensitivity to undercutting was observed on top weld bead surfaces in all three aging/welding conditions; that is, solution treated and aged prior to welding, cold rolled and aged prior to welding, and welded in the solution treated condition. Figures 101 and 102 illustrate this effect on weld cross-sections in aged material.

Micrographs of weld cross-sections in aged B120VCA are presented in Figures 101 through 106. The weld of Figure 101 was produced with a focused beam at a moderately fast welding speed. The undercutting induced by the sharply focused beam can be seen in this photograph. Previous experience has shown that undercutting can be eliminated in most cases by using 60 cycle beam oscillation. Figures 102 and 103 illustrate the effect of welding with 1.5 KW of beam power using "Y" beam oscillation and circular beam oscillation. Figures 104 and 105 show the extensive heat effect resulting from welding with an oscillated beam at 2.1 and 2.24 KW respectively.

The effect of "X" beam oscillation upon weld quality is shown in Figure 106. This weld was produced at a relatively slow speed (22 ipm) using a slightly defocused beam (a comparatively small spot size, however, when compared to the beam used to produce the welds shown in Figures 104 and 105). The settings associated with the weld of Figure 106 were chosen for the final weld settings for B120VCA titanium.

B120VCA Titanium Final-weld Evaluation Results

With the exception of some smooth, shallow undercutting all final welds in B120VCA exhibited smooth, continuous, and crack-free weld beads. Radiographic and dye-penetrant inspection indicated that no cracking or porosity was present in the final welds.

Representative examples of the final butt welds in all three of the material conditions welded are illustrated in Figures 107 through 118. Figures 107, 108, 109, and 110 illustrate, respectively, 10X photographs of the top and bottom weld beads of the final welds in solution treated and aged B120VCA, a 20X photograph of the weld cross-section, and a 100X photomicrograph of the weld-zone microstructure. Figures 111 through 114 and 115 through 118 present identical illustrations for final butt welds in material welded in the solution-treated condition and aged after welding and

material welded in the cold rolled and aged condition.

Room-temperature tensile test results for the final electron beam weldments are presented in Table 18.

The ductile-to-brittle transition temperature for electron beam weldments in all three aging/welding conditions of B120VCA are summarized in Table 19. The effect of increasing temperature on transverse bend ductility for all conditions is shown in Figure 119. For reference the base-metal results are included on the same plot.

Results of internal-notch fracture toughness tests are summarized in Table 20. A complete compilation of data used for the calculation of G_c for the B120VCA final weldments can be found in Table 26 in the Appendix

Microhardness surveys taken across the weld zones of all three aging/welding conditions are plotted in Figures 120 through 122. In order to eliminate the hardness variations which can result from grain boundary effects, microhardness surveys for all titanium welds were taken using a 2 kilogram load rather than the 0.2 kilogram load used for base-metal hardness determinations.

D6AC Steel Trial-weld Evaluation Results

Electron beam welds in both the 0.290- and 0.090-inch D6AC steel exhibited sound, non-porous microstructures when welded with a variety of settings. Welds with highest-quality surface appearance and optimum weld-zone characteristics were associated with welding performed using a moderately high energy beam of approximately 0.015-inch diameter.

In general, trial weld beads were characterized by a slightly irregular and rough surface texture. A defocused beam was used to overcome this surface roughness in the 0.090-inch material. The use of a clean-up pass was investigated for the thicker 0.290-inch D6AC.

Figures 123 to 128 illustrate weld cross-sections in 0.090-inch plate. The effect of welding with a focused beam at a relatively fast speed is shown in Figure 123. The surface irregularity and some undercutting can be seen in the cross-section of this trial weld. The welds in Figures 124 through 127 illustrate the effects of beam oscillation (X, Y and circular) upon weld quality. The use of circular beam oscillation eliminated a good portion of the top weld bead irregularity and undercutting; however, the quality of the bottom weld bead was poor. Figures 128 and 129 show welds produced using beams defocused to a diameter of 0.010 inch and 0.015 inch respectively. The settings associated with Figure 129 were selected as the final weld settings for 0.090-inch D6AC.

The 0.290-inch D6AC responded to similar welding conditions in a manner identical to the 0.090-inch material. Therefore, a two-pass welding technique was investigated as an alternate method of improving the surface

quality of the D6AC weldments. The weld in Figure 130 was produced using a low energy clean-up pass to smooth the top bead. The settings used to produce the weld shown in this photograph were chosen as the final weld settings for 0.290-inch D6AC. Figure 131 exhibits a weld containing an intergranular crack. In general, the crack was associated with the plane of weakness occasionally present as a result of the columnar grain growth in the weld fusion zone.

D6AC Steel Final-weld Evaluation Results

Visual inspection of final welds indicated that the weld beads were smooth and crack-free. Inspection by normal radiographic, dye penetrant, and magnetic particle techniques revealed that the welds were free of any porosity or cracking. Metallographic evaluation of a sampling of 0.290-inch final welds (subsequent to mechanical property testing) revealed the presence of a fine line-crack through the columnar grains in the center of the weld zone. These cracks were not detectable by the 2 percent penetrameter radiographic sensitivity used for normal weldment radiographic inspection.

Figures 132 through 147 show examples of the final weldments in both the 0.090- and 0.290-inch D6AC. Photographs of top and bottom weld beads, a 20X photograph of the weld cross-section, and a 100X photomicrograph of the weld-zone microstructure are presented for each welding/heat treatment combination. Figures 132 through 135 present illustrations for the final butt welds in 0.090-inch D6AC welded in the annealed condition and heat treated after welding. Final butt welds in 0.090-inch D6AC welded in the heat-treated condition are shown in Figures 136 through 139. Figures 140 through 143 and 144 through 147 illustrate the final butt welds for the 0.290-inch D6AC welded in the annealed condition and heat treated after welding and the 0.290-inch D6AC welded in the heat-treated condition.

Results of room-temperature tensile tests performed on final butt weldments in the 0.090-inch thick D6AC are presented in Table 21.

Electron beam weldment ductile-to-brittle transition temperatures for all welding/heat treatment combinations of the 0.090-inch plate are summarized in Table 22. The increase in transverse bend ductility with increasing temperature is shown in Figure 148 for the 0.090-inch weldments. For reference base-metal results are included on the same plot.

Internal-notch fracture toughness test results are presented in Table 23. Specimen data used for the computation of G_c for the D6AC is presented in Table 26 in Appendix.

The results of microhardness surveys taken across the weld zones of all welding/heat treatment conditions are plotted in Figures 149 through 156. For the 0.290-inch D6AC welds hardness surveys were taken across both the single pass and clean-up pass weld zones and the zone of heat-affect resulting from the second pass.

Results of Tests (Continued)

Impact tests performed upon 0.290-inch D6AC final butt welds are summarized in Table 24.

Discussion of Results

Base-metal Discussion

Visual inspection of all base metal in the as-received condition indicated that, with the exception of the thicker D6AC steel, all material was of acceptable quality for welding evaluation. The thicker D6AC steel (0.300 inch) was received in the hot-rolled condition and consequently exhibited considerable surface roughness due to the presence of a tenacious rolling scale. This scale was removed, however, when the 0.300-inch D6AC was surface ground to remove the decarburized surface layer discussed previously.

The chemical analyses of the base metals (Table 7) were within normally acceptable limits.

Metallographic examination of the base metals revealed that decarburization was present in both thicknesses of D6AC steel. The decarburized surface layer shown in Figure 61 extended approximately 0.015 inch below the surface and undoubtedly resulted from the hot rolling of both plate thicknesses. The presence of this decarburization seriously impaired the surface hardenability of the D6AC plate, and its removal was a prerequisite to uniform heat treatment of the steel.

Both the D6AC steel and the B120VCA titanium exhibited excellent heat treatment and aging response as indicated by the high strength levels attained as a result of thermal treatment. The heat treatment procedure for D6AC steel outlined in the description of tests was chosen for optimum properties at a minimum strength level of 240,000 psi (Rc50). The double temper (2T700) used for both thicknesses of the D6AC is a common heat treating practice for high-strength structural steels. The second tempering treatment provides an additional stress relief and tempers any martensite that may have formed from retained austenite during the first temper.

The aging treatments chosen for the solution treated and the solution treated and 50% cold rolled B120VCA titanium produced relatively high strength levels compared to those presently used in industry. The exceptionally high strength of the solution treated and aged material (220,000 psi ultimate and 201,000 psi yield strength) was a result of the long aging treatment (72 hours). Present industrial practice is based on attaining a strength-to-density ratio of 1×10^6 (inch) which, in the case of B120VCA titanium whose density is 0.175 pounds per cubic inch, would have been satisfied by a strength level of 175,000 psi. The higher strength level was, however, chosen in order to investigate the effects of electron beam welding on titanium base metal aged to strength levels in excess of 200,000 psi.

The tensile properties of all base metals (Table 9) were well within the ranges of expected values. The cold-rolled B120VCA titanium exhibited exceptionally high strength upon aging, with a 12 hour treatment resulting in a tensile strength of 244,000 psi (Figure 3). Both thicknesses of D6AC steel responded quite well to heat treatment and the 240,000 psi strength

level was easily achieved. 0.050-inch Mo-0.5% Ti base metal exhibited a room-temperature tensile strength far superior to similar base metal used during the investigation of the electron beam welding of Mo-0.5% Ti under a previous program.

Room-temperature tensile properties of 0.050-inch tungsten base metal were not obtained. The extreme brittleness of the material results in part from surface imperfections that act as stress concentration sites and promote brittle fracture. Every reasonable precaution was taken to eliminate notches, laminations and other defects that could cause premature brittle failure. This included careful machining, chemical polishing of specimens before testing, and use of the room-temperature tensile testing fixture shown in Figure 8. Still defects were present that initiated failure at relatively low strength values.

The tungsten specimens tested at temperatures in the range of 2200 F to 2800 F all failed in a ductile manner at reasonably uniform values. Therefore, these data are considered valid.

The tensile strength of the 0.040-inch beryllium base metal was relatively high when compared to the reported base-metal tensile properties of similar material used during programs conducted to evaluate conventional fusion welding of beryllium.

The bend-test data (Table 10) indicate that with the exception of annealed 0.090-inch D6AC, solution treated B120VCA, 0.100-, 0.050- and 0.005-inch Mo-0.5% Ti, and 0.005-inch tungsten ductile-to-brittle transition temperatures of base metals were generally above room temperature.

The results of fracture-toughness tests on solution-treated B120VCA titanium base-metal specimens indicated the material to have such high fracture toughness that the G_c* values (1768 - 2137 $\frac{\text{inch-lb.}}{\text{inch}^2}$) were not considered valid; i.e., the ratio of net section stress to yield strength was much greater than unity. The fracture surfaces exhibited 100% oblique (45°) shear separation and a fibrous appearance. All load-deflection curves peaked prior to fast fracture, indicating the extreme fracture toughness of solution-treated titanium.

Solution treated and aged (900° F - 72 hrs.) B120VCA titanium base metal exhibited low fracture toughness properties (G_c* ranging from 72.1 to 121.5 $\frac{\text{inch-lb.}}{\text{inch}^2}$). The fracture surfaces contained a flat granular zone bordered occasionally by shear lips which totaled up to 15% of specimen thickness. Analysis of results and load-deflection curves indicated that wing-crack pop-in coincided with catastrophic failure.

Solution treated, cold-rolled, and aged (800° F - 12 hrs.) B120VCA titanium base metal exhibited the lowest base-metal fracture toughness properties

(G_c^* ranging from 28.1 to 38.3 $\frac{\text{inch-lb.}}{\text{inch}^2}$). The fracture surfaces contained a flat granular zone bordered occasionally by shear lips totalling only 5% of specimen thickness. Analysis of results and load-deflection curves indicated that wing-crack pop-in was coincident with catastrophic failure.

Fracture-toughness tests on base-metal specimens in both aged conditions indicate that the B120VCA titanium alloy at the ultra high strength level of 244,000 psi and yield strength/density ratio of 1.37×10^6 (inch) is less than optimum for high pressure applications. Furthermore the fracture-toughness test results obtained for B120VCA indicate the necessity for choosing an aging treatment and attendant strength level on the basis of fracture-toughness properties as well as standard mechanical properties.

Fracture-toughness test results on both thicknesses of D6AC steel base metal in the annealed condition indicated extremely high fracture toughness properties for this alloy. G_c^* values were not considered valid because the net section stress was much greater than the yield strength; in almost every case, annealed D6AC specimens were completely fractured during slow crack growth. The fracture surfaces indicated 100 percent oblique shear failure and had a fibrous appearance. The load-deflection curves peaked considerably before complete failure. However, the crack length at the onset of fast fracture was determined from an apparent modulus drawn from the origin of the load-deflection curve to the point of maximum load rather than the point of fast fracture or complete failure.

Valid G_c^* values could have been determined for the annealed, extremely tough D6AC (or the solution-treated B120VCA) if large enough specimens were tested. The K_{Nc} determination for non-valid tests was made, however, in order to obtain some meaningful fracture toughness value from the 3-inch wide specimens. K_{Nc} closely approaches the K_{1c} value[2] (or plane strain fracture toughness index) which represents a fracture toughness property of an infinitely wide specimen or, practically speaking, a minimum value of Kc. Thus, for a given material and heat-treat condition, the K_{Nc} value should be constant. The scatter (up to $\pm$ 13% for annealed D6AC) is attributed to the difficulty in picking the exact point of deviation from linearity of the apparent modulus.

The 0.090-inch D6AC steel base metal in the heat-treat condition (2T700) exhibited high fracture toughness properties (G_c^* values greater than 1100 $\frac{\text{inch-lb.}}{\text{inch}^2}$). Some specimens were so tough that the G_c^* values were not considered valid. The fracture surfaces exhibited 100 percent oblique shear failure and were occasionally characterized by orthogonal shear rather than single shear. A chevron effect characteristic of fast fracture usually accompanied orthogonal shear. The fracture surfaces had a dull-gray fibrous appearance.

Discussion of Results (Continued)

The heat treated 0.290-inch D6AC steel base metal exhibited fairly low fracture toughness (G_c* values around 200 $\frac{\text{inch-lb.}}{\text{inch}^2}$). The fracture surfaces exhibited a granular zone bordered by shear lips totalling 20% of specimen thickness. A severe decrease in fracture toughness with increasing thickness is characteristic of most high-strength steels in a certain thickness range which is frequently between 0.1 inch and 0.2 inch at room temperature.

Impact tests performed on 0.290-inch D6AC base metal failed to generate any reliable results. The unnotched, substandard Izod impact specimen was chosen in order to ensure the most meaningful impact results for electron beam weldments. Due to the small overall weld bead widths, location of a notch in a welded impact specimen was not considered practical and an unnotched specimen was designed for impact testing. As can be seen from Table 13, base-metal specimens were not fractured by the impact testing machine. The results, therefore, do not lend themselves to any reasonable interpretation.

Discussion of Results (Continued)

Beryllium Trial-weld Discussion

Best results were obtained in electron beam welding of beryllium using moderately high power densities and slow welding speeds. When welding speeds were increased, or when extremely high power densities were used, columnar grain growth lead to weld cracking.

Because of the toxic nature of beryllium, metallographic specimens were prepared on a subcontract basis at facilities outside of Hamilton Standard. Consequently, the long lead times that were involved in obtaining metallographic information on the welds made it necessary to evaluate trial welds, and choose final weld settings, solely on the basis of visual examination of weld beads.

The effect of welding at a relatively slow welding speed with a focused beam of moderate power is shown in Figure 62. The crack evident in the weld cross-section is characteristic of all welds in beryllium produced at these settings.

The weld in Figure 63 illustrates the effect of welding at a fast speed with a focused beam of relatively high power. The weld zone assumed the classical wedge shape associated with high-energy-density electron beam welding; however, the fusion zone grains are columnar and highly oriented. This condition, in general, induced low strength and ductility. In fact, viewing through the visual optics, formation of the crack was noted immediately after completion of the weld.

The weld shown in Figure 64 was produced using a focused beam of relatively high power and longitudinal beam oscillation. Experience with tungsten welding[1] has shown that this type of deflection creates a more randomly oriented grain structure in the fusion zone, leading to improved weld strength. However, essentially no improvement was realized when this technique was applied to beryllium.

Circular beam oscillation has been used with good success to induce random grain orientation in several materials. Figure 65 shows a beryllium weld produced using circular beam oscillation. This technique offered no improvement in grain quality when applied to beryllium. Increased effective spot size, as a result of the circular beam movement, made the weld zone relatively large.

Figure 66 illustrates a cross-section of a beryllium weld produced at a slow welding speed using a slightly defocused beam. Beam diameter was 0.015 inch. Although the grain pattern is somewhat columnar, the results are encouraging because of the extremely narrow weld zone.

A fusion zone microstructure approaching a more randomly oriented grain pattern is shown in Figure 67. This weld was produced by moderating the power density (decreasing accelerating voltage to 75 KV) and increasing the beam diameter to 0.020 inch. The weld shown in Figure 67 has a larger

weld zone than that shown in Figure 66 and columnar grain growth is evident at the boundaries of the weld zone. However, the fusion grains in the interior of the weld zone are relatively small in size and randomly oriented. The settings used to produce this weld were chosen to be the final weld settings for 0.040-inch beryllium solely on the basis of visual appearance.

A further decrease in accelerating voltage (to 65 KV) resulted in the weld illustrated in Figure 68. The grains are small in size and show little evidence of columnar growth. It appears that welding conditions somewhat between those used for the welds in Figures 66 and 68 should develop the desired narrow, but randomly oriented weld zone.

The columnar grain structure resulting from welding at fast speeds with a beam of relatively high specific power is to date unexplainable. Experience with metals other than beryllium (as shown with the other metals welded during this program) has always indicated a decrease in grain size and orientation with increasing welding speeds. Beryllium, the exception, exhibits the opposite effect.

It appears that due to a combination of its high thermal conductivity and high specific heat, beryllium is extremely sensitive to thermal input. The fast cooling rate associated with the low-energy input from welding with relatively high-power-densities and fast travel speeds results in severe weld cracking along grain boundaries. This is due primarily to the high degree of orientation of the columnar grains towards the center of the weld zone. With TIG welding it has been reported[3] that the tendency towards hot-tearing decreases with slower welding speeds and increased preheat.

Controlled cooling appears to be necessary to produce the optimum weld-zone microstructures. This is accomplished by moderating the power density and decreasing the welding speed. Of course, the ideal weld-zone would be small in over-all size while exhibiting a fine-grained, random microstructure. The results shown in Figure 66 indicate that such a weld structure is attainable by using moderately high voltages in combination with lower beam currents, while maintaining the slow welding speeds.

Beryllium Final-weld Discussion

The consistent production of sound crack-free butt welds in beryllium indicates that beryllium sheet is reproducibly weldable by electron beam techniques.

In all cases, the size of the weld beads, the fusion zone, and grain size were less than those generally obtained in arc welds in the same material thickness.

As previously mentioned, the metallographic evaluation of beryllium trial-weld microstructures was not performed until after final weld settings were chosen and manufacture of mechanical property test specimens was initiated. Therefore, the conditions selected for welding tensile and

bend specimens were based on visual examination of the weld bead and were not based on metallographic evaluations. In fact, metallographic work conducted subsequent to final welding and testing indicated that further improvement in grain size, random grain orientation, and size of fusion zone can be expected with somewhat different welding conditions as illustrated by the random grain orientation of Figure 68.

The room-temperature tensile strength of electron beam welded 0.040-inch beryllium sheet was consistently about 65 percent of base-metal strength. The consistency of tensile strength values is an indication of the uniformity of electron beam welds in this material. The elongation obtained in electron beam weldments tested at room temperature was lower than that obtained for base metal. However, it should be noted that in weld fractures a very high proportion of the strain is absorbed within the very narrow weld zone. Thus, a very high degree of local ductility could be masked by the overall gauge-length measurement (one (1) inch gauge section).

Figure 73 shows the continuous approach of the tensile strength of the weld to that of the base metal with increasing temperature. At 1000 F, even though all of the welded specimens failed in the welds, the base-metal and weld ultimate and yield strengths were essentially the same. Based on the data shown in Figure 73, the tensile strength of electron beam weldments at 1000 F is equivalent to base-metal strength.

In general, electron beam butt welds in beryllium sheet exhibited tensile strength properties at both room and elevated temperatures in excess of similar joints produced either by conventional welding techniques[3] or low voltage electron beam welding[4].

The correlation of electron beam bend ductility data for the 0.040-inch beryllium weldments (as well as electron beam welds in any other material) is difficult for many reasons. Techniques of testing differ among the various investigators, making intercomparison of test data an almost impossible task. Secondly, and perhaps most significantly, the over-all dimensions of electron beam welds as compared with welds produced by conventional fusion welding techniques are drastically different. Whereas in bend testing conventionally produced welds in beryllium, all bending strains can be absorbed in a fusion zone perhaps 0.250-inch wide (a width far exceeding a 1T bend-radius mandrel), electron beam welds must absorb all the bending strain in a total weld zone width smaller than the bend radius utilized, in this case 0.050 inch. Therefore, for electron beam welds, the less ductile weld metal must absorb all of the bending strain while the parent metal surrounding it remains relatively unstrained. In addition, the weldments tested were chosen solely on the basis of visual appearance, not metallographic evaluation. Therefore, the results of bend ductility testing shown in Figure 74 cannot be interpreted as being representative of optimum electron beam welds in beryllium. The less ductile, highly oriented columnar grains present on the edge of the fusion zone (Figure 67) undoubtedly contribute to the low bend ductility values exhibited by the weldments tested.

Discussion of Results (Continued)

It is apparent that the weld of Figure 68, because of its completely random fine grained structure, should exhibit superior strength and bend ductility. This weld was produced at lower energy and at a slower welding speed than the weld tested and discussed above.

It is of interest to note that during some company sponsored beryllium welding, weldments were produced at power inputs of 42 KW/linear inch. Metallographic evaluation of these weldments revealed the presence of porosity within the fusion zone. In order to determine the most probable cause of porosity in beryllium weldments a comparison was made of the power inputs used to produce these porous welds and the power inputs used to produce the sound welds during the beryllium phase of the program being reported upon. The sound welds produced for the subject program were produced at a power input of 17.4 KW/linear inch. The weldments produced during the company sponsored effort at power inputs of 42 KW/linear inch represent a power input increase of approximately 140%.

W. T. Hess et al[4] have reported an interdependence of power input and chamber pressure upon vaporization ability. At a pressure of 10^{-4} mm. Hg., the theoretical boiling point of beryllium is 1440 K which is below its melting point of 1550 K. This indicates that beryllium should sublime below its melting point. Since welding during the company sponsored phase was performed with 2.4 times the power used during initial welding (for the subject program), it is entirely conceivable that some vaporization threshold exists, beyond which a given power input will cause gas evolution in the molten weld metal at a rate in excess of the rate of out-gassing from the molten surface. This excess gas results in the detected porosity.

Molybdenum-0.5% Titanium to Tungsten Trial-weld Discussion

Sound, fully penetrated welds were obtained with beam locations varied within rather wide limits (up to 0.010 inch on either side of the joint centerline) indicating a high degree of weldability for the Mo-0.5% Ti/ tungsten joint combination. All of the welds illustrated are sound and crack-free; however, weld zone characteristics differ. Some difference in cross-sectional thickness between the Mo-0.5% Ti and tungsten base metal can be noted from the trial weld cross-sections. This, however, in no way detracts from the soundness of the welds.

As discussed under Results of Tests, joint characteristics were found to be highly dependent upon beam location. Alignment of the electron beam on the joint centerline, or on the Mo-0.5% Ti side of the joint up to a maximum of 0.010 inch from the centerline, resulted in a "braze type" of joint rather than a fusion weld; with the Mo-0.5% Ti parent metal acting as the braze alloy. The weld shown in Figure 75 illustrates the effect of welding with the beam located on the joint centerline. Extensive recrystallization has occurred in the Mo-0.5% Ti joint member while little, if any, alloying has occurred between the Mo-0.5% Ti and the tungsten. The higher melting material, tungsten, did not completely reach a molten state and small islands of unmelted tungsten can be observed in the fusion zone.

This effect becomes more pronounced as the beam location is moved further into the Mo-0.5% Ti, Figure 76.

By moving the location of beam impingement onto the tungsten side of the joint, complete fusion of both members is obtained. A microstructure of a weld produced by welding with the beam 0.010 inch on the tungsten is shown in Figure 77. This joint exhibits a fusion zone and fused grains typical of electron beam welds in either tungsten or Mo-0.5% Ti; however, the fusion and recrystallized zones are excessively large.

Placing the beam location 0.006 inch from the joint centerline produced the weld shown in Figure 78. The fusion and recrystallized grain sizes are relatively fine and the weld exhibits a depth-to-width ratio about the same as either the tungsten or Mo-0.5% Ti weldments in the same thickness. The settings used to produce this weld were chosen as the final settings for 0.100-inch Mo-0.5% Ti/tungsten.

The 0.050-inch Mo-0.5% Ti/tungsten trial welds displayed similar reactions to variation of beam location as did the 0.100-inch welds. Therefore, in order to restrict the extent of fusion and recrystallization, location of the beam on the tungsten side of the joint was again required. Figure 81 illustrates a weld produced with the beam 0.005 inch on the tungsten side of the joint. These settings represent the final weld settings for 0.050-inch Mo-0.5% Ti/tungsten.

Weld beads, rather than weld cross-sections, were used to evaluate the trial welds in 0.005-inch Mo-0.5% Ti/tungsten. Weld cross-sections in such thin material are of insufficient thickness to assume characteristic weld-zone patterns. However, meaningful results can be obtained by viewing the weld bead solidification patterns.

Initially, trial butt welding of 0.005-inch Mo-0.5% Ti to tungsten was concentrated upon the determination of the effects of beam location (relative to the butted joint) upon weld properties. In general, welds produced by butting the two materials and welding with beam impingement locations varying from the molybdenum side of the joint to the tungsten side of the joint were characterized by discontinuities within the fusion zone. When heated by the beam, the extremely thin tungsten sheet appeared to ripple at the joint interface causing discontinuities in the weld after solidification. In most cases the discontinuities were the holes or gaps through the entire weld thickness shown in Figure 82.

Since the holes in the fusion zone were most probably caused by a lack of weld metal in the gap areas due to either poor joint fit-up or edge preparation, attempts were made at welding the 0.005-inch Mo-0.5% Ti/tungsten joints using a "filler metal" technique. The presence of excess base metal in the joint area did in fact eliminate any holes or discontinuities within the weld zone.

Sound butt welds, free of any discontinuities, were produced using the

technique illustrated in Figure 85. The joint configuration shown in this drawing permits welding with a minimum of fixturing and edge preparation. Early in the trial butt welding of the 0.005-inch Mo-0.5% Ti/tungsten it became evident that joint fit-up was a most critical parameter. Because of the relatively thin sheet cross-sections being joined, unless mating edges were in intimate contact along the entire length of weld optimum welding results could not be obtained. Since welding of the joint shown in Figure 85 is performed with a beam of considerably larger diameter than the sheet overlap (beam diameter approximately 0.010 inch), joints welded by this technique show no evidence of prior overlap and function as conventionally butt-welded sheet. Figure 84 illustrates a weld in 0.005-inch Mo-0.5% Ti/tungsten using the overlap technique. The settings used to produce this weld were chosen as the final weld settings for 0.005-inch sheet.

In summary, trial welding of Mo-0.5% Ti to tungsten indicated that the best welds were produced when the beam was impinged on the tungsten side of the joint. A modification of joint design was necessary for the 0.005-inch thick material in order to eliminate several of the problems associated with joint fit-up and edge preparation.

Molybdenum-0.5% Titanium to Tungsten Final-weld Discussion

The final butt welds, illustrated in Figures 86 through 96, demonstrate the extreme weldability of the dissimilar metal joint Mo-0.5% Ti to tungsten by the electron beam technique. In each material thickness the weld fusion and recrystallized zones and grain sizes are comparable to those developed in electron beam welds in either of the two base metals[1]; comparison with conventionally produced arc welds indicates that the electron beam weld fusion and recrystallized zones and grain sizes are considerably smaller.

The minute amount of porosity found in the 0.100 and 0.050-inch welds is most probably a result of the difference in melting points of the two materials. This porosity, which became evident only after electropolishing of weld cross-sections (mechanical polishing techniques were used during the initial weld evaluation phases), could undoubtedly be eliminated by performing welding of slightly slower travel speeds; thereby allowing greater time for the molten weld metal to out-gas under the influence of the vacuum.

The room-temperature tensile properties of electron beam welds in 0.050-inch Mo-0.5% Ti welded to tungsten are slightly lower than tensile strengths exhibited by electron beam welds in Mo-0.5% Ti welded to itself[1]. Comparison with the room-temperature tensile properties of electron beam welded tungsten is difficult due to the lack of valid tensile data for 0.050-inch tungsten welds tested at room temperature. The electron beam welds in Mo-0.5% Ti welded to tungsten that were tensile tested at room temperature exhibited extremely brittle fracture surfaces. Failure has occurred in the tungsten recrystallized zone and is intergranular in nature. The reduced ductility of the tungsten recrystallized grains is most probably the main factor contributing to the relatively low room-temperature tensile strengths shown by the Mo-0.5% Ti/tungsten welds.

Discussion of Results (Continued)

Figure 97 shows the continuous approach of the tensile strength of the Mo-0.5% Ti/tungsten welds to that of both base metals with increasing temperature. For reference, the elevated-temperature tensile properties of electron beam welds in 0.050-inch Mo-0.5% Ti and tungsten to themselves respectively are shown on the same figure along with the base metal. The tensile strengths of Mo-0.5% Ti/tungsten welds exceed strengths of electron beam welded Mo-0.5% Ti and tungsten at 1600 and 1900 F. At 2200 F the electron beam welded Mo-0.5% Ti/tungsten demonstrated tensile strengths essentially equivalent to base-metal strength and to the strength of electron beam welds in Mo-0.5% Ti and tungsten at the same temperature. With the exception of two specimens tested at 2200 F, all failures occurred, as expected, in the tungsten recrystallized grains. The increased ductility of the Mo-0.5% Ti base-metal recrystallized zone relative to the tungsten in the 1600 to 2200 F temperature range undoubtedly contributes to the superior ability of the Mo-0.5% Ti side of the joint to withstand elastic strains at the temperatures tested. The two tensile failures occurring in the Mo-0.5% Ti base metal at 2200 F clearly demonstrate the ability of electron beam welds in Mo-0.5% Ti/tungsten to retain base-metal strength at temperatures approaching the recrystallization temperature of the less-refractory joint component (approximately 2450 F).

The results indicate that electron beam welded butt joints of Mo-0.5% Ti welded to tungsten possess strength properties equal to or exceeding similar welds in Mo-0.5% Ti or tungsten welded to themselves, at service temperatures in the range of 1600 to 2200 F. Although comparable data for arc welds is not available, the fact that electron beam welds in Mo-0.5% Ti and tungsten have demonstrated load-carrying capacities 50 percent greater than conventionally produced weldments serves as an indication of the improvement that can be realized for the dissimilar metal joint Mo-0.5% Ti welded to tungsten.

As was anticipated, the electron beam welds in each thickness (0.005, 0.050, and 0.100 inch) of Mo-0.5% Ti welded to tungsten exhibited transverse bend ductilities that fell in the range between the bend ductilities exhibited by electron beam welds in similar thicknesses of Mo-0.5% Ti and tungsten respectively. In general, the less ductile tungsten recrystallized grains were the limiting factor for Mo-0.5% Ti/tungsten weldment bend ductility.

Hokanson and Kern[1], in an earlier investigation into the electron beam welding of the refractory metals tungsten and Mo-0.5% Ti to themselves, have thoroughly discussed the difficulties associated with the interpretation of electron beam weld bend-test data. In brief, one must consider several factors that contribute to apparent weld ductility: (1) welds were tested in the as-welded condition, that is, the weld beads were not finish ground; (2) Mo.0.5% Ti and tungsten are sensitive to surface condition; (3) the relatively narrow electron beam weld zone induces an extreme concentration of stress in a relatively small, less ductile fusion zone, therefore, the outermost fiber stresses in the weld zone reach extremely high values with very little deflection of the specimen.

Discussion of Results (Continued)

Considering the above-mentioned factors it can be seen that the type of bend test employed does not accurately reflect the true ductility of electron beam welds when data are compared with base-metal or arc-weld data obtained from similar test conditions. However, the relatively small grain sizes and limited fusion and recrystallized zones obtained in electron beam welds should contribute to comparatively superior service ductility over arc welds in similar material thicknesses.

B120VCA Titanium Trial-weld Discussion

The weldability of the B120VCA titanium alloy is readily demonstrated by the welds shown in Figures 101 through 106. Sound welds were produced using a wide range of settings; however, due to the extreme fluidity of this titanium alloy less latitude was available in choosing a final weld setting which produced a weld bead with no undercutting.

The weld of Figure 101 was produced using a sharply focused beam at a moderately fast welding speed (50 ipm). The fusion zone exhibits the classical wedge shape. However, the weld is characterized by a notch-like undercut. This undercutting was observed in all conditions of material welded, that is, welded both prior and subsequent to aging.

Early in trial welding the extreme sensitivity to undercutting of the B120VCA titanium alloy was noted. Consequently, the greatest portion of trial welding was devoted to the development of weld settings which would produce a weld with optimum bead surface quality while retaining the advantages associated with electron beam welding.

The weld of Figure 102, produced with a beam oscillated transversely with respect to the joint, represents an attempt to eliminate the undercutting effects of Figure 101. The sharp notch-like undercut has been effectively smoothed to less of a notch effect. Undercutting is, however, still present.

The effects of welding with a circularly oscillated beam are illustrated in Figure 103. The weld bead undercut has been eliminated; however, the slower welding speed and circular beam oscillation has resulted in rather wide fusion and heat-affected zones.

The weld-zone characteristics induced by welding with an oscillated beam will, of course, vary with the oscillation amplitude. The welds in Figures 104 and 105 while non-undercut, exhibit extended fusion and heat-affected zones. Welding with a beam oscillated either in the transverse direction or in a circular manner can effectively eliminate weld bead undercutting; however, the effect of a widely oscillated beam is to produce excessively wide fusion and heat-affected zones.

An oscillated beam can effectively eliminate weld bead undercutting by creating a favorable distribution of beam energy within the immediate area being welded. From examination of the weld cross-sections in Figures 103

through 105 it is obvious that a circularly oscillated beam produces a more distinct weld bead than a beam deflected in the transverse direction. The fusion and heat-affected zones, however, are too extensive to be considered as optimum weld microstructures.

In an attempt to eliminate the extensive heat effect resulting from welding with a circularly oscillated beam, welds were produced using a beam oscillated longitudinally with respect to the joint. An example is shown in Figure 106. The fusion and heat-affected zones are slightly wider than with a non-oscillated beam (Figure 101); however, undercutting has been minimized to the extent of not being apparent from the weld cross-section shown in this photograph.

The production of smooth, non-undercut weld beads in the 0.125-inch B120VCA is dependent upon welding with a beam of relatively higher power (approximately 1 KW) than would be generally associated with a plain penetration weld pass to an equivalent depth. The use of 0.075-inch longitudinal oscillation, in combination with a slow welding speed and a relatively small diameter beam, minimizes the heat effect associated with the settings used to produce the weld shown in Figure 106. The settings used to produce this weld were chosen as the final settings for the welding of 0.125-inch B120VCA titanium.

Summarizing the trial welding of B120VCA titanium, welds with minimum top bead undercutting were produced by welding at a slow welding speed with a slightly defocused beam of relatively high energy. Beam oscillation along the weld was required to produce weld beads of acceptable quality.

B120VCA Final-weld Discussion

The consistent production of sound butt welds in all aging/welding conditions of B120VCA indicates that this material is reproducibly weldable by electron beam techniques.

The final butt welds are illustrated in Figures 107 through 118. In every case, the size of the fusion zones, the heat-affected zones, and the grain sizes were less than those generally published for conventionally produced fusion welds in the same material thickness. The average weld grain size for electron beam welds in B120VCA titanium was 0.005 inch. Comparable data for single pass TIG square butt welds in B120VCA titanium indicate average weld grain sizes of 0.016 inch.

Examination of Figures 101 and 106 indicates that a further decrease in overall weld dimensions and weld grain size can be achieved when welding is performed at increased welding speeds and the weld bead width is decreased. However, the notch-like undercutting associated with the weld settings of Figure 101 makes this weld unacceptable from a structural standpoint. The sinking or undercutting problem in B120VCA appears to be inherent to welds produced with non-oscillated beams. Since maximum strength and ductility are commonly associated with electron beam welds exhibiting the classical

parallel sided fusion zone (Figure 101), some compromise must be made to attain maximum structural integrity. This compromise will have to be either welding with B120VCA titanium filler metal or grinding weld beads subsequent to welding to remove the weld bead undercut.

Since all final butt welds for mechanical property evaluation were tested with the weld beads in the as-welded condition, final weld settings were selected to produce welds with non-undercut weld beads. Therefore, while results of final weld evaluation can be considered representative of electron beam welds in B120VCA, they should not be taken as the maximum or optimum properties obtainable.

The tensile strengths exhibited by electron beam welds in all three aging/welding conditions of B120VCA titanium varied from sixty percent of base-metal strength for welds in the cold-rolled and aged condition, to seventy-five percent of base-metal strength for welds in solution treated material that were aged subsequent to welding. The elongation obtained in weldments tested in both the aged and welded condition and the welded and aged condition were lower than that obtained for base metal. Welds in the cold rolled and aged condition exhibited ductility superior to the cold-rolled and aged base metal.

The tensile test results (Table 18) indicate a high degree of uniformity for electron beam produced weldments in all three welding/aging conditions. Welds produced in both solution treated and aged and cold-rolled and aged material exhibited an expected uniformity, with maximum ultimate tensile strengths exceeding 155,000 psi for each case. The electron beam welds produced in solution-treated B120VCA base metal and aged after welding exhibited ultimate tensile strengths approximately 20,000 psi higher than the welds produced in aged material.

The reduced weld zone hardness for welds produced in both aged conditions, and the reduced ductility resulting from the relatively large grain size (approximately, however, one-fourth that of TIG weld fusion zone grains) as compared to base metal, undoubtedly contribute to the reduction in the tensile strength of the electron beam welds. All tensile failures initiated and propagated through the heat-affected zone. Considering that the less-ductile weld zone grains must absorb all plastic strain during the tensile test, it is reasonable to assume that providing no weld defects are present the narrower fusion-zone width at the bottom of the weld cross-section achieves maximum plastic strain before the wider fusion zone at the weld top. Failure, therefore, always initiates at the bottom of the heat-affected zone and propagates along the less-ductile interface between the heat-affected zone and the base metal. This failure mechanism would apply to all three aging/welding conditions of B120VCA, with tensile strength variations resulting from differences in fusion-zone hardness.

The results indicate that electron beam welds in all three aging/welding conditions possess tensile strengths in excess of similar joints produced by arc welding techniques in similar materials. A slight improvement in weld ductility is also noted.

Discussion of Results (Continued)

For all welding/aging conditions of B120VCA titanium, bend angles greater than 20 degrees were not achieved at test temperatures up to the prior aging temperature (700 or 800 F). From examination of Figure 119 it is apparent that cold-rolled and aged base metal exhibited similar low ductility; in fact, the ductilities exhibited by electron beam welds produced in material in both the solution treated and aged (STAW) and the cold-rolled and aged (CRAW) condition were superior to the cold-rolled and aged base metal.

The ductile-to-brittle transition curves for electron beam welds in the STAW and CRAW B120VCA titanium exhibit parallel behavior. This parallelism undoubtedly results from the similarity in weld-zone hardness profiles for both conditions when welding was performed subsequent to aging. The extreme similarity can be noted from examination of the hardness profiles in Figures 120 and 122 for the STAW and CRAW condition, respectively. The slightly lower fusion-zone hardness in the CRAW condition (ranging from 29 to 31 Rc as compared to 29 to 33 for STAW welds) undoubtedly is the reason for the slightly higher maximum bend angle (20 degrees as compared to 19 degrees).

The solution treated, welded, and aged B120VCA appeared to exhibit the most brittle behavior of any welding/aging conditions of B120VCA titanium investigated. Although the fusion zone was aged to a hardness level equivalent to the surrounding base metal, all bending strain must be absorbed in the relatively less-ductile fusion zone resulting in what appears to be low ductility.

Results of internal-notch fracture-toughness tests on welds in solution treated and aged (900°F - 72 hr.) (STAW) B120VCA titanium showed considerable variation (G_c^* ranging from 300.7 to 1762). G_c^* values in the range of 1368 to 1762 resulted from non-valid tests; i.e. $\sigma x / \sigma ys >> 1$ indicating that the test was not valid but reflecting extremely high fracture toughness. The 1/2 crack length at fast fracture (a) and the gross section stress (σo) varied from 0.55 to 0.090 inch and 47,900 to 81,800 psi respectively. The fracture toughness equation, $G_c^* = \frac{\sigma o^2 W}{E} \tan \frac{\pi a}{W}$ indicates that variations in (a) and (σo) of these magnitudes can produce a wide range of G_c^* values. Load-deflection curves for some of the tougher specimens peaked prior to the onset of fast fracture. The fracture surfaces had a fibrous appearance and indicated partial or full shear failure separation. Percent shear was not tabulated for most welded specimens since interpretation of fracture appearance in terms of shear lip existence was difficult in the narrow electron beam weld zone.

Electron beam welds in solution treated, cold rolled, and aged (800°F - 12 hr.) (CRAW) B120VCA titanium exhibited G_c^* values ranging from 257.6 to 618.1. The fracture surfaces had a partially fibrous appearance and indicated partial shear failure.

Welds in solution-treated material which were aged (900°F - 72 hrs.) after welding (STWA) exhibited the lowest fracture-toughness properties for electron beam welds in the B120VCA alloy. (G_c^* ranging from 97.7 to

123.1). The fracture surfaces were characterized by a granular appearance and no shear lips. The fracture toughness of STWA welds was equivalent to that of comparable base-metal aged specimens (G_c* ranging from 72.1 to 121.5).

The range of fracture-toughness properties exhibited by all welding/aging combinations of electron beam welds in B120VCA must be interpreted on the basis of a number of factors. Slight variations in hardness exist across the weld zone creating a ductility gradient within each weld tested. During testing, crack propagation occurs along random paths and can be influenced by hardness and ductility variations.

Electron beam welds in solution treated and aged B120VCA titanium exhibited fracture toughness far superior to equivalently-aged base metal. This behavior undoubtedly resulted from the greater ductility associated with the lower strength level of the electron beam weld zone. As expected, the extremely high strength level of the base metal with its attendant low ductility resulted in less than optimum fracture toughness in the electron beam welds.

Comparison of the fracture-toughness of electron beam welds in B120VCA titanium with arc welds produced in similar base metal (Table 127 Appendix) indicates that in spite of the high base-metal strength level (approximately thirty-three percent higher yield strength), electron beam welds exhibited greater than one-hundred percent improvement in fracture toughness over arc welds. Considerable improvement was also shown over previously produced high-voltage electron beam welds with weld-bead surfaces ground flush.[5]

As was previously discussed, electron beam welding techniques developed for B120VCA titanium were less-than optimum due to the extreme sensitivity of this alloy to weld bead undercutting. The establishment of optimum weld-bead quality as a criteria for acceptable electron beam welds made it necessary to modify welding techniques in order to eliminate weld-bead undercutting. The relatively wide fusion and heat-affected zones of the welds shown in Figures 109, 113, and 117 result from welding with less-than optimum electron beam welding parameters. With the development of special welding techniques utilizing base-metal composition filler metal to eliminate undercutting, weld zone characteristics similar to those obtained in the weld shown in Figure 101 can be achieved. This relatively narrow, parallel-sided weld zone, with its restricted heat-affected zones and rapid quench rate (ensuring retention of the beta phase) should, undoubtedly, offer a further improvement in weld strength and ductility.

D6AC Steel Trial-weld Discussion

The wide range of settings used in the production of electron beam welds in D6AC indicates the weldability of this alloy. The welds illustrated in Figures 123 through 130 are representative of the many welds produced by a variety of settings. Almost all of the welds illustrated are sound and crack-free. Definite differences do exist in weld quality.

Discussion of Results (Continued)

Surface defects similar to these encountered with the B120VCA titanium were noticed early in the evaluation of trial welds in D6AC. Considerable surface roughness and undercutting was encountered throughout the trial welding portion of the program. This weld bead surface roughness appears to be inherent to the D6AC material; in fact, other investigators[6] have reported this effect when electron beam welding D6AC. Welds produced in the consumable-electrode vacuum-cast type material used for welding during this program appear to be more susceptible to bead surface roughness than welds produced in vacuum cast material.

The effects of welding with a focused beam are illustrated in Figure 123. The weld exhibits the classical wedge-shaped fusion zone; however, the top bead surface is considerably rough and undercut. All trial welds produced in both thicknesses of the D6AC with a focused, non-oscillated beam exhibited the surface discontinuities shown in Figure 123.

Welding with a beam oscillated longitudinally with respect to the joint being welded produced the weld of Figure 124. The surface roughness has effectively been smoothed out. The fusion zone of the weld is considerably large at the top surface and decreases in a distinct taper.

An attempt to smooth the top bead surface and reduce the sharp taper of the weld zone is illustrated in Figure 125. This weld, produced with a beam oscillated transversely with respect to the joint being welded at a relatively fast welding speed exhibits considerably larger zones of fusion and heat affect. The notch-like undercutting was not eliminated.

Experience with B120VCA titanium has shown that non-undercut welds can be produced using moderately high beam energy, beam oscillation, and relatively slow welding speeds. The welds presented in Figures 126 and 127 represent attempts at eliminating bead undercut by welding with a higher power density beam using transverse and circular beam oscillation respectively. Undercutting has been reduced; however, the weld zones are large and considerable bottom weld-bead roughness is present on the weld shown in Figure 127.

Bottom weld bead roughness was eliminated through the use of a slightly defocused beam (Figures 128 and 129). Both the fusion and heat-affected zones have been slightly increased. However, overall weld-bead quality has been improved. The weld settings associated with Figure 129 were chosen for final welding of 0.090-inch D6AC.

As with the 0.125-inch B120VCA, a compromise between optimum electron beam weld-zone characteristics and good visual appearance was necessary for the 0.090-inch D6AC welds. The rough weld-bead surface obtained as a result of welding with a focused beam made it necessary to sacrifice the deep-narrow weld zone in favor of the visually acceptable smooth, continuous weld bead resulting from welding with a 0.015-inch diameter beam.

The 0.290-inch D6AC reacted to like welding conditions in a manner similar to the 0.090-inch material. Therefore, trial welds with acceptable

weld beads were produced using a slightly defocused beam; however, the settings used to produce these welds in the thicker D6AC were not chosen as the final weld settings for the thicker D6AC material.

The surface irregularities present on the weld beads of the 0.290-inch D6AC extended approximately 0.010 inch below the surface of the weldment. During trial welding it was observed that the irregularities on the top weld bead were associated only with fully penetrated welds. Weld beads of incompletely penetrated weld passes exhibited a sound appearance. Therefore, a second weld pass at lower energy settings could effectively clean-up the surface discontinuities present on the single-pass weld bead. The cross-section of a weld in 0.290-inch D6AC produced using a two-pass technique is shown in Figure 130.

The two-pass welding technique used to produce the weld of Figure 130 consisted of an initial pass using a sharply focused beam deflected slightly in the transverse direction, followed by a second clean-up pass made with a beam oscillated in a circular manner to a 0.040-inch diameter circle. The weld exhibits the classical parallel-sided shape of a high-voltage electron beam weld. The second weld pass has effectively smoothed the weld-bead surface and eliminated the defects induced by the initial weld pass.

The relatively high depth-to-width ratio of the weld shown in Figure 130 (approximately 5:1) results from performing the initial welding using "optimum electron welding conditions", i.e. relatively high energy and fast welding speed. The clean-up pass smooths the surface irregularities but does not affect the weld-zone characteristics. The settings used to produce the weld in Figure 130 were chosen as the final weld settings for 0.290-inch D6AC.

During the trial welding phase weld cracking was noted in the 0.290-inch material. For example the weld of Figure 131 illustrates an intergranular crack extending upwards through the center of the weld zone. In general, it was found that most of the cracks initiated in the root of the weld where weld bead surface discontinuities were present and that the cracks propagated upward through the center of the weld along the centerline of the symmetrical columnar grain solidification pattern. The center of the weld being the last to solidify, naturally exhibits a less-ductile microstructure as a result of the more rapid cooling rate. Since it was found during subsequent welding that cracking could be eliminated through post-welding thermal treatment, it is evident that shrinkage stresses from solidification were not responsible alone for cracking.

D6AC Steel Final-Weld Discussion

The production of sound butt welds in D6AC is highly dependent upon optimization of weld-zone ductility through immediate post-welding thermal treatment. The combination of the extremely high hardenability of this alloy and the extremely rapid quench rates associated with high-voltage electron beam welding, creates a solidification mechanism which produces a

brittle, highly oriented martensite in the fusion zone. Unless this martensite is tempered immediately, either by a post-weld tempering treatment or a full heat treatment, an extremely high susceptibility towards brittle behavior exists in the as-welded fusion zone.

Welds produced in both thicknesses of D6AC steel (0.090 and 0.290 inch) exhibited a tendency towards brittle behavior when welded in the heat-treated condition and tested as-welded. However, welds in the thicker base metal were characterized by a greater tendency towards brittle failure, with most mechanical-test failures occurring in the weld zone even though no apparent welding defects were present.

The final butt welds in both thicknesses of D6AC, illustrated in Figures 132 through 147, represent attempts to obtain electron beam weldments with good overall visual appearance and optimum properties. For all heat treatment/aging conditions the size of the fusion zones, the heat-affected zones, and the grain size were less than those generally obtained by arc welding in the same material thicknesses. This is especially true for electron beam welds in the 0.290-inch thick material.

The apparent widening at the bottom of the weld zone in the 0.090-inch weldments, resulted from the particular welding conditions used to obtain good surface quality. Welding was performed using a beam defocused to a 0.015-inch diameter. The result of defocusing is to bring the beam focal, or cross-over point, slightly above the surface of the weldment. This effectively permits the beam to diffuse as it passes through the gaseous plasma present in the fusion zone during welding, creating the wider fusion zone at the bottom of the weld. The undesirable wider weld zone resulting from welding with a defocused beam was the principle reason for developing a two-pass technique as an alternate method of eliminating weld-bead discontinuities.

As can be seen in Figure 130, the two-pass welding technique produced a weld zone configuration typical of high-power-density electron beam welding. The extremely deep and narrow weld zone is characterized by minimal fusion and heat-affected zone widths. However, because of the less-ductile microstructure of the fusion zone in the as-welded D6AC steel, a two-pass welding technique has inherent disadvantages. The effect of solidification stresses from the second clean-up welding pass is to place the bottom of the initial through-penetrated weld in tension. The tensile stresses in many instances induced cracking along the less-ductile columnar grain interface along the centerline of the weld. Figure 131 illustrates this effect.

An immediate post-welding temper (two hours at 600 F) resulted in an improvement in weld zone ductility for 0.290 inch D6AC; however, cracking did occur in several tempered weldments. A post-welding heat treatment (i.e. a complete austenitizing and double temper treatment) contributed somewhat to improved weld ductility; however, a large precentage of the welds cracked during heat treatment either as a result of rough handling or thermal shock.

Because of the relatively poor ductility exhibited by the 0.290-inch

Discussion of Results (Continued)

D6AC welds during preliminary mechanical property tests, mechanical property testing of final welds in the thicker D6AC was restricted to tensile evaluation of welds tempered immediately after welding.

With relatively few exceptions electron beam welds in 0.090-inch D6AC did not exhibit the low ductility and brittle fracture behavior that characterized welds in the thicker material. The less-than-optimum electron beam welding parameters used to weld this thinner material did not induce the quenching severity present in the 0.290-inch welds. Since cooling rate can influence the fracture transition temperature, it is evident that the less severe cooling of the 0.090-inch welds resulted in more ductile weld-zone behavior.

Results of tensile tests in 0.090-inch D6AC (Table 21) indicate that electron beam welds in all heat treatment/welding combinations of the thinner D6AC retain from ninety to ninety-five percent of heat-treated base-metal tensile strength. The highest tensile strengths were exhibited by welds given a complete heat treatment after welding; however, the elongation obtained in welds tempered immediately after welding was slightly higher.

Hardness profiles for welds in 0.090-inch D6AC (Figures 149-151) show a decrease in hardness in the heat-affected zones of welds tested either as welded or with a post-welding temper. In most cases, failure occurred in this zone of relatively lower strength; however, some failures did occur in the base metal. Welds that were completely heat treated after welding displayed uniform hardness across the weld zone and base metal. The occurrence of failure for welds heat treated after welding was distributed equally between the base metal and the weld zone.

As was previously stated, tensile tests were performed only upon 0.290-inch D6AC welds that were tempered immediately after welding. The results of tensile tests performed upon tempered electron beam welds in 0.290-inch D6AC indicate that in many cases the welds exhibited equivalent heat-treated base-metal strength. Elongation obtained in these welds was in general lower than base metal.

The extremely high strength exhibited by the tempered 0.290-inch D6AC welds indicates that the welds were tempered fast enough to relieve the stresses induced by the clean-up pass. The relatively low strength of weld HWS 29-1 indicated that the clean-up-pass induced stresses were not relieved in time to prevent cracking. Welds exhibiting intermediate tensile strengths indicate only partially stress-relieved structures.

Electron beam welds in all heat treatment/welding conditions of 0.090-inch D6AC and in 0.290-inch D6AC welded in the heat-treated condition and tempered immediately after welding possessed tensile strengths in excess of welds in similar material produced by conventional arc welding techniques.

The effect of post-welding thermal treatment on the ductility of electron beam welds in 0.090-inch D6AC is shown in Figure 148. The ductile-to-brittle transition curves exhibit, as expected, a noticeable improvement in weldment ductility for welds completely heat treated after welding. In

order to obtain a more meaningful comparison of transition temperatures for D6AC steel base metal and weld, the ductile-to-brittle transition temperature has been redefined as the temperature at the midpoint of the ductile-to-brittle transition range with respect to bend angle.

Applying the above definition of transition temperature to Figure 148, weldments in 0.090-inch D6AC steel that were completely heat treated after welding exhibited a transition temperature of 500 F as compared to 470 F for heat-treated base metal. Welds in heat-treated base metal that were tested either as-welded or with an immediate post-welding temper exhibited identical transition temperatures (550 F). The overall ductility of the weldments with a post-welding temper was, however, higher than as-welded ductility.

As was previously discussed, comparison of electron beam weldment ductility with data for arc welds is extremely difficult because of the severity of the 1.6T bend radius for electron beam welds.

Transverse bend ductility data is not reported for 0.290-inch D6AC welds. The high crack-susceptibility of welds in the thicker D6AC tended to mask true weld ductility and rendered bend test data invalid.

The fracture toughness exhibited by electron beam welds in 0.090-inch D6AC steel in all heat treatment/welding combinations was lower than the fracture toughness of heat-treated base metal. This can be explained on the basis of the reduced ductility and highly oriented columnar grain solidification pattern in the fusion zone.

Table 23 summarizes the results of fracture-toughness tests performed upon all three heat treatment/welding combinations. Fracture-toughness tests conducted on 0.090-inch D6AC steel specimens welded in the heat-treated condition (HW), revealed the effect of the extremely hard and brittle martensite present in untempered electron beam welds in this material. All specimens failed either during fatigue cracking, test setup (2000 lb. preload), or at test loads less than 6000 lbs. Fracture surfaces exhibited a granular appearance and indicated cleavage failure. The fracture-toughness data for HW specimens was not reported.

Welds produced in heat-treated base metal and tempered (600 F - 2 hrs.) after welding (HWS), exhibited fracture toughness (G_c*) values ranging from 189.3 to 249.8. The fracture surfaces generally exhibited a granular appearance and occasionally indicated low partial shear failure. High magnification macroscopic examination revealed that the flat zone between occasional shear lips coincided with the central plane of the fusion zone resulting from columnar grain growth.

Welds in annealed D6AC which were heat treated after welding (WH), exhibited the highest fracture-toughness (G_c* values ranging from 288.3 to 726.3). The fracture surfaces exhibited a fibrous appearance. Partial or full shear failure mechanism was indicated by shear lips totalling sixty to one-hundred percent of specimen thickness. High magnification macroscopic examination indicated that in specimens exhibiting partial shear failure, the

flat zone between shear lips coincided with the border between the fusion and the heat-affected zone.

As was discussed under B120VCA Titanium Final-weld Discussion, the range of fracture-toughness properties exhibited by all heat treatment/welding conbinations must be interpreted on the basis of several factors. Slight variations in weld-bead and weld-zone geometry can occur from weld to weld. The presence of a non-uniform hardness level within the weld zone creates a ductility gradient. Since during fracture-toughness testing crack propagation occurs along random paths, variable hardness, ductility, and geometry can influence the crack path.

Examination of the hardness profiles for 0.090-inch D6AC welds (Figures 149 through 151) gives some indication of the hardness variation present within welds in each heat treatment/welding condition. The hardness profile for 0.090-inch D6AC heat treated after welding (Figure 149) is relatively constant, with a uniform hardness existing across the weld zone and surrounding base metal. Therefore, the crack paths can vary over a wider range when compared to those in the HWS specimens. Although crack propagation was initiated in the weld (notch tips located at weld centerline), they could continue either in the weld zone, particularly at the fusion/heat-affected zone interface, or cross into the tougher base metal. In fact, welds in the WH condition exhibiting fracture-toughness values in the high range generally had larger shear lips (indicating shear failure) and eventually failed in the base metal.

Microstructural differences (i.e. the degree of recrystallization of the columnar-grained weld fusion zones induced by post-welding heat treatment) offer another possible explanation for variation in fracture-toughness properties of the WH welds. The heat treatment chosen for use during the subject program included a one-hour hardening treatment at 1600 F. Late in the program it was discovered that this austenitizing treatment did not always produce full recrystallization of the weld zone in the 0.090 inch D6AC steel.

The weld zone microstructures shown in Figures 135 and 143 illustrate differences in degree of fusion zone recrystallization occurring after heat treatment of welds in annealed material.

The results of fracture-toughness tests performed on all three heat treatment/welding conditions of 0.090-inch D6AC steel indicate that maximum fracture toughness is obtained from welds fully heat treated after welding. Welds produced in heat-treated material that were tempered immediately after welding exhibited lower fracture-toughness. The presence of the brittle untempered martensite in welds in heat-treated material tested as-welded, resulted in premature brittle fracture during preliminary phases of testing. For welds fully heat treated after welding, fracture-toughness up to 65% of base metal was obtained.

Data obtained during impact testing of 0.290-inch D6AC welds (Table 24) further bears out the need for an immediate post-welding thermal treatment. The specimen used, an unnotched substandard Izod specimen, was chosen in

order to eliminate the need for locating a notch or key-hole in the narrow electron beam weld zone. Failure did not occur during impact testing of base-metal specimens. Tests performed on welds were valid, however, with failure occurring either completely in the weld zone or partially in the base metal. Welds with an immediate post-weld temper exhibited superior impact properties. No data was obtained for welds completely heat treated after welding because of fracture of weldments during heat treatment.

The results of mechanical property tests performed on both 0.090- and 0.290-inch D6AC indicate the need for an immediate post-welding thermal treatment. For all types of mechanical tests performed (tensile, transverse bend, internal-notch fracture toughness, and impact) superior strength and ductility were exhibited by welds subjected to either an immediate temper or complete heat treatment after welding.

LIST OF REFERENCES

1. Hokanson, H. A., and Kern, W. I., "Electron Beam Welding of Tungsten and Molybdenum", ASD TR61-461, Dec., 1961.

2. Boyle, R. W., Sullivan, A. M., and Krafft, J. M., "Determination of Plane-Strain Fracture Toughness with Sharply Notched Sheets", Welding Journal, Sept., 1962, pp. 428s - 432s.

3. MacPherson, B. M., and Beaver, W. W., "Fusion Welding of Beryllium", WADD TR 60-917, Apr., 1961.

4. Hess, W. T., Lander, H. J., and White, S. S., "Electron Beam Welding of Beryllium", Proceedings, Third Symposium on Electron Beam Technology, Alloyd Electronics Corporation, Boston, 1961.

5. Brody, R. P., and Helfrich, W. E., "Fifth Quarterly Report on Research and Development of Titanium Rocket Motor Case", WAL TR No. 766.2/1-4.

6. Roth, R. E., and Bratkovich, N. F., "Characteristics and Strength Data of Electron Beam Welds in Four Representative Materials", paper presented at AWS National Fall Meeting, Sept., 1961.

TABLE 1

Test Material

Material	Thickness (inches)	Quantity Sq. Ft.	Billet/Heat Number
B120VCA Titanium	0.250	11.25	D - 1684
B120VCA Titanium	0.125	34.5	D - 2617
B120VCA Titanium	0.125	6.1	D - 496
Ladish D6AC Steel	0.300	48	06765
Ladish D6AC Steel	0.100	48	06251
Molybdenum-0.5% Titanium	0.050	3.6	KDTM 702A
Pure Tungsten	0.050	5.4	M-61-1-68
Beryllium	0.040	10.0	Sheet No. 30A
Molybdenum-0.5% Titanium*	0.100	4.9	T-5077-A2
Molybdenum-0.5% Titanium*	0.005	3.5	T-5042-A2-2
Pure Tungsten*	0.100	3.5	U4.5-2974
Pure Tungsten*	0.005	3.0	U4.5-2974

*Material transferred to program from previous program conducted under Air Force Contract AF 33(616)-7439 Task Number 735102

TABLE 2

Metallographic Techniques

Material	Polishing Technique	Etchant	Etching Technique
B120VCA Titanium	Mechanical Polish	a. 3.5% HNO_3 + 1.5% HF + H_2O	Swab Etch
		b. 6% HNO_3 + 1% HF + H_2O	
		c. 3 gms $Pb(NO_3)_2$ + 25% HNO_3 + 1% HF + H_2O	
D6AC Steel	Mechanical Polish	2% Nital	Swab Etch
Mo-0.5% Ti and Tungsten	a. Mechanical Polish	a. Murikami's Etch	Swab Etch
	b. Electropolish 5% H_2SO_4 + 1.25% HF + Methanol	b. Murikami's Etch	Swab Etch
Beryllium	Mechanical Polish	Polarized Light (not etched)	

TABLE 3

Bend Mandrel Radii

Material	Thickness (inches)	Bend Radius (T = sheet thickness)
B120VCA Titanium	0.125	1.25T
D6AC	0.290	1.6 T
D6AC	0.090	1.6 T
Mo-0.5% Ti	0.100	1.5 T
Mo-0.5% Ti	0.050	1.25T
Mo-0.5% Ti	0.005	4.0 T
Tungsten	0.100	1.5 T
Tungsten	0.050	1.25T
Tungsten	0.005	4.0 T
Beryllium	0.040	1.1 T

TABLE 4

Cleaning Procedures

Material	Cleaning Procedure
D6AC	a. Anodic Clean - Water rinse b. 50% Aqueous solution HCl c. Water Rinse
B120VCA	a. 110 F Solution of 1 part HF + 10 parts HNO_3 + 20 parts H_2O b. Water Rinse c. 150 F Solution 30% H_2SO_4 d. Water Rinse
Mo-0.5% Ti	a. 180 F Solution of 10% NaOH + 5% $KMnO_4$ + 85% H_2O - 5-minute immersion, Followed by b. Room temperature-solution of 15% HCl + 15% H_2SO_4 + 10% CrO_3 + 60 % H_2O c. Water Rinse
Tungsten	a. 1-minute immersion in solution of 50% HF + 50% HNO_3 b. Water Rinse
Beryllium	a. 1-minute immersion in solution of 2% HF + 40% HNO_3 + 58% H_2O b. Water Rinse

TABLE 5

Trial Welding - Condition Ranges

Material Thickness (in.)	Accelerating Voltage (KV)	Beam Current (Ma)	Welding Speed (ipm)	Oscillation Amplitude (in.)	Pulsing Conditions	Other
0.125 B120VCA	90 to 150	3 to 15	15 to 100	X: 0 to 0.200 Y: 0 to 0.050	10 to 3000 cps 0.05 to 10 ms	beam diameter up to 0.025 in.
0.090 D6AC	50 to 150	3 to 21	5 to 100	X: 0 to 0.200 Y: 0 to 0.50	10 to 3000 cps 0.05 to 10 ms	beam diameter up to 0.025 in.
0.290 D6AC	100 to 150	5 to 21	3 to 40	X: 0 to 0.200 Y: 0 to 0.50	10 to 300 cps 0.05 to 10 ms	a. beam diameter up to 0.025 in. b. 2-pass technique
0.100 Mo/Tungsten	120 to 150	7 to 20	4 to 100	X: 0 to 0.200 Y: 0 to 0.050		Beam location 0.00 to 0.010 in. on tungsten
0.050 Mo/Tungsten	100 to 150	5 to 20	5 to 100	X: 0 to 0.200 Y: 0 to 0.050		Beam location 0.00 to 0.010 in. on tungsten
0.005 Mo/Tungsten	65 to 150	0.5 to 5	10 to 100	X: 0 to 0.200 Y: 0 to 0.050		a. Beam location 0.00 to 0.005 in on tungsten b. joint overlap up to 0.010 in.
0.040 Beryllium	50 to 120	2 to 15	5 to 100	X: 0 to 0.200 Y: 0 to 0.050	1 to 300 cps 0.05 to 10 ms	beam diameter up to 0.025 in.

NOTE: X - Oscillation along weld seam
Y - Oscillation across weld seam

TABLE 6

Final Butt Welding Settings

Material Thickness (inch)	Condition	Accelerating Voltage (KV)	Beam Current (ma)	Welding Speed (ipm)	Oscillation Amplitude (inch)	Other
0.125 B120VCA	Weld - Age - Test	150	7	22	0.075 X	
0.125 B120VCA	Age - Weld - Test	150	7	22	0.075 X	
0.125 B120VCA	Cold Roll - Age - Weld - Test	150	7	22	0.075 X	
0.290 D6AC	Weld - Heat Treat - Test	150	21	24	0.005 Y	Initial Pass
		110	5	20	0.040 Circular	Clean-up Pass
0.290 D6AC	Heat Treat - Weld - Test	150	21	24	0.005 Y	Initial Pass
		110	5	20	0.040 Circular	Clean-up Pass
0.290 D6AC	Heat Treat - Weld - Stress Relieve - Test	150	21	24	0.005 Y	Initial Pass
		110	5	20	0.040 Circular	Clean-up Pass
0.090 D6AC	Weld - Heat Treat - Test	150	15	58		Defocused Beam (0.015-inch diameter)
0.090 D6AC	Heat Treat - Weld - Test	150	15	58		Defocused Beam (0.015-inch diameter)
0.090 D6AC	Heat Treat - Weld - Stress Relieve - Test	150	15	58		Defocused Beam (0.015-inch diameter)
0.100 Mo-0.5% Ti/Tungsten		145	15	27		Beam Located 0.006 inch on Tungsten
0.050 Mo-0.5% Ti/Tungsten		145	14	45		Beam Located 0.005 inch on Tungsten
0.005 Mo-0.5% Ti/Tungsten		70	3.25	60		0.005-inch Joint overlap
0.040 Beryllium		75	6	15		Defocused Beam (0.020-inch diameter)

TABLE 7

Base-metal Chemical Analyses

B120VCA Titanium

Thickness (inch)	Heat No.	V	Cr	Al	Fe	C	H	O	N
0.250	D-1684	12.65	10.10	2.82	.15	0.04	0.009	0.134	0.034
0.125	D-2617	13.5	10.9	3.2	.15	0.025	0.006	0.123	0.027
0.125	D-496	13.7	10.9	3.1	.16	0.023	0.007	0.127	0.027

D6AC Steel

Thickness (inch)	Heat No.	C	Si	Mn	S	P	Cr	V	Mo	Ni
0.300	06765	0.46	0.26	0.67	0.005	0.006	1.12	0.08	1.05	0.57
0.100	06251	0.45	0.22	0.66	0.006	0.010	1.07	0.08	0.93	0.59

Mo-0.5% Ti

Thickness (inch)	Heat No.	C	Ti	O (ppm)	N (ppm)	H (ppm)
0.100	T-5077-A2	0.026	0.46	9	55	100
0.050	KDTM 702A	0.020	0.44	7	52	81
0.005	7-5042A2-2	0.029	0.44	7	100	50

Tungsten

Thickness (inch)	Heat No.	O (ppm)	N (ppm)	H (ppm)	C
0.100	U4.5-2974	200	70	10	
0.050	M61-1-68	27	2	1	0.004
0.005	U4.5-2974	200	70	10	

Beryllium

Thickness (inch)	Sheet No.	BeO	Fe	Si	Al	Mg	Mn	Ni
0.040	30A	1.30	0.10	0.022	0.035	0.022	0.010	0.010

Note: All Compositions Are Percent Unless Otherwise Noted.

TABLE 8

Room Temperature Base-metal Hardness Properties

Material	Thickness (Inch)	Condition	VHN	Equivalent "R_c"
B120VCA	0.125	Solution Treated	386	32.1
B120VCA	0.125	Solution Treated and Aged	320	39.4
B120VCA	0.125	Solution Treated and Cold Rolled	440	44.5
B120VCA	0.125	Solution Treated, Cold Rolled and Aged	446	44.5
		(Direct Rockwell Measurement)		49.5
D6AC	0.090	Annealed	183	(6.4)
D6AC	0.090	Heat Treated to 2T700	548	52.1
D6AC	0.290	Annealed	220	(15.6)
D6AC	0.290	Heat Treated to 2T700	528	51
Mo-0.5% Ti	0.100	As Received	324	--
Mo-0.5% Ti	0.100	Recrystallized	186	--
Mo-0.5% Ti	0.050	As Received	285	--
Mo-0.5% Ti	0.050	Recrystallized	218	--
Mo-0.5% Ti	0.005	As Received	325	--
Mo-0.5% Ti	0.005	Recrystallized	193	--
Tungsten	0.100	As Received	457	--
Tungsten	0.100	Recrystallized	351	--
Tungsten	0.050	As Received	507	--
Tungsten	0.050	Recrystallized	411	--
Tungsten	0.005	As Received	467	--
Tungsten	0.005	Recrystallized	379	--

TABLE 9

Base-metal Tensile Properties

B120VCA ST	Solution Treated	B120VCA STA	Solution Treated and Aged
B120VCA CR	Cold Rolled	B120VCA CRA	Cold Rolled and Aged
D6AC ANN	Annealed	D6AC 2T700	Heat Treated
Mo-0.5% Ti AR	As-received	Tungsten AR	As-received
Beryllium AR	As-received		

Material	Thickness (Inch)	Test Temp. (F)	Condition	Tensile Strength psi	Yield Strength (0.2% Offset, psi)	% Elongation 2 Inch	% Elongation 1 Inch
B120VCA	0.125	RT	ST	135,000	132,000		23.5
B120VCA	0.125	RT	ST	135,000	130,500		25.5
B120VCA	0.125	RT	ST	135,000	131,500		25.5
B120VCA	0.125	RT	ST	134,500	129,000		27
B120VCA	0.125	RT	ST	133,000	128,000		27
B120VCA	0.125	RT	ST	133,000	131,000		28
B120VCA	0.125	RT	STA	226,000	205,000		5
B120VCA	0.125	RT	STA	206,700	190,700		6
B120VCA	0.125	RT	STA	233,800	207,000		4
B120VCA	0.125	RT	STA	222,500	203,000		5
B120VCA	0.125	RT	CR	193,000	183,500	5	8
B120VCA	0.125	RT	CR	197,000	188,000	5	8
B120VCA	0.125	RT	CR	193,000	188,000	5	8
B120VCA	0.125	RT	CR	195,500	188,500	5	7
B120VCA	0.125	RT	CR	193,200	183,000	4.5	8
B120VCA	0.125	RT	CR	191,500	182,500	5	8
B120VCA	0.125	RT	CR	194,000	189,000	5	8
B120VCA	0.125	RT	CR	190,500	181,000	5	8
B120VCA	0.125	RT	CRA	244,000	237,500		2
B120VCA	0.125	RT	CRA	244,000	241,000		2
B120VCA	0.125	RT	CRA	243,000	240,000		4
B120VCA	0.125	RT	CRA	244,000	242,000		4

TABLE 9

Base-metal Tensile Properties (Continued)

Material	Thickness (Inch)	Test Temp. (F)	Condition	Tensile Strength psi	Yield Strength (0.2% Offset, psi)	% Elongation 2 Inch	% Elongation 1 Inch
D6AC	0.090	RT	ANN	87,800	64,800	26	36
D6AC	0.090	RT	ANN	87,400	59,500	24	36
D6AC	0.090	RT	ANN	88,000	62,300	24	36
D6AC	0.090	RT	ANN	88,000	65,000	24	26
D6AC	0.090	RT	ANN	86,500	56,000	24	28
D6AC	0.090	RT	ANN	88,300	58,200	25	30
D6AC	0.090	RT	ANN	88,100	63,500	23	27
D6AC	0.090	RT	ANN	88,300	61,700	24	25
D6AC	0.090	RT	ANN	88,200	58,200	23	26
D6AC	0.090	RT	ANN	88,500	62,600	25	36
D6AC	0.090	RT	2T700	256,000	230,000	7	10
D6AC	0.090	RT	2T700	254,000	232,000	6	10
D6AC	0.090	RT	2T700	253,000	228,000	6	10
D6AC	0.090	RT	2T700	257,000	229,000	6	10
D6AC	0.090	RT	2T700	252,000	228,000	7	10
D6AC	0.090	RT	2T700	251,000	228,000	7	11
D6AC	0.090	RT	2T700	254,000	229,000	6	10
D6AC	0.090	RT	2T700	249,000	228,000	6	10
D6AC	0.090	RT	2T700	258,000	229,000	7	10
D6AC	0.290	RT	ANN	89,000	57,700	22	25
D6AC	0.290	RT	ANN	90,900	59,300	26	31
D6AC	0.290	RT	ANN	90,700	63,500	24	25
D6AC	0.290	RT	ANN	91,400	56,600	23	28
D6AC	0.290	RT	ANN	89,400	63,100	25	26
D6AC	0.290	RT	ANN	88,600	65,400	27	37
D6AC	0.290	RT	ANN	88,900	63,000	24	36
D6AC	0.290	RT	ANN	89,000	62,700	23	28
D6AC	0.290	RT	2T700	249,000	230,000	7	10
D6AC	0.290	RT	2T700	257,000	225,000	7	10
D6AC	0.290	RT	2T700	257,000	227,000	6	10

TABLE 9

Base-metal Tensile Properties (Continued)

Material	Thickness (Inch)	Test Temp. (F)	Condition	Tensile Strength psi	Yield Strength (0.2% Offset, psi)	% Elongation 2 Inch	% Elongation 1 Inch
D6AC	0.290	RT	2T700	252,000	230,000	7	10
D6AC	0.290	RT	2T700	254,000	227,000	6	11
D6AC	0.290	RT	2T700	255,000	226,000	7	10
D6AC	0.290	RT	2T700	248,000	225,000	7	11
D6AC	0.290	RT	2T700	253,000	228,000	7	10
Mo-0.5% Ti	0.050	RT	AR	130,000	112,000		10.2*
Mo-0.5% Ti	0.050	RT	AR	131,500	111,200		9.7*
Mo-0.5% Ti	0.050	RT	AR	127,600	109,200		11.3*
Mo-0.5% Ti	0.050	1600	AR	91,200	84,200		3.8*
Mo-0.5% Ti	0.050	1600	AR	92,500	81,300		3.8*
Mo-0.5% Ti	0.050	1600	AR	94,600	80,500		3.8*
Mo-0.5% Ti	0.050	1900	AR	70,900	60,600		8.6*
Mo-0.5% Ti	0.050	1900	AR	68,700	64,100		8.6*
Mo-0.5% Ti	0.050	1900	AR	68,500	50,400		6.5*
Mo-0.5% Ti	0.050	2200	AR	28,600	27,700		30.6*
Mo-0.5% Ti	0.050	2200	AR	26,900	23,900		34.9*
Mo-0.5% Ti	0.050	2200	AR	30,300	26,900		30.1*
Tungsten	0.050	RT	AR	Failed in Gripping Pins			
Tungsten	0.050	RT	AR	Failed in Gripping Pins			
Tungsten	0.050	2200	AR	57,200	50,400	5	
Tungsten	0.050	2200	AR	59,400	49,500	5	
Tungsten	0.050	2200	AR	54,600	47,900	5	
Tungsten	0.050	2500	AR	25,600	25,000	20	
Tungsten	0.050	2500	AR	34,200	29,700	15	
Tungsten	0.050	2500	AR	31,200	29,000	23	
Tungsten	0.050	2800	AR	13,450	7,900	26	
Tungsten	0.050	2800	AR	13,100	9,400	24	

TABLE 9

Base-metal Tensile Properties (Continued)

Material	Thickness (Inch)	Test Temp. (F)	Condition	Tensile Strength psi	Yield Strength (0.2% Offset, psi)	% Elongation 2 Inch	% Elongation 1 Inch
Beryllium	0.040	80	AR	70,100	42,500	18	
Beryllium	0.040	80	AR	70,200	41,700	20	
Beryllium	0.040	80	AR	68,100	42,600	14	
Beryllium	0.040	1000	AR	25,600	24,400	16	
Beryllium	0.040	1000	AR	25,600	25,000	20	
Beryllium	0.040	1000	AR	24,700	24,500	17	

* Percent elongation in 1.86 inch.

TABLE 10

Base-metal Ductile-to-brittle Transition Temperatures

Material	Thickness (inch)	Condition	Ductile-to-brittle Transition Temperature
B120VCA	0.125	Solution Treated	< RT
B120VCA	0.125	Solution Treated and Aged	750 F
B120VCA	0.125	Cold Rolled and Aged	*
D6AC	0.090	Annealed	< RT
D6AC	0.090	Heat Treated	470 F
Mo-0.5% Ti	0.100	As Received	< RT
Mo-0.5% Ti	0.050	As Received	< RT
Mo-0.5% Ti	0.005	As Received	< RT
Tungsten	0.100	As Received	820 F
Tungsten	0.050	As Received	300 F
Tungsten	0.005	As Received	< RT
Beryllium	0.040	As Received	400 F

* 30 Degree Bend Angle Not Achieved At Testing Temperatures up to 800 F (Aging Temperature)

TABLE 11

Base Metal And Weldment Mechanical Property Data For Mo-0.5% Ti And Tungsten Welded During Air Force Contract AF 33(616)-7439 Task No. 735102

Tensile Properties

Material	Thickness (inch)	Test Temp. of	Condition	Tensile Strength (psi)	Yield Strength (0.2% offset, psi)	Elong. (%)
Mo-0.5% Ti	0.050	RT	Base Metal	92,630	76,000	2.5
Mo-0.5% Ti	0.050	1600	Base Metal	65,000	59,370	8
Mo-0.5% Ti	0.050	1900	Base Metal	55,930	48,260	10
Mo-0.5% Ti	0.050	2200	Base Metal	36,390	32,300	19
Mo-0.5% Ti	0.050	RT	Weldment	80,600	79,400	
Mo-0.5% Ti	0.050	1600	Weldment	54,830	49,700	7
Mo-0.5% Ti	0.050	1900	Weldment	40,050	39,100	6.3
Mo-0.5% Ti	0.050	2200	Weldment	35,810	31,400	6
Tungsten	0.050	RT	Base Metal	82,700		
Tungsten	0.050	1900	Base Metal	58,580	53,700	8
Tungsten	0.050	2500	Base Metal	39,750	37,600	19
Tungsten	0.050	2800	Base Metal	11,5200	7,300	55
Tungsten	0.050	RT	Weldment			
Tungsten	0.050	1900	Weldment	31,390	28,700	4
Tungsten	0.050	2500	Weldment	28,310	24,810	4
Tungsten	0.050	2800	Weldment	12,050	8,090	51

Bend Properties

Material	Thickness (inch)	Condition	Ductile-to-brittle Transition Temp.	Bend Radius
Mo-0.5% Ti	0.050	Base Metal	170 F	1.25 T
Mo-0.5% Ti	0.050	Weldment	350 F	1.25 T
Tungsten	0.050	Base Metal	600 F	1.25 T
Tungsten	0.050	Weldment	1025 F	1.25 T

TABLE 12

Base-metal Fracture Toughness Test Results

Material	Thickness (Inch)	Condition	a (inch)	σx (psi)	G_c* $\frac{\text{in.-lb.}}{\text{in}^2}$	K_c* (ksi $\sqrt{\text{in}}$)	K_{Nc}(c) (ksi $\sqrt{\text{in}}$)	% Shear Lip
B120VCA	0.125	ST	0.92	214,000(a)	2,137	177	79.8	100
B120VCA	0.125	ST	0.79	188,700(a)	1,768	161	(d)	100
B120VCA	0.125	ST	0.84	213,100(a)	2,023	172	88.0	100
B120VCA	0.125	STA	0.54	50,000	121.5	41.0		15
B120VCA	0.125	STA	0.52	37,500	72.1	33.5		15
B120VCA	0.125	STA	0.54	42,600	93.4	39.1		0
B120VCA	0.125	STCRA	0.55	22,300	28.1	20.8		0
B120VCA	0.125	STCRA	0.54	23,800	33.5	22.8		5
B120VCA	0.125	STCRA	0.58	25,800	38.3	24.3		10
D6AC	0.090	ANN	1.40(b)	738,900	2,198	258	54.9	100
D6AC	0.090	ANN	1.34(b)	461,800	1,381	269	56.0	100
D6AC	0.290	ANN	1.40(b)	∞	93,420	1690	48.4	100
D6AC	0.290	ANN	1.40(b)	∞	90,000	1660	62.1	100
D6AC	0.090	HT	1.01(b)	297,300	1,496	214	67.5	100
D6AC	0.090	HT	0.94	235,100	1,135	186		100
D6AC	0.090	HT	0.87	230,800	1,113	184		100

TABLE 12

Base-metal Fracture Toughness Test Results (Continued)

Material	Thickness (Inch)	Condition		a (inch)	σx (psi)	G_c* $\frac{\text{in.-lb.}}{\text{in}^2}$	K_c*	K_{Nc}(c) $\frac{}{(\text{ksi}\sqrt{\text{in}})}$	% Shear Lip
D6AC	0.290	HT		0.80	97,100	212	80.5		20
D6AC	0.290	HT		0.77	88,700	181	74.3		20
D6AC	0.290	HT	(b)(e)	1.00	128,400	282	92.8	42.0	20

(a)- $\frac{\sigma x}{\sigma ys}$ is greater than 1; 1st indication that test is not valid.

(b)- 2a is greater than about 0.6W; 1st indication that test is not valid.

(c)- K_{Nc} computed only for nonvalid tests.

(d)- Chart not suitable for K_{Nc} determination.

(e)- Large 1/2 crack length, a, is probably a result of the abnormally high a_o value due to an extra-large fatigue crack.

TABLE 13

0.290-Inch D6AC Steel Base-metal Impact Test Results

Material	Condition	Impact Strength (Ft-lbs)	Hardness (R_c)
D6AC	Annealed	91 NF*	38.5 **
D6AC	Annealed	93 NF	37.5
D6AC	Annealed	95 NF	37.5
D6AC	Heat Treated	120 NF	51.5
D6AC	Heat Treated	120 NF	51.5
D6AC	Heat Treated	120 NF	51.5

Specimen Type: Unnotched Substandard Izod

* NF - Specimen Not Failed During Test

** Material annealed after heat treatment to 2T700 condition

TABLE 14

Electron Beam Weld Tensile Properties

0.040-Inch Beryllium

Test Temperature (F)	Ultimate Strength (psi)	Yield Strength (psi)	Elongation (% in 1 inch)
80	43,400	None	0
80	44,400	None	0
80	47,200	43,900	0.5
500	42,800	34,100	18.5
500	42,600	33,300	9.5
500	42,000	34,000	9.5
1000	25,600	23,400	3.5
1000	24,700	23,800	3.5
1000	24,700	23,400	3.5

TABLE 15

Electron Beam Weld Ductile-to-brittle Transition Temperature

0.040-Inch Beryllium

Condition	Ductile-to-brittle Transition Temperature	Bend Radius
Electron Beam Welded	1040 F	1.1 T
Base Metal	400 F	1.1 T

TABLE 16

Electron Beam Weld Tensile Properties
0.050-Inch Mo-0.5% Ti Welded to Tungsten

Material	Thickness (Inch)	Test Temp. (F)	Tensile Strength (psi)	Yield Strength (0.2% Offset, psi)	% Elongation In 2 Inches	Failure Location
Mo-0.5% Ti/tungsten	0.050	RT	49,600	None	0.9	Tungsten HAZ
Mo-0.5% Ti/tungsten	0.050	RT	50,400	None	0.9	Tungsten HAZ
Mo-0.5% Ti/tungsten	0.050	1600	65,600	61,100	2	Tungsten HAZ
Mo-0.5% Ti/tungsten	0.050	1600	57,800	54,600	1.5	Tungsten HAZ
Mo-0.5% Ti/tungsten	0.050	1600	54,000	51,000	1.5	Tungsten HAZ
Mo-0.5% Ti/tungsten	0.050	1900	47,700	45,600	2	Tungsten HAZ
Mo-0.5% Ti/tungsten	0.050	1900	55,700	53,100	1.5	Tungsten HAZ
Mo-0.5% Ti/tungsten	0.050	1900	53,100	48,600	1.5	Tungsten HAZ
Mo-0.5% Ti/tungsten	0.050	2200	30,320	29,340	15.6	Mo-0.5% Ti BM
Mo-0.5% Ti/tungsten	0.050	2200	30,200	28,400	10.3	Tungsten HAZ
Mo-0.5% Ti/tungsten	0.050	2200	29,400	28,200	16.9	Mo-0.5% Ti BM

TABLE 17

Electron Beam Weld Ductile-to-brittle Transition Temperatures
0.050-Inch Mo-0.5% Ti Welded to Tungsten

Material	Thickness (Inch)	Ductile-to-brittle Transition Temperature (F)	Comparative Weldment Transition Temperature*		Comparative Base-metal Transition Temperature (F)	
			Mo-0.5% Ti	Tungsten	Mo-0.5% Ti	Tungsten
Mo-0.5% Ti/tungsten	0.100	750	530	>900	<RT	820
Mo-0.5% Ti/tungsten	0.050	800	350	1025	<RT	300
Mo-0.5% Ti/tungsten	0.005	140	RT	435	<RT	<RT

*Reference 1.

TABLE 18

Electron Beam Weld Tensile Properties B120VCA Titanium

* WA - Welded in the Solution-treated Condition and Aged Subsequent to Welding
** AW - Welded in the 72 Hour at 900 F Aged Condition
*** CAW - Welded in the 50% Cold Rolled and 12 Hour at 800 F Aged Condition
‡ HAZ - Heat-affected Zone

Material	Thickness (inch)	Condition	Tensile Strength (psi)	Yield Strength (0.2% offset psi)	% Elongation 2"	1"	1/4"	Failure Location
B120VCA	0.125	WA*	177,500	None		2	8	HAZ‡
B120VCA	0.125	WA	167,200	None		2	6	HAZ
B120VCA	0.125	WA	171,500	None		2	8	HAZ
B120VCA	0.125	WA	176,000	None		1	4	HAZ
B120VCA	0.125	WA	157,000	None		3	8	HAZ
B120VCA	0.125	WA	168,000	None		3	4	HAZ
B120VCA	0.125	WA	155,500	None		1	4	HAZ
B120VCA	0.125	WA	151,000	None		1	4	HAZ
B120VCA	0.125	WA	176,000	None		1	4	HAZ
B120VCA	0.125	AW**	149,500	149,500	2	4		HAZ
B120VCA	0.125	AW	151,500	150,000	2	4		HAZ
B120VCA	0.125	AW	145,500	145,500	2	3		HAZ
B120VCA	0.125	AW	149,500	149,500	2	3		HAZ
B120VCA	0.125	AW	153,300	153,300	2	4		HAZ
B120VCA	0.125	AW	147,500	147,500	2	4		HAZ
B120VCA	0.125	AW	154,000	153,900	2	4		HAZ
B120VCA	0.125	AW	152,100	152,100	1.5	3		HAZ
B120VCA	0.125	AW	151,400	151,400	1.5	3		HAZ
B120VCA	0.125	AW	151,500	150,500	2	4		HAZ
B120VCA	0.125	AW	153,500	152,500	2	4		HAZ
B120VCA	0.125	AW	152,000	152,000	3	6		HAZ
B120VCA	0.125	AW	153,500	152,900	3	6		HAZ
B120VCA	0.125	AW	152,300	152,300	2	4		HAZ
B120VCA	0.125	AW	154,000	154,000	1.5	3		HAZ
B120VCA	0.125	AW	148,000	148,000	1.5	3		HAZ
B120VCA	0.125	AW	157,900	155,100		3	8	HAZ

TABLE 18

Electron Beam Weld Tensile Properties B120VCA Titanium (Continued)

Material	Thickness (inch)	Condition	Tensile Strength (psi)	Yield Strength (0.2% offset psi)	% Elongation 2"	1"	1/4"	Failure Location
B120VCA	0.125	AW	154,900	152,200		4	12	HAZ
B120VCA	0.125	AW	153,600	151,100		4	16	HAZ
B120VCA	0.125	AW	147,500	146,000		5	20	HAZ
B120VCA	0.125	CAW***	151,000	146,100		6	18	HAZ
B120VCA	0.125	CAW	145,800	142,000		6	18	HAZ
B120VCA	0.125	CAW	145,600	143,200		6	18	HAZ
B120VCA	0.125	CAW	153,200	150,300		4	12	HAZ
B120VCA	0.125	CAW	135,800	135,800		4	12	HAZ
B120VCA	0.125	CAW	143,800	141,500		5	18	HAZ
B120VCA	0.125	CAW	158,000	152,000		5	18	HAZ
B120VCA	0.125	CAW	147,400	147,400		4	12	HAZ
B120VCA	0.125	CAW	159,000	156,000		4	16	HAZ
B120VCA	0.125	CAW	153,200	151,800		4	12	HAZ
B120VCA	0.125	CAW	142,000	142,000		4	12	HAZ
B120VCA	0.125	CAW	142,500	141,000		6	20	HAZ
B120VCA	0.125	CAW	150,000	148,700		4	8	HAZ
B120VCA	0.125	CAW	152,000	150,000		3	8	HAZ
B120VCA	0.125	CAW	152,100	150,800		3	10	HAZ
B120VCA	0.125	CAW	150,200	149,000		4	10	HAZ
B120VCA	0.125	CAW	154,200	151,100		4	16	HAZ
B120VCA	0.125	CAW	156,000	152,000		4	8	HAZ
B120VCA	0.125	CAW	155,500	152,200		3	12	HAZ
B120VCA	0.125	CAW	158,200	156,800		3	8	HAZ
B120VCA	0.125	CAW	137,900	137,000		3	12	HAZ
B120VCA	0.125	CAW	148,500	147,500		4	16	HAZ
B120VCA	0.125	CAW	152,000	150,000		4	16	HAZ
B120VCA	0.125	CAW	152,500	152,500		4	12	HAZ
B120VCA	0.125	CAW	147,800	147,800		4	16	HAZ
B120VCA	0.125	CAW	153,200	151,800		4	8	HAZ
B120VCA	0.125	CAW	151,900	148,500		5	20	HAZ

TABLE 19

Electron Beam Weld Ductile-to-brittle Transition Temperature

0.125-inch B120VCA Titanium

Material	Condition	Ductile-to-brittle Transition Temperature	Bend Radius
B120VCA	Welded-Aged 72 hrs. at 900F	* (Maximum Bend Angle 19 degrees)	1.25T
B120VCA	Aged 72 hrs. at 900 F - Welded	* (Maximum Bend Angle 16 degrees)	1.25T
B120VCA	Cold Rolled and Aged 12 hrs. at 800F - Welded	* (Maximum Bend Angle 20 degrees)	1.25T
B120VCA	Solution Treated - Base Metal	< RT	1.25T
B120VCA	Aged 72 hrs. at 900F - Base Metal	750 F	1.25T
B120VCA	Cold Rolled and Aged 12 hrs. at 800F - Base Metal	* (Maximum Bend Angle 17 degrees)	1.25T

Note

* 30-degree bend angle not achieved at temperatures up to prior aging temperature.

TABLE 20

Electron Beam Weld Fracture Toughness Test Results

0.125-inch B120VCA Titanium

Material	Thickness (Inch)	Condition	a(inch)	σx (psi)	G_c* $\frac{\text{in.} - \text{lb.}}{\text{in}^2}$	K_c* (ksi $\sqrt{\text{in}}$)	% Shear Lip
B120VCA	0.125	STAW	0.61	114,500	560.4	93.2	(a)
B120VCA	0.125	STAW	0.55	83,200	300.7	68.3	-
B120VCA	0.125	STAW	0.90	246,100	1657.	160.3	-
B120VCA	0.125	STAW	0.84	229,900	1762.	165.2	-
B120VCA	0.125	STAW	0.67	117,400	565.0	93.6	-
B120VCA	0.125	STWA	0.68	50,400	103.8	40.1	-
B120VCA	0.125	STWA	0.69	54,100	118.7	42.9	-
B120VCA	0.125	STWA	0.63	48,100	97.7	38.9	-
B120VCA	0 125	STAW	0.76	174,600	1358.	145.1	-
B120VCA	0.125	STCRAW	0.565	82,700	296.3	67.8	-
B120VCA	0.125	STCRAW	0.64	121,200	618.1	97.9	-
B120VCA	0.125	STCRAW	0.76	102,800	496.4	87.7	-
B120VCA	0.125	STCRAW	0.60	104,500	544.0	91.8	-
B120VCA	0.125	STWA	0.645	49,500	123.1	43.7	-
B120VCA	0.125	STCRAW	0.72	105,700	257.6	63.2	-

(a) Percent shear not reported for most welded specimens because of (interpretation) (measurement) difficulties.

TABLE 21

Electron Beam Weld Tensile Properties

0.290- And 0.090-Inch D6AC Steel

* WH - Welded in the Solution-treated Condition and Heat Treated Subsequent to Welding
** HW - Welded in the Heat-treated Condition
*** HWS - Welded in the Heat-treated Condition and Stress-relieved 1 hr. at 600F Immediately After Welding
*
* BM - Base Metal
*
*
* HAZ - Heat-affected Zone
[a] FZ - Fusion Zone

Material	Thickness (inch)	Condition	Tensile Strength (psi)	Yield Strength (0.2% offset psi)	% Elongation 2"	1"	1/4"	Failure Location
D6AC	0.090	WH*	232,000	218,000		5		BM * *
D6AC	0.090	WH	247,000	232,000		2	12	HAZ *
D6AC	0.090	WH	237,000	227,000		2	12	HAZ *
D6AC	0.090	WH	241,000	218,200		6		BM
D6AC	0.090	WH	240,000	225,000		5		BM
D6AC	0.090	WH	244,000	222,000		5		BM
D6AC	0.090	WH	238,000	220,000				BM
D6AC	0.090	WH	239,000	222,000		2	8	HAZ
D6AC	0.090	WH	228,000	226,500		2	8	HAZ
D6AC	0.090	WH	238,500	221,000		6		BM
D6AC	0.090	WH	241,000	221,500	2	4	12	FZ[a]
D6AC	0.090	WH	231,500	222,000	1	2	8	FZ
D6AC	0.090	WH	240,000	224,500	1	2	8	FZ
D6AC	0.090	WH	94,000	None	0.5	1	4	FZ
D6AC	0.090	HW 1**	241,000	227,000	2	3	8	HAZ
D6AC	0.090	HW 1	236,000	220,500	3	4	8	HAZ
D6AC	0.090	HW 1	244,000	232,000	2	4	8	HAZ

TABLE 21 (Continued)

Electron Beam Weld Tensile Properties

0.290- And 0.090-Inch D6AC Steel

Material	Thickness (inch)	Condition	Tensile Strength (psi)	Yield Strength (0.2% offset psi)	% Elongation 2"	1"	1/4"	Failure Location
D6AC	0.090	HW 2	172,000	None	1	2	4	HAZ
D6AC	0.090	HW 2	224,000	None	1	2	8	HAZ
D6AC	0.090	HW 2	221,000	217,500	1	2	8	HAZ
D6AC	0.090	HW 2	249,000	240,000	5	10		Base Metal
D6AC	0.090	HW 3	228,000	222,000	1	2	6	HAZ
D6AC	0.090	HW 3	244,000	240,000	4	8		Base Metal
D6AC	0.090	HW 3	243,000	239,000	4	8		Base Metal
D6AC	0.090	HW 4	145,500	None	0	0	0	HAZ
D6AC	0.090	HW 4	175,500	None	0	0	0	HAZ
D6AC	0.090	HW 4	118,200	None	0	0	0	HAZ
D6AC	0.090	HW 4	143,000	None	0	0	0	HAZ
D6AC	0.090	HW 4	172,100	None	0	0	0	HAZ
D6AC	0.090	HW 4 ***	172,000	None	0	0	0	HAZ
D6AC	0.090	HWS 2	236,500	223,000	4	6	20	HAZ
D6AC	0.090	HWS 2	235,000	224,000	3	6	24	HAZ
D6AC	0.090	HWS 2	238,500	229,500	3	6	20	HAZ
D6AC	0.090	HWS 2	239,000	226,000	3	6	20	HAZ
D6AC	0.090	HWS 2	236,000	226,000	3	6	20	HAZ
D6AC	0.090	HWS 2	241,000	224,500	3	6	18	HAZ
D6AC	0.090	HWS 1	228,000	218,500	2	4	16	HAZ
D6AC	0.090	HWS 1	232,000	223,500	3	6	16	HAZ
D6AC	0.090	HWS 1	233,000	228,500	2.5	3	12	HAZ
D6AC	0.090	HWS 1	231,000	222,000	2.5	3	12	HAZ
D6AC	0.090	HWS 1	227,500	222,000	1	2	8	HAZ
D6AC	0.090	HWS 1	225,500	221,000	2	3	12	HAZ

TABLE 21 (Continued)

Electron Beam Weld Tensile Properties

0.290- And 0.090-Inch D6AC Steel

Material	Thickness (inch)	Condition	Tensile Strength (psi)	Yield Strength (0.2% Offset psi)	% Elongation 2"	1"	1/4"	Failure Location
D6AC	0.290	HWS 25-1	254,000	232,000	5	8	16	FZ
D6AC	0.290	HWS 25-3	251,000	233,000	3	4	8	FZ
D6AC	0.290	HWS 25-4	255,000	236,000	5	8	16	FZ
D6AC	0.290	HWS 27-1	240,000	230,000	2	4	8	FZ
D6AC	0.290	HWS 27-3	223,000	None	1	2	8	FZ
D6AC	0.290	HWS 27-4	250,000	231,000	6	10	10	FZ
D6AC	0.290	HWS 28-1	248,000	Not Measured	3	6	8	FZ
D6AC	0.290	HWS 28-2	248,500	232,000	3	5	12	FZ
D6AC	0.290	HWS 28-3	250,000	235,000	3	6	8	FZ
D6AC	0.290	HWS 28-4	249,000	236,000	5	8	18	FZ
D6AC	0.290	HWS 30-2	241,000	228,000	2	4	8	FZ
D6AC	0.290	HWS 30-3	229,000	None	1	2	8	FZ
D6AC	0.290	HWS 30-4	241,000	225,000	3	6	8	FZ
D6AC	0.290	HWS 35-1	239,000	Not Measured	1.5	2	8	FZ
D6AC	0.290	HWS 35-2	237,000	232,500	1	2	4	FZ
D6AC	0.290	HWS 35-4	247,000	233,000	4	8	18	FZ
D6AC	0.290	HWS 36-1	241,000	Not Measured	1.5	2	8	FZ
D6AC	0.290	HWS 36-2	242,000	235,000	1.5	3	8	FZ
D6AC	0.290	HWS 36-3	249,000	235,000	3	6	17	FZ
D6AC	0.290	HWS 36-4	225,000	None	1	2	8	FZ
D6AC	0.290	HWS 29-1	25,900	None	0	0	0	FZ
D6AC	0.290	HWS 30-1	180,500	None	0.5	1	4	FZ

TABLE 22

Electron Beam Weld Ductile-to-brittle Transition Temperatures

0.090-inch D6AC Steel

Material	Condition	Ductile-to-brittle Transition Temperature	Bend Radius
D6AC	Welded - Heat Treated	500 F	1.6T
D6AC	Heat Treated - Welded	550 F	1.6T
D6AC	Heat Treated - Welded - Stress Relieved	550 F	1.6T
D6AC	Annealed - Base Metal	< RT	1.6T
D6AC	Heat Treated - Base Metal	470 F	1.6T

TABLE 23

Electron Beam Weld Fracture Toughness Test Results

0.090-inch D6AC Steel

Material	Thickness (Inch)	Condition	a(inch)	σx (psi)	G_c* $\frac{\text{in. - lb.}}{\text{in}^2}$	K_c* (ksi $\sqrt{\text{in}}$)	% Shear Lip
D6AC	0.090	HWS	0.73	90,000	189.3	76.0	-
D6AC	0.090	HWS	0.795	103,400	237.7	85.1	-
D6AC	0.090	HWS	0.79	102,600	235.0	84.7	-
D6AC	0.090	HWS	0.75	102,400	202.2	78.5	-
D6AC	0.090	HWS	0.71	111,100	249.8	87.3	-
D6AC	0.090	WH	0.93	194,200	720.6	148.3	90
D6AC	0.090	WH	0.705	107,300	288.3	93.8	60
D6AC	0.090	WH	0.88	158,700	533.5	127.6	100
D6AC	0.090	WH	0.70	115,200	315.9	98.2	60
D6AC	0.090	WH	0.76	177,600	726.3	148.8	100
D6AC	0.090	WH	0.81	156,200	573.6	132.3	100

TABLE 24

Electron Beam Weld Impact Test Results

0.290-inch D6AC Steel

Condition	Impact Strength Ft-Lbs	Location of Failure	Hardness (Rc)
HW*	2.0	Weld	50.5
HW*	1.5	Weld	51
HW*	1.5	30% in Base Metal	51
HW*	3.0	30% in Base Metal	51
HW*	1.0	Weld	51
HW**	10.0	95% in Base Metal	50
HW**	0	Weld	50
HW**	0	30% in Base Metal	49.5
HW**	0	Weld	50.5
HW**	0	Weld	50
HWS*	3.0	20% in Base Metal	50.5
HWS*	5.0	30% in Base Metal	50.5
HWS*	4.0	10% in Base Metal	50.5
HWS*	4.0	10% in Base Metal	50.5
HWS*	2.5	30% in Base Metal	50.5
HWS**	39.0	50% in Base Metal	50.5
HWS**	40.0	60% in Base Metal	50.5
HWS**	15.0	30% in Base Metal	50.5
HWS**	44.0	40% in Base Metal	50.5
HWS**	41.0	40% in Base Metal	50.5

* Specimen tested with face of weld in tension

** Specimen tested with root of weld in tension

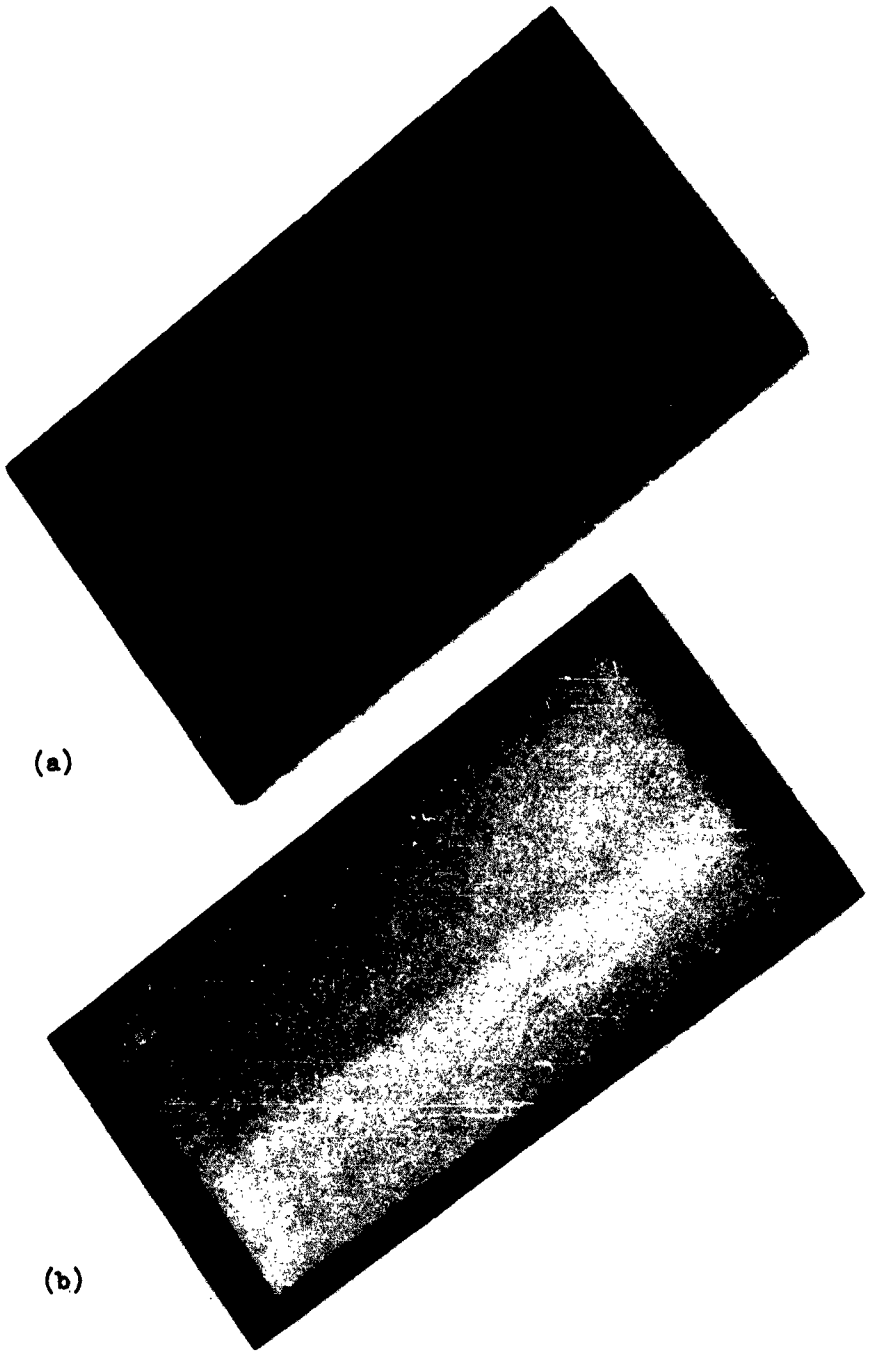

Figure 1. 0.290-Inch D6AC Base Metal
a. As received
b. After grinding

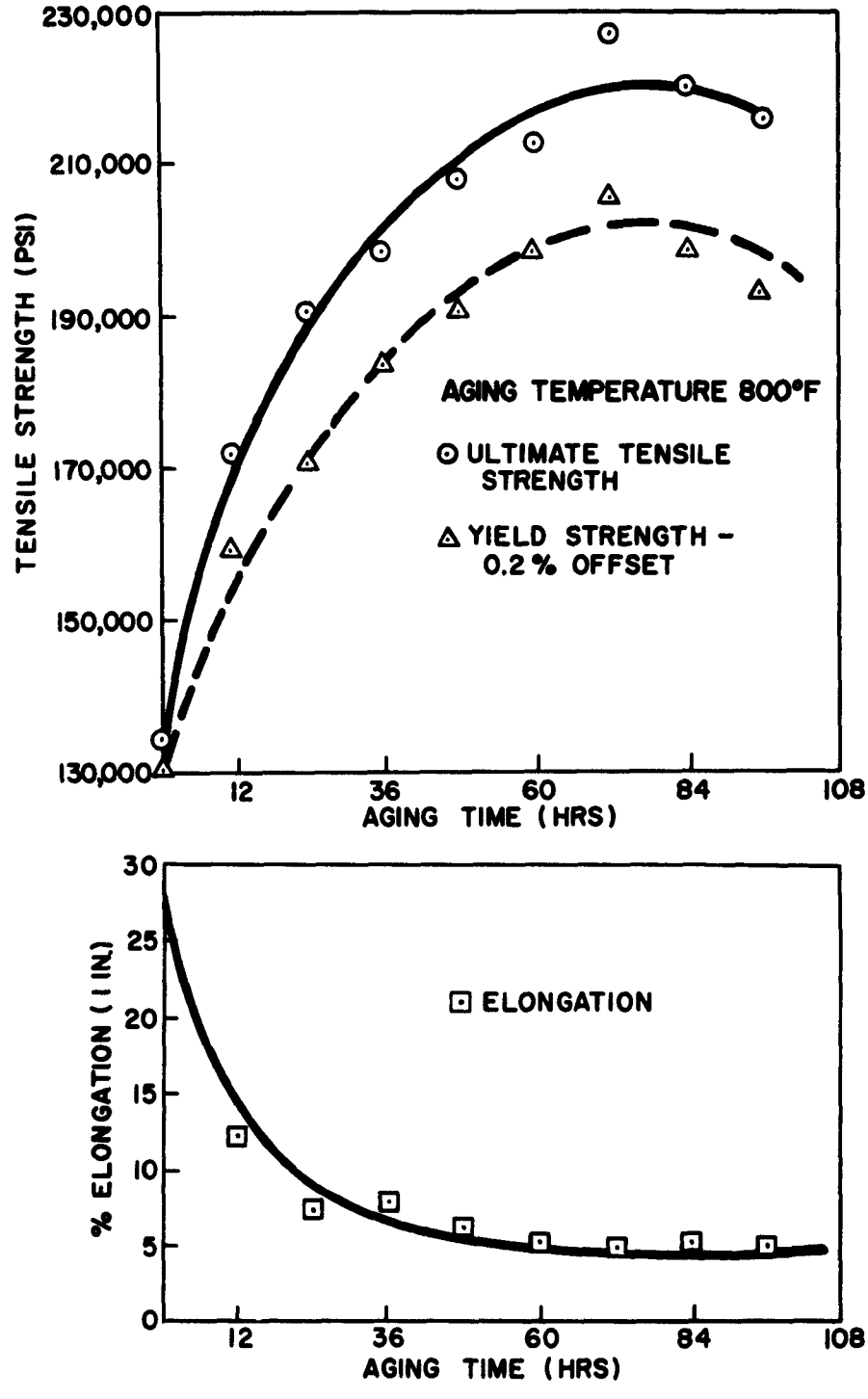

Figure 2. Aging Characteristics of Solution Treated 0.125-Inch B120VCA Titanium Plate

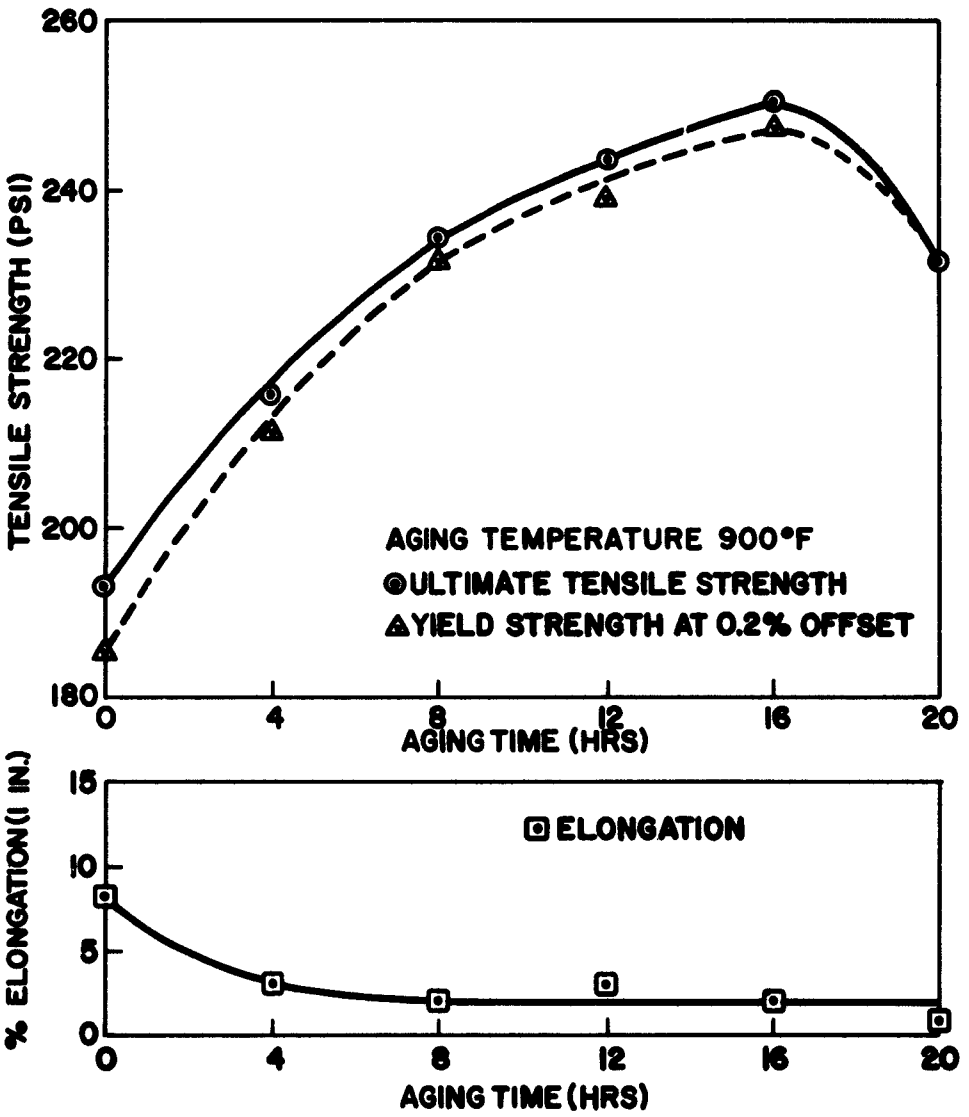

Figure 3. Aging Characteristics of Solution Treated and 50% Cold Rolled 0.125-Inch B120VCA Titanium Plate

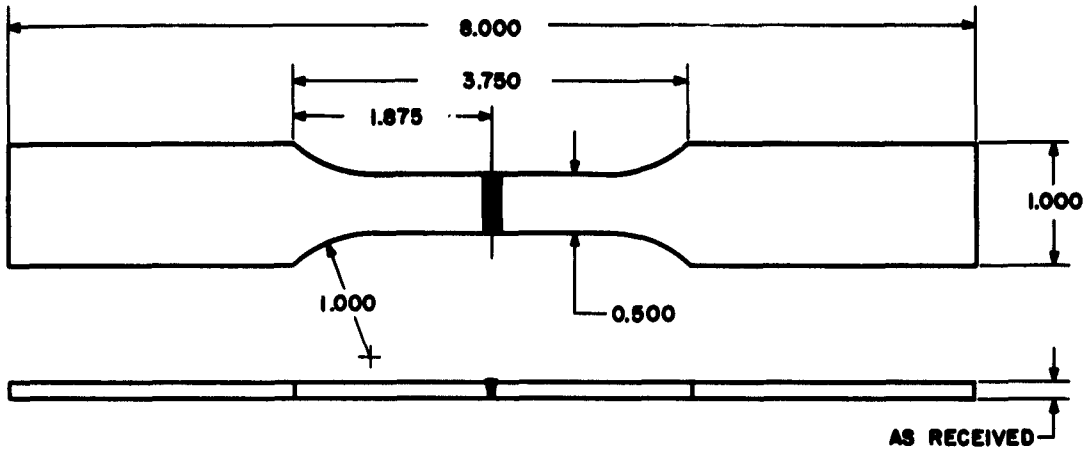

Figure 4. Room-Temperature Tensile Specimen Drawing (D6AC Steel and B120VCA Titanium)

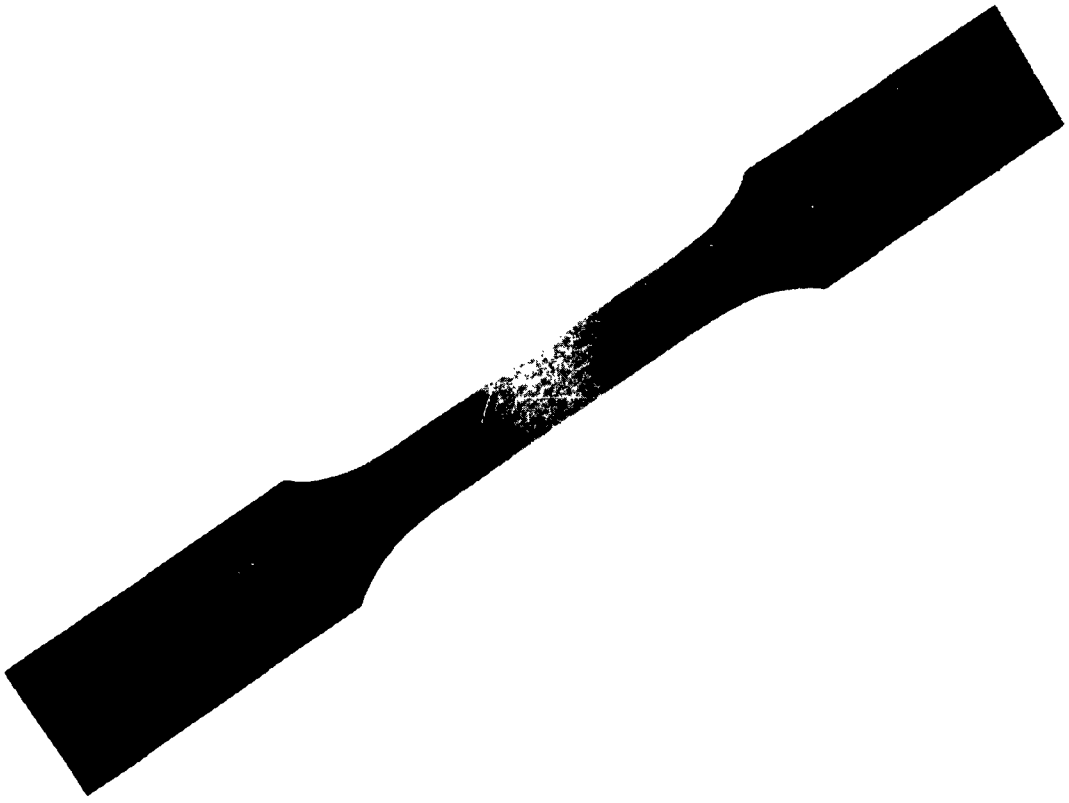

E8624-8

Figure 5. Room-Temperature Tensile Specimen (D6AC Steel and B120VCA Titanium)

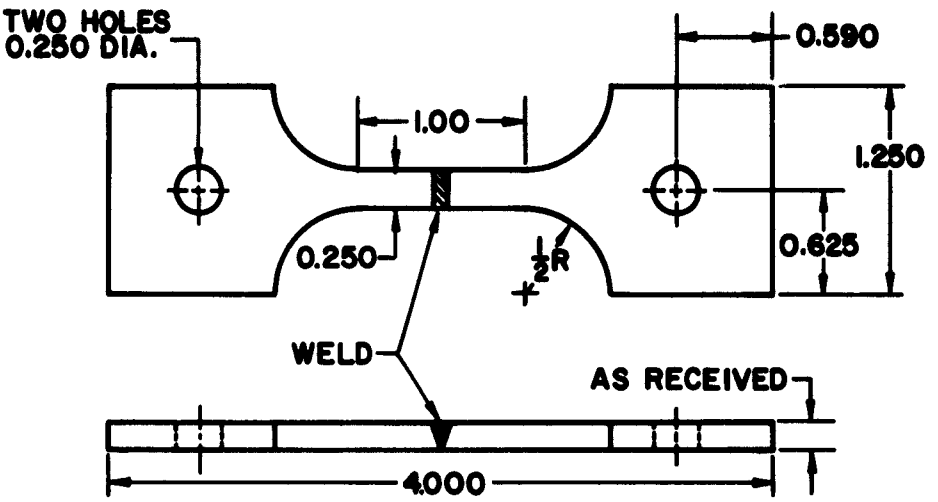

NOTE: ALL DIMENSIONS IN INCHES

Figure 6. Room and Elevated-temperature Tensile Specimen Drawing (Mo-0.5% Ti, Tungsten, and Beryllium)

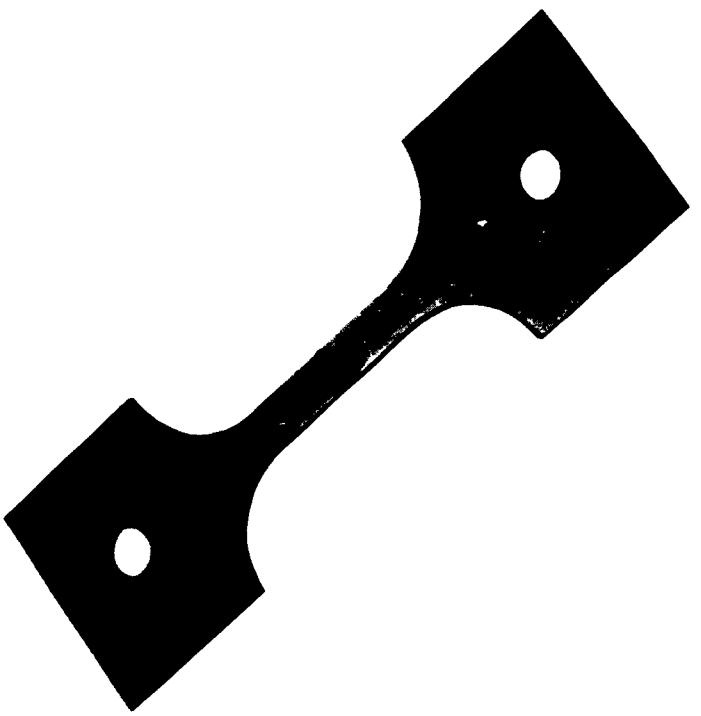

K 8625-8 Figure 7. Room and Elevated-temperature Tensile Specimen (Mo-0.5% Ti, Tungsten, and Beryllium)

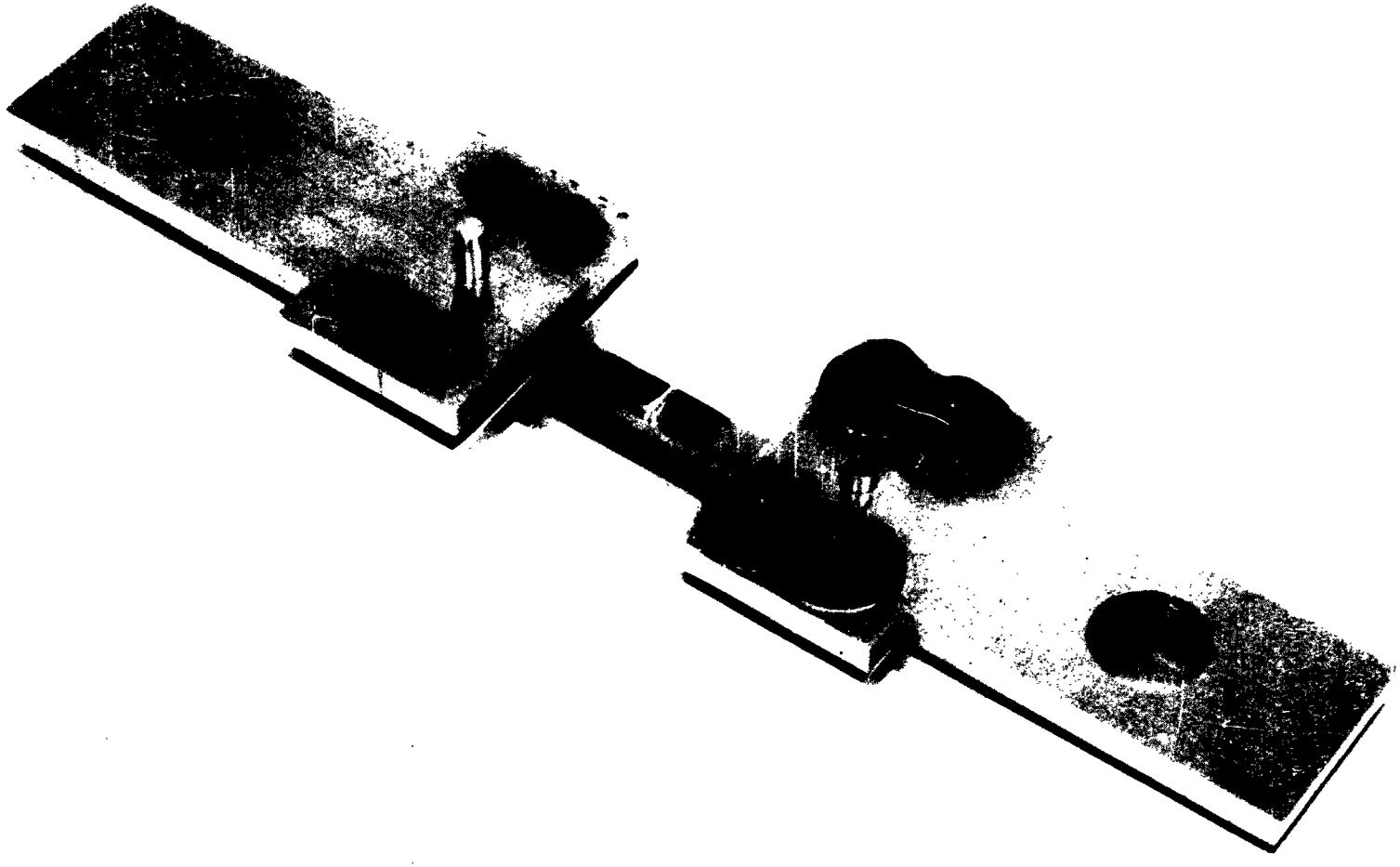

S-32470

Figure 8. Room-temperature Tensile Testing Fixture

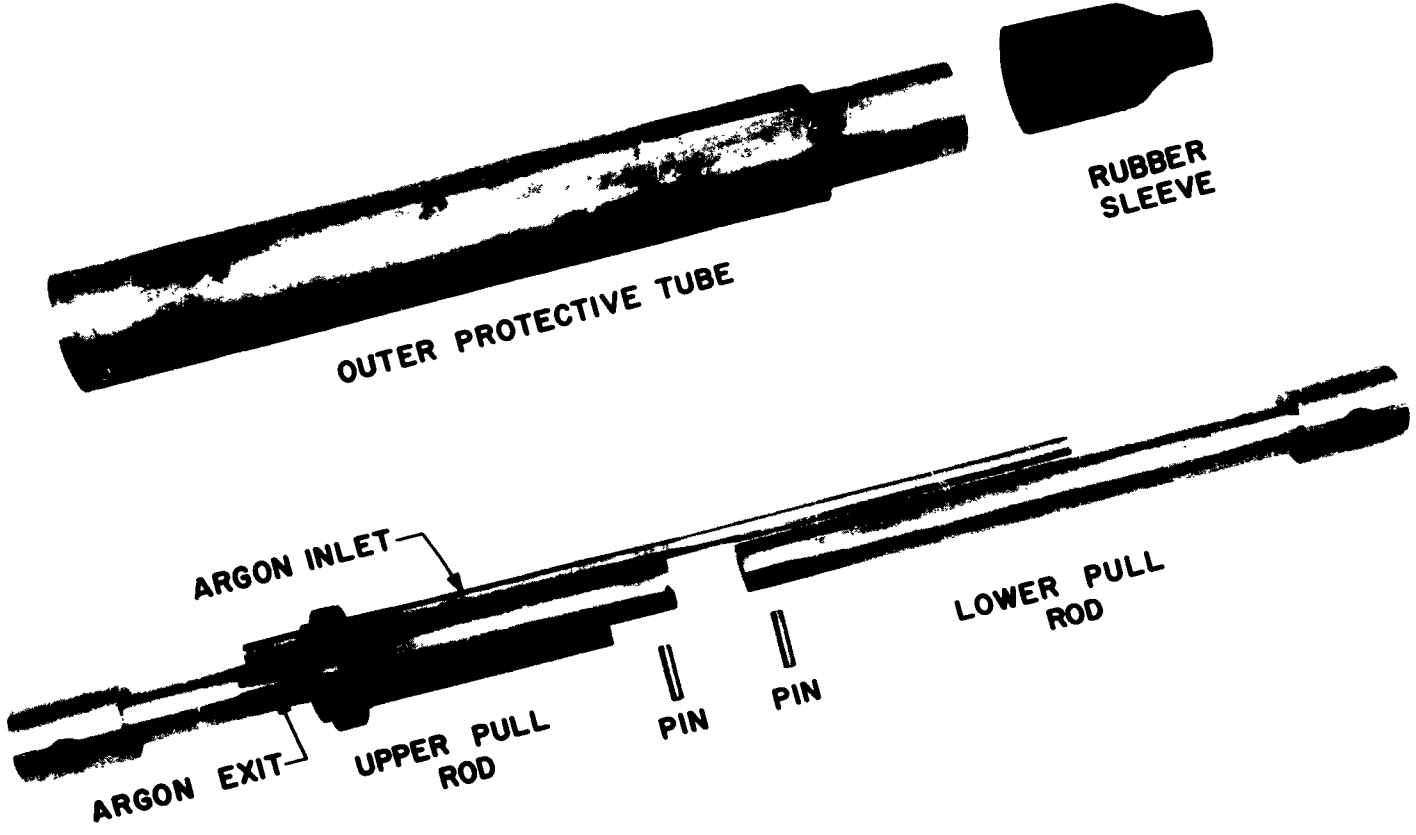

EB765—4

Figure 9. Beryllium Tensile Testing Encapsulation Assembly

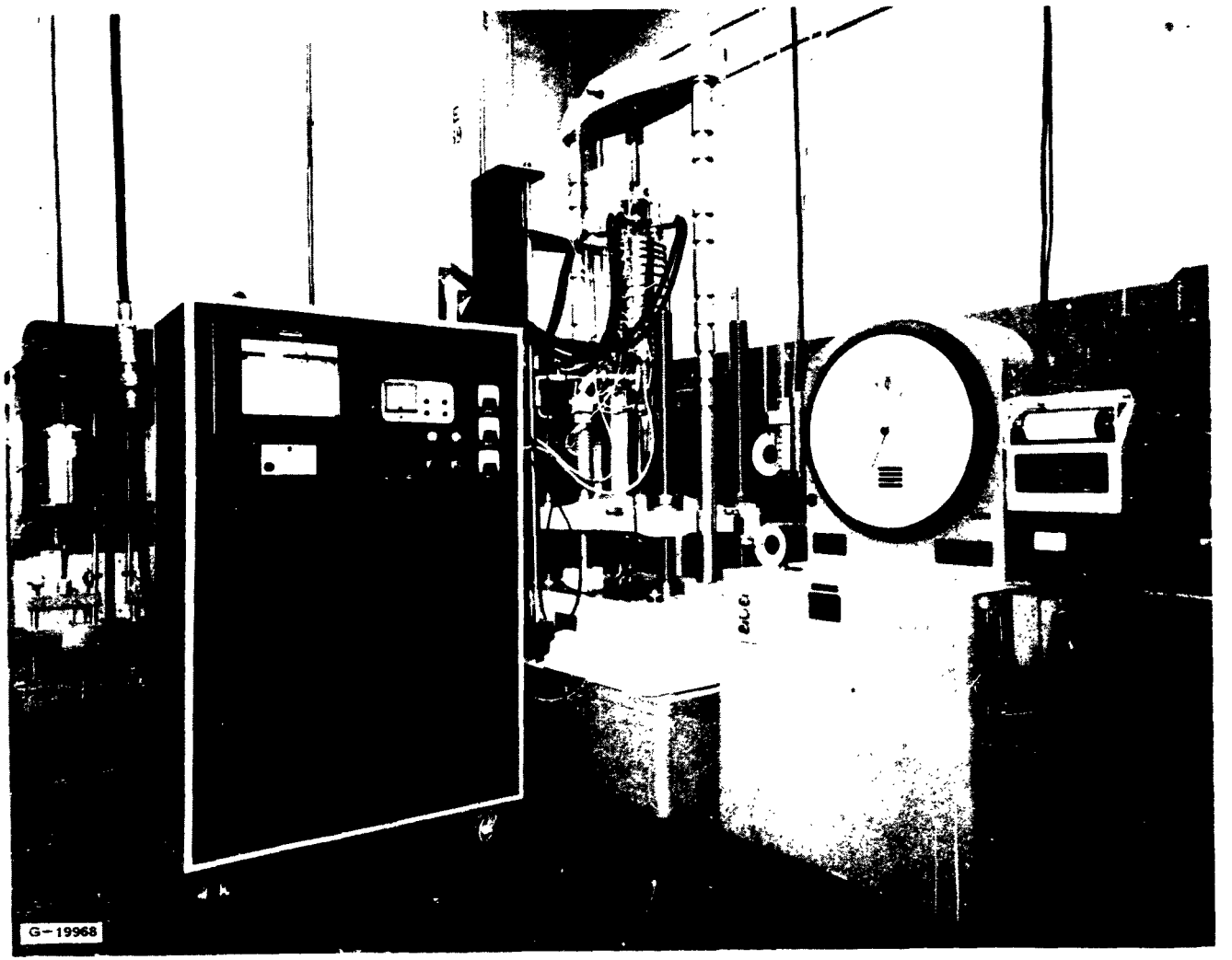

Figure 10. Elevated-temperature Tensile Testing Setup

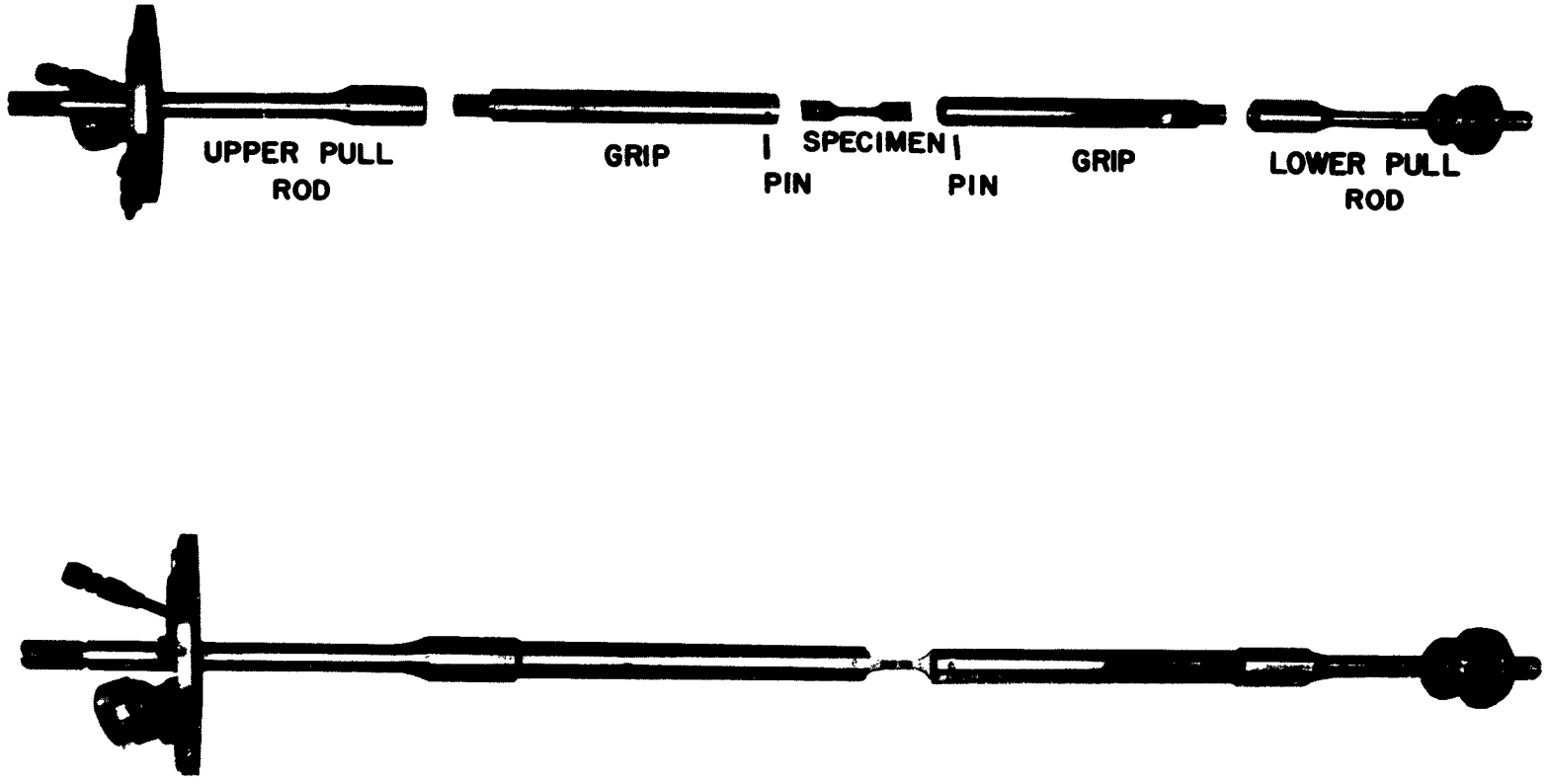

S-32463 Figure 11. Elevated-temperature Tensile Pull-rod and Grip Assembly; Exploded and Assembled

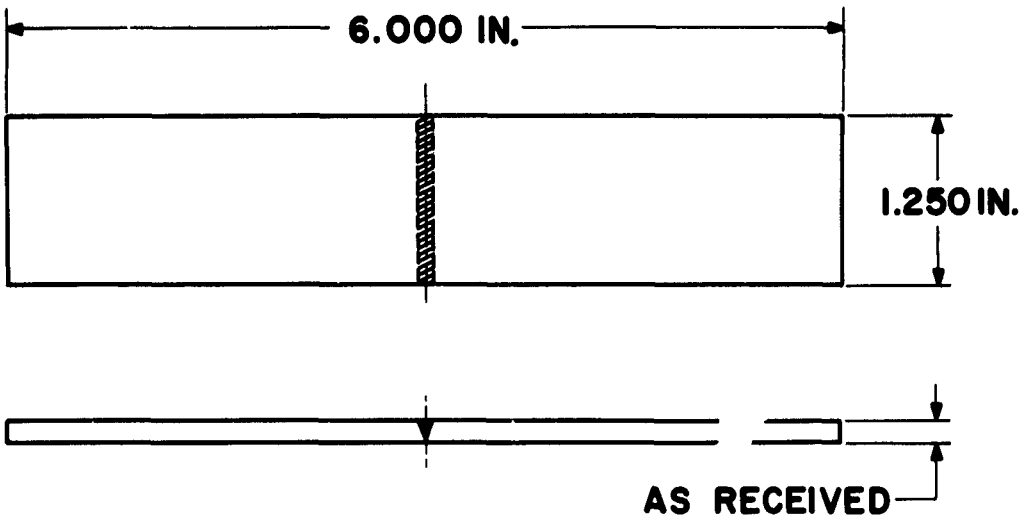

Figure 12. Bend Specimen Drawing
(D6AC Steel and B120VCA Titanium)

K 8826-8

Figure 13. Bend Specimen
(D6AC Steel and B120VCA Titanium)

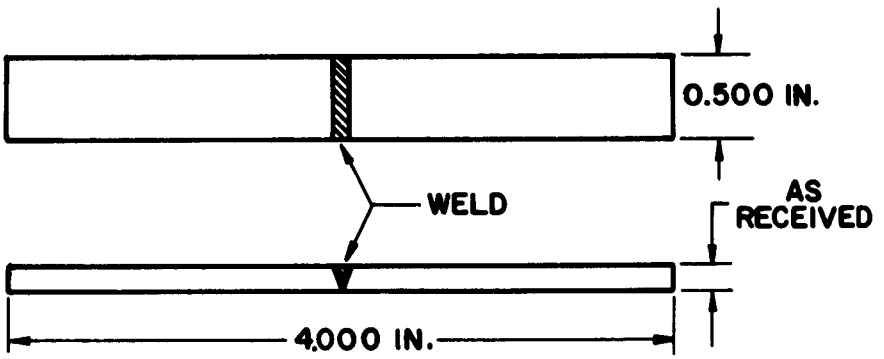

Figure 14. Bend Specimen Drawing
(Mo-0.5% Ti, Tungsten, and Beryllium)

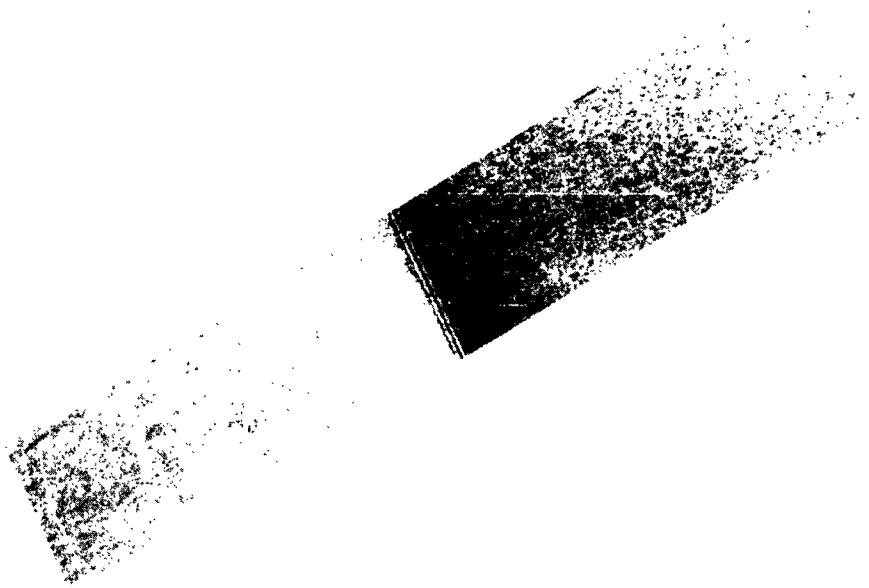

EB827-8

Figure 15. Bend Specimen
(Mo-0.5% Ti, Tungsten, and Beryllium)

EB769-4

Figure 16. Elevated-temperature Bend-test Setup

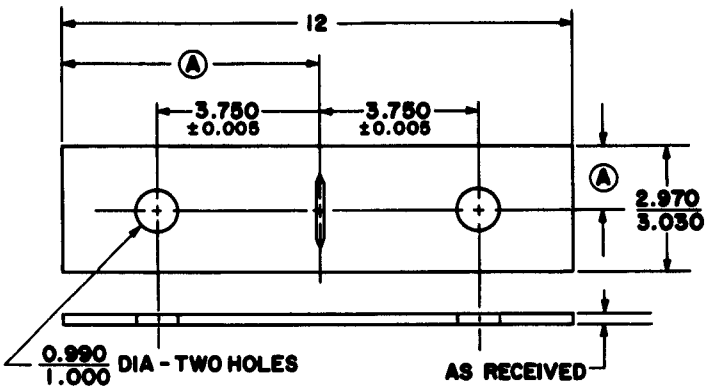

Figure 17. Internal-notch Tensile Specimen Drawing (D6AC Steel and B120VCA Titanium)

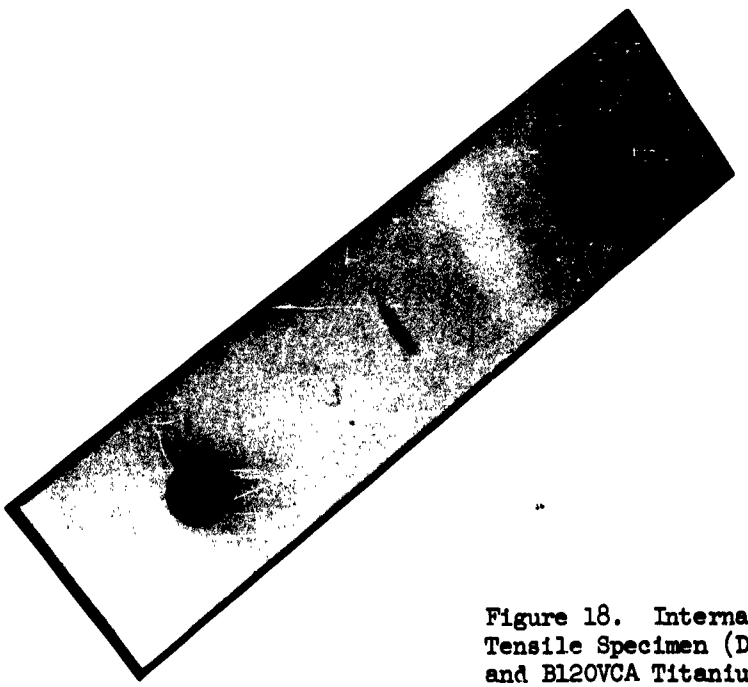

EB827-8

Figure 18. Internal-notch Tensile Specimen (D6AC Steel and B120VCA Titanium)

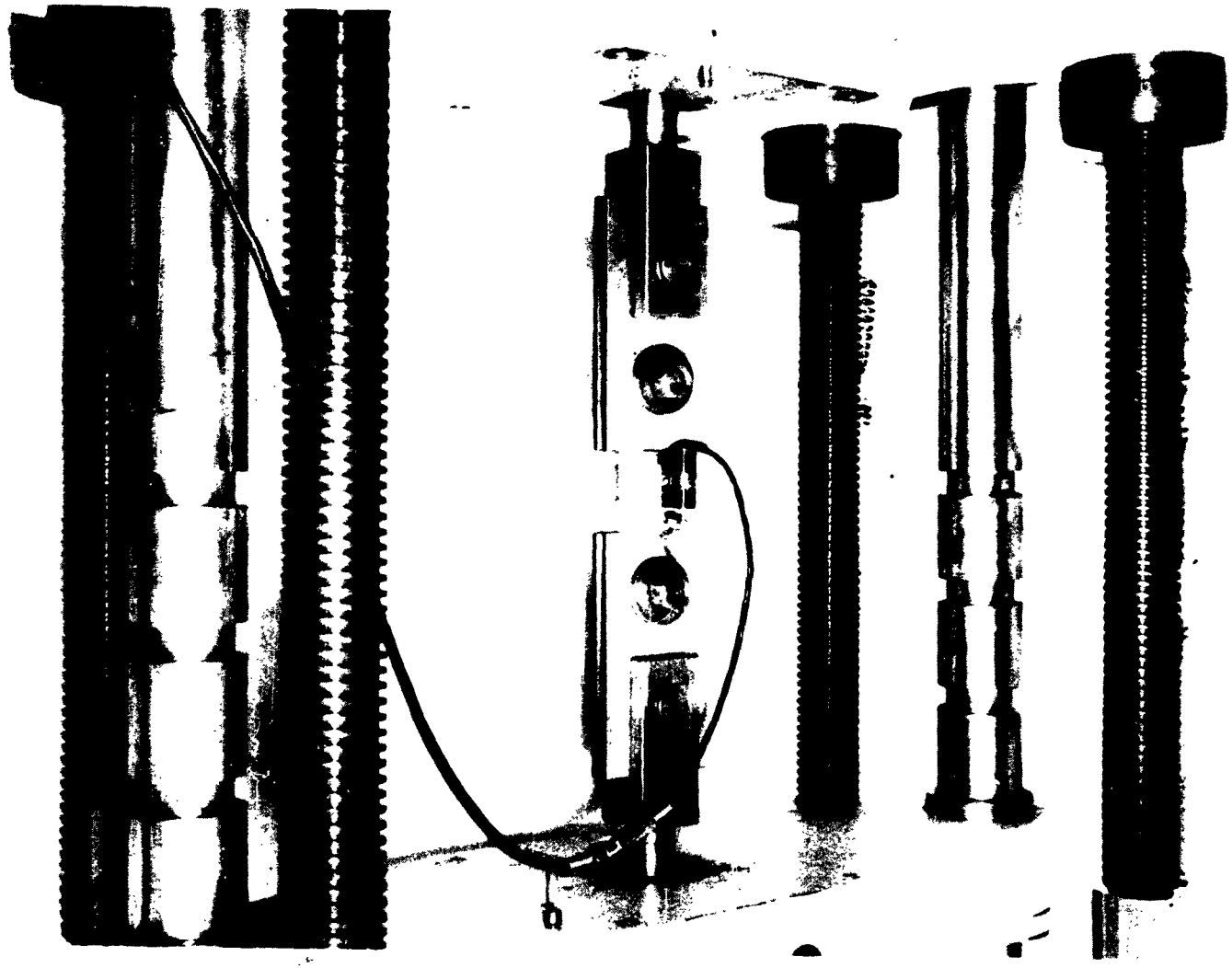

EB767-4

Figure 19. Internal-notch Tensile Testing Setup

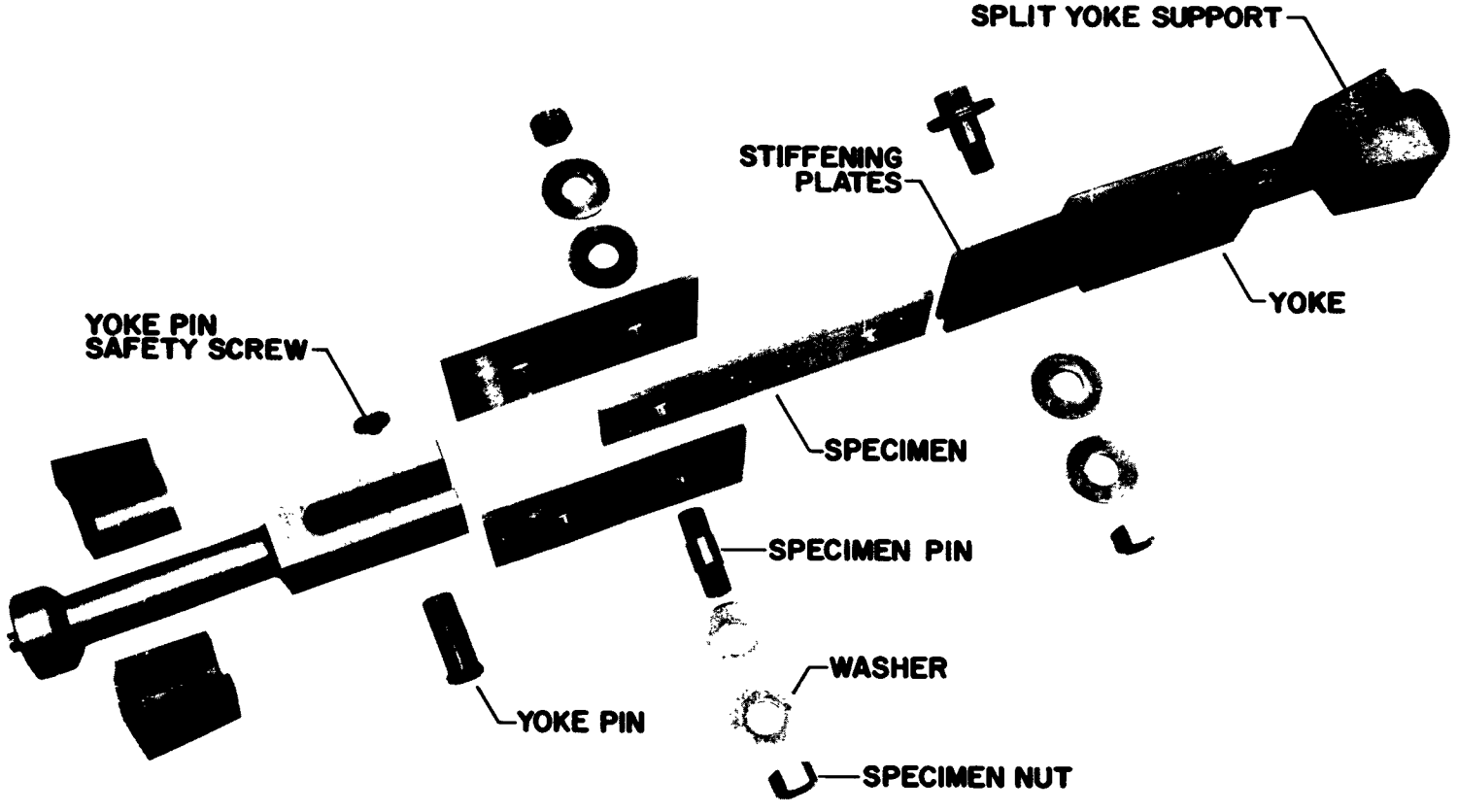

EB766-4

Figure 20. Internal-notch Tensile Clamping Fixtures

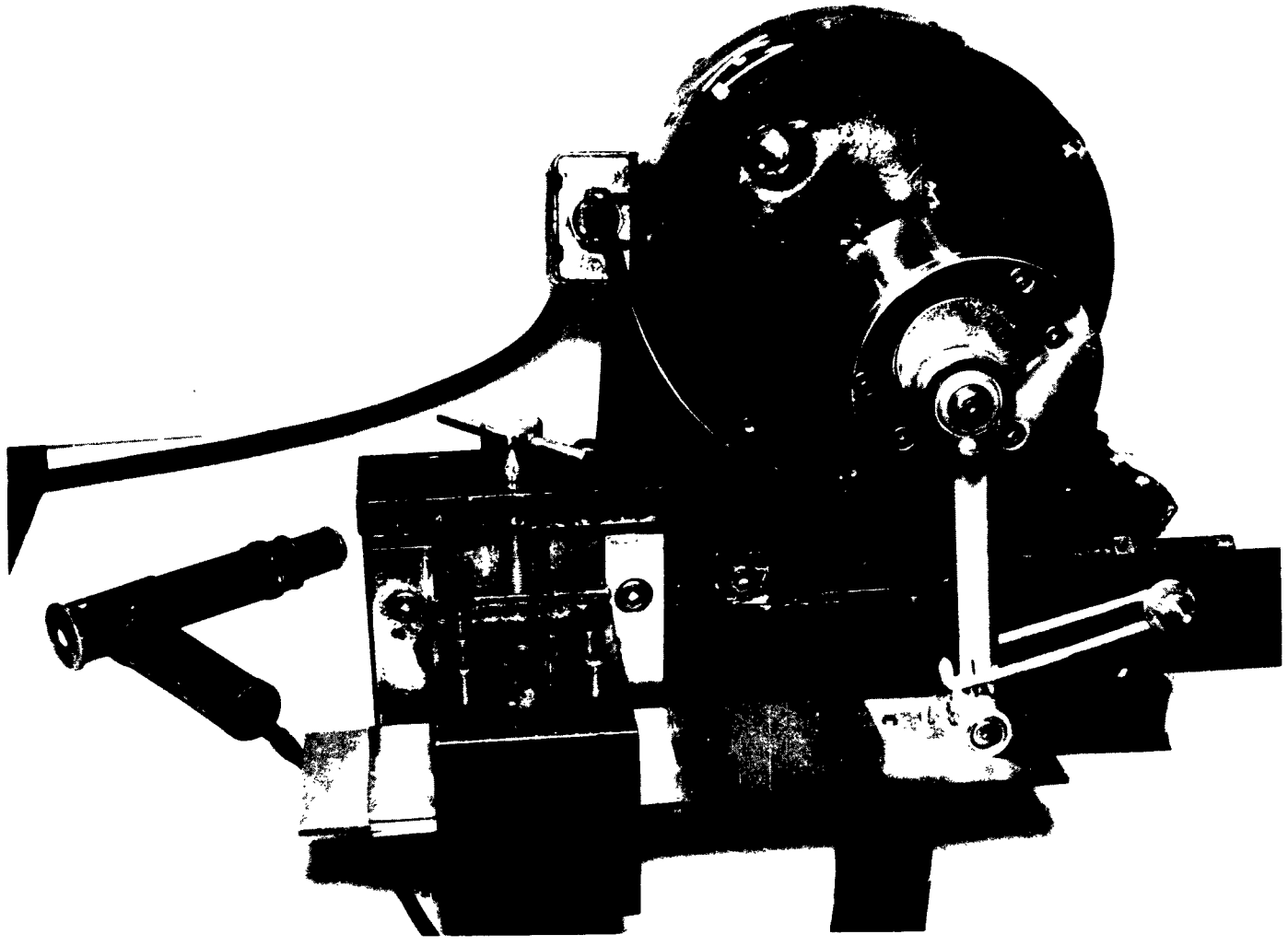

EB768-4

Figure 21. Krouse Plate Cyclic Bending Machine

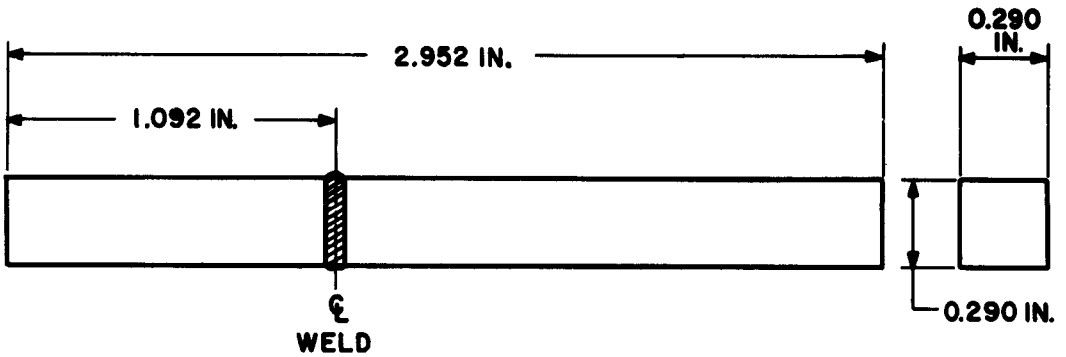

Figure 22. Impact Specimen Drawing (D6AC)

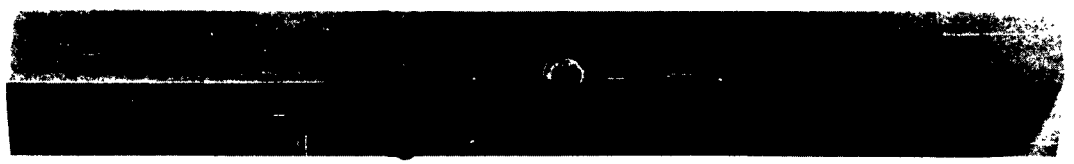

E8829-8

Figure 23. Impact Specimen (D6AC)

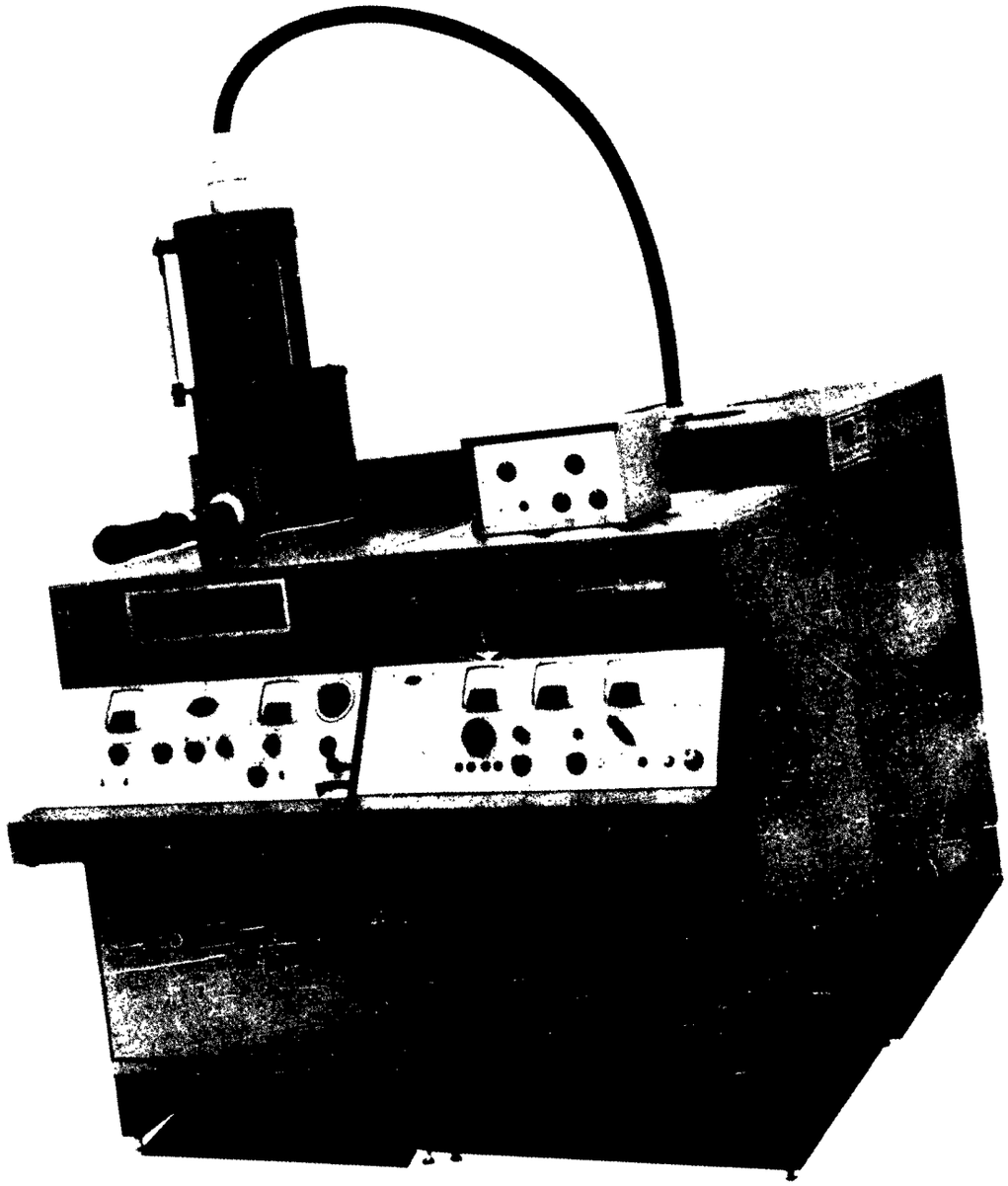

EB633-8 Figure 24. Hamilton-Zeiss Electron Beam Welding Machine

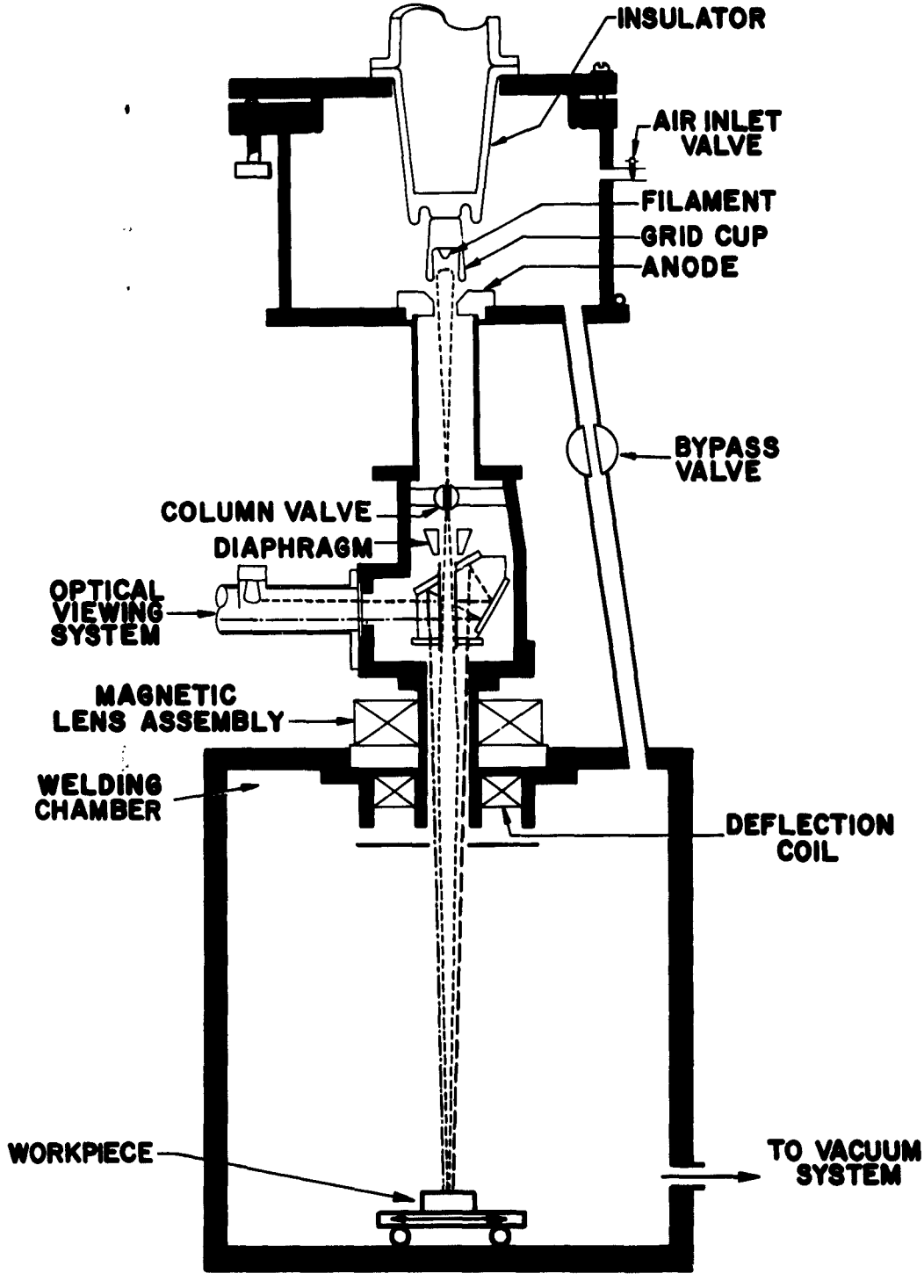

Figure 25. Electron Beam Welding Machine Schematic

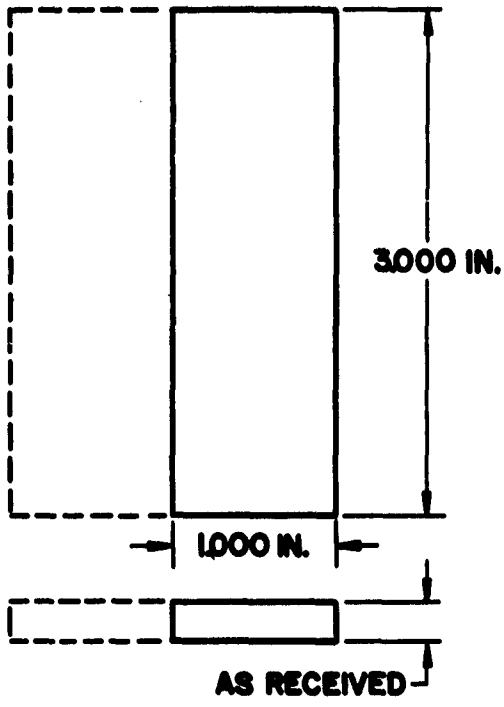

Figure 26. Trial Weld Specimen Drawing
(D6AC Steel and B120VCA Titanium)

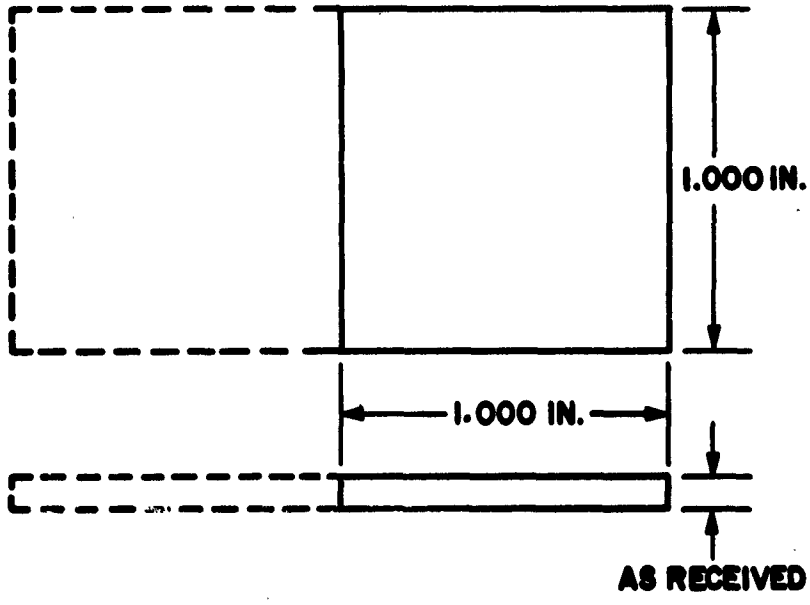

Figure 27. Trial Weld Specimen Drawing
(Mo-0.5% Ti/tungsten, beryllium)

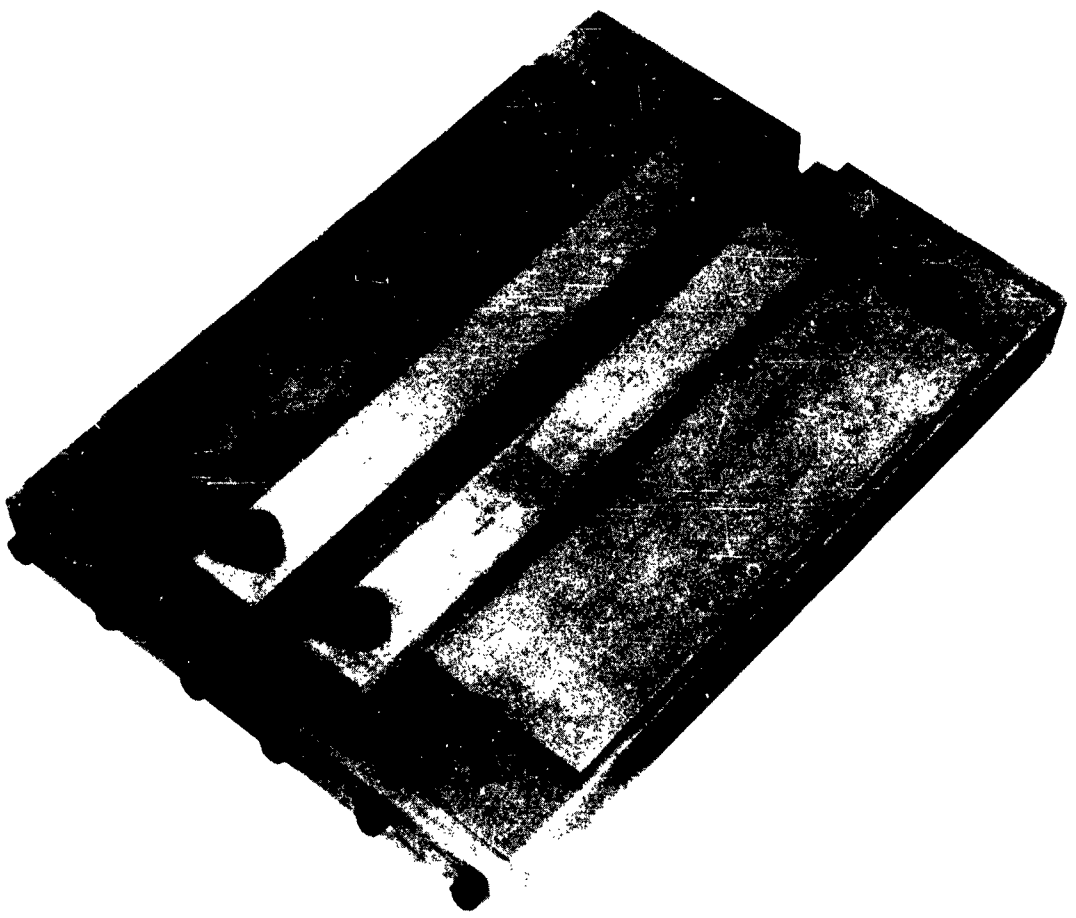

KMS30-8

Figure 28. Typical Welding Fixture

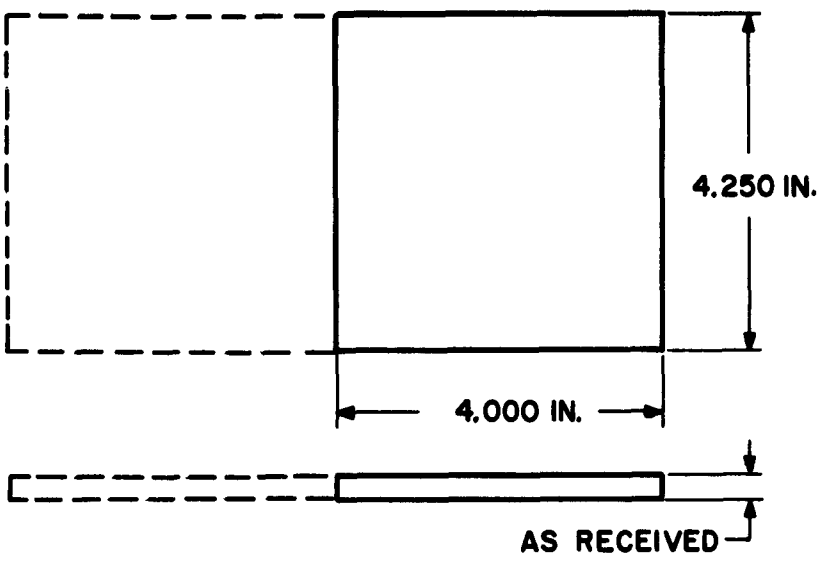

Figure 29. Final Butt-weld Specimen Drawing for Tensile Evaluation (D6AC Steel and B120VCA Titanium)

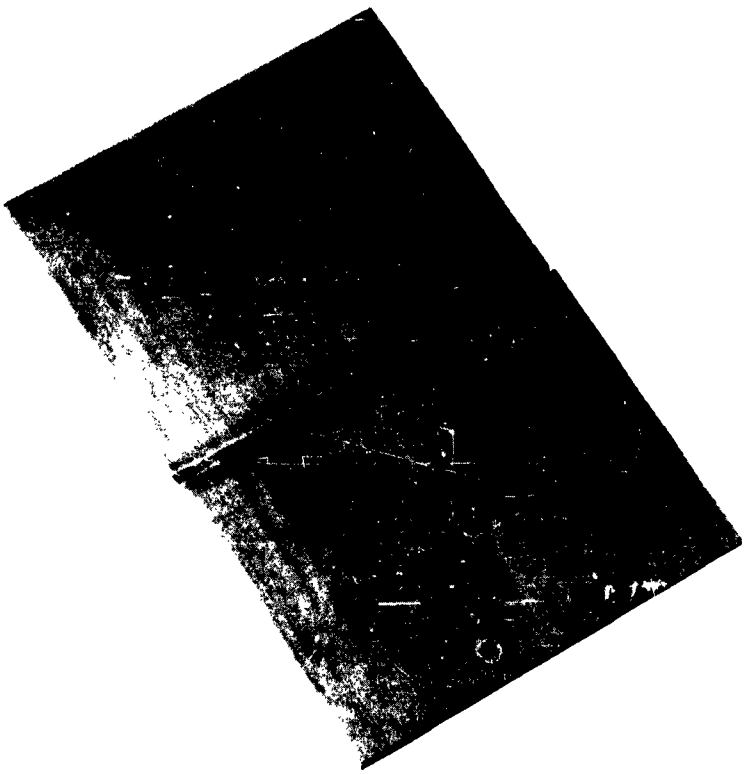

EM831-8 Figure 30. Final Butt-weld Specimen for Tensile Evaluation (D6AC Steel and B120VCA Titanium)

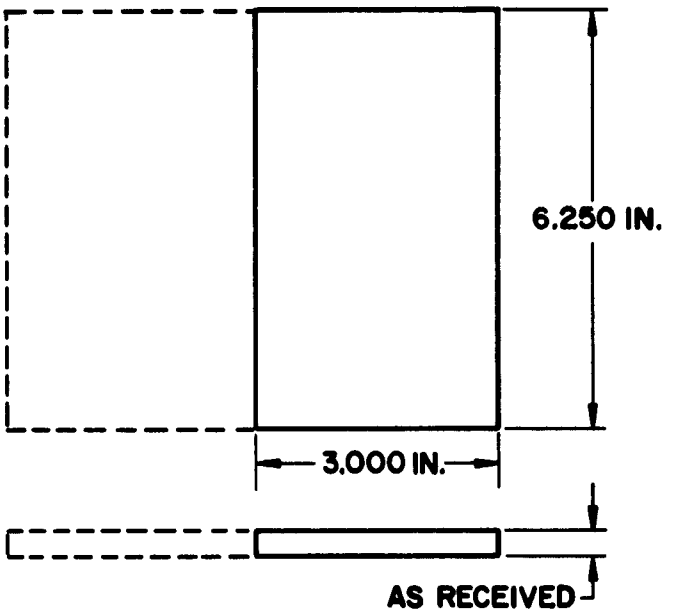

Figure 31. Final Butt-weld Specimen Drawing for Bend Evaluation (D6AC Steel and B120VCA Titanium)

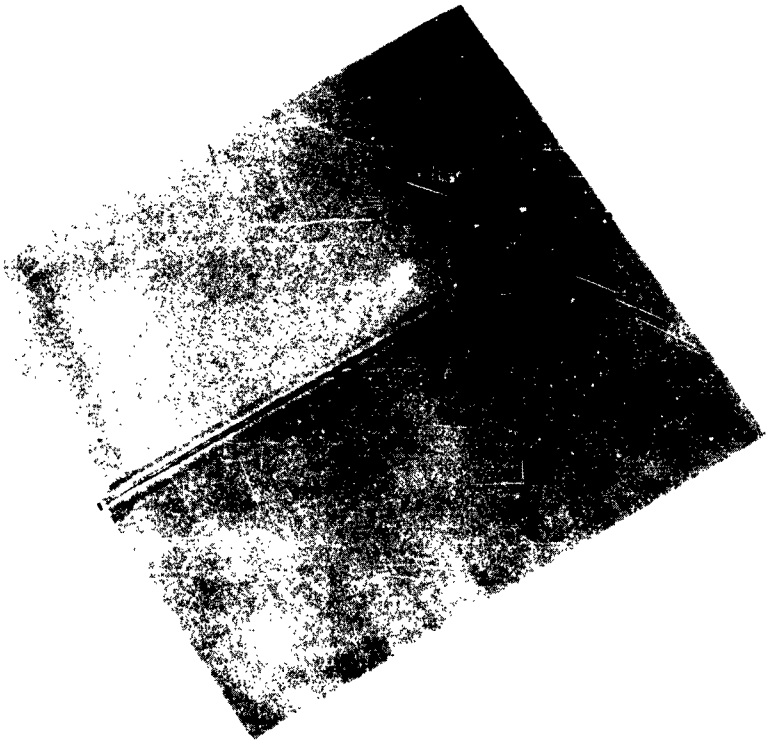

EB832-8 Figure 32. Final Butt-weld Specimen for Bend Evaluation (D6AC Steel and B120VCA Titanium)

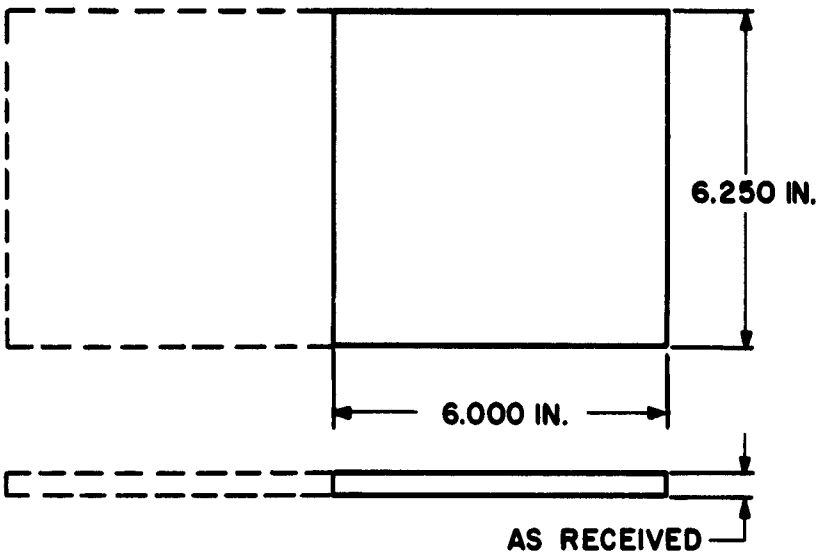

Figure 33. Final Butt-weld Specimen Drawing for Internal-Notch Tensile Evaluation (D6AC Steel and B120VCA Titanium)

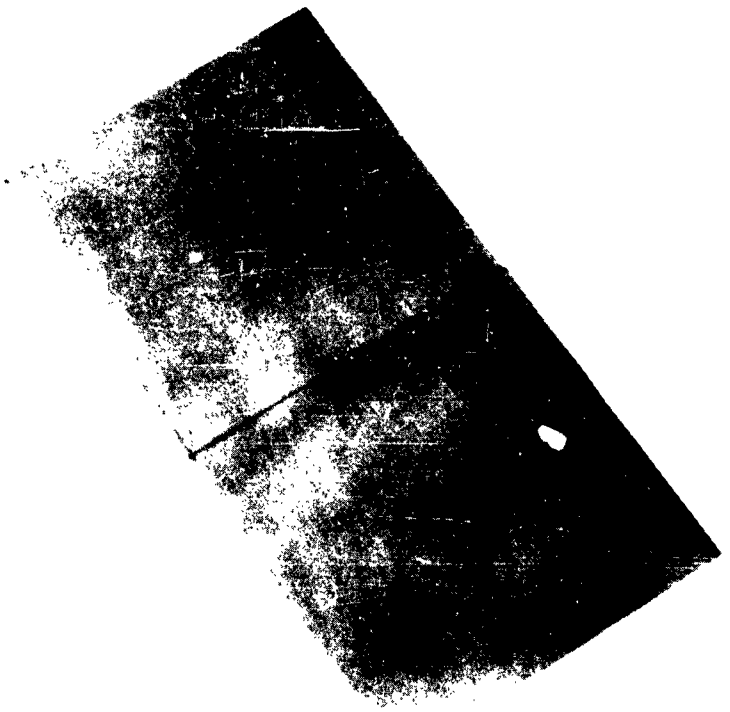

KM833-8 Figure 34. Final Butt-weld Specimen for Internal-Notch Tensile Evaluation (D6AC Steel and B120VCA Titanium)

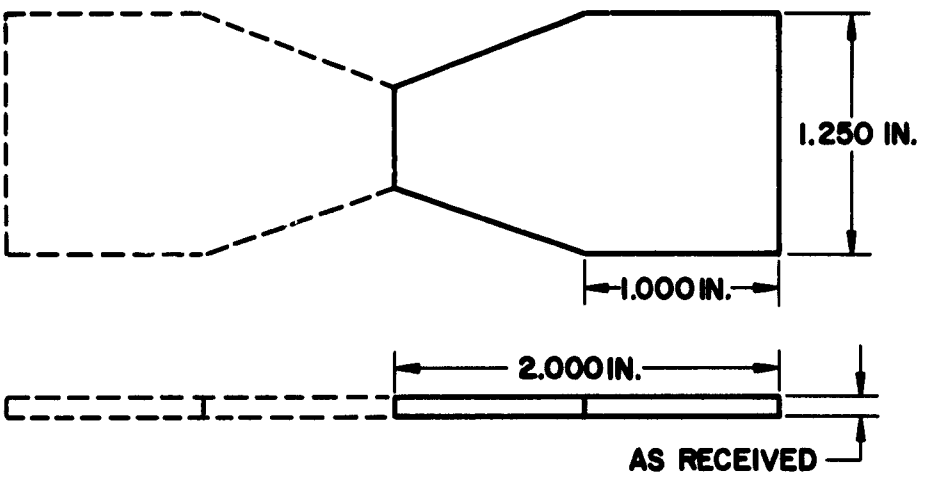

Figure 35. Final Butt-weld Specimen Drawing for Tensile Evaluation (Mo-0.5% Ti/tungsten, and beryllium)

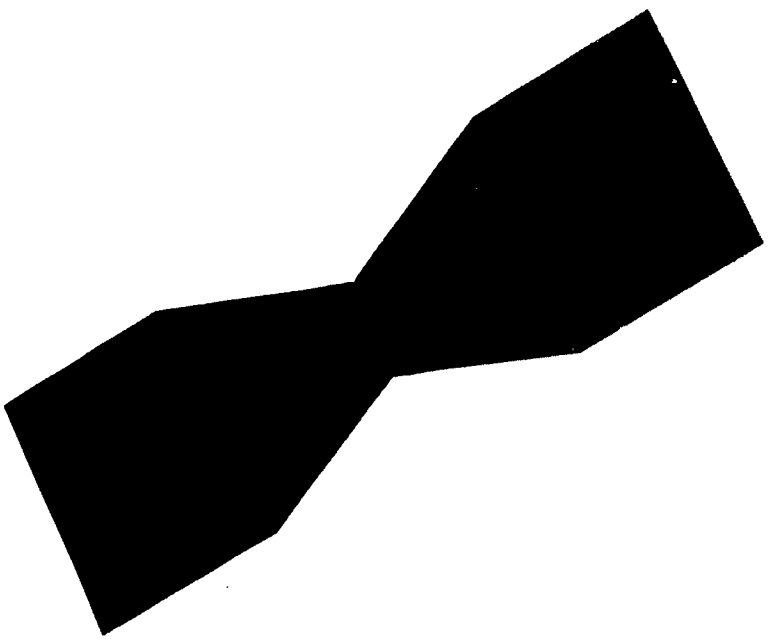

K8834-8 Figure 36. Final Butt-weld Specimen for Tensile Evaluation (Mo-0.5% Ti/tungsten, and beryllium)

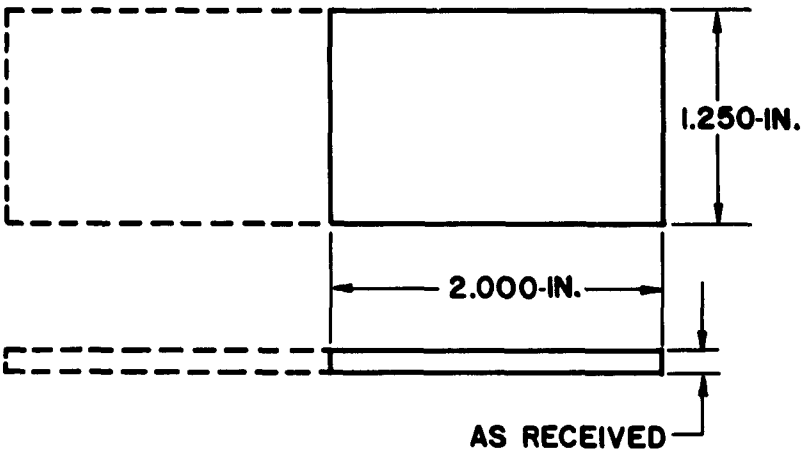

Figure 37. Final Butt-weld Specimen Drawing for Bend Evaluation (Mo-0.5% Ti/tungsten, and beryllium)

S-32490 Figure 38. Final Butt-weld Specimen for Bend Evaluation (Mo-0.5% Ti/tungsten, and beryllium)

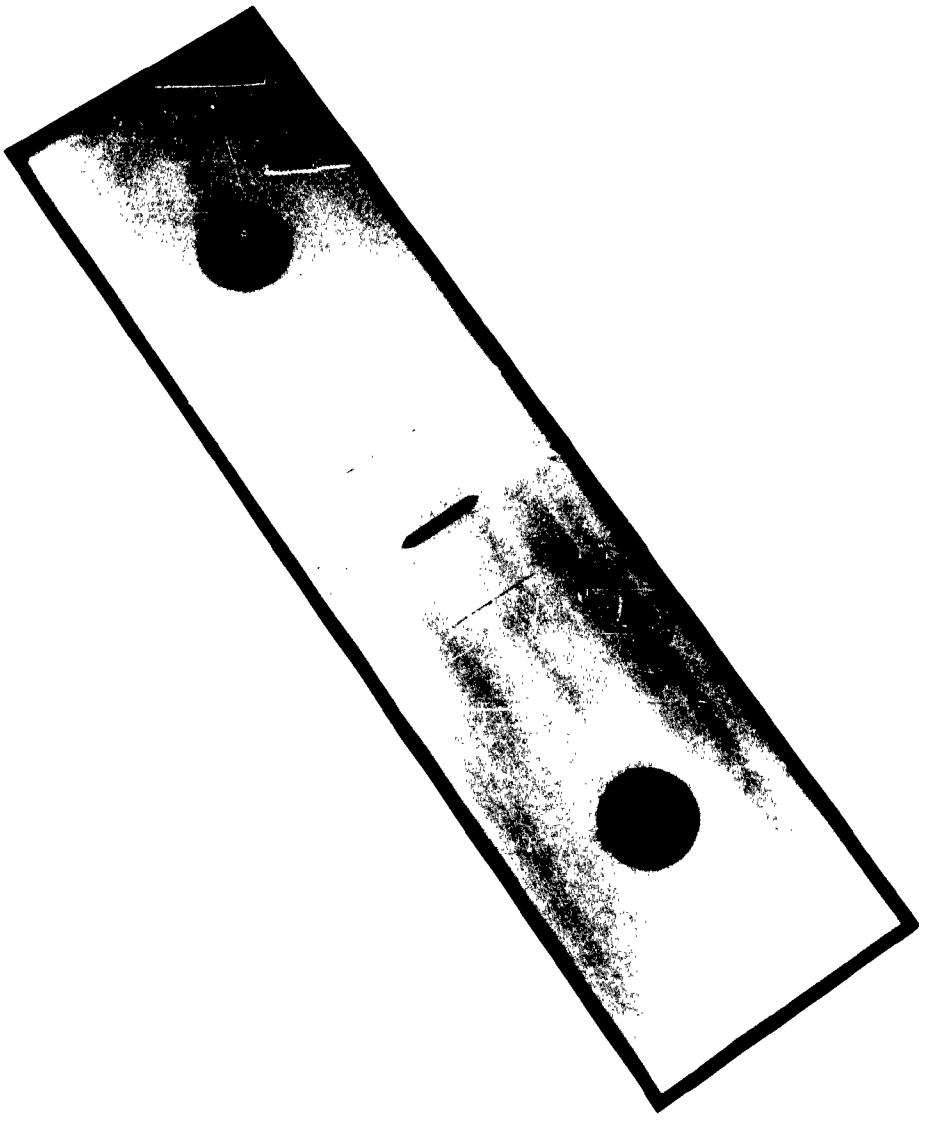

EM835-8 Figure 39. Welded Internal-Notch Tensile Specimen

Figure 40. B120VCA Titanium Base Metal; 0.125-Inch Solution Treated; X200

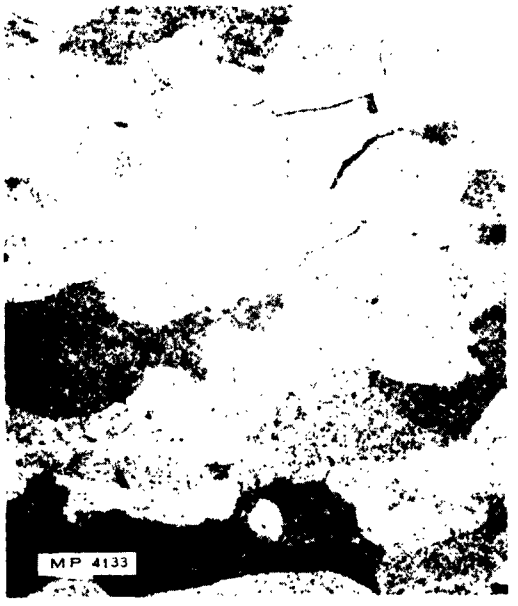

Figure 41. B120VCA Titanium Base Metal; 0.125-Inch Solution Treated; After Aging 72 Hours at 900 F;X200

Figure 42. B120VCA Titanium Base Metal; 0.125-Inch 50% Cold Rolled; X200

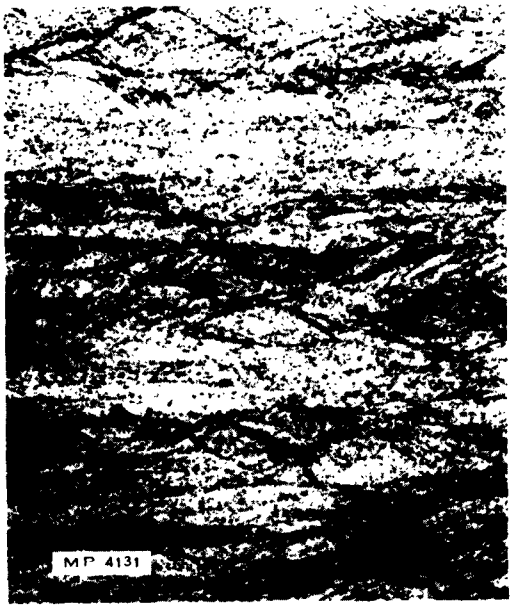

Figure 43. B120VCA Titanium Base Metal; 0.125-Inch 50% Cold Rolled; After Aging 12 Hours at 800F;X200

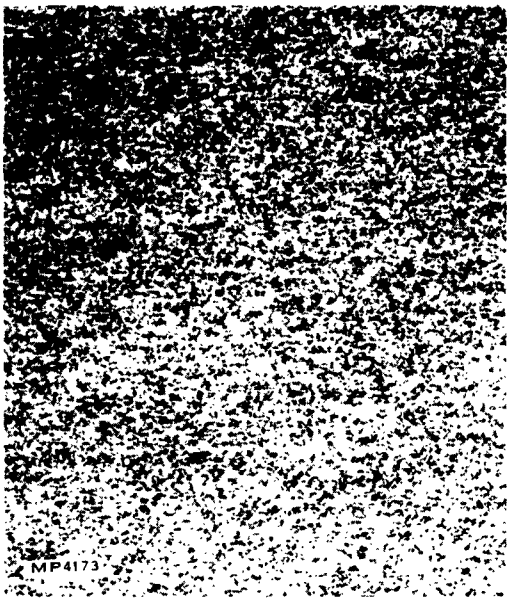

Figure 44. D6AC Steel Base Metal; 0.090-Inch Annealed; X200

Figure 45. D6AC Steel Base Metal; 0.090-Inch Annealed; After Heat Treatment to 2T700; X200

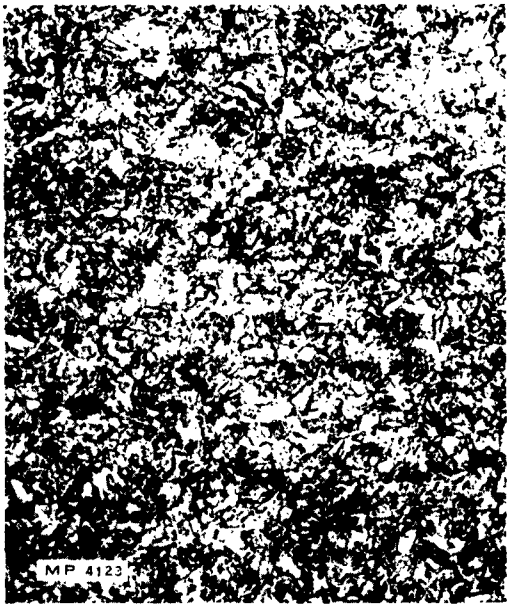

Figure 46. D6AC Steel Base Metal; 0.290-Inch Annealed; X200

Figure 47. D6AC Steel Base Metal; 0.290-Inch Annealed; After Heat Treatment to 2T700; X200

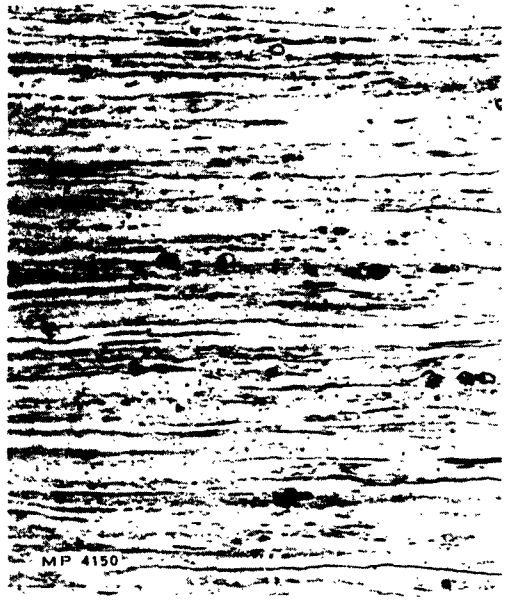

Figure 48. Mo-0.5% Ti Base Metal; 0.100-Inch As-received; X200

Figure 49. Mo-0.5% Ti Base Metal; 0.100-Inch Recrystallized; X200

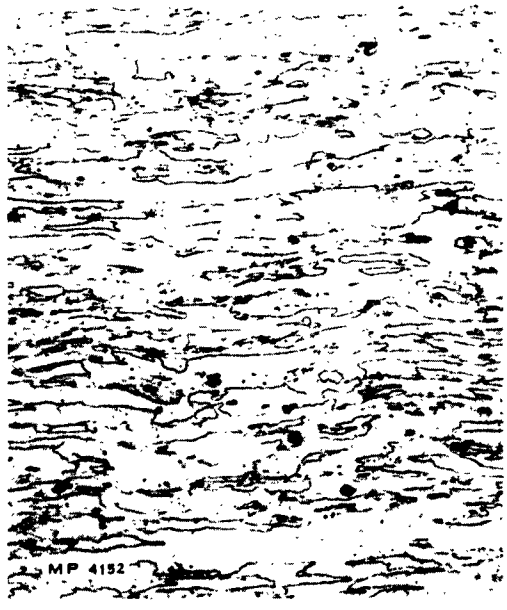

Figure 50. Mo-0.5% Ti Base Metal; 0.050-Inch As-received; X200

Figure 51. Mo-0.5% Ti Base Metal; 0.050-Inch Recrystallized; X200

Figure 52. Mo-0.5% Ti Base Metal; 0.005-Inch As-received; X200

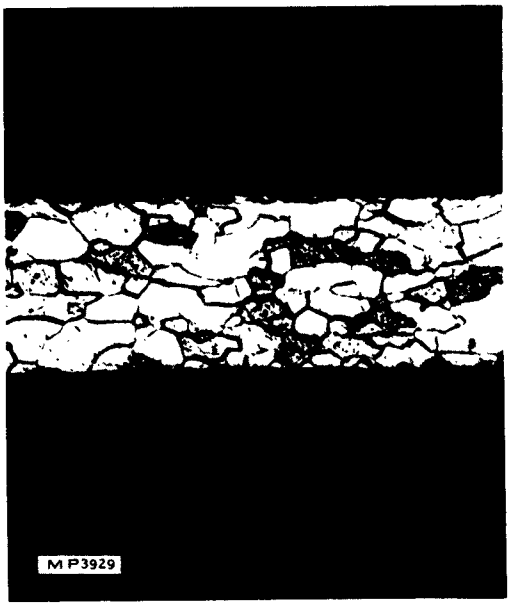

Figure 53. Mo-0.5% Ti Base Metal; 0.005-Inch Recrystallized; X200

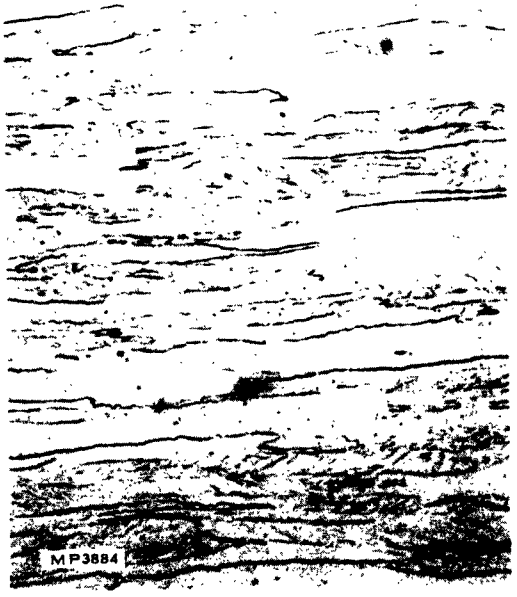

Figure 54. Tungsten Base Metal; 0.100-Inch As-received; X200

Figure 55. Tungsten Base Metal; 0.100-Inch Recrystallized; X200

Figure 56. Tungsten Base Metal; 0.050-Inch As-received; X200

Figure 57. Tungsten Base Metal; 0.050-Inch Recrystallized; X200

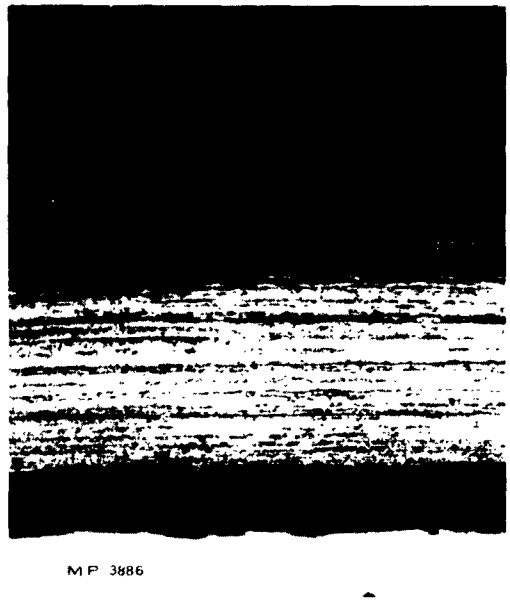

Figure 58. Tungsten Base Metal; 0.005-Inch As-received; X200

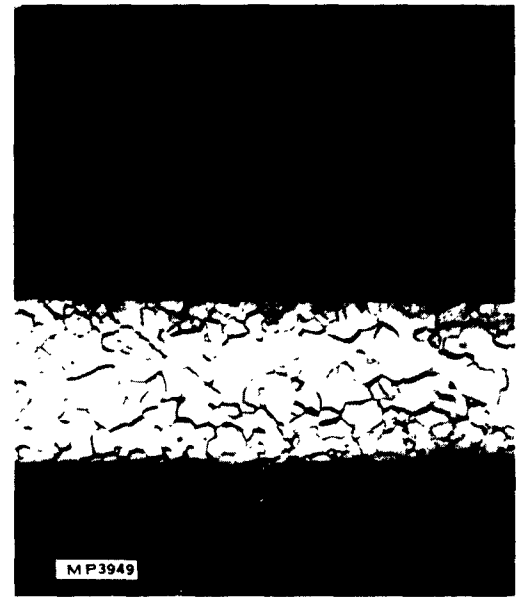

Figure 59. Tungsten Base Metal; 0.005-Inch Recrystallized; X200

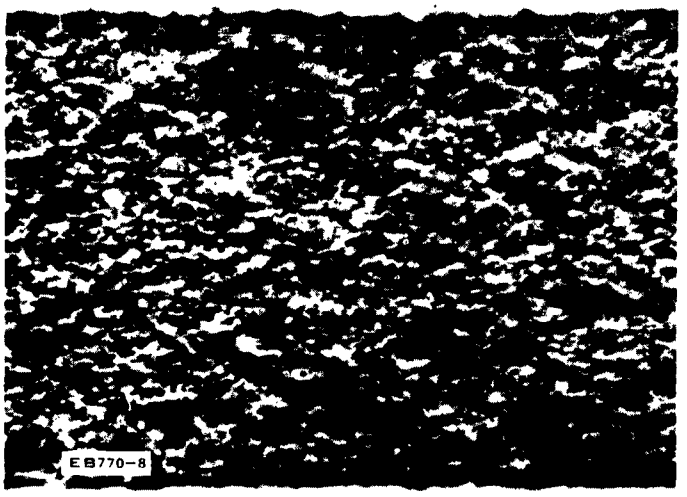

Figure 60. Beryllium Base Metal;
0.040-Inch As-received; X200

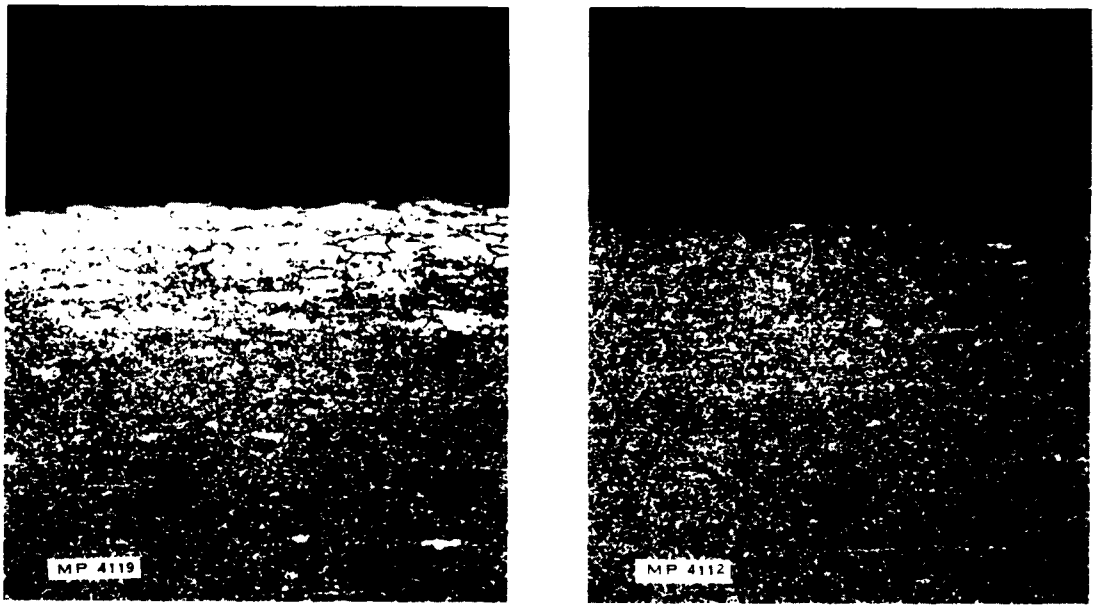

a. As-received

b. After Grinding

Figure 61. 0.090-Inch D6AC
Base Metal Cross-section; X200

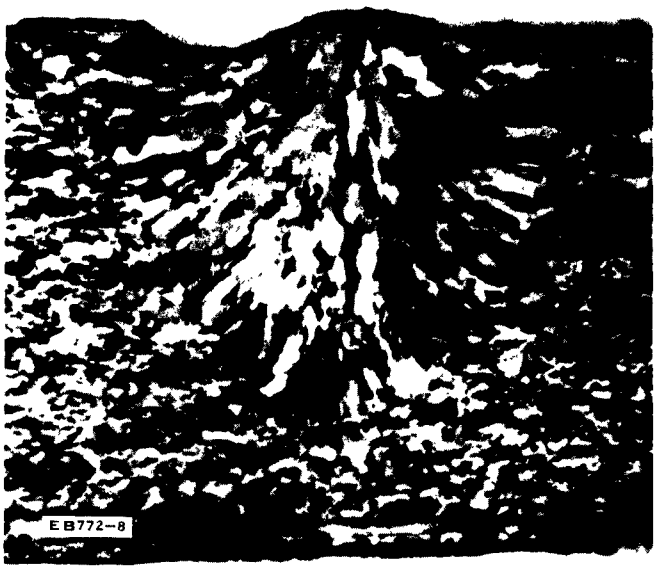

Figure 62. Trial Weld Cross-section; 0.040-Inch Beryllium; X70; 100 KV, 12 ma, 27 ipm

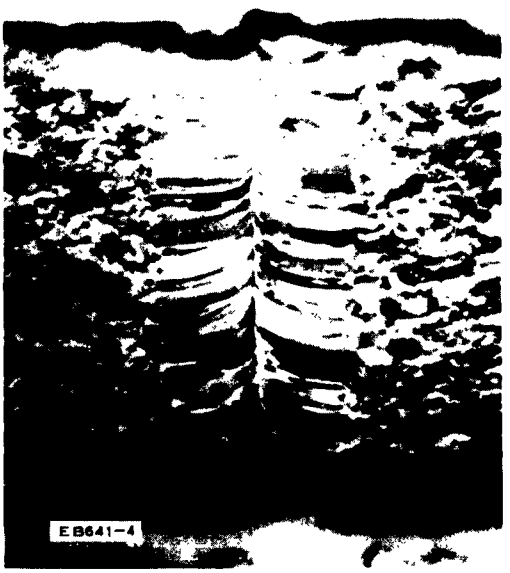

Figure 63. Trial Weld Cross-section; 0.040-Inch Beryllium; X70; 120 KV, 7 ma, 80 ipm

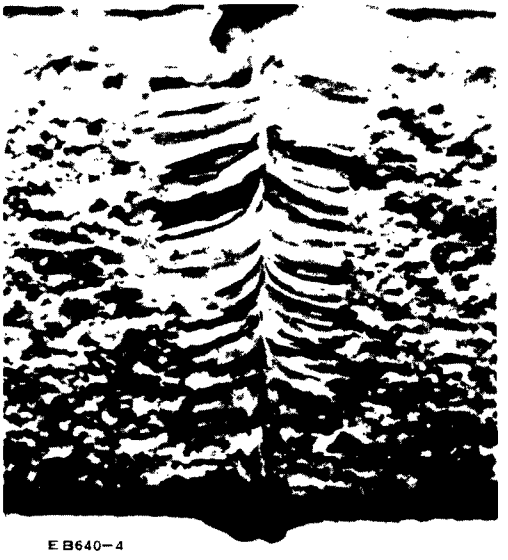

Figure 64. Trial Weld Cross-section; 0.040-Inch Beryllium; X70; 120 KV, 7 ma, 80 ipm, Longitudinal Beam Oscillation

Figure 65. Trial Weld Cross-section; 0.040-Inch Beryllium; X70; 120 KV, 7 ma, 80 ipm, Circular Beam Oscillation

Figure 66. Trial Weld Cross-section; 0.040-Inch Beryllium; X70; 110 KV, 2.5 ma, 15 ipm, 0.015-Inch Diameter Beam

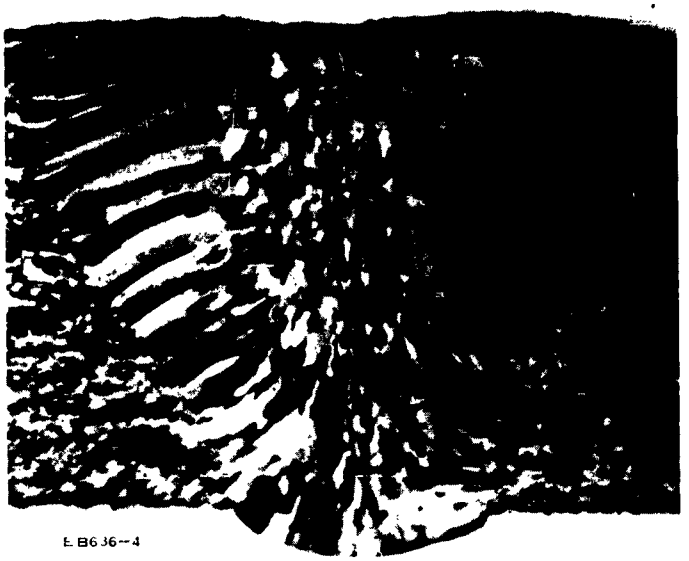

Figure 67. Trial Weld Cross-section; 0.040-Inch Beryllium; X70; 75 KV, 6 ma, 15 ipm, 0.020-Inch Diameter Beam

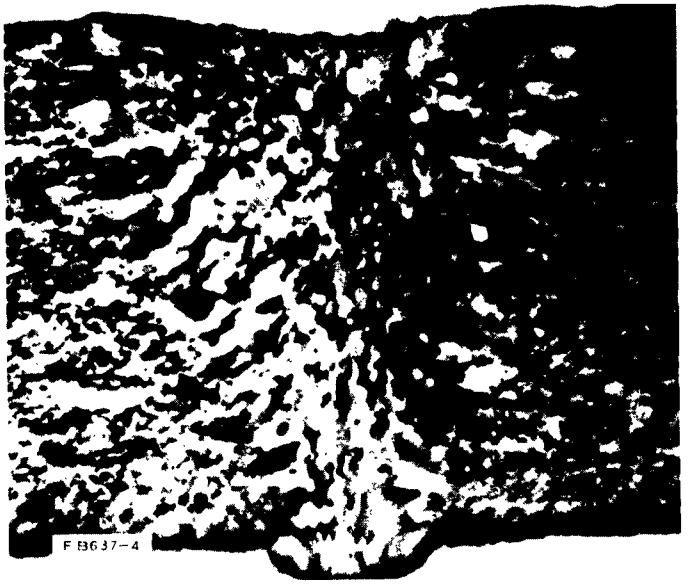

Figure 68. Trial Weld Cross-section; 0.040-Inch Beryllium; X70; 65 KV, 7 ma, 15 ipm, 0.020-Inch Diameter Beam

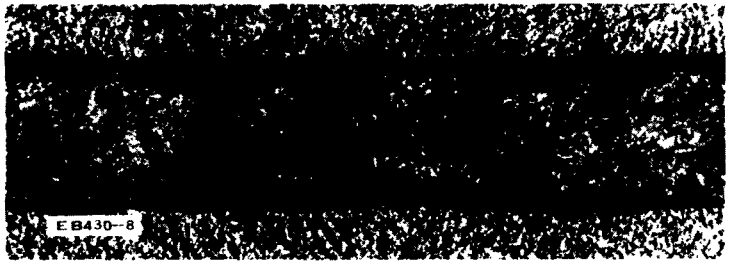

Figure 69. Final Weld Top Bead;
0.040-Inch Beryllium; X10

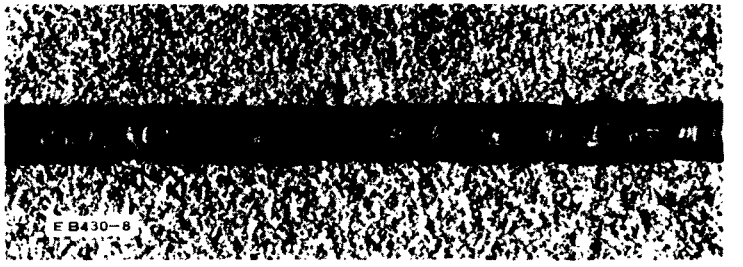

Figure 70. Final Weld Bottom Bead;
0.040-Inch Beryllium; X10

Figure 71. Final Weld Cross-section;
0.040-Inch Beryllium; X70

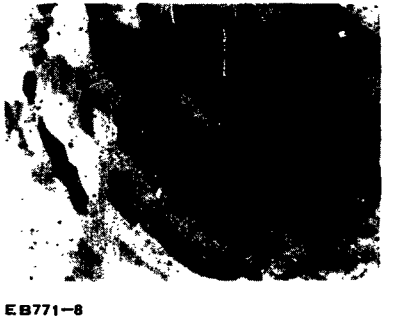

Figure 72. Final Weld Microstructure;
0.040-Inch Beryllium; X100

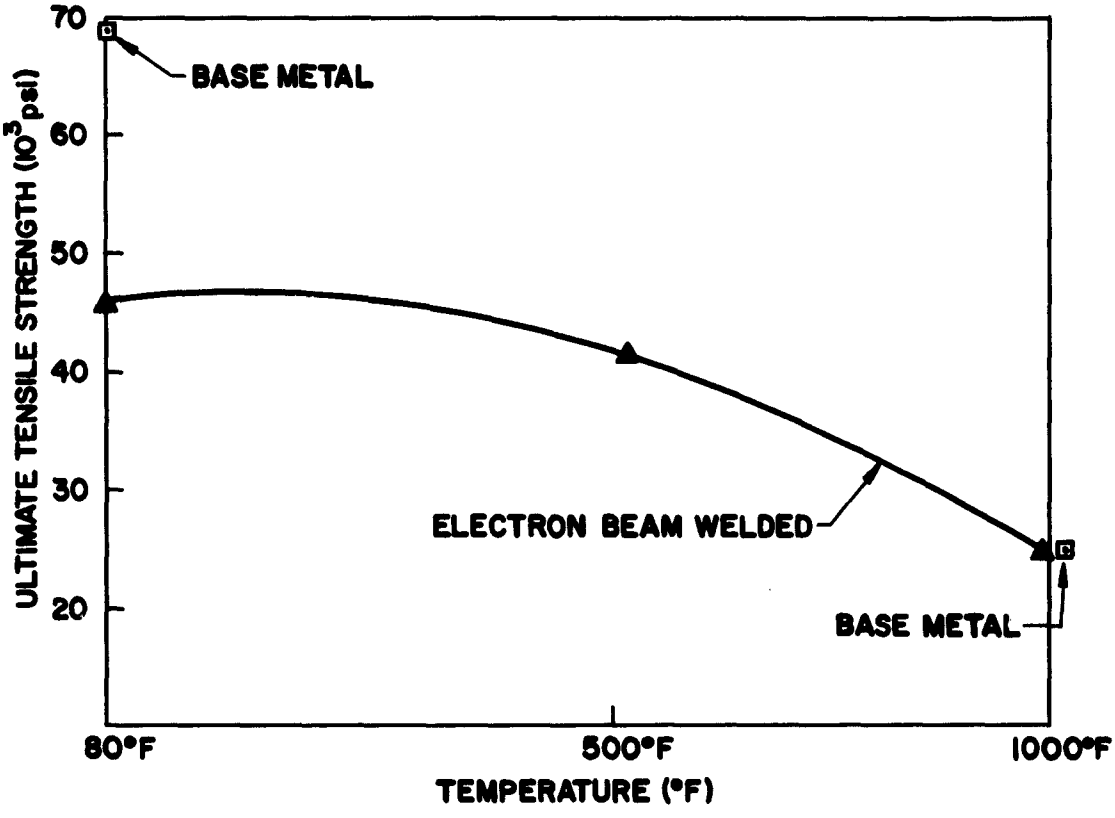

Figure 73 Ultimate Tensile Strength vs. Temperature; 0.040-Inch Beryllium Welds

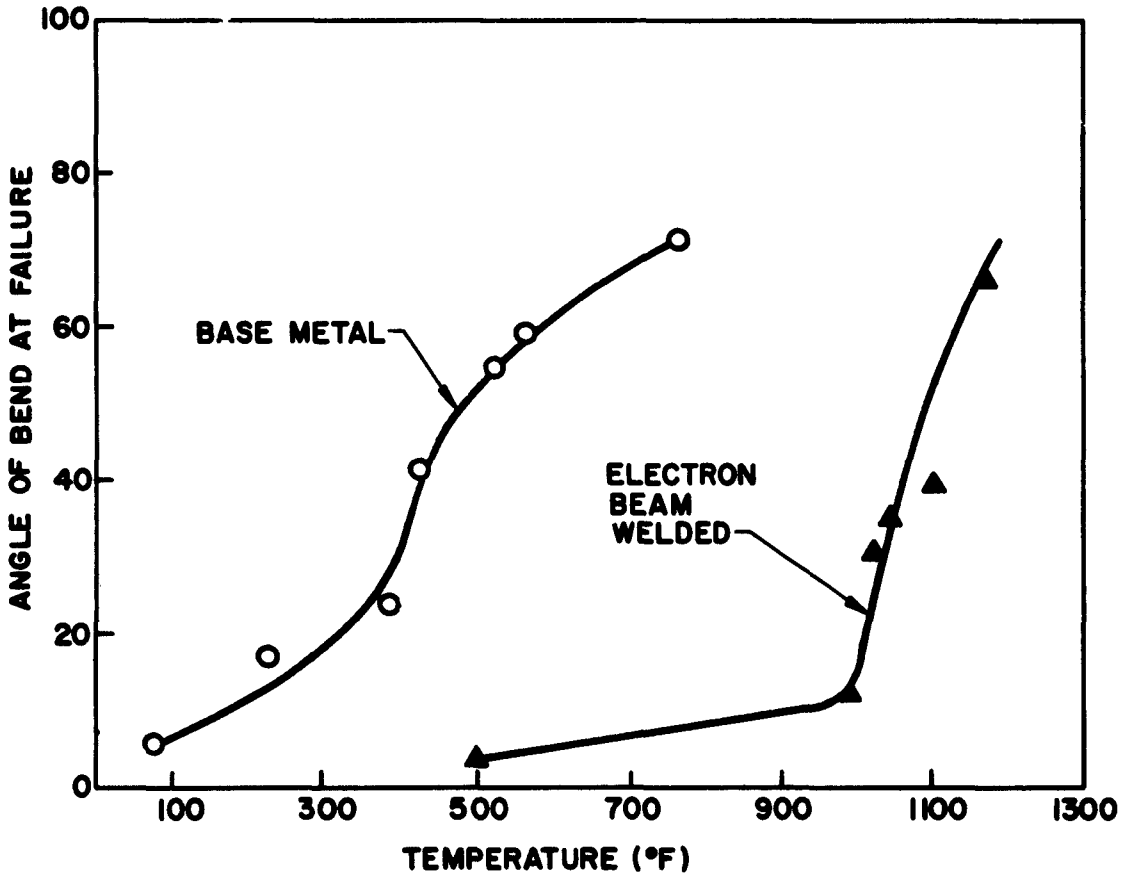

Figure 74. Bend Angle vs. Temperature; 0.040-Inch Beryllium Welds

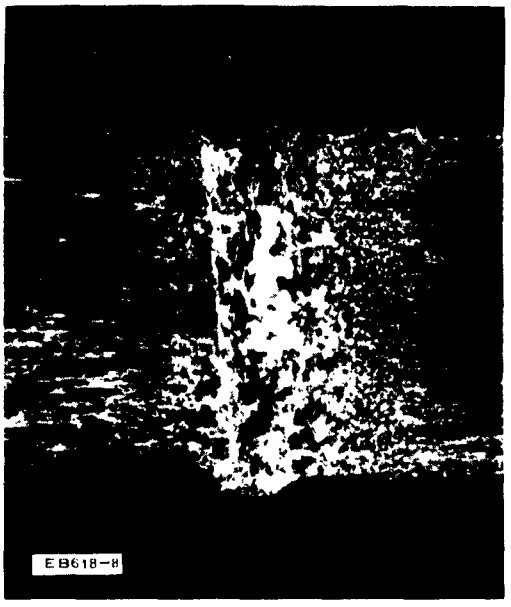

Figure 75. Trial Weld Cross-section; X20; 0.100-Inch Mo-0.5% Ti/Tungsten; Beam Located on Joint Centerline

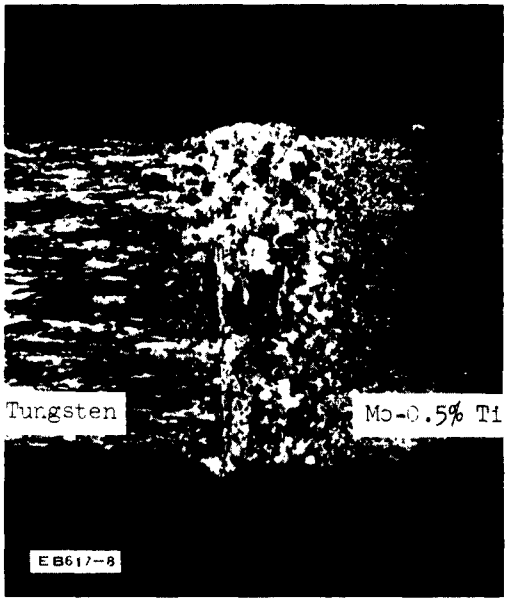

Figure 76. Trial Weld Cross-section; X20; 0.100-Inch Mo-0.5% Ti/Tungsten; Beam Located 0.010 Inch in Mo-0.5% Ti

Figure 77. Trial Weld Cross-section; X20; 0.100-Inch Mo-0.5% Ti/Tungsten; Beam Located 0.010 Inch Tungsten

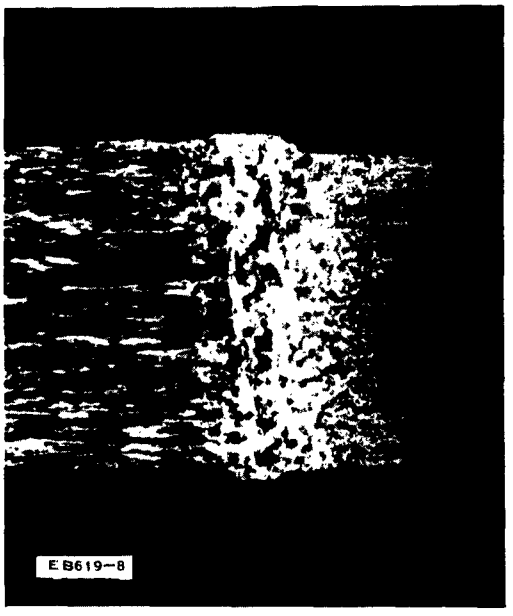

Figure 78. Trial Weld Cross-section; X20; 0.100-Inch Mo-0.5% Ti/Tungsten; Beam Located 0.006 Inch in Tungsten

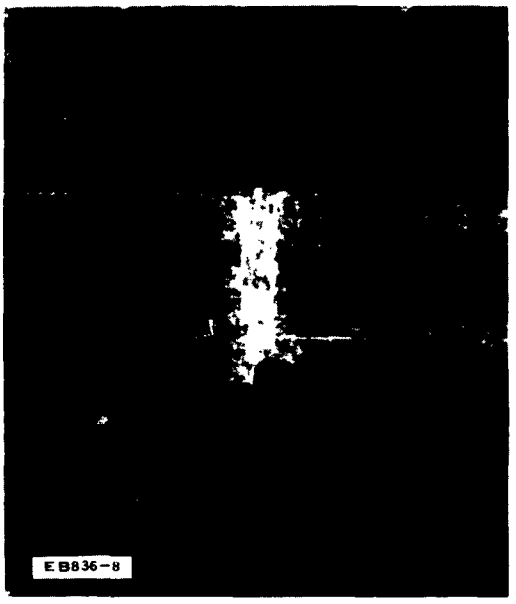

Figure 79. Trial Weld Cross-section; X20; 0.050-Inch Mo-0.5% Ti/Tungsten; Beam Located on Joint Centerline

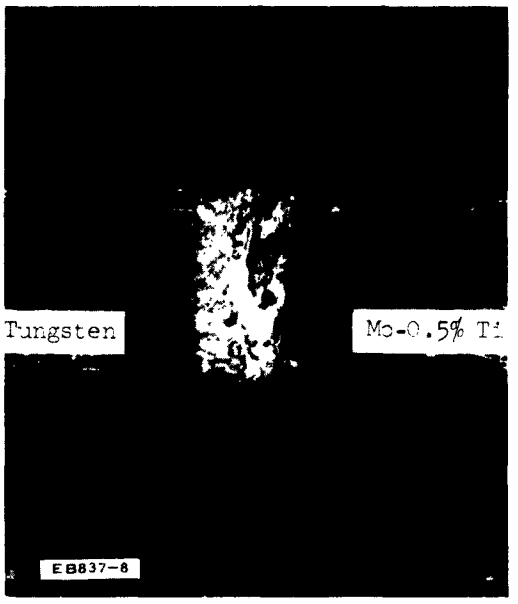

Figure 80. Trial Weld Cross-section; X20; 0.050-Inch Mo-0.5% Ti/Tungsten; Beam Located 0.005 Inch in Mo-0.5% Ti

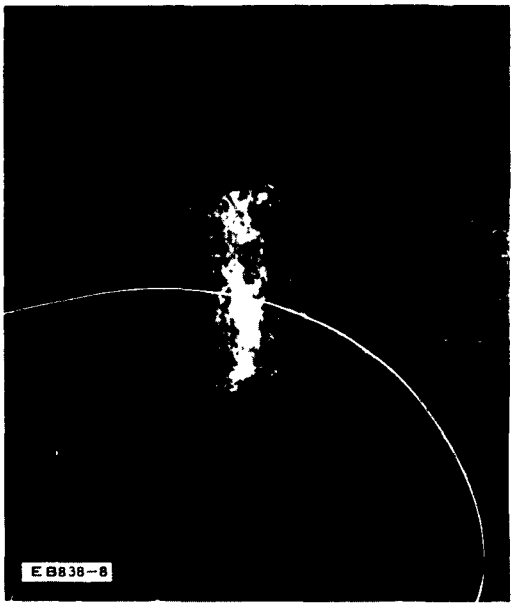

Figure 81. Trial Weld Cross-section; X20; 0.050-Inch Mo-0.5% Ti/Tungsten; Beam Located 0.005 Inch in Tungsten

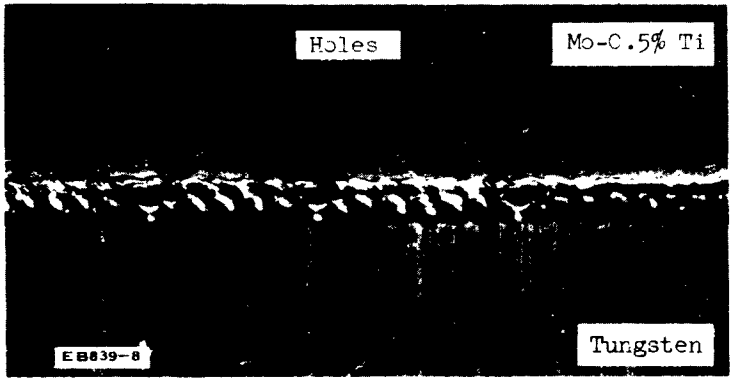

Figure 82. Trial Weld Bead; X10 0.005-Inch Mo-0.5% Ti/Tungsten; Beam Located on Joint Centerline

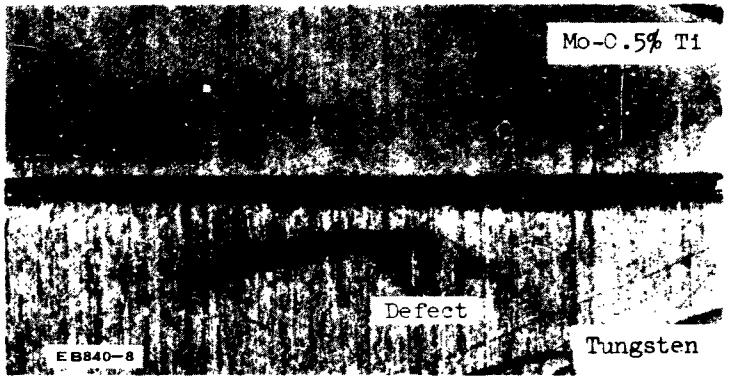

Figure 83. Trial Weld Bead; X10 0.005-Inch Mo-0.5% Ti/Tungsten; Beam Located 0.002 Inch in Tungsten

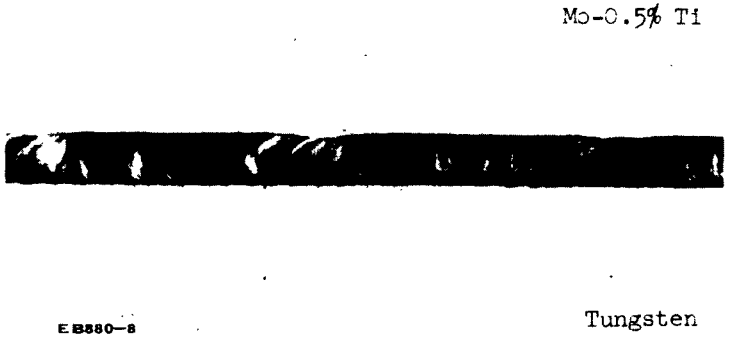

Figure 84. Trial Weld Bead; X10 0.005-Inch Mo-0.5% Ti/Tungsten; 0.005-Inch Joint Overlap

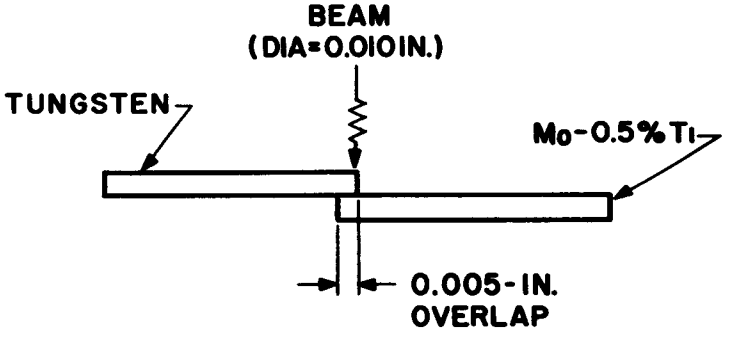

Figure 85. Modified Joint Design for Thin Sheet Weldments

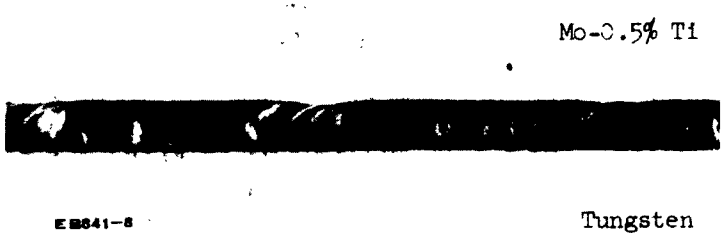

Figure 86. Final Weld Top Bead; X10
0.005-Inch Mo-0.5% Ti/Tungsten

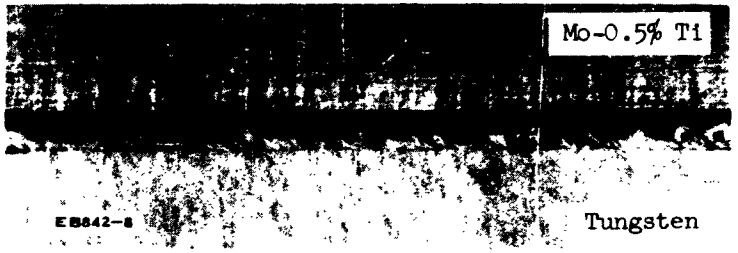

Figure 87. Final Weld Bottom Bead; X10
0.005-Inch Mo-0.5% Ti/Tungsten

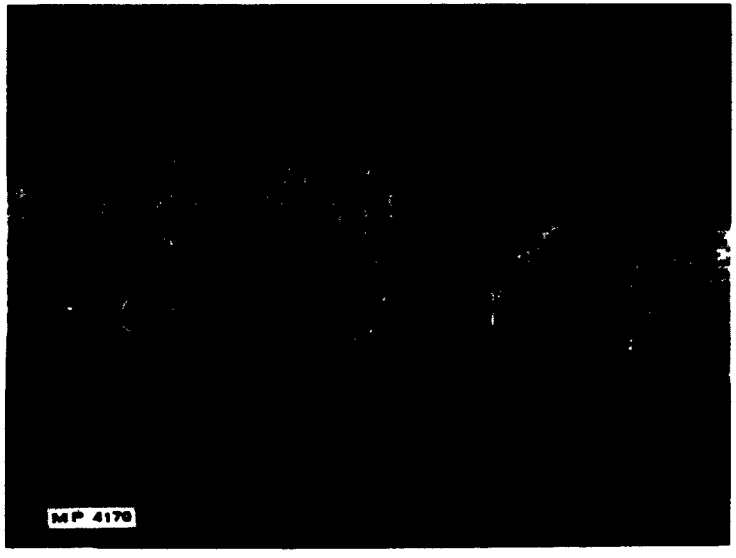

Figure 88. Final Weld Microstructure;
X200 0.005-Inch Mo-0.5% Ti/Tungsten

Figure 89. Final Weld Top Bead; X10
0.050-Inch Mo-0.5% Ti/Tungsten

Figure 90. Final Weld Bottom Bead; X10
0.050-Inch Mo-0.5% Ti/Tungsten

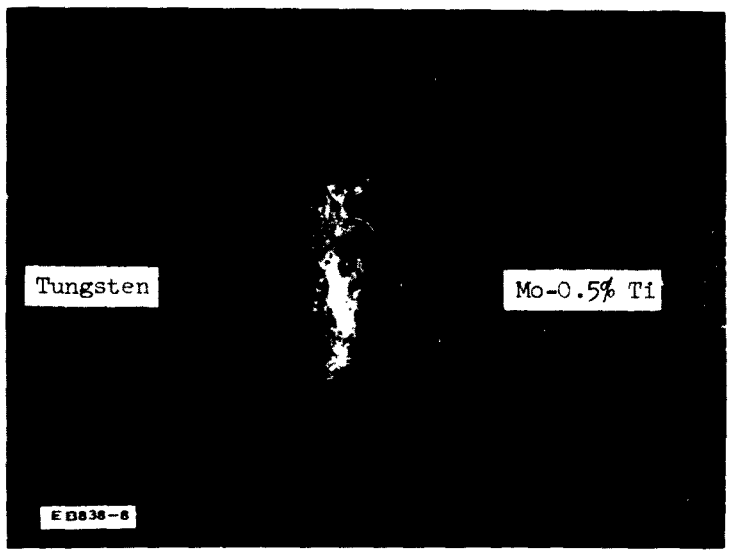

Figure 91. Final Weld Cross-section; X20
0.050-Inch Mo-0.5% Ti/Tungsten

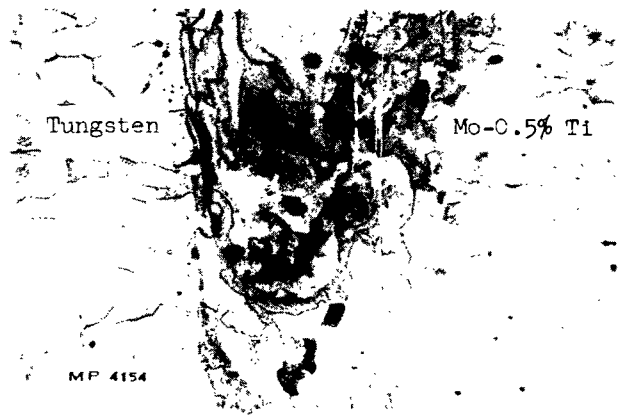

Figure 92. Final Weld Microstructure;
X100 0.050-Inch Mo-0.5% Ti/Tungsten

Figure 93. Final Weld Top Bead; X10
0.100-Inch Mo-0.5% Ti/Tungsten

Figure 94. Final Weld Bottom Bead; X10
0.100-Inch Mo-0.5% Ti/Tungsten

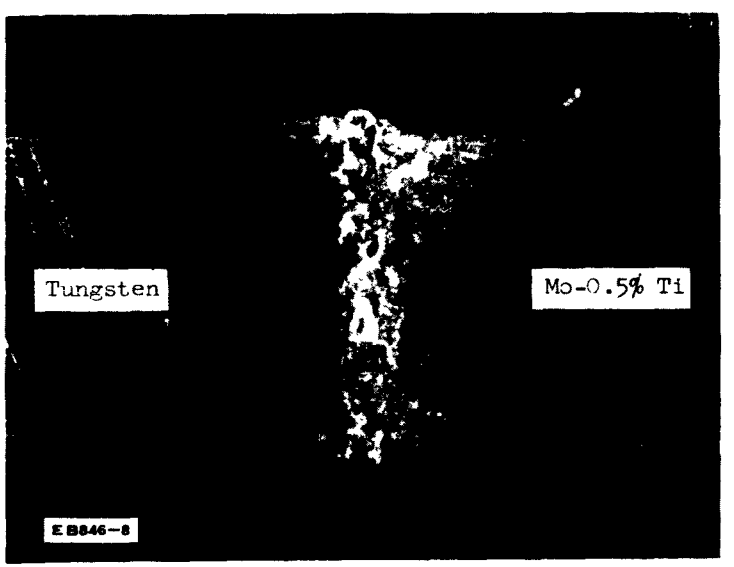

Figure 95. Final Weld Cross-section; X20
0.100-Inch Mo-0.5% Ti/Tungsten

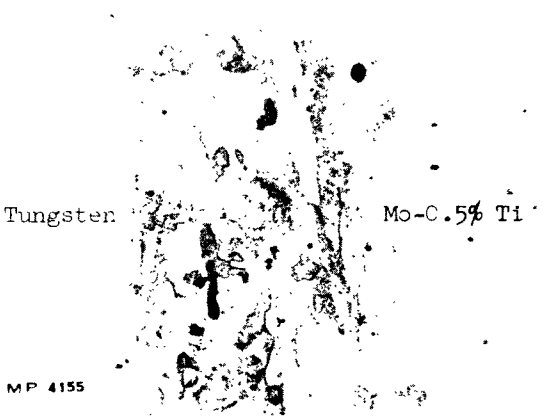

Figure 96. Final Weld Microstructure;
X100 0.100-Inch Mo-0.5% Ti/Tungsten

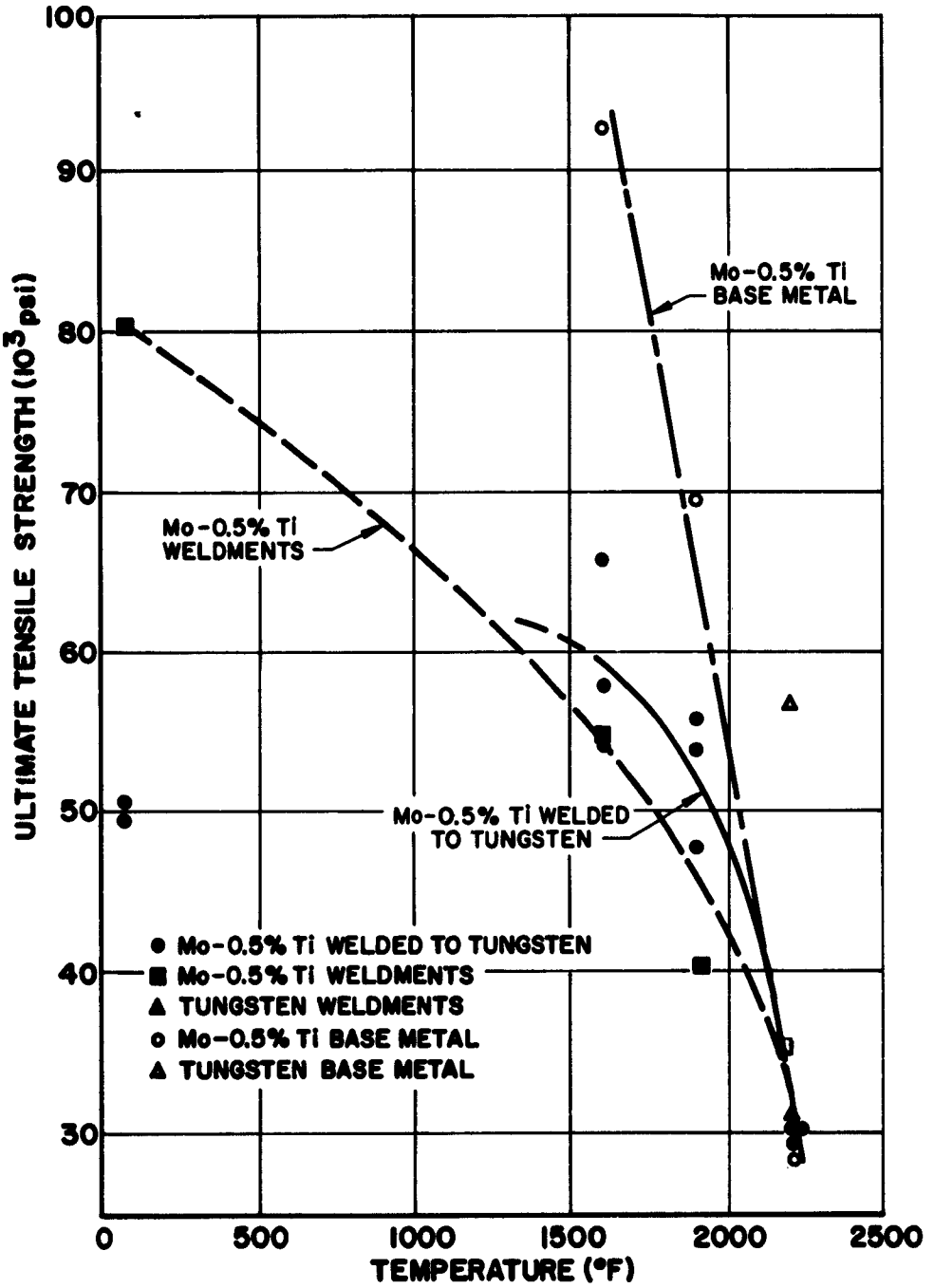

Figure 97. Ultimate Tensile Strength vs. Temperature; 0.050-inch Mo-0.5% Ti/Tungsten Welds

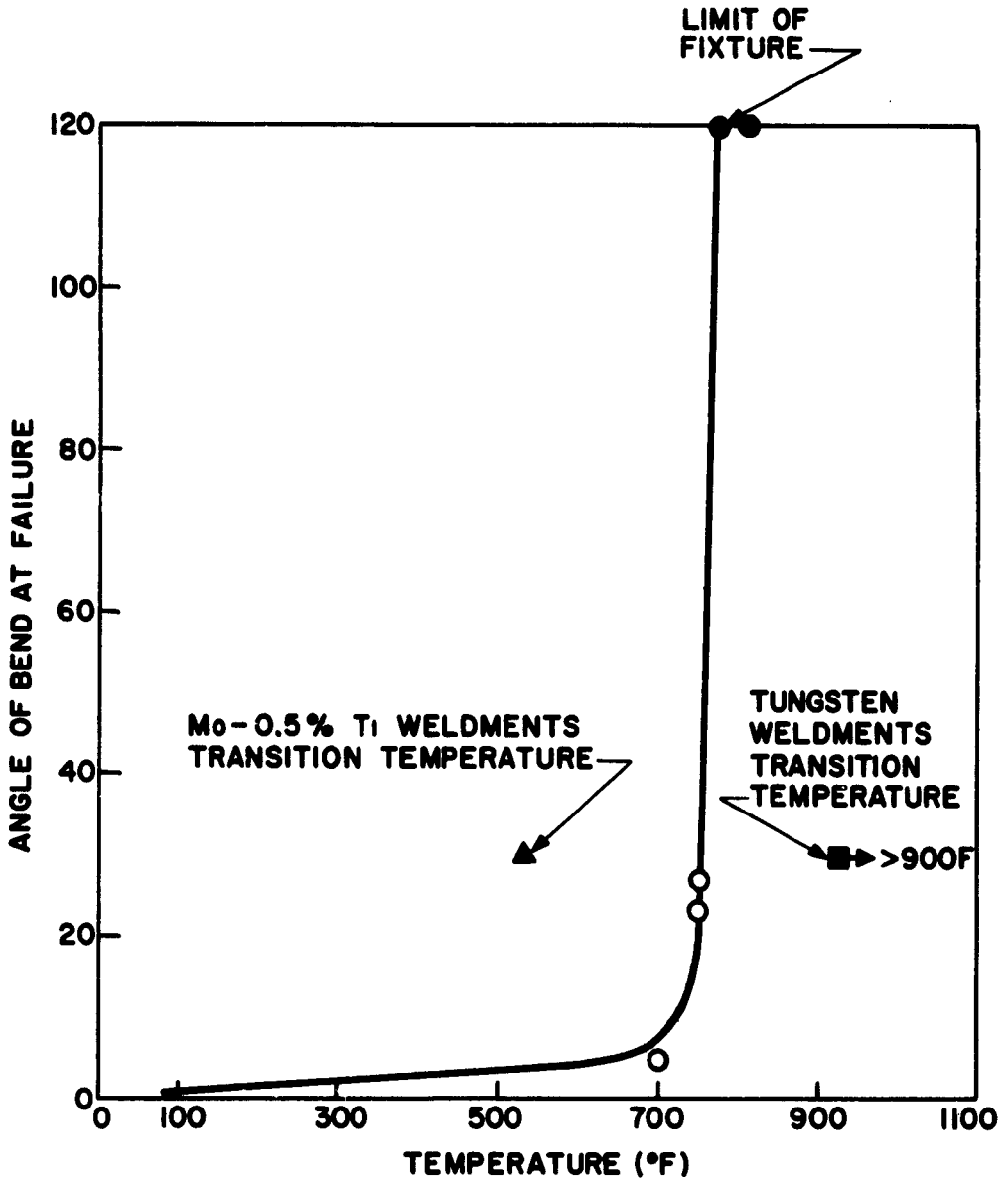

Figure 98. Bend Angle vs. Temperature; 0.100-Inch Mo-0.5% Ti/Tungsten Welds

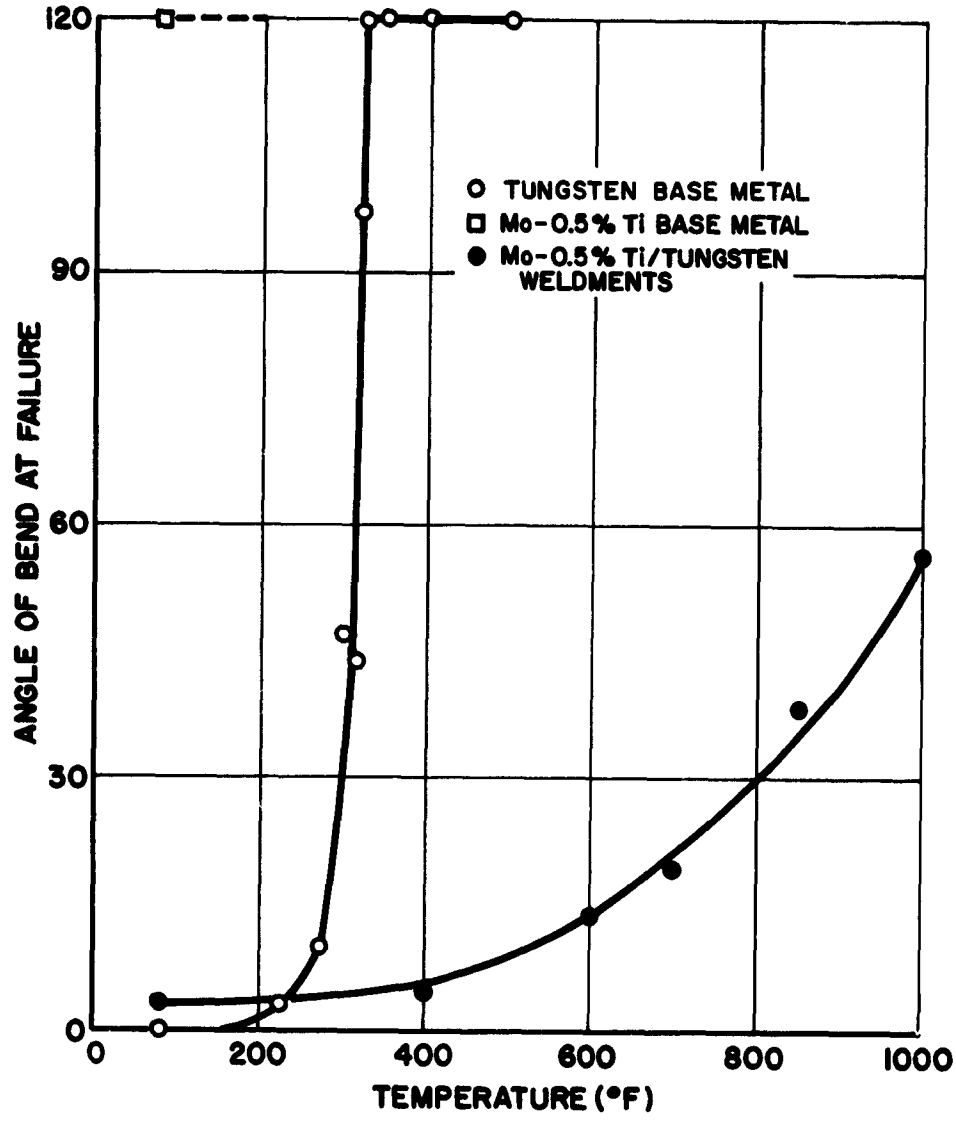

Figure 99. Bend Angle vs. Temperature; 0.050-Inch Mo-0.5% Ti/Tungsten Welds

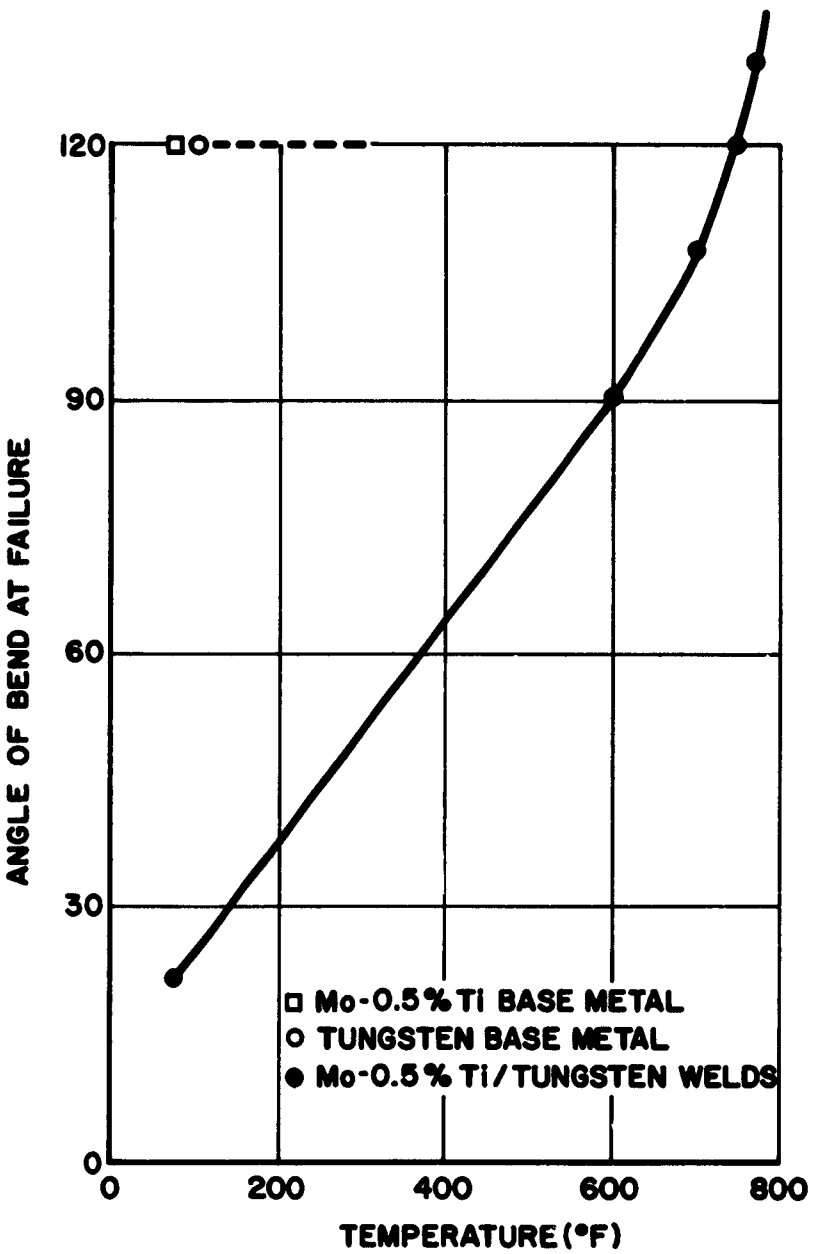

Figure 100. Bend Angle vs. Temperature; 0.005-Inch Mo-0.5% Ti/Tungsten Welds

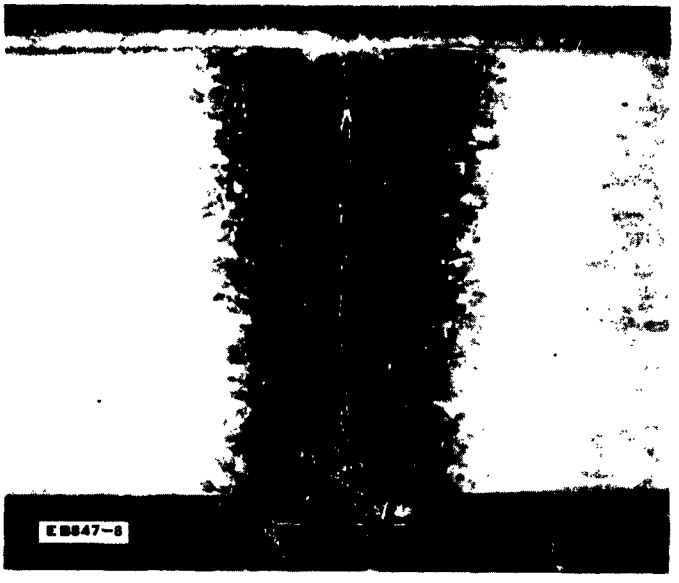

Figure 101. Trial Weld Cross-section; X20; 0.125-inch B120VCA Ti; 150 KV, 10 ma, 50 ipm

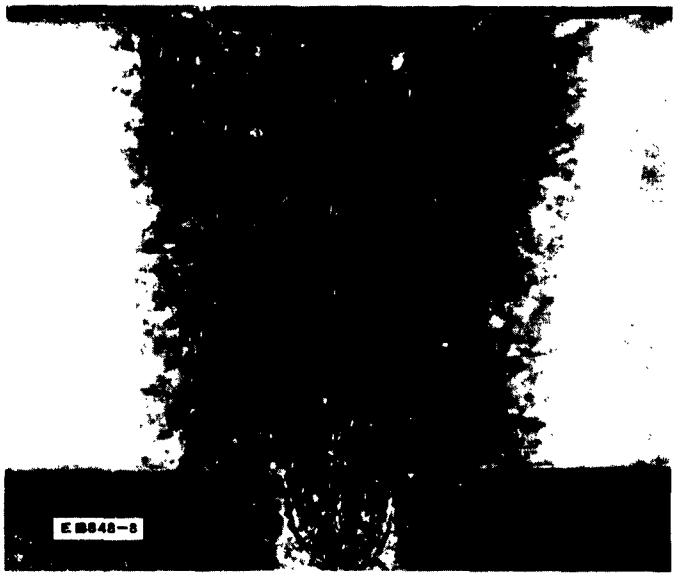

Figure 102. Trial Weld Cross-section; X20; 0.125-Inch B120VCA Ti; 150 KV, 10 ma, 50 ipm, 0.020-Inch Y Oscillation

Figure 103. Trial Weld Cross-section; X20; 0.125-inch B120VCA Ti; 150 KV, 10 ma, 40 ipm, 0.020-inch Circular Oscillation

Figure 104. Trial Weld Cross-section; X20; 0.125-Inch B120VCA Ti; 140 KV, 15 ma, 50 ipm, 0.020-Inch Y Oscillation

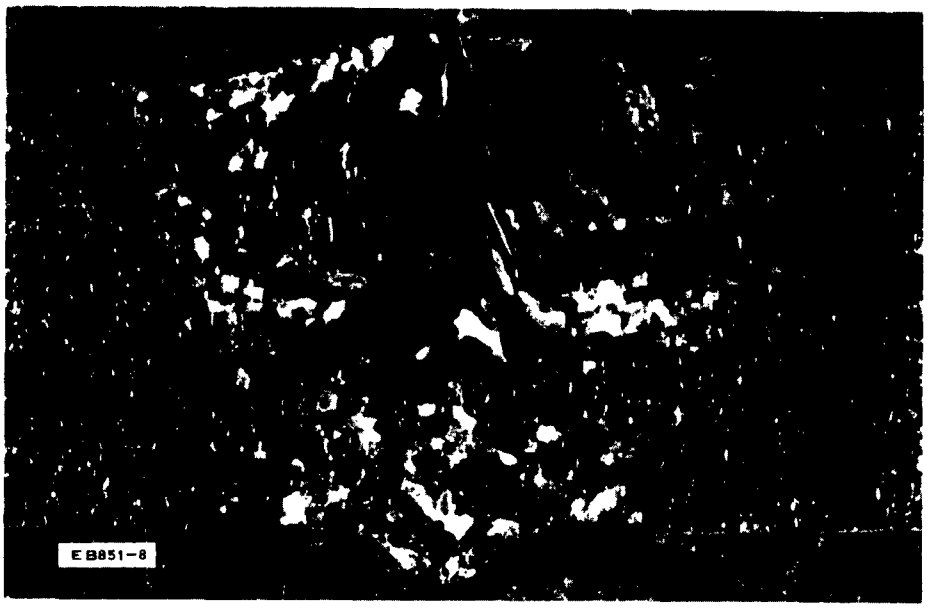

Figure 105. Trial Weld Cross-section; X20; 0.125-inch B120VCA Ti; 140 KV, 16 ma, 40 ipm, 0.020-inch Circular Oscillation

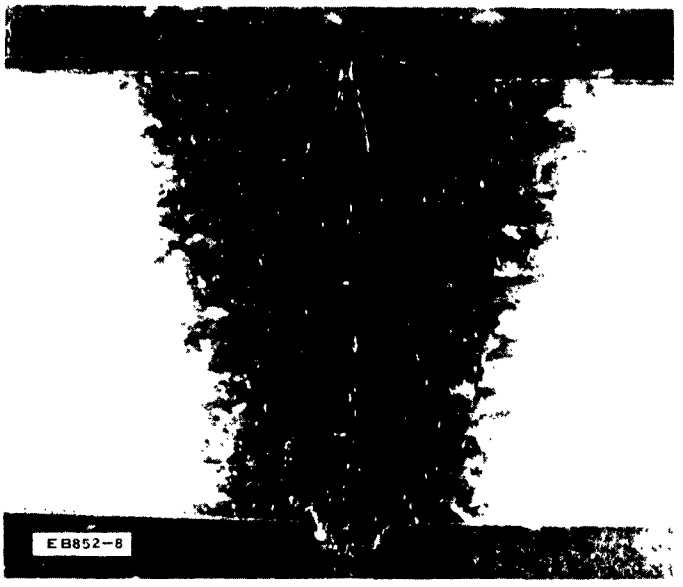

Figure 106. Trial Weld Cross-section; X20; 0.125-inch B120VCA Ti; 150 KV, 7 ma, 22 ipm, 0.075-inch X Oscillation

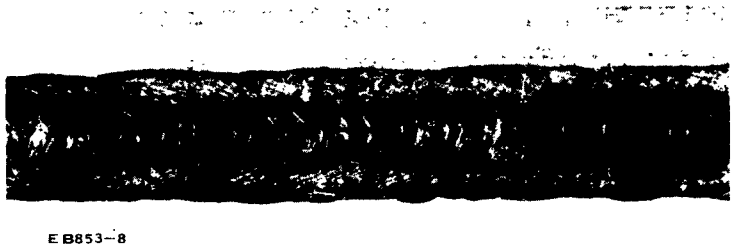

Figure 107. Final Weld Top Bead; X10; 0.125-Inch B120VCA Ti; Welded In The Solution Treated and Aged Condition

Figure 108. Final Weld Bottom Bead; X10; 0.125-Inch B120VCA Ti; Welded In The Solution Treated and Aged Condition

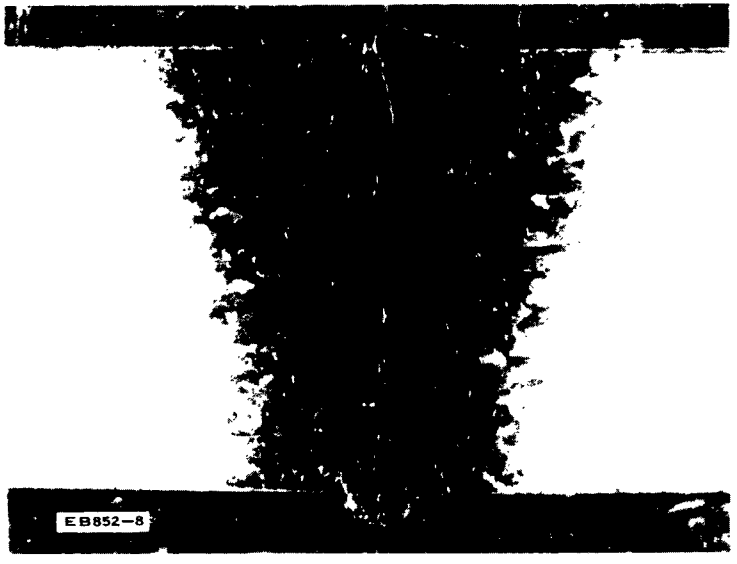

Figure 109. Final Weld Cross-section; X20; 0.125-Inch B120VCA Ti; Welded in the Solution Treated and Aged Condition

Figure 110. Final Weld Microstructure; X100; 0.125-Inch B120VCA Ti; Welded in the Solution Treated and Aged Condition

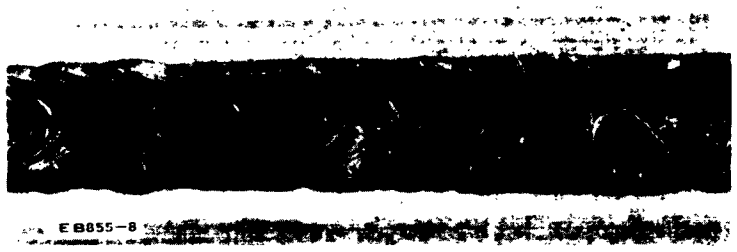

Figure 111. Final Weld Top Bead; X10; 0.125-Inch B120VCA Ti; Welded in the Solution-Treated Condition and Aged After Welding

Figure 112. Final Weld Bottom Bead; X10; 0.125-Inch B120VCA Ti; Welded in the Solution-Treated Condition and Aged After Welding

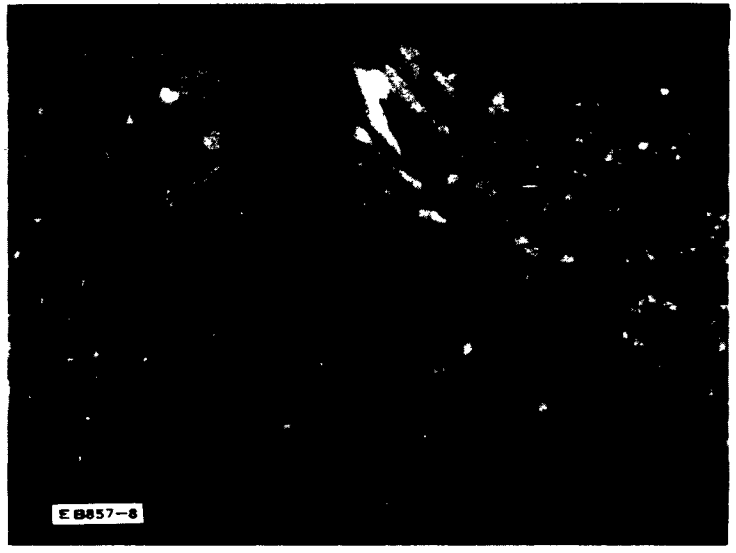

Figure 113. Final Weld Cross-section; X20; 0.125-Inch B120VCA Ti; Welded in the Solution-Treated Condition and Aged After Welding

Figure 114. Final Weld Microstructure; X100; 0.125-Inch B120VCA Ti; Welded in the Solution-Treated Condition and Aged After Welding

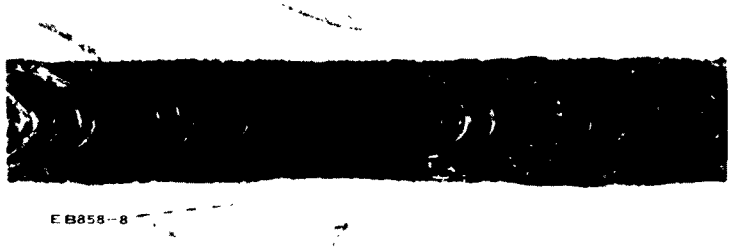

Figure 115. Final Weld Top Bead; X10; 0.125-Inch B120VCA Ti; Welded in the Solution-Treated, Cold Rolled, and Aged Condition

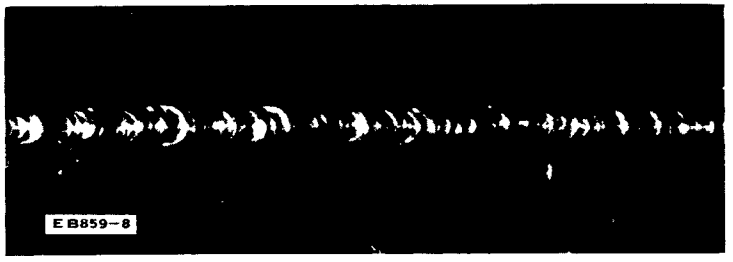

Figure 116. Final Weld Bottom Bead; X10; 0.125-Inch B120VCA Ti; Welded in the Solution Treated, Cold Rolled, and Aged Condition

Figure 117. Final Weld Cross-Section; X20; 0.125-Inch B120VCA Ti; Welded in the Solution-Treated, Cold Rolled, and Aged Condition

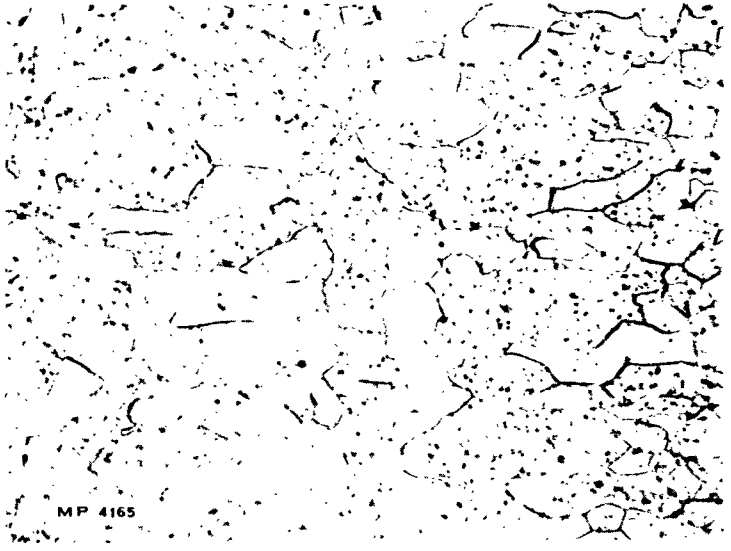

Figure 118. Final Weld Microstructure; X100; 0.125-Inch B120VCA Ti; Welded in the Solution-Treated, Cold Rolled, and Aged Condition

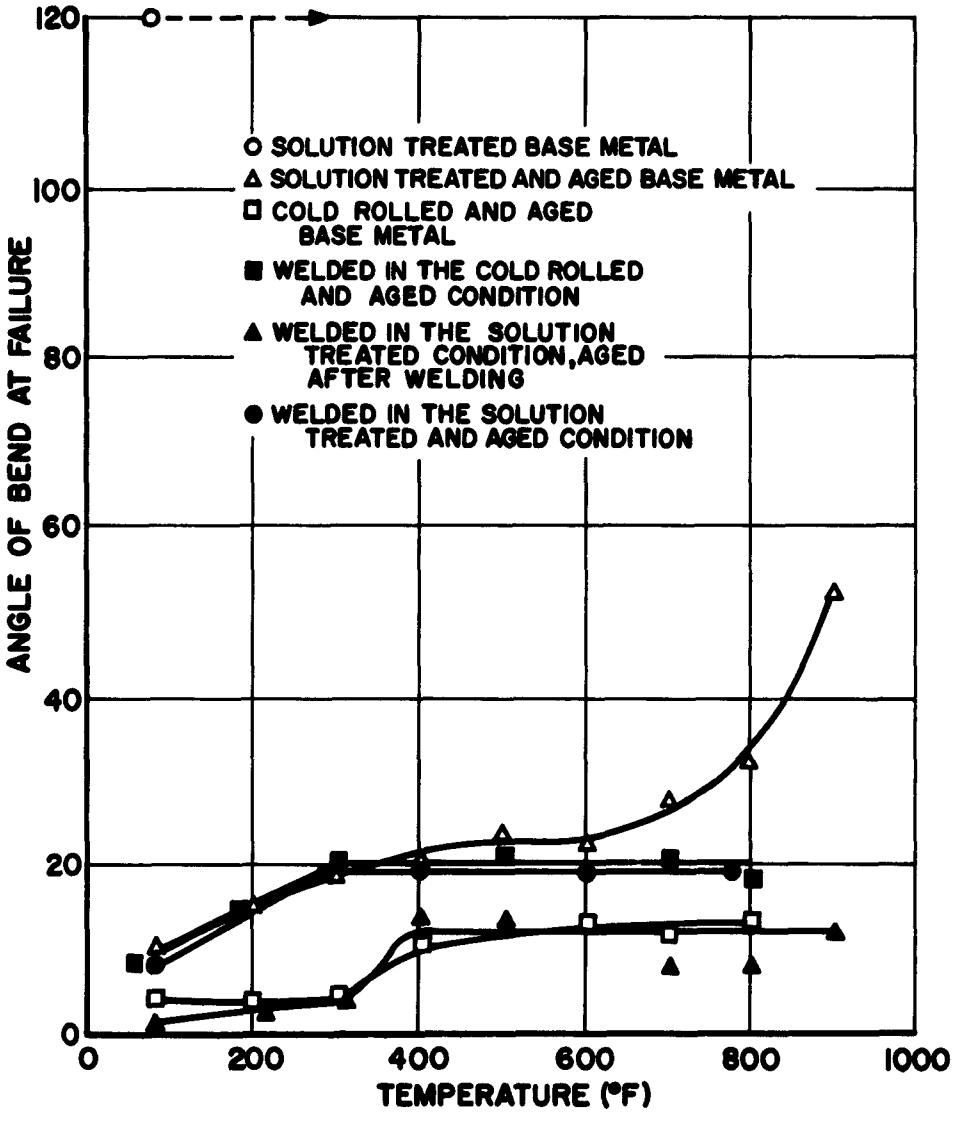

Figure 119. Bend Angle vs. Temperature; 0.125-Inch B120VCA Titanium Weldments

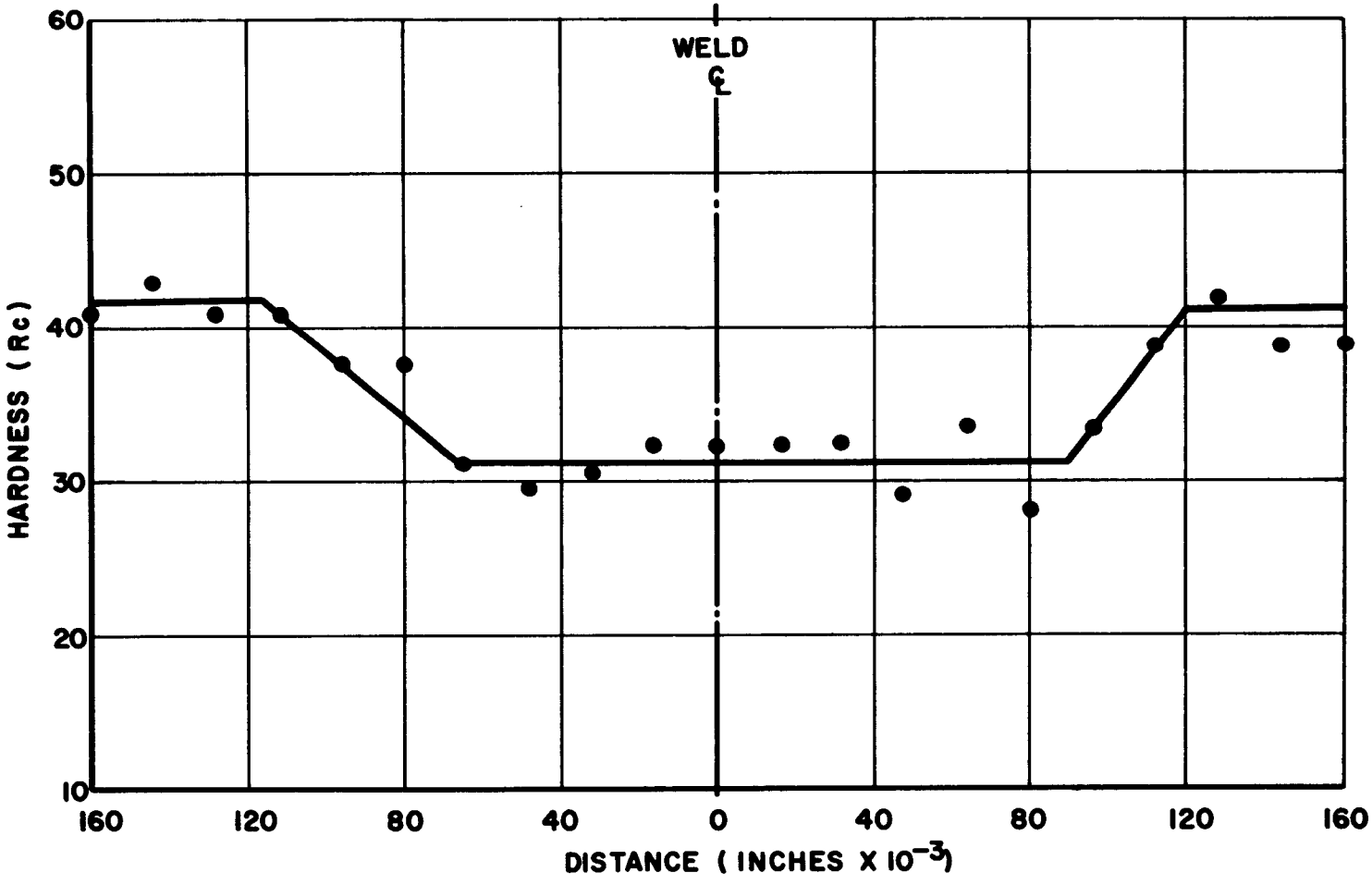

Figure 120. Hardness Profile; 0.125-Inch B120VCA Titanium; Welded in the Solution Treated and Aged Condition

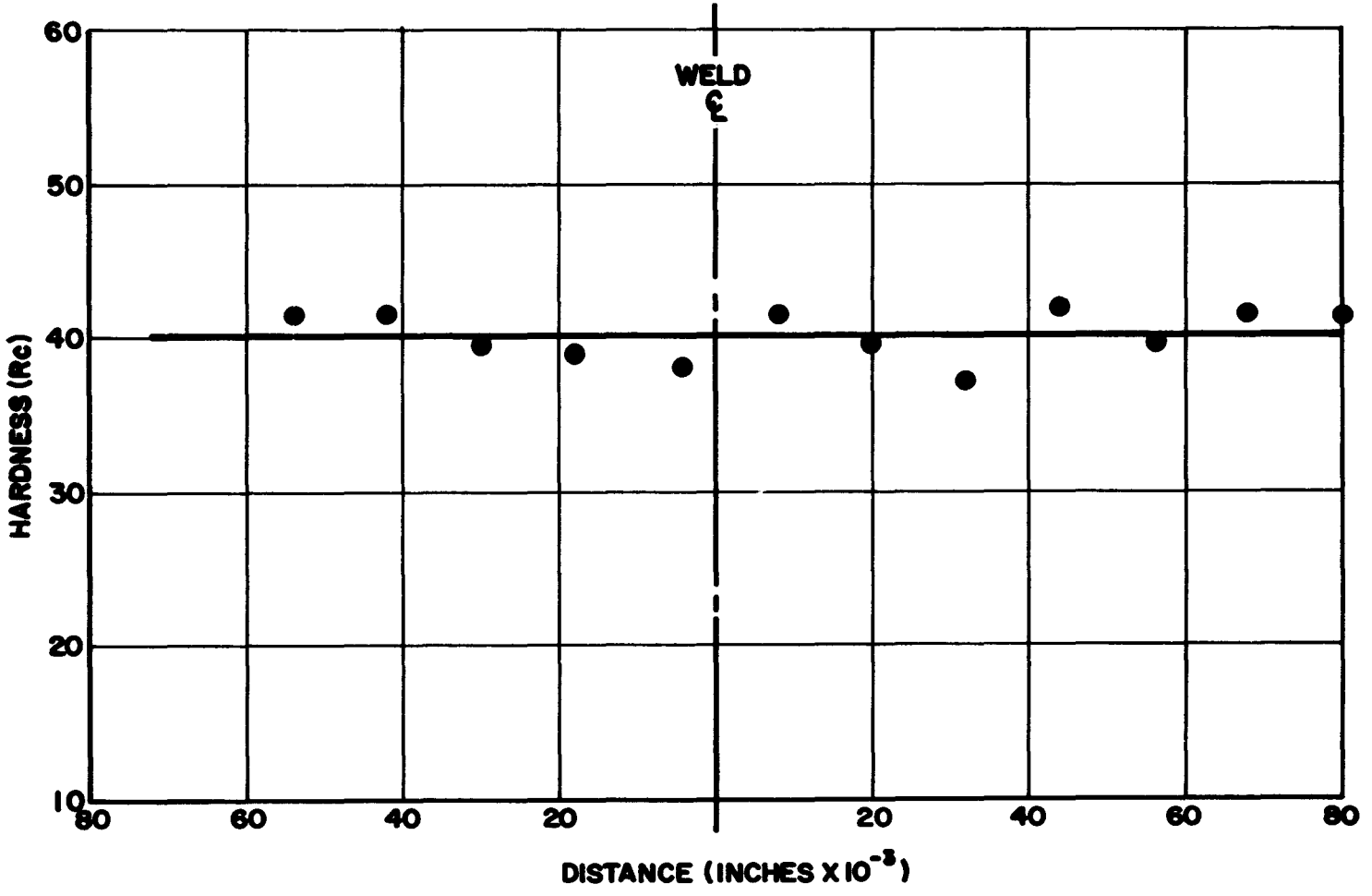

Figure 121. Hardness Profile; 0.125-Inch BI20VCA Titanium; Welded in the Solution-treated Condition and Aged After Welding

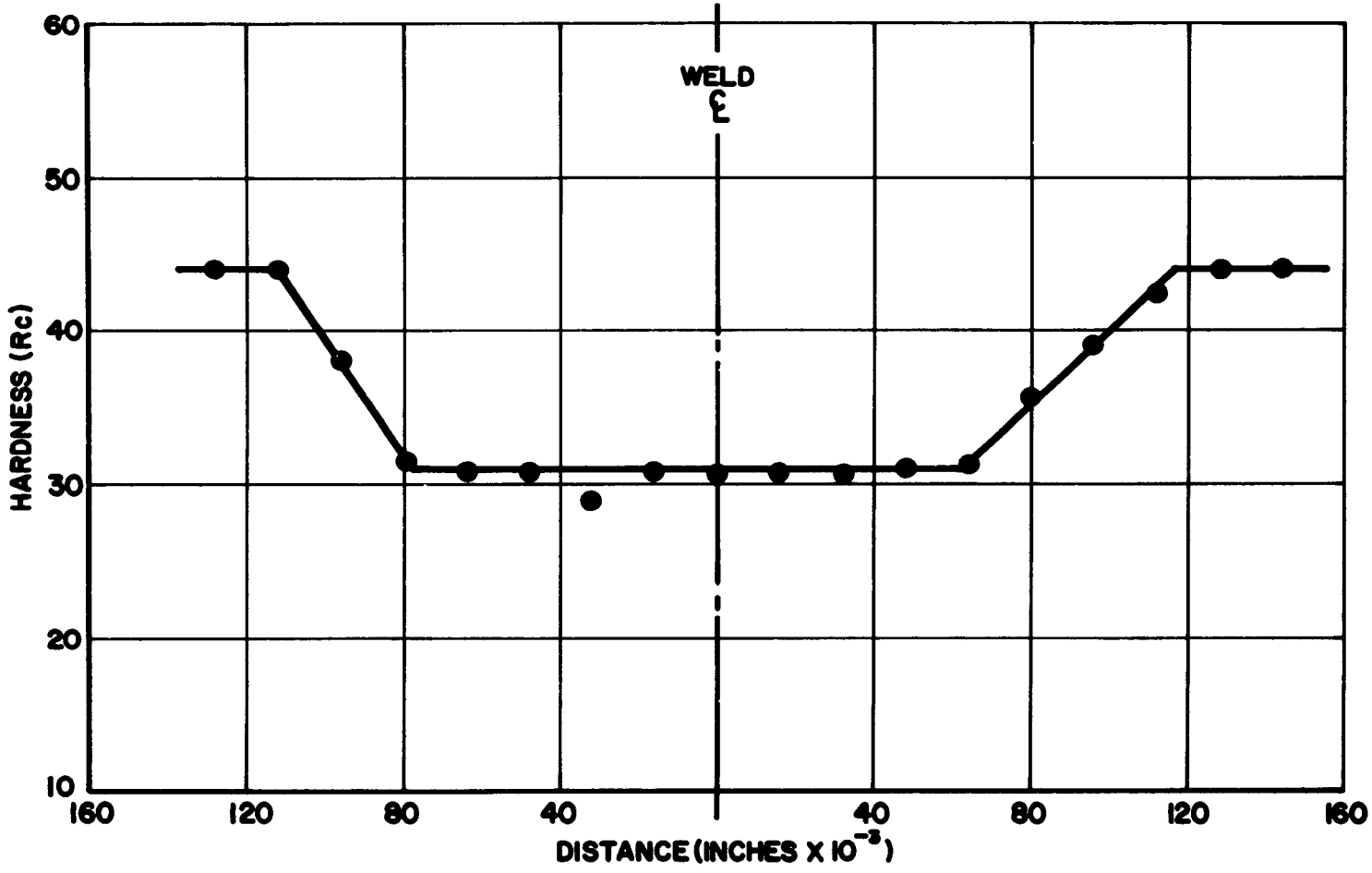

Figure 122. Hardness Profile; 0.125-Inch B120VCA Titanium; Welded in the Solution Treated, Cold Rolled, and Aged Condition

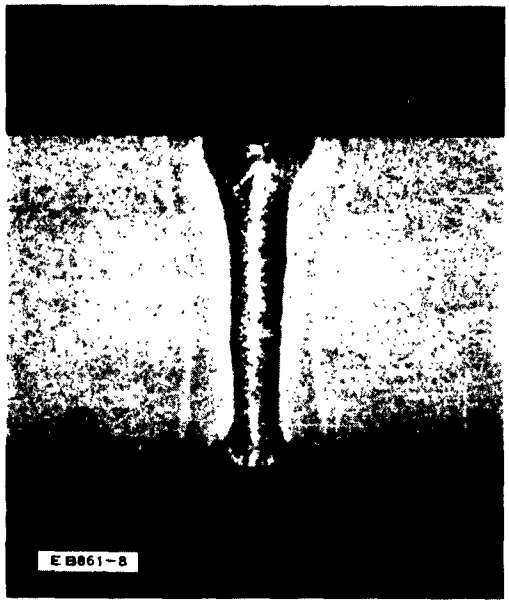

Figure 123. Trial Weld Cross-section; X20; 0.090-Inch D6AC; 130KV, 15 ma, 60 ipm

Figure 124. Trial Weld Cross-section; X20; 0.090-Inch D6AC; 150 KV, 10 ma, 55 ipm, 0.010-Inch X Oscillation

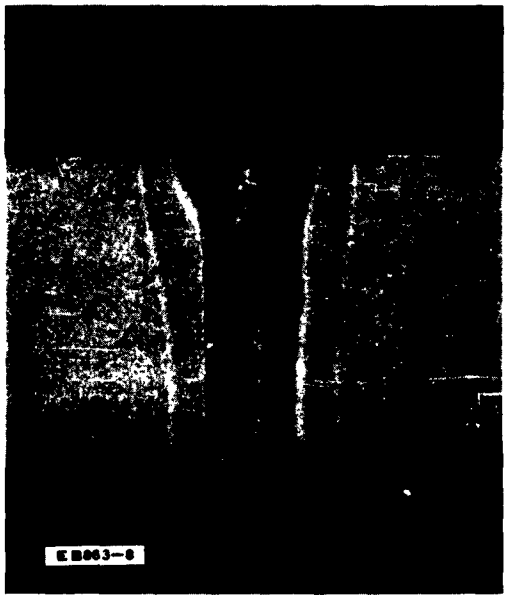

Figure 125. Trial Weld Cross-section; X20; 0.090-Inch D6AC; 130 KV, 15 ma, 70 ipm, 0.010-Inch Y Oscillation

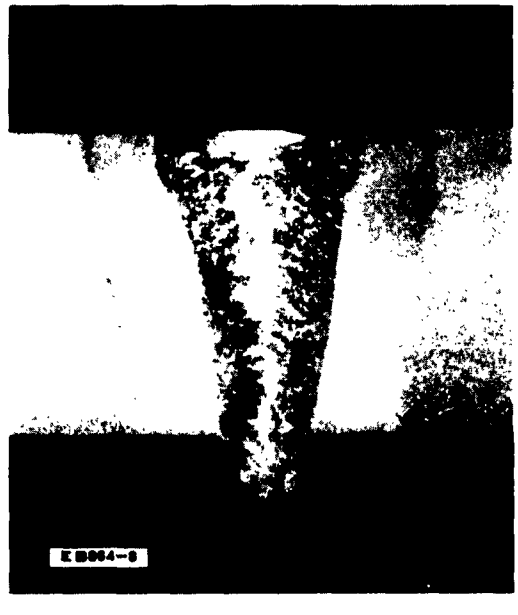

Figure 126. Trial Weld Cross-section; X20; 0.090-Inch D6AC; 150 KV, 10 ma, 55 ipm, 0.015-Inch Y Oscillation

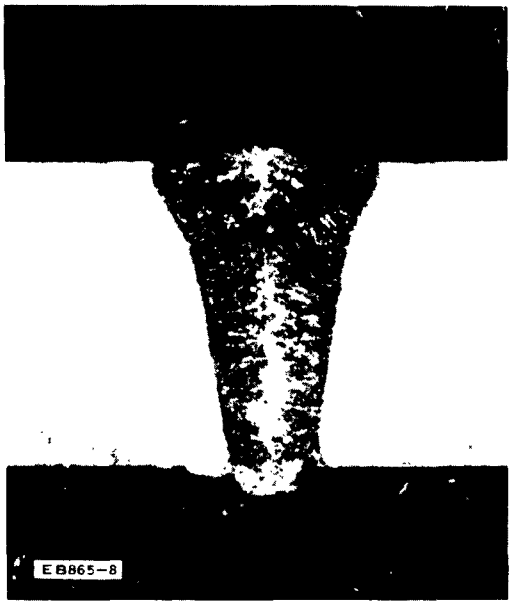

Figure 127. Trial Weld Cross-section; X20; 0.090-Inch D6AC; 150 KV, 10 ma, 55 ipm, 0.015-Inch Circular Oscillation

Figure 128. Trial Weld Cross-section; X20; 0.090-Inch D6AC; 150 KV, 11 ma, 50 ipm, 0.010-Inch Diameter Beam

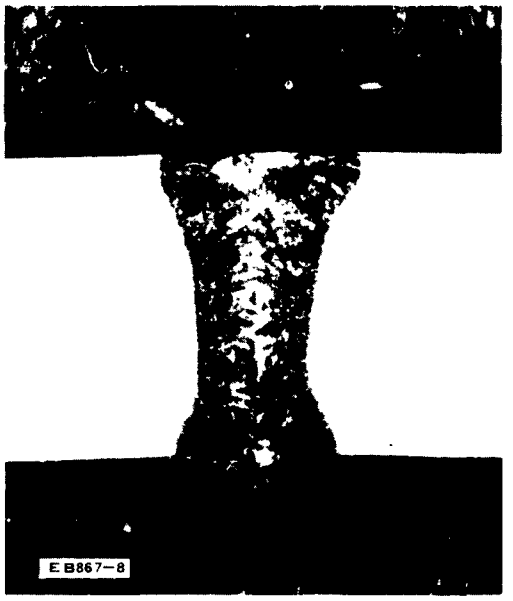

Figure 129. Trial Weld Cross-section; X20; 0.090-Inch D6AC; 150 KV, 15 ma, 58 ipm, 0.015-Inch Diameter Beam

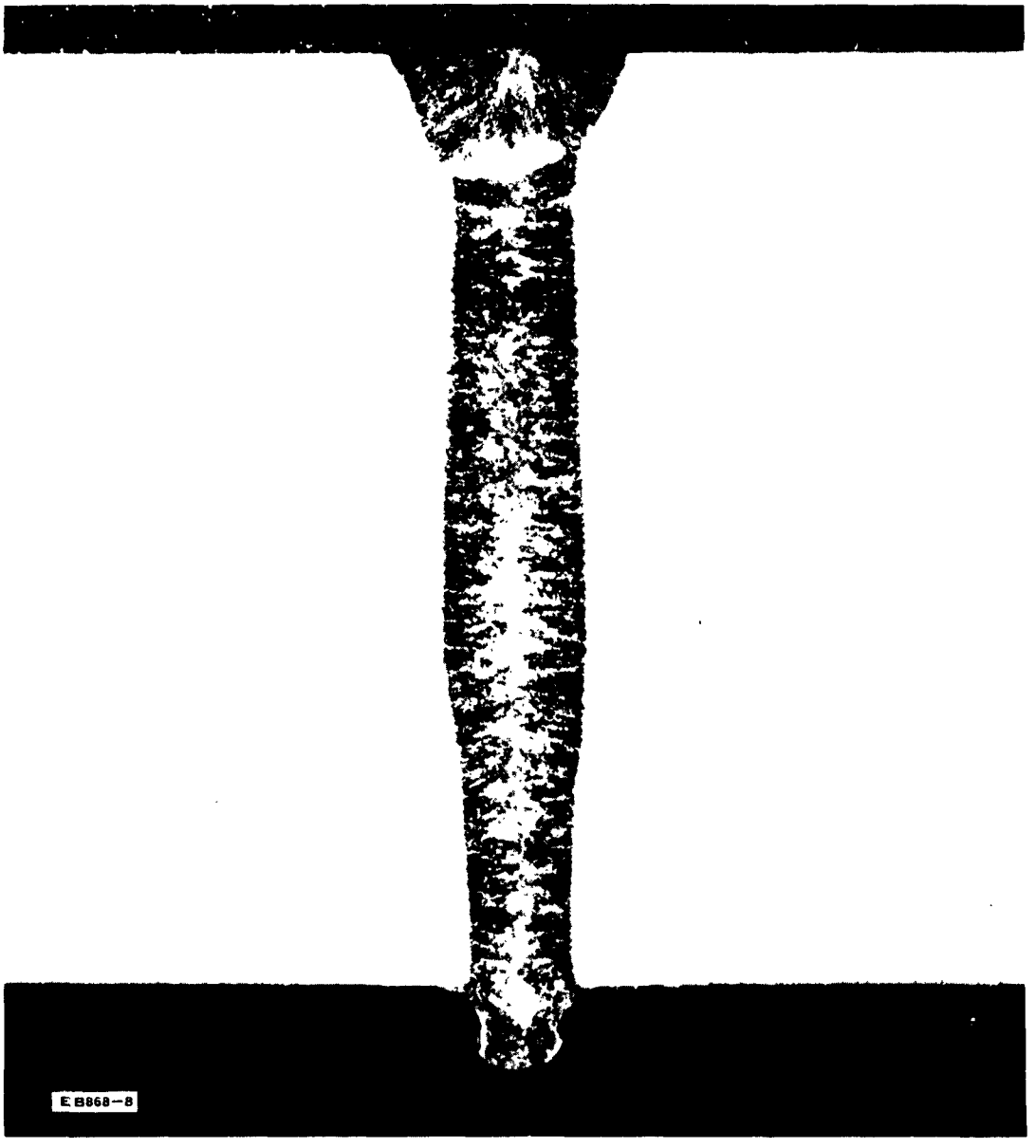

Figure 130. Trial Weld Cross-section; X20; 0.290-Inch D6AC; 150 KV, 21 ma, 24 ipm, 0.005-Inch Y Oscillation, With Second Clean-up Pass

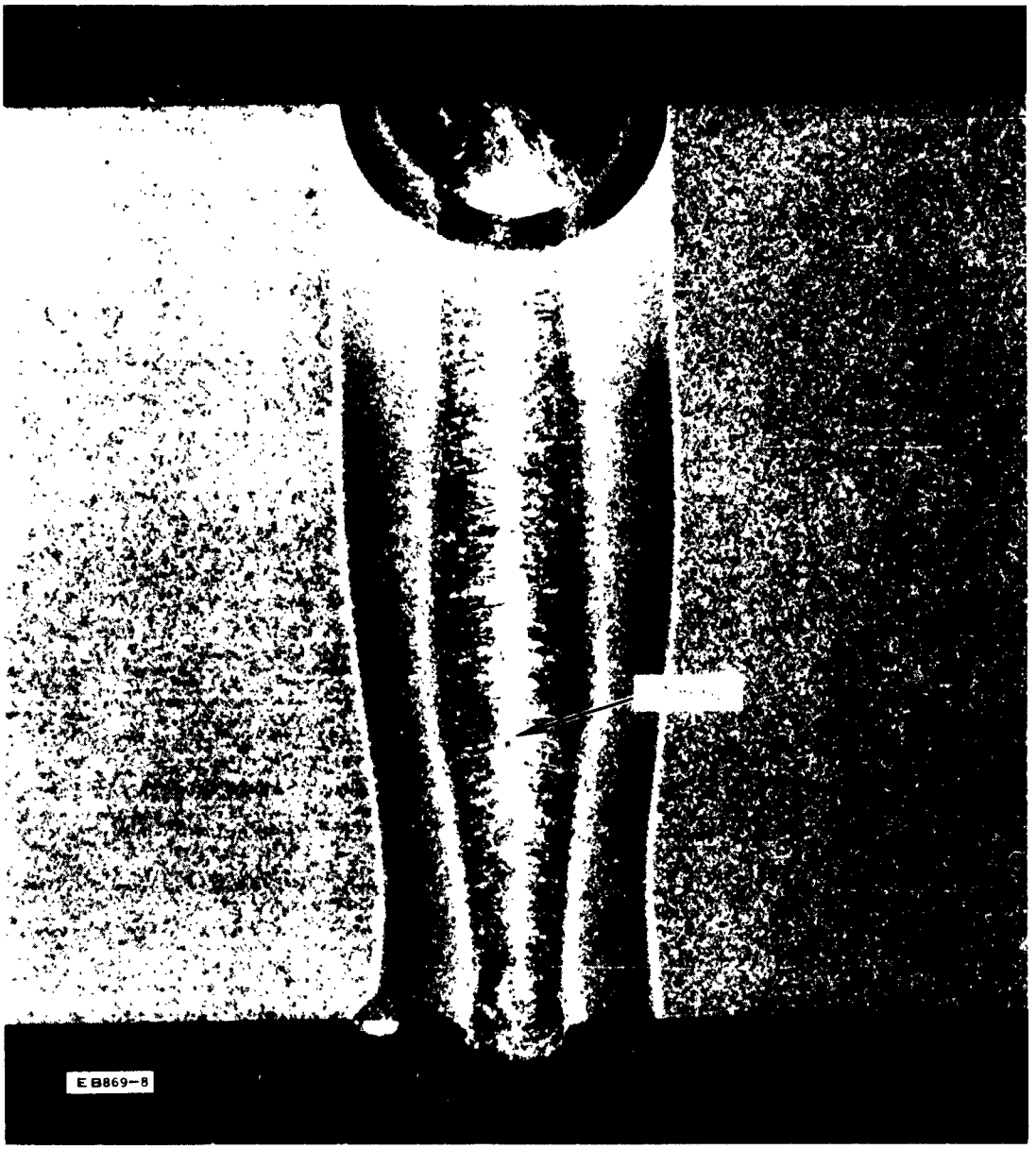

Figure 131. Trial Weld Cross-section; X20; 0.290-Inch D6AC

Figure 132. Final Weld Top Bead; X10; 0.090-Inch D6AC; Welded in the Annealed Condition and Heat Treated After Welding

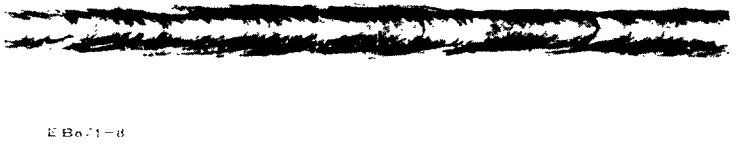

Figure 133. Final Weld Bottom Bead; X10; 0.090-Inch D6AC; Welded in the Annealed Condition and Heat Treated After Welding

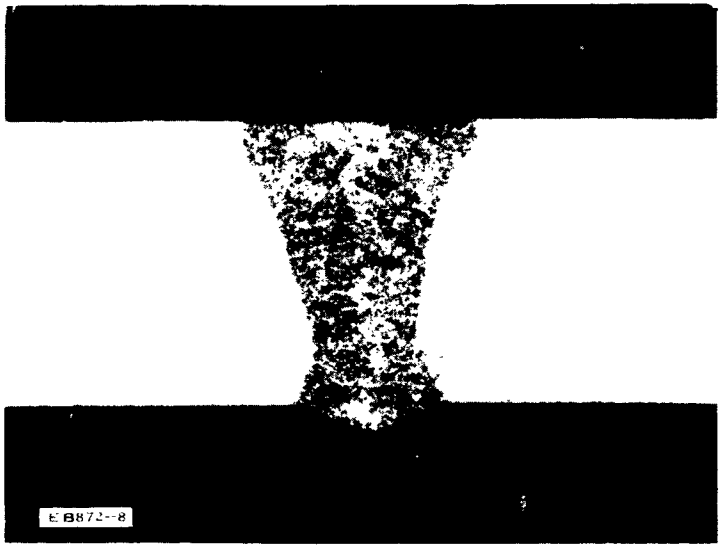

Figure 134. Final Weld Cross-section; X20; 0.090-Inch D6AC; Welded in the Annealed Condition and Heat Treated After Welding

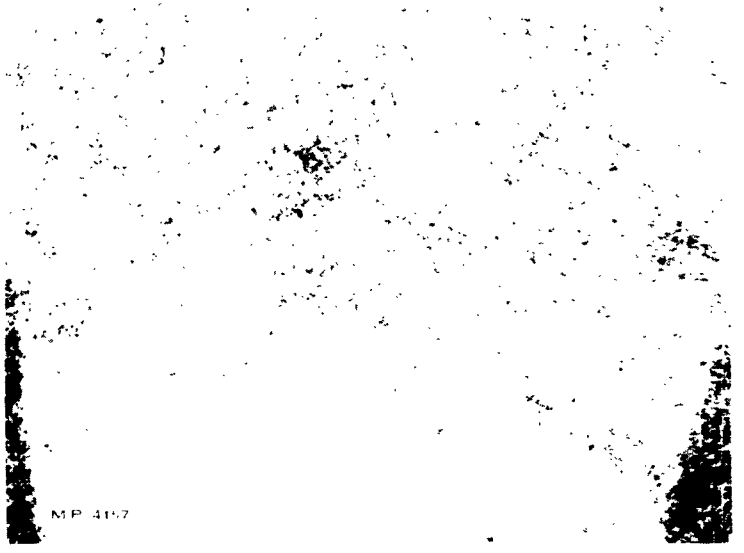

Figure 135. Final Weld Microstructure; X100; 0.090-Inch D6AC; Welded in the Annealed Condition and Heat Treated After Welding

Figure 136. Final Weld Top Bead; X10; 0.090-Inch D6AC; Welded in the Heat Treated Condition

Figure 137. Final Weld Bottom Bead; X10; 0.090-Inch D6AC; Welded in the Heat Treated Condition

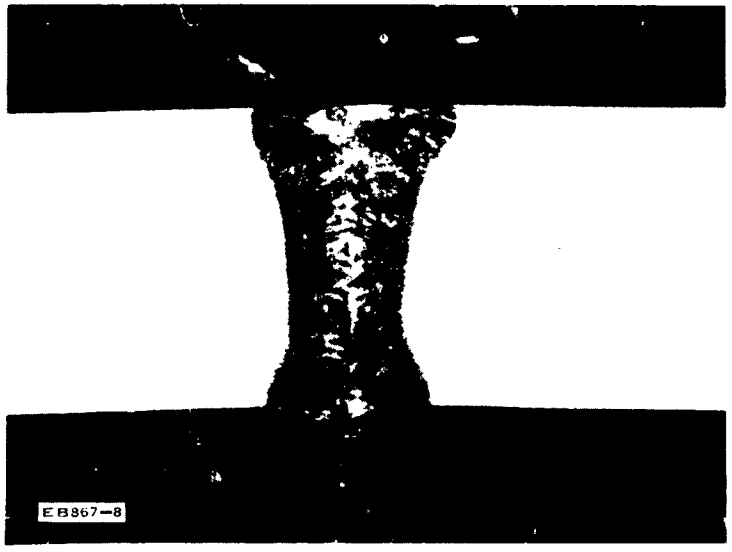

Figure 138. Final Weld Cross-section; X20; 0.090-Inch D6AC; Welded in the Heat Treated Condition

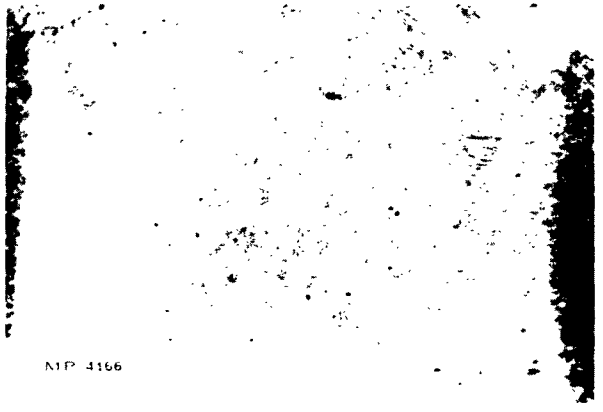

Figure 139. Final Weld Microstructure; X100; 0.090-Inch D6AC; Welded in the Heat Treated Condition

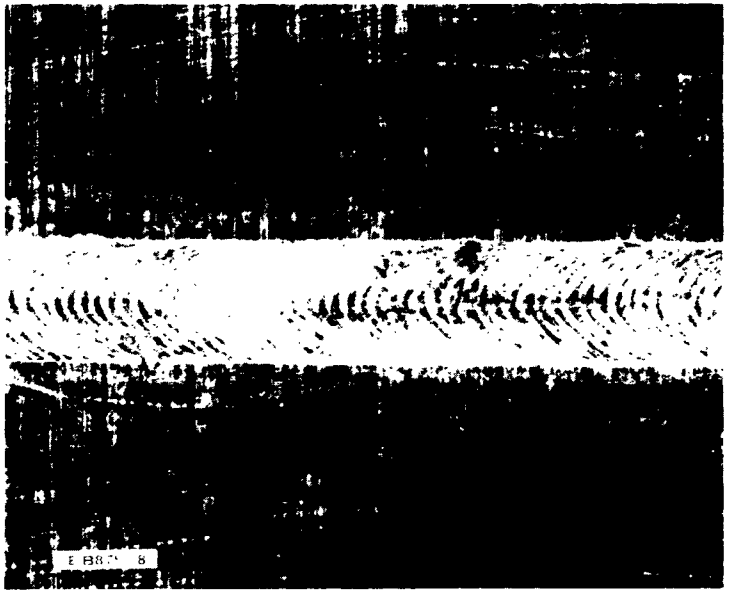

Figure 140. Final Weld Top Bead; X10; 0.290-Inch D6AC; Welded in the Annealed Condition and Heat Treated After Welding

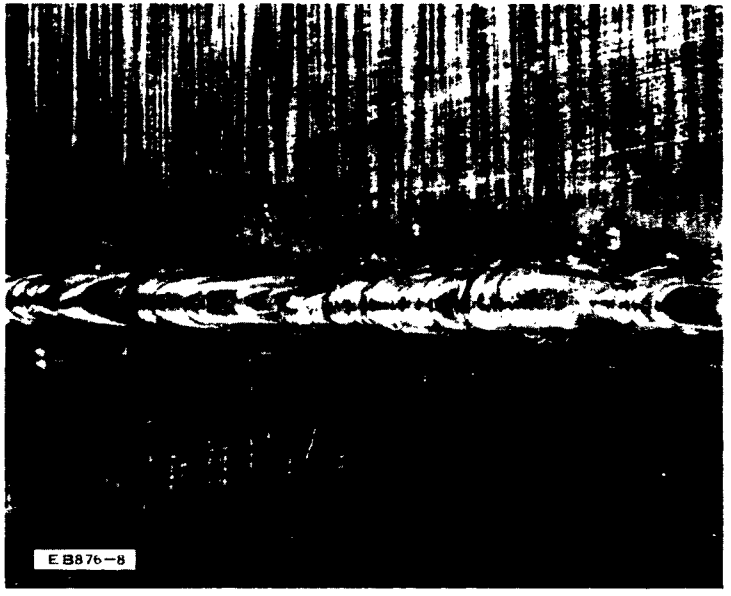

Figure 141. Final Weld Bottom Bead; X10; 0.290-Inch D6AC; Welded in the Annealed Condition and Heat Treated After Welding

Figure 142. Final Weld Cross-section; X20; 0.290-Inch D6AC; Welded in the Annealed Condition and Heat Treated After Welding

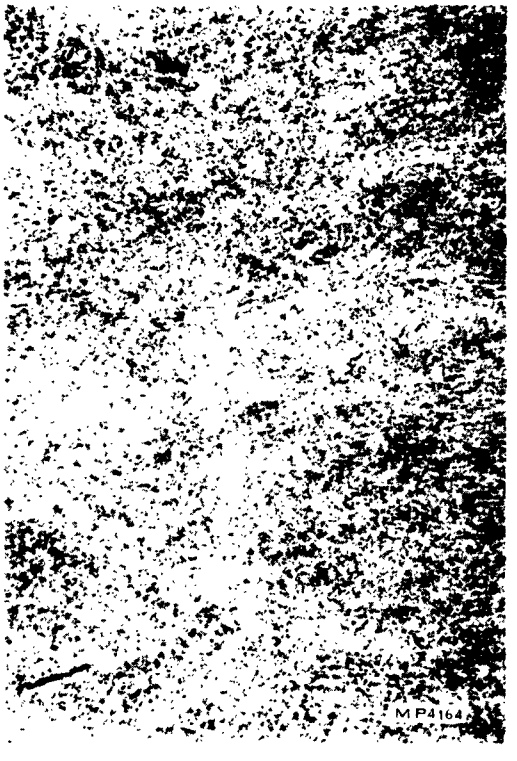

Figure 143. Final Weld Microstructure; X100; 0.290-Inch D6AC; Welded in the Annealed Condition and Heat Treated After Welding

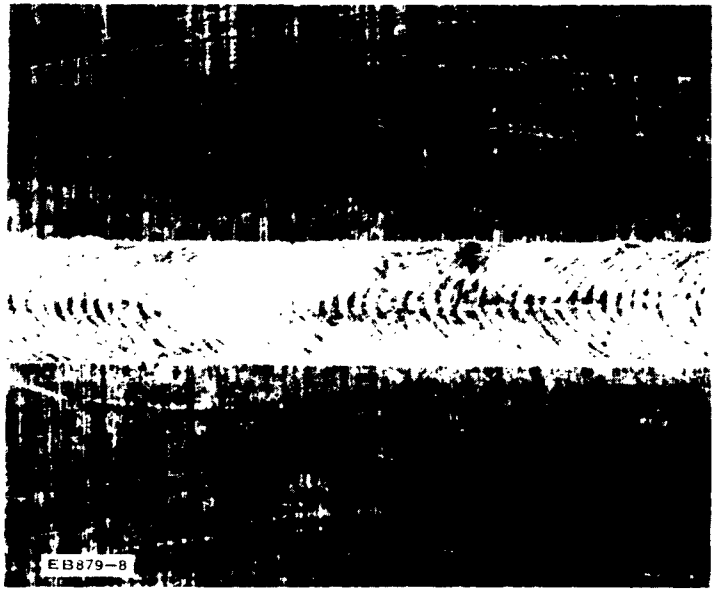

Figure 144. Final Weld Top Bead; X10; 0.290-Inch D6AC; Welded in the Heat Treated Condition

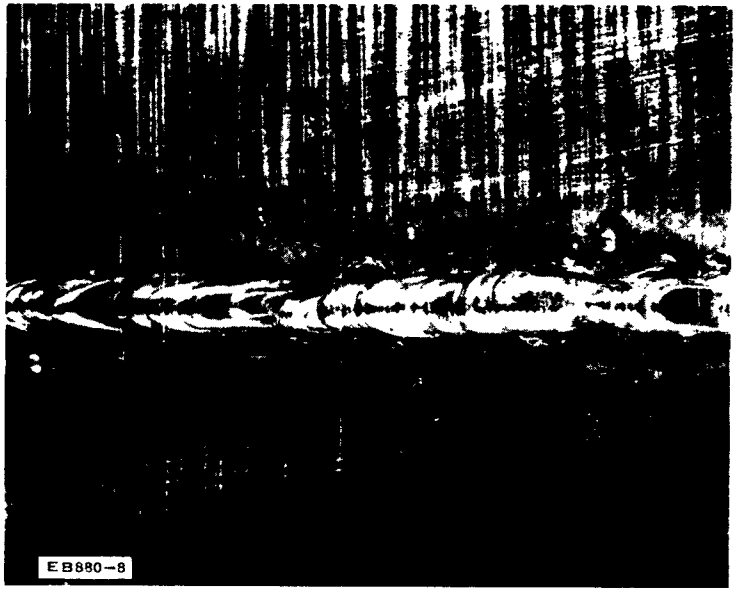

Figure 145. Final Weld Bottom Bead; X10; 0.290-Inch D6AC; Welded in the Heat Treated Condition

Figure 146. Final Weld Cross-section; X20; 0.290-Inch D6AC; Welded in the Heat Treated Condition

Figure 147. Final Weld Microstructure; X100; 0.290-Inch D6AC; Welded in the Heat Treated Condition

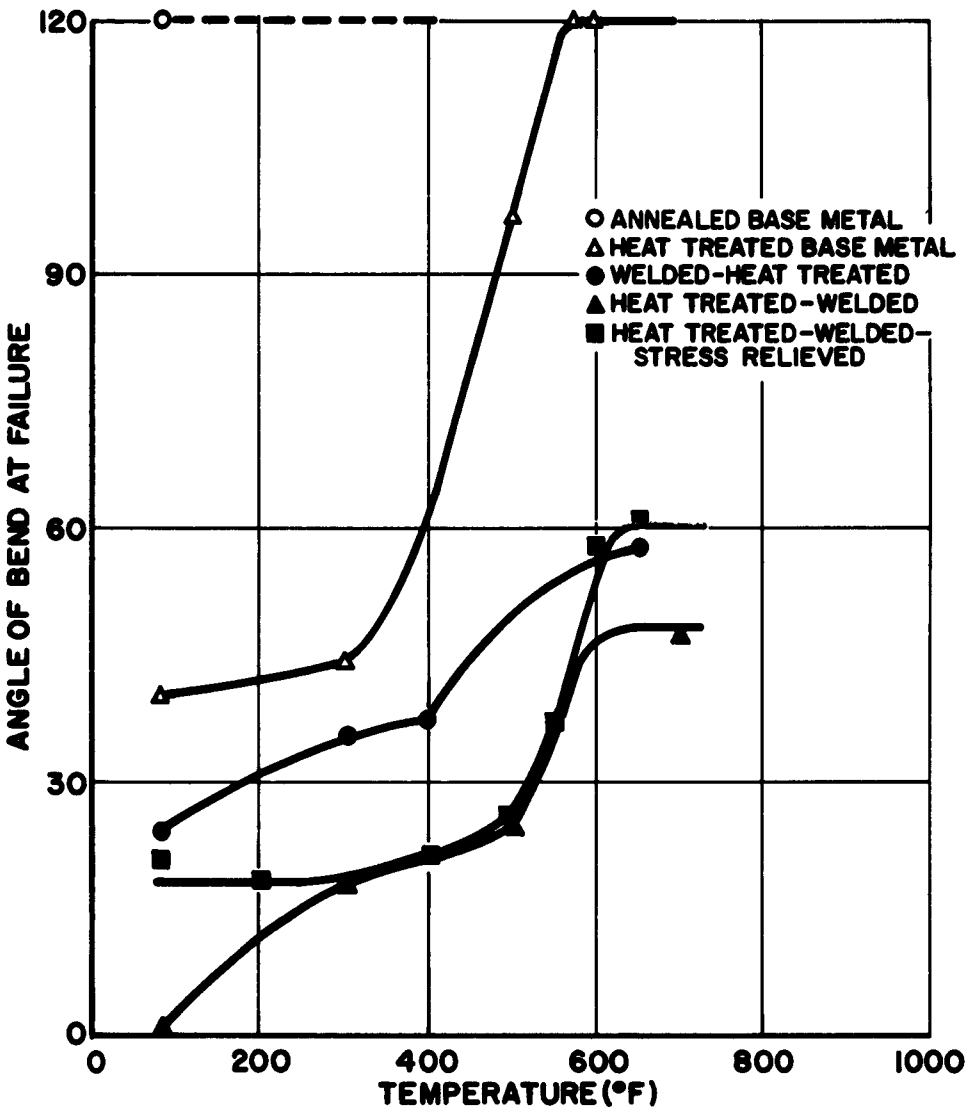

Figure 148. Bend Angle vs. Temperature; 0.090-Inch D6AC Steel

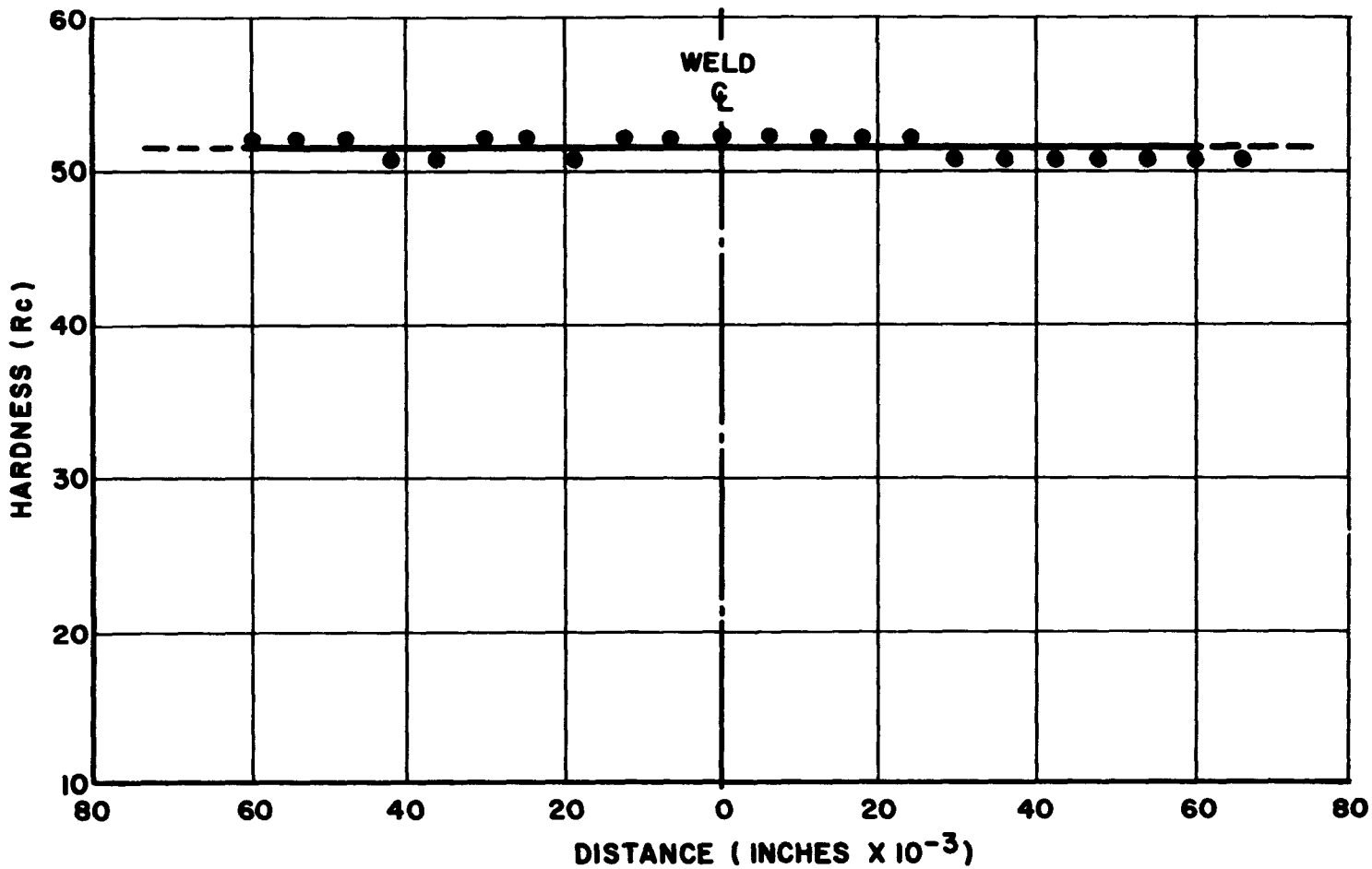

Figure 149. Hardness Profile; 0.090-Inch D6AC; Welded in the Annealed Condition and Heat Treated After Welding

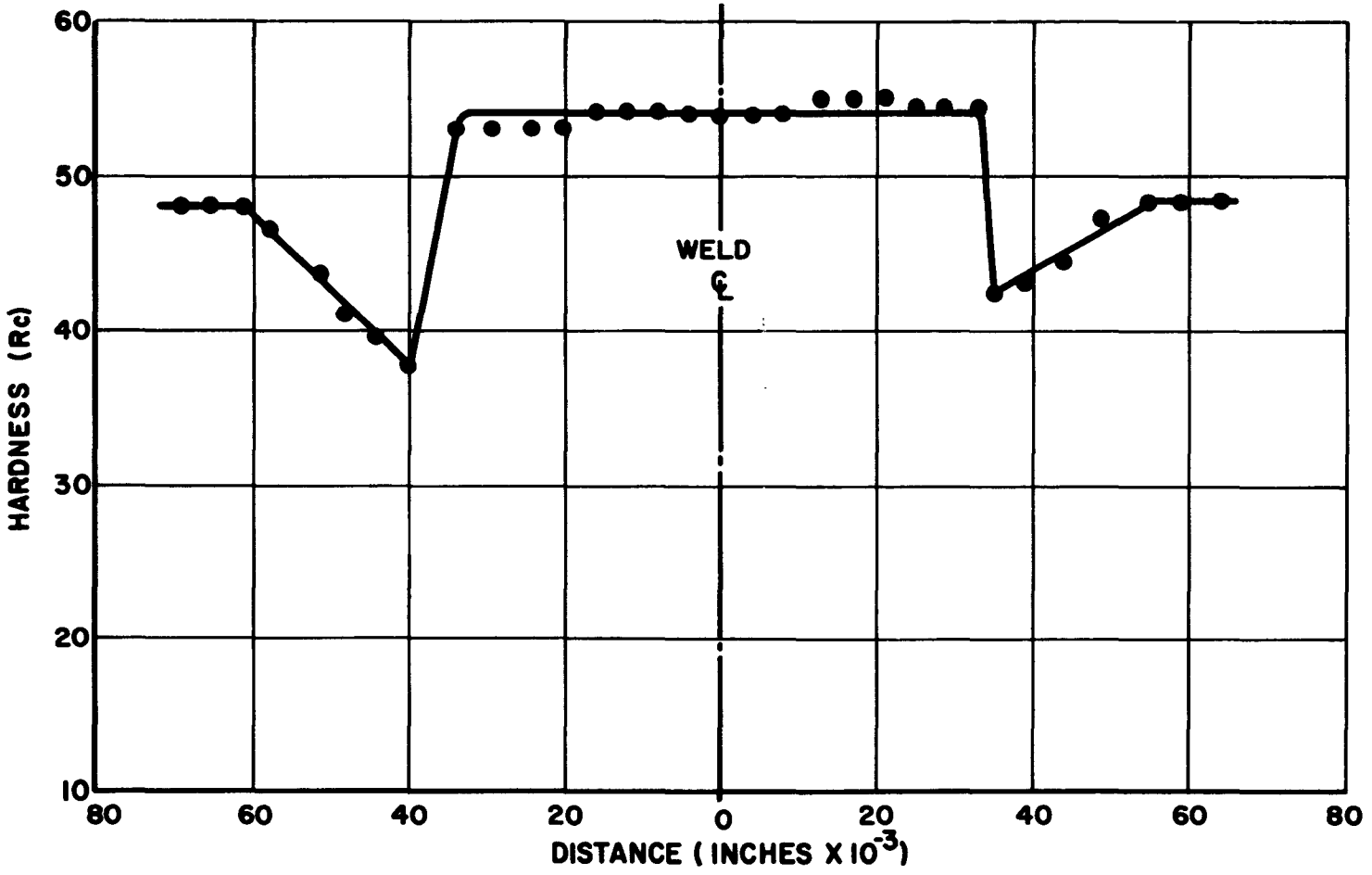

Figure 150. Hardness Profile; 0.090-Inch D6AC; Welded in the Heat Treated Condition

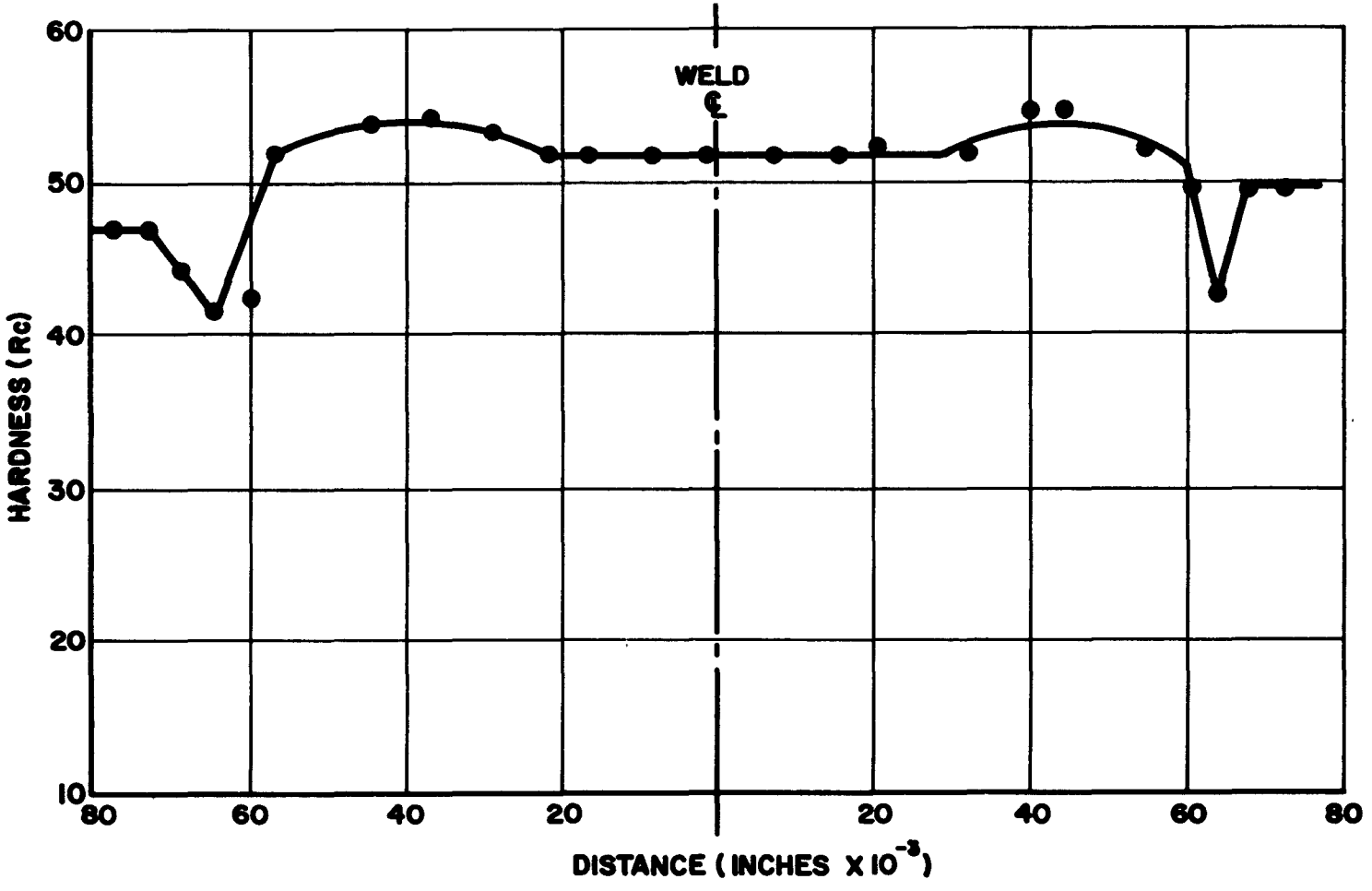

Figure 151. Hardness Profile; 0.090-Inch D6AC; Welded in the Heat Treated Condition; Stress Relieved After Welding

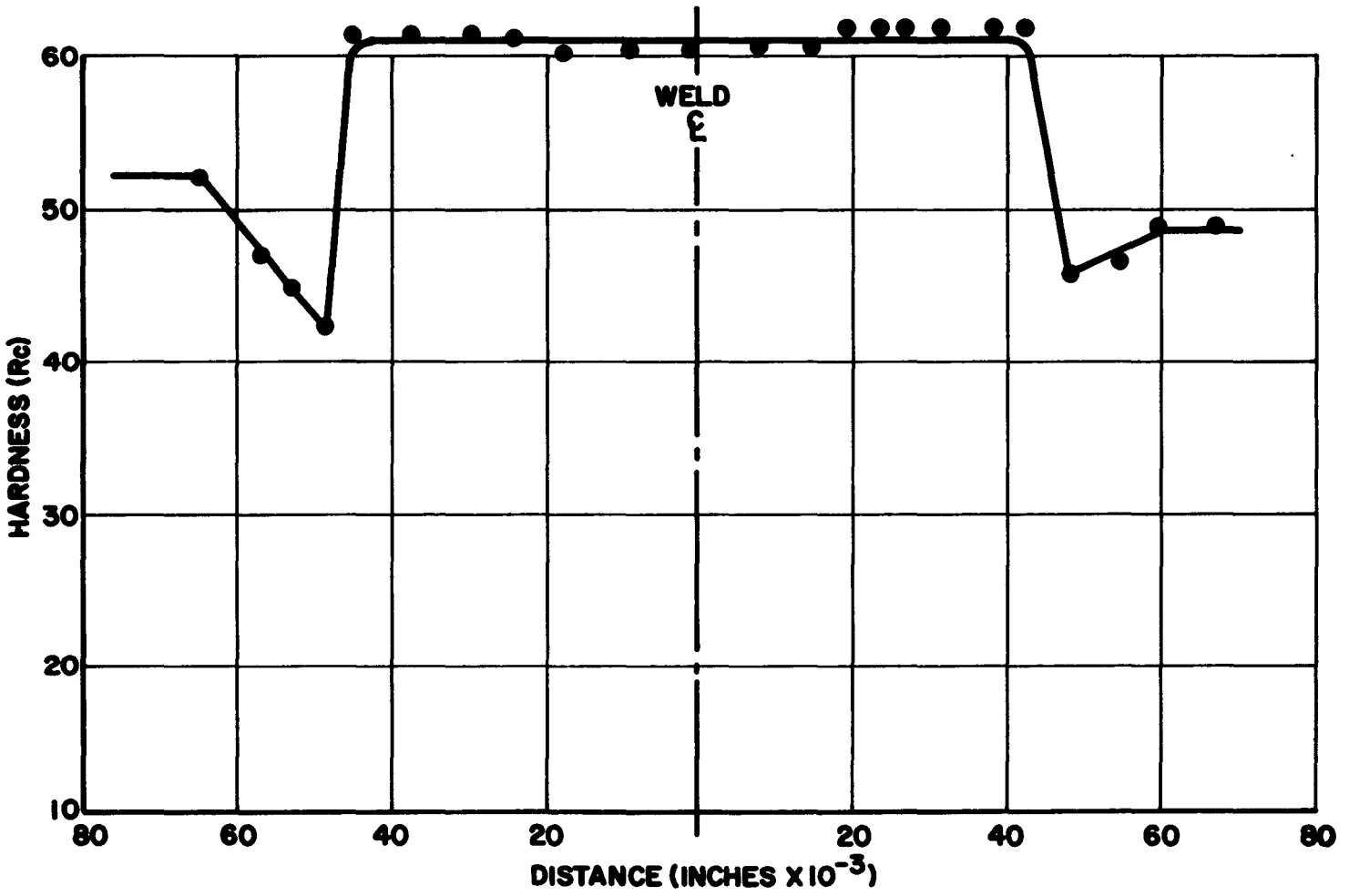

Figure 152. Hardness Profile; 0.290-Inch D6AC; Welded in the Heat Treated Condition; Through Region of Single Pass

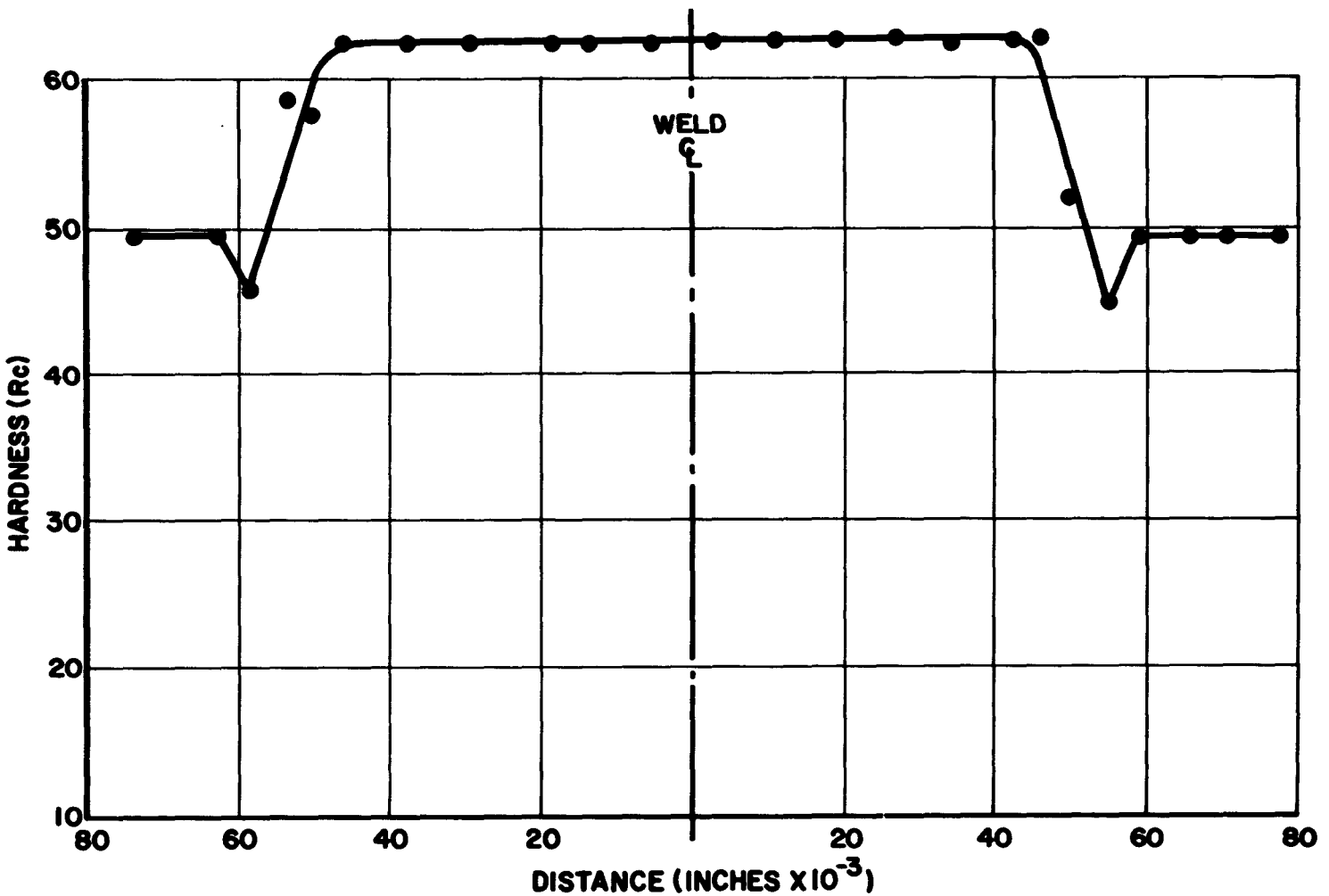

Figure 153. Hardness Profile; 0.290-Inch D6AC; Welded in the Heat Treated Condition; Through Region of Clean-up Pass

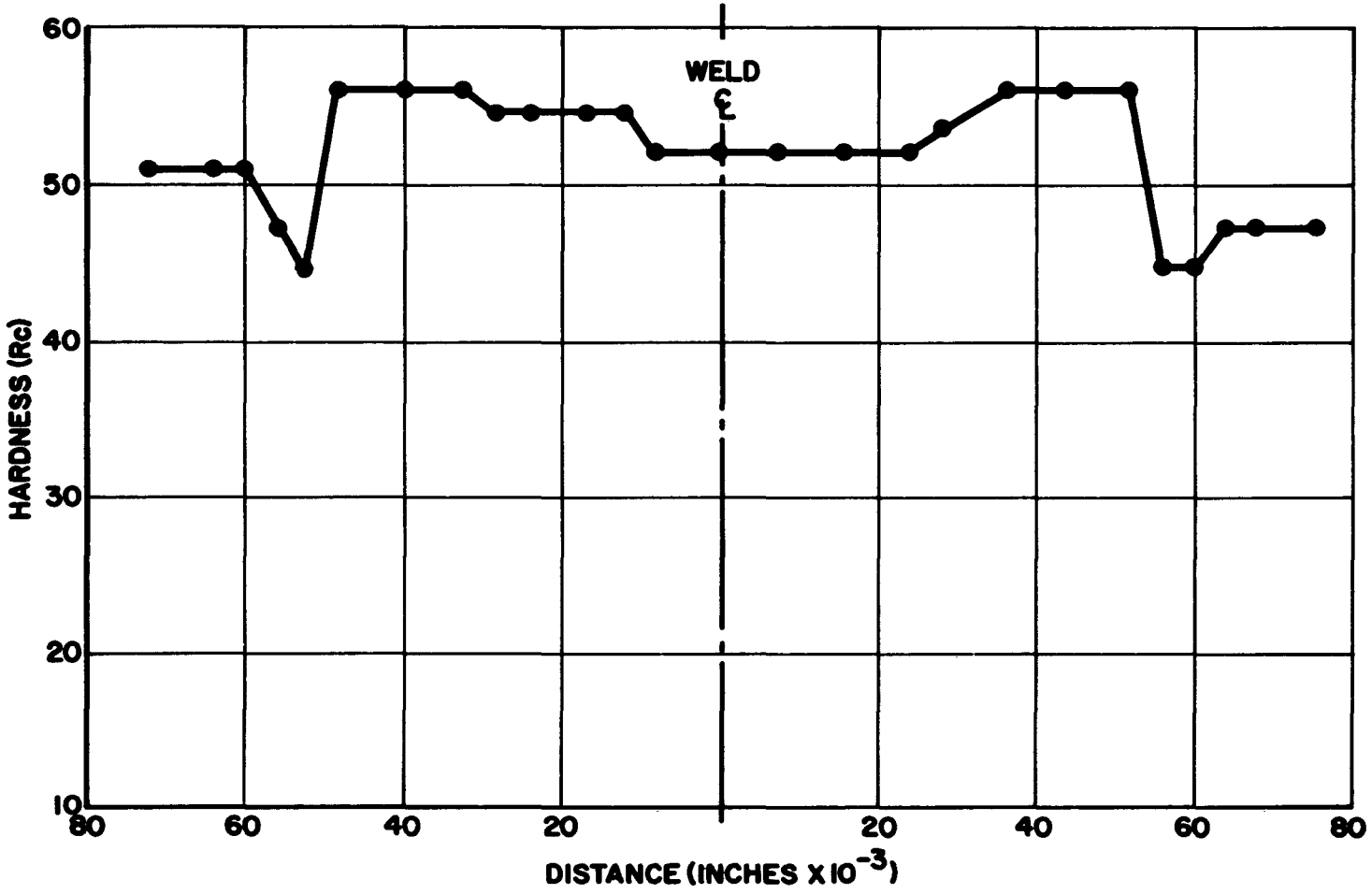

Figure 154. Hardness Profile; 0.290-Inch D6AC; Welded in the Heat Treated Condition; Through Region of Heat-affect from Clean-up Pass

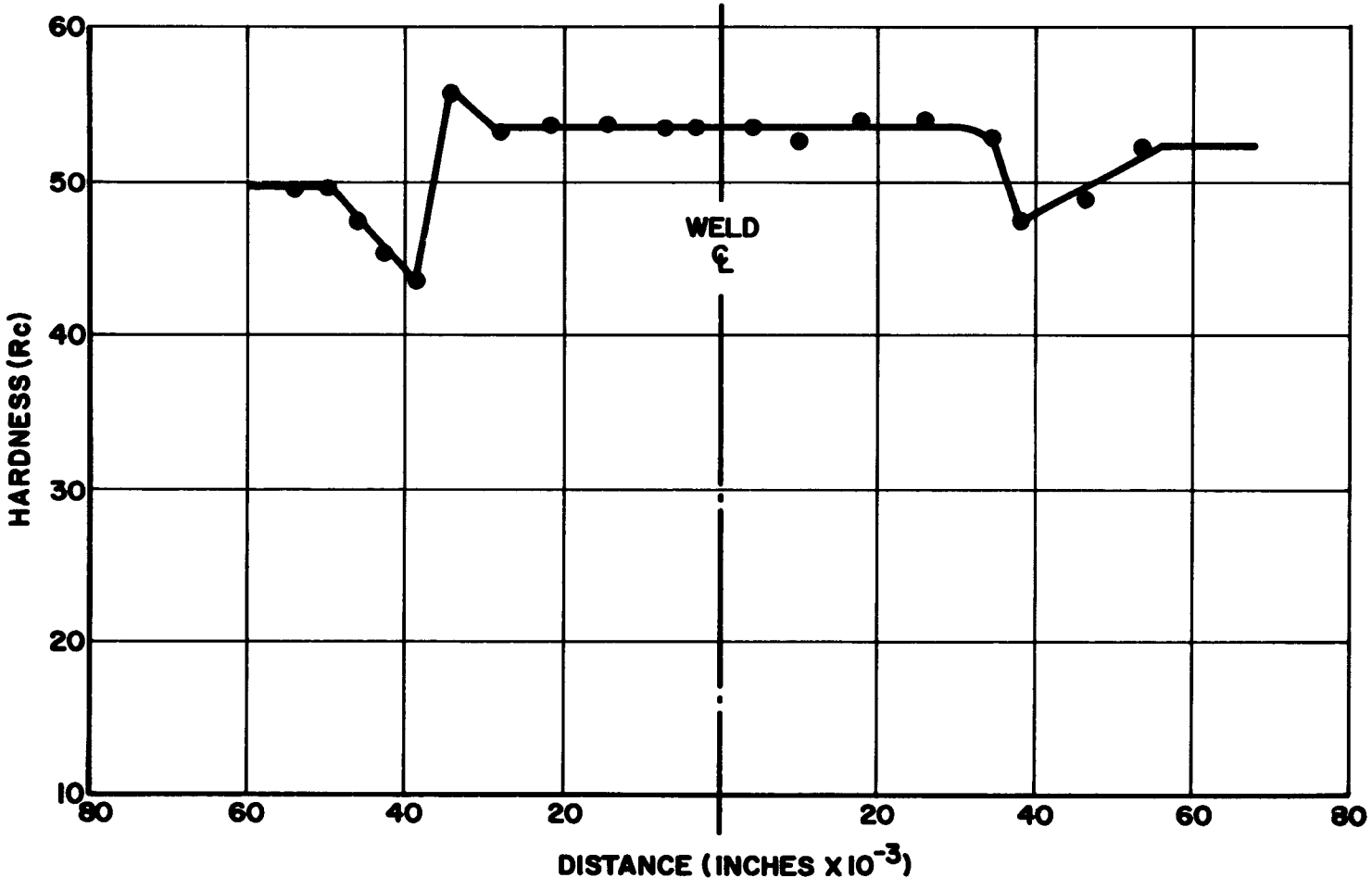

Figure 155. Hardness Profile; 0.290-Inch D6AC; Welded in the Heat Treated Condition and Stress Relieved After Welding; Through Region of Clean-up Pass

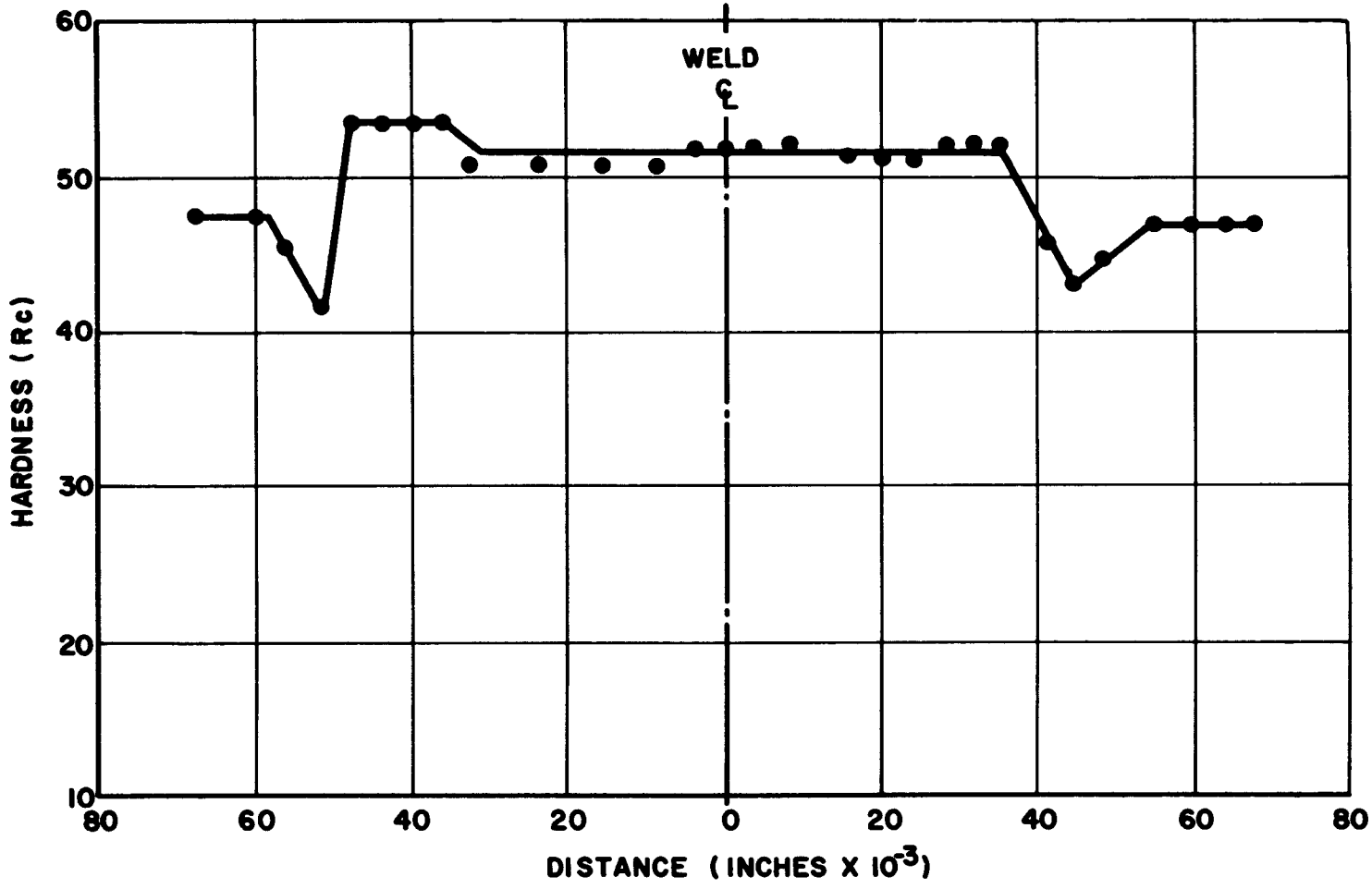

Figure 156. Hardness Profile; 0.290-Inch D6AC; Welded in the Heat Treated Condition and Stress Relieved After Welding; Through Region of Single Pass

APPENDIX

Evaluation of Fracture Toughness

APPENDIX

Evaluation of Fracture Toughness

The fracture toughness value ("G_c") indicates the ability of a material to resist failure due to the propagation of an already-present through-crack during load application. It should be noted that standard mechanical tests do not measure this property; i.e. the tensile test, the fatigue test, the standard notch tensile test, and even the standard impact test which measures the energy to fail an unnotched or notched specimen by causing a crack which ultimately leads to failure.

Fracture toughness tests are currently being used to determine the relative merit of different high strength materials for use in rocket cases at specific levels of yield strength. While the yield strength may be readily measured from a load-deflection curve of an unnotched tensile specimen, fracture toughness evaluation is somewhat more involved since measurement of crack growth of a notched tensile specimen is needed in addition to the load-deflection curve. Specifically, determination of the slow crack growth up to the onset of fast fracture is necessary. This crack length is then used to calculate "G_c", the value of the energy necessary for rapid crack extension (also known as the critical crack extension force, fracture extension force, or fracture toughness).

A comprehensive survey of techniques 1 through 21 currently being used to evaluate fracture toughness was conducted prior to final choice of the evaluation method used in the subject program.

Briefly, edge-notch tensile tests were eliminated because they are currently considered more applicable as a screening method. Precracked Charpy-specimen tests are still in the early stages of development, and in any case, although economical, are not readily suitable for testing electron beam weldments in the as-welded condition. Various bend tests are in the early stages of development, and bulge tests are not considered applicable for the butt-welds being tested.

The center-notch tensile test was finally chosen because of its accuracy, particular suitability for electron beam weldments, and general acceptance by industry. However, the ink-staining technique originally proposed for measuring slow crack growth was dropped for three reasons: 1) considerable judgment as to the quantity of ink applied to the notch root was required--too much ink caused ink splatter at fast fracture which in turn caused an overestimate of fast fracture crack length, and too little ink caused exhaustion of the fluid prior to fast fracture which in turn caused an underestimate of the fast fracture crack length; 2) ink has been proved to cause an environmental effect which leads to an erroneous G_c evaluation; and 3) ink staining techniques are insensitive to the stress field disturbance resulting from plastic flow relaxation at the crack tip and thus necessitate a correction factor for the plastic zone at the crack tip in the calculation of G_c.

The specimen used for center notch tensile testing was shown in

Figures 17 and 18. Internal notching of the specimen was accomplished by spark-erosion machining. A two-ampere discharge current was used to produce a smooth sided cut and a maximum notch tip radius of 0.005 inch. The notch tips were then fatigue cracked by alternate bending in a Krouse plate cyclic bending machine. Base-metal specimens were easily through-cracked, (except for an infinitesimally small section at the neutral axis) using zero (0) mean stress.

Because of weld metal protrusion, welded specimens required a small mean stress causing more tension on the root side in order to produce fairly even "wing" cracks.

In a valid fracture - toughness test the crack-tip plastic zone is small in relation to the crack dimensions and the elastic stress field[19]. Under such conditions the effective stiffness of the specimen containing the crack will be a function of the extent by which the specimen has been parted by the crack. With crack growth, less of the section remains to support the load, and the strains become correspondingly higher, with the result that the load to extension ratio or elastic modulus decreases. Ideally, a load - extension curve between points on either side of a centrally notched plate should show an initially constant slope characteristic of the notch length. Then as a crack propagates from the notch, a decrease in slope similar to the onset of plastic flow in an unnotched specimen would appear. This curve would differ from a normal stress-strain curve, however, in that upon unloading it would return to the origin along a straight line, the slope of which would be characteristic of the total crack length attained. Accordingly, a line drawn from the origin to any point on the curve would have a slope characteristic of the crack length attained at that point. Thus, measurement of extension of the notched specimen during loading up to the onset of fast fracture (the point of maximum load in a valid fracture toughness test) should provide a measure of the crack length at that point.

Applying the fracture-mechanics discussed above, a calibration curve[20] was drawn for two 3-inch wide specimens of different materials (refer to Figure A1). The apparent elastic moduli of the specimens were determined for a variety of center-slot lengths. The percent (%) decrease in modulus vs. increasing crack length was plotted. It was found that the curves were essentially linear for slot lengths between 1 and 1.5 (or even 1.8 inches) and furthermore, that the curves for the two different materials were very close together. From the slope of the curve in the straight-line range, an expression for crack growth as a function of percent decrease in the apparent modulus was obtained: crack growth (in.)=(% decrease in modulus) x (0.0185). It has been further proposed[21], that within the limits of experimental error, this relationship holds true for all materials that lend themselves to fracture-toughness evaluation.

An extensometer was used to measure the displacement across the notch of the sheet specimen. The displacement and maximum load were converted into an apparent modulus. Percent decrease in modulus was calculated from ratio of apparent modulus to actual modulus of the load-deflection curve

(see Figure A2). The crack growth was then obtained from the calibration curve of percent decrease in modulus versus crack length (Figure A1).

An extensometer - compliance gauge was used for initial fracture toughness tests. It soon became evident, however, that the extensometer was being severely shock-loaded upon fracture of the more brittle specimens. Also, because of the built-in magnification factor of the compliance gauge, and the limited range of the extensometer, the displacement across the notch of the more ductile specimens could not be measured. Therefore, the compliance gauge was eliminated and a new 2-inch gauge length, medium magnification, medium range, extensometer was modified in order to measure all types of specimens tested during the subject program.

Certain slight errors are possible in current methods of evaluation of fracture toughness. Human errors can occur during measurement of $2a_o$ and determination of the slow crack growth by a graphical method. The determination of the 1/2 crack length (a), by the technique described above is believed to be more accurate than the ink-staining technique and safer perhaps than a calculation technique[19] which could incorporate up to a 10 percent error in a direct elastic modulus determination (as a result of inherent tensile machine error). The graphical method used allows[20] for a cancellation of errors in modulus determination since it is based on the difference between the initial modulus and the apparent modulus.

APPENDIX (Continued)

Notes

In order for a fracture toughness test to be valid, the conditions below must be satisfied.

1. A nominal specimen limitation of $16t < W < 45t$ was adopted by the ASTM Committee* for the following reasons: if the width of the specimen is greater than 16 times the thickness the propagation of a nominal 2a crack or flaw can be contained or even stopped within the elastic stress field, i.e. the plastic zone at the crack tip should not exceed the elastic stress field of the specimen, otherwise the elastic stress analysis upon which fracture toughness determinations are based would be violated; if the width of a thin sheet specimen is greater than 45 times the thickness the specimen may tend to buckle during the test.

2. The initial slot length ($2a_0$) should be 30 to 40 percent of the specimen width ($0.3\ W < 2a_0 < 0.4\ W$). This nominal limitation on internal-slot length was adopted by the ASTM Committee in order to ensure the validity of the fracture-toughness test with respect to the original elastic stress analysis.

3. The 2a crack length should not exceed 0.6 W (W referring to specimen width). If the 0.6 W crack length is exceeded, the specimen is too ductile for a valid fracture toughness determination. A similar limitation imposed by the ASTM Committee is $\sigma_x \leq \sigma_{ys}$, or that the net section stress should not exceed the tensile yield strength in a valid fracture toughness test.

4. Due to the technique of measurement all fracture toughness values reported have been inherently corrected for the plastic zone at the crack tip. Therefore, fracture toughness values are reported as G_c^* or K_c^*, the asterisk symbolizing inclusion of the plastic zone correction.

*ASTM Committee on Fracture Testing of High Strength Sheet Materials

APPENDIX (Continued)

List of Symbols

P = maximum load at onset of fast fracture (lbs.)

W = specimen width (in.)

t = sheet thickness (in.)

a_0 = 1/2 initial center-slot length = $\frac{\text{notch length + fatigue cracks}}{2}$ (in.)

a = 1/2 crack length at onset of fast fracture = $\frac{2a_0 + \text{slow crack growth}}{2}$ (in.)

$\Phi = \frac{\pi a}{W}$ (radians)

E = elastic modulus (psi)

$\sigma 0$ = gross section stress = $\frac{P}{Wt}$ (psi)

σx = net section stress = $\frac{P}{(W-2a)\,t}$ (psi)

σys = yield strength (psi)

ρ = density (lbs./in. ^{3})

R = notch strength = $\frac{P}{(W - 2a_0)\,t}$ (psi)

G_c^* = fracture toughness $(\frac{\text{in. lb.}}{\text{in.}^2})$ [Corrected for plastic zone at crack tips]

K_c^* = critical crack toughness index (ksi $\sqrt{\text{in.}}$)

K_{1c} = plane-strain fracture toughness index (ideal)

K_{Nc} = opening mode or plane-strain toughness index (ksi $\sqrt{\text{in.}}$)

APPENDIX (Continued)

List of Symbols (Continued)

G_{Nc} = plane-strain fracture toughness $\left(\frac{\text{in. lb.}}{\text{in.}^2}\right)$

P_{Nc} = load at minor instability; crack pop-in or deviation of apparent modulus from linearity (lbs.)

μ = Poisson's Ratio

σ_{Nc} = opening-mode gross stress = $\frac{P_{Nc}}{Wt}$

APPENDIX (Continued)

List of Equations

$$G_c^* = \frac{\sigma_o^2 \ W}{E} \tan \Theta \quad \text{where } \Theta = \frac{\pi a}{W}$$

$$G_c^* = \frac{K_c^{*2}}{E} \quad \text{or} \quad K_c^* = \sqrt{E \ G_c^*}$$

$\frac{\sigma ys}{\rho}$ = yield strength: density ratio (in.)

$\frac{R}{\sigma ys}$ = notch strength: yield strength ratio

$$G_{Nc} = \frac{\sigma_{Nc}^2 \ W}{E} \tan \frac{\pi a_o}{W}$$

$$K_{Nc} = \sqrt{\frac{E}{1 - \mu^2} \ G_{Nc}}$$

$$(K_{Nc} \cong K_{1c})$$

APPENDIX

Sample Calculation

Sample calculation for specimen #102, 0.090" D6AC base-metal heat treated to the 2T700 condition.

1. Determine gross section stress, $\sigma o = \frac{P}{Wt}$ (psi)

$$\frac{24{,}100 \text{ lb.}}{(2.90 \text{ in.})(0.090 \text{ in.})} = 92{,}400 \text{ psi}$$

2. Determine 1/2 crack length at onset of fast fracture (a) by method shown in Figure A-2.

$$\frac{20{,}700 \text{ lb.} - 12{,}800 \text{ lb.}}{20{,}700 \text{ lb.}} \times 100 = \text{percent decrease in modulus} = 38.1\%.$$

$$(38.1\%) \times (0.0185) = \text{Crack Growth} = 0.70 \text{ in.}$$

$$\frac{2a_o + \text{Crack Growth}}{2} = a \qquad \frac{1.04 + 0.70}{2} = 0.87 \text{ in.}$$

3. Calculate fracture toughness, $G_c^* = \frac{\sigma o^2 W}{E} \tan \theta \left(\frac{\text{in-lb}}{\text{in}^2} \right)$

where $\theta = \frac{\pi a}{W}$ (radians)

$$\frac{(92.4)^2 \times 10^6 \times 2.90}{30.5 \times 10^6} \tan \left[\frac{\pi (.87)}{2.90} \times \frac{360}{2\pi} \right]^\circ = 1113 \ \frac{\text{in.-lb.}}{\text{in}^2}$$

4. Calculate critical crack toughness index, $K_c^* = \sqrt{E \, G_c^*}$ (ksi$\sqrt{\text{in}}$)

$$\sqrt{30.5 \times 10^6 \times 1113} = 184 \text{ ksi} \sqrt{\text{in.}}$$

5. Calculate net section stress, $\sigma x = \frac{P}{(W-2a)t}$ (psi)

$$\frac{24{,}100}{(2.90-1.74)(0.090)} = 230{,}800 \text{ psi}$$

APPENDIX

Bibliography

1. Special ASTM Committee on Fracture Testing of High-Strength Sheet Materials (FTHSSM), "Fracture Testing of High-Strength Sheet Materials", ASTM Bulletin No. 243, Jan., 1960, pp. 29 - 40; No. 244, Feb., 1960, pp. 18 - 28.

2. Warga, J. J., "Use of the Center-notch Tensile Test to Evaluate Rocket-Chamber Materials", American Welding Society Meeting in Los Angeles, Calif., Apr. 25 - 29, 1960.

3. ASTM FTHSSM Committee, "The Slow Growth and Rapid Propagation of Cracks", Materials Research & Standards, May, 1961, pp. 389 - 393.

4. ASTM FTHSSM Committee, "NASA - NRL Cooperative Program on Specimens Intended for Fracture Toughness Measurements", Materials Research & Standards, Nov., 1961, pp. 877 - 885.

5. Boyle, R. W., Sullivan, A. M., and Krafft, J. M., "Determination of Plane-Strain Fracture Toughness With Sharply Notched Sheets", Welding Journal, Sept., 1962, pp. 428s - 432s.

6. Manning, R. D., et al, "Simulated Service Tests of Steels for Solid-Propellant Missile Motor Cases", Materials Research & Standards, Part I, May, 1962, pp. 392 - 395; Part II, June, 1962, pp. 469 - 475.

7. Morrison, J. D., Kattus, J. R., and Salzman, W. R., "An Investigation of the Crack-Propagation Resistance of High-Strength Alloys and Heat-Resistant Alloys", Report to be Published.

8. Romine, H. E., "Summary Review of Fracture Toughness Results on Titanium Alloys Being Considered for Solid-Propellant Rocket Motor Cases", NWL Report No. 1798.

9. Campbell, J. E., and Achback, W. P., "Current Tests for Evaluating Fracture Toughness of Sheet Metals at High Strength Levels", DMIC Report No. 124, Jan., 1960.

10. Marschall, C. W., "The Factors Influencing the Fracture Characteristics of High-Strength Steel", DMIC Report No. 147, Feb., 1961.

11. Spretnak, J. W., "A Summary of the Theory of Fracture in Metals", DMIC Report No. 157, Aug., 1961.

12. Hertzberg, R. W., "Fracture Toughness & Notch Sensitivity of AISI 4340 Steel", M.I.T. Thesis, Apr., 1961.

13. Irwin, G. R., Private Communication

APPENDIX

Bibliography (Continued)

14. Srawley, J. E., Private Communication

15. Krafft, J. M., Private Communication

16. Orner, G. M. and Hartbower, C. E., "Sheet Fracture Toughness Evaluated by Charpy Impact and Slow Bend", Welding Journal, Sept., 1961, pp. 405s - 416s.

17. Irwin, G. R., "Fracture Testing of High-Strength Sheet Materials Under Conditions Appropriate for Stress Analysis" NRL Report No. 5486, July, 1960.

18. Romine, H. E., and Kies, J. A., "The Effects of Titanium Alloy Composition, Microstructure, and Processing Variables in Meeting Minimum Toughness Requirements for Motor Cases", 6th Titanium Meeting, New York University, Sept., 1960.

19. Boyle, R. W., "A Method for Determining Crack Growth in Notched Sheet Specimens", Materials Research & Standards, Aug., 1962, pp. 646 - 651.

20. Orner, G. M., "Metallurgical Variables Affecting Fracture Toughness in High-Strength Sheet Alloys", Report to be Published.

21. Orner, G. M., Private Communication

22. Brody, R.P., Hauser, H.A., Helfrich, W.E., and Schwind, H.L., "Research and Development of Titanium Motor Case", Program Covering July, 1960 to December, 1962. Final report to be published by Pratt & Whitney Aircraft Division of United Aircraft Corporation.

TABLE 25

Base-metal Fracture Toughness Data and Results

Specimen No.	Material	Condition	Thickness (t)(inch)	Width (W) (inch)	a_o (inch)	Elastic Modulus (E)(psi x 10^6)	Max. Load (P)(lbs.)	a (inch)
56	B120VCA	ST	0.125	3.10	0.52	14.7	33,700	0.92
57	B120VCA	ST	0.125	3.00	0.52	14.7	33,500	0.79
58	B120VCA	ST	0.125	2.90	0.52	14.7	32,500	0.84
61	B120VCA	STA	0.125	2.90	0.54	15.5	10,750	0.54
63	B120VCA	STA	0.125	3.10	0.52	15.5	9,660	0.52
65	B120VCA	STA	0.125	2.90	0.54	15.5	9,700	0.54
48	B120VCA	STCRA	0.125	2.90	0.55	15.5	5,400	0.55
49	B120VCA	STCRA	0.125	2.80	0.54	15.5	5,480	0.54
50	B120VCA	STCRA	0.125	2.70	0.58	15.5	5,620	0.58
F77	D6AC	ANN	0.090	3.00	0.52	30.5	13,300	1.40 (b)
F79	D6AC	ANN	0.090	3.00	0.51	30.5	13,300	1.34(b)
83	D6AC	ANN	0.290	2.80	0.57	30.5	48,500	1.40(b)
84	D6AC	ANN	0.290	2.80	0.58	30.5	47,550	1.40(b)
F26	D6AC	HT	0.090	2.90	0.55	30.5	23,550	1.01(b)
F25	D6AC	HT	0.090	3.00	0.53	30.5	23,700	0.94
102	D6AC	HT	0.090	2.90	0.52	30.5	24,100	0.87
85	D6AC	HT	0.290	2.90	0.54	30.5	36,600	0.80
101	D6AC	HT	0.290	2.90	0.54	30.5	35,000	0.77
F22	D6AC	HT	0.290	2.90	0.63	30.5	33,500	1.00(b)(e)

(a) $\frac{\sigma x}{\sigma ys} \gg 1$; Initial indication that test is not valid.

(b) 2a > Approximately 0.6 W; Initial indication that test is not valid.

(c) K_{Ic} computed, non-valid tests only.

(d) Curve of Load vs. deflection not suitable for K_{Ic} determination.

(e) Large 1/2 crack length (a) probably a result of the abnormally high a_o value due to extra large fatigue crack.

(f) Values for σys and $\sigma ys/\rho$ are average values for each heat treated condition.

TABLE 25

Base-metal Fracture Toughness Data and Results (Continued)

σ_o(psi)	σ_x(psi)	G_c^* $\left(\frac{\text{in. lbs}}{\text{in.}^2}\right)$	K_c^* (ksi$\sqrt{\text{in.}}$)	Percent Shear Lip	K_{Ic}(c) (ksi$\sqrt{\text{in}}$)	σ_{ys}(psi)	σ_{ys}/ρ(f) (inch)	Specimen No.
86,900	214,000(a)	2137	177	100	79.8	130,000	745,000	56
89,400	188,700(a)	1768	161	100	(d)	130,300	745,000	57
89,500	213,100(a)	2023	172	100	88.0	130,300	745,000	58
29,600	50,000	108.1	41.0	15		201,000	1,149,000	61
24,900	33,500	72.1	33.5	15		201,000	1,149,000	63
27,500	42,600	93.4	39.1	0		201,000	1,149,000	65
14,900	22,300	28.1	20.8	0		240,000	1,371,000	48
16,300	23,800	33.5	22.8	5		240,000	1,371,000	49
16,600	25,800	38.3	24.3	10		240,000	1,371,000	50
49,200	738,900	2198.0	258	100	54.9	61,200	216,000	F77
49,200	461,800	1381.0	269	100	56.0	61,200	216,000	F79
59,600	∞	93,420	1690	100	48.4	61,200	216,000	83
58,500	∞	90,000	1660	100	62.1	61,200	216,000	84
90,400	297,300	1496.	214	100	67.5	229,100	810,000	F26
87,800	235,100	1135.	186	100		229,100	810,000	F25
92,400	230,800	1113.	184	100		229,100	810,000	102
43,600	97,100	212	80.5	20		229,100	810,000	85
41,600	88,700	181.0	74.3	20		229,100	810,000	101
39,800	128,400	282.0	92.8	20	42.0	229,100	810,000	F22

TABLE 26

Electron Beam Weld Fracture Toughness Data and Results

Specimen No.	Material	Condition	Thickness (t)(inch)	Width (W) (inch)	a_o (inch)	Max. Load (P)(lbs.)	Elastic Modulus (E)(10 x psi)	a(inch)
F56	B120VCA	AW	0.125	2.60	0.53	19,750	15.5	0.61
F12	B120VCA	AW	0.125	2.59	0.51	15,500	15.5	0.55
F9	B120VCA	AW	0.125	2.59	0.51	24,300	15.5	0.90
F10	B120VCA	AW	0.125	2.59	0.53	26,150	15.5	0.84
F14	B120VCA	AW	0.125	2.59	0.53	18,350	15.5	0.67
F30	B120VCA	AW	0.125	2.86	0.51	29,250	15.5	0.76
10	B120VCA	WA	0.125	2.60	0.52	7,810	15.5	0.68
17	B120VCA	WA	0.125	2.60	0.53	8,250	15.5	0.69
22	B120VCA	WA	0.125	2.60	0.51	8,050	15.5	0.63
7	B120VCA	WA	0.125	3.00	0.52	10,580	15.5	0.645
F1	B120VCA	CAW	0.125	2.57	0.52	15,100	15.5	0.565
F3	B120VCA	CAW	0.125	2.60	0.52	20,000	15.5	0.64
F4	B120VCA	CAW	0.125	2.96	0.52	18,500	15.5	0.76
F6	B120VCA	CAW	0.125	2.96	0.51	23,000	15.5	0.60
F7	B120VCA	CAW	0.125	2.84	0.52	18,500	15.5	0.72
F41	D6AC	EWB	0.090	2.60	0.55	11,800	30.5	0.71
F42	D6AC	EWB	0.090	2.88	0.515	11,500	30.5	0.73
F40	D6AC	EWB	0.090	2.88	0.51	12,000	30.5	0.795
F34	D6AC	EWB	0.090	2.88	0.53	12,000	30.5	0.79
F35	D6AC	EWB	0.090	2.59	0.52	10,050	30.5	0.75

TABLE 26

Electron Beam Weld Fracture Toughness Data and Results (Continued)

Specimen No.	Material	Condition	Thickness (t)(inch)	Width (W) (inch)	a_o (inch)	Max. Load (P)(lbs.)	Elastic Modulus (E)(10 x psi)	a(inch)
F29	D6AC	WH	0.090	3.00	0.54	19,400	30.5	0.81
F57	D6AC	WH	0.090	2.89	0.55	18,000	30.5	0.93
F58	D6AC	WH	0.090	3.00	0.53	15,350	30.5	0.705
F35a	D6AC	WH	0.090	2.94	0.54	16,850	30.5	0.88
F61	D6AC	WH	0.090	2.88	0.52	15,350	30.5	0.70
F32	D6AC	WH	0.090	2.89	0.57	21,800	30.5	0.76

(a) Percent shear not reported for most welded specimens because of difficulties in interpreting fracture surfaces.

(b) Average values for σys and $\sigma ys/\rho$.

TABLE 26

Electron Beam Weld Fracture Toughness Data and Results (Continued)

σ_o(psi)	σ_x(psi)	G_c $\left(\frac{\text{in. lbs}}{\text{in.}^2}\right)$	K_c (ksi$\sqrt{\text{in.}}$)	Percent Shear Lip[b]	σ_{ys}(psi)[c]	σ_{ys}/ρ [d] (inch)	Specimen No.
60,800	114,500	560.4	93.2		151,000	863,000	F56
47,900	83,200	300.7	68.3		151,000	863,000	F12
75,100	246,100	1657.0	160.3		151,000	863,000	F9
80,800	229,900	1762.0	165.2		151,000	863,000	F10
56,700	117,400	565.0	93.6		151,000	863,000	F14
81,800	174,600	1,358.0	145.1		151,000	863,000	F30
24,000	50,400	103.8	40.1				10
25,400	54,100	118.7	42.9				17
24,800	48,100	97.7	38.9				22
28,200	49,500	123.1	43.7				7
46,600	82,700	296.3	67.8		148,100	846,000	F1
61,500	121,200	618.1	97.9		148,100	846,000	F3
50,000	102,800	496.4	87.7		148,100	846,000	F4
62,200	104,500	544.0	91.8		148,100	846,000	F6
52,100	105,700	257.6	63.2		148,100	846,000	F7
50,400	111,100	249.8	87.3		224,100	792,000	F41
44,400	90,000	189.3	76.0		224,100	792,000	F42
46,300	103,400	237.7	85.1		224,100	792,000	F40
46,300	102,600	235.0	84.7		224,100	792,000	F34
43,100	102,400	202.2	78.5		224,100	792,000	F35

TABLE 26

Electron Beam Weld Fracture Toughness Data and Results (Continued)

σ_o (psi)	σ_x (psi)	G_c ($\frac{\text{in. lbs}}{\text{in.}^2}$)	K_c (ksi$\sqrt{\text{in.}}$)	Percent Shear Lip (b)	σ_{ys} (psi) (c)	σ_{ys}/ρ (d) (inch)	Specimen No.
71,900	156,200	573.6	132.3	100	223,200	789,000	F29
69,200	194,200	720.6	148.3	90	223,200	789,000	F57
56,900	107,300	288.3	93.8	60	223,200	789,000	F58
63,700	158,700	533.5	127.6	100	223,200	789,000	F35a
59,200	115,200	315.9	98.2	60	223,200	789,000	F61
84,200	177,600	726.3	148.8	100	223,200	789,000	F32

TABLE 27

B120VCA Titanium Fracture-toughness Property Comparison

Specimen	Bead Condition	Heat Treat Condition	σ ys(Weld) (psi)	σ ys(Base Metal) (psi)	G_c* $\frac{\text{in.-lb.}}{\text{in}^2}$	Thickness (inch)	Source
Base Metal	N.A.	STCRA	N.A.	240	23-38	0.125	HSD
Base Metal	N.A.	STA	N.A.	201	72-121	0.125	HSD
Base Metal	N.A.	STCRA	N.A.	202	~75	~0.125	PWA
Base Metal	N.A.	STA	N.A.	196	~121	0.063	NRL
Base Metal	N.A.	STA	N.A.	179	~256	0.150	NWL
EB Weld	Intact	STAW	151	201	300-1762	0.125	HSD
EB Weld	Intact	STCRAW	148	240	258-618	0.125	HSD
EB Weld	Intact	STWA	~166	201	98-123	0.125	HSD
EB Weld	Ground Flush	STCRAW	~135	~180	240-440	0.140	PWA
TIG Weld	Intact	STCRAW	~120	~180	218-246	0.140	PWA

Notes

N.A. - Not Applicable

1. All specimens used were center-notch tensile (3" x 12") for all sources.
2. All notches were located in center of weld for all sources.
3. HSD utilized fatigue cracking; however, a non-ink stain technique.
4. PWA and NRL utilized fatigue cracking and ink stain technique.
5. NWL utilized ground notch-tips with less than 0.001" radius and ink stain technique.
6. G_c* values above 1350 for HSD-STAW specimens resulted from non-valid tests although extreme fracture toughness was indicated.
7. PWA - Pratt and Whitney Aircraft Division of United Aircraft Corporation, East Hartford, Conn.[22]
8. NRL - U.S. Naval Research Laboratory, Washington, D.C.[4]
9. NWL - U.S. Naval Weapons Laboratory, Dahlgren, Va.[18]

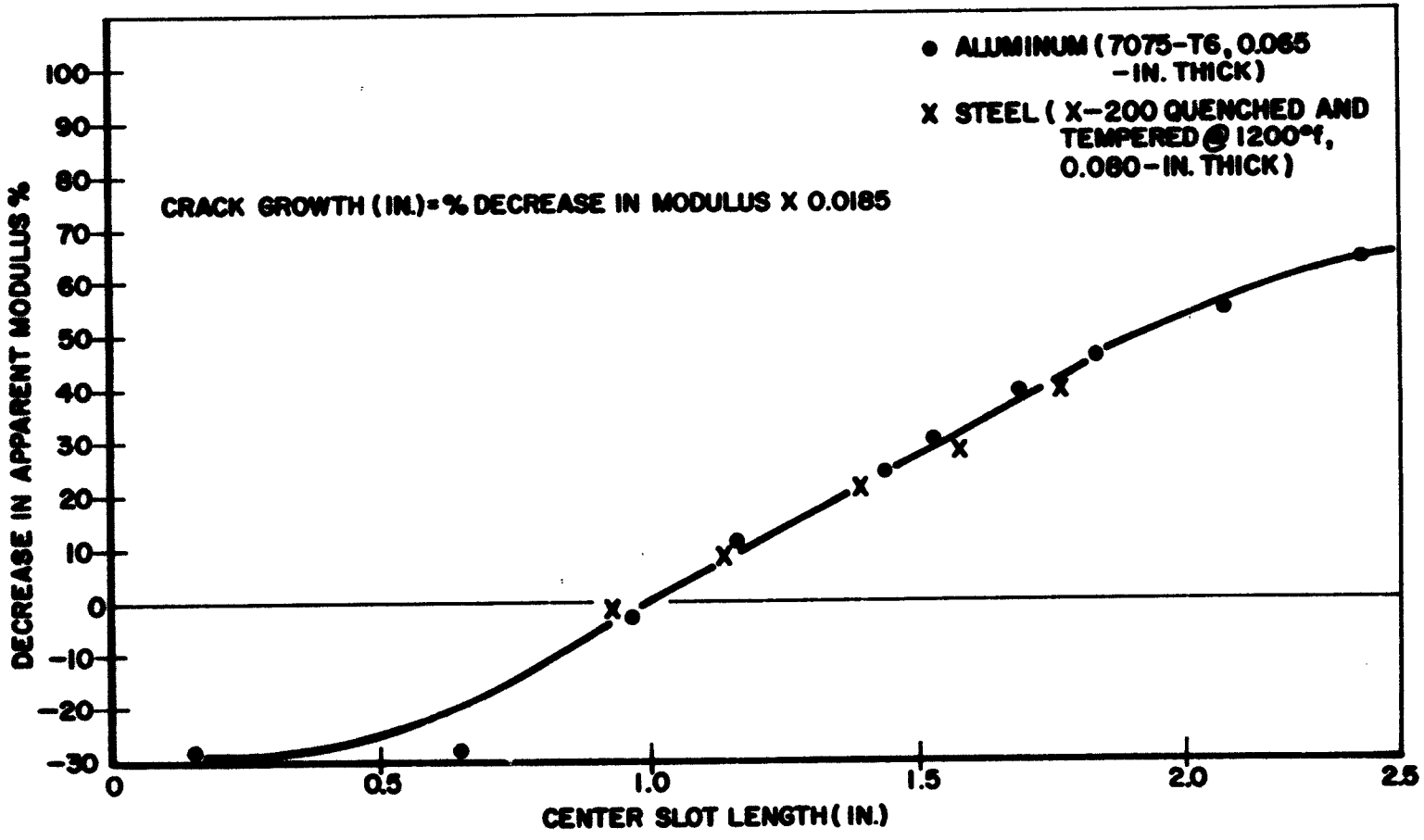

Figure 157 Decrease in Apparent Modulus vs. Crack Length in Three-Inch Wide Center-notched Specimens

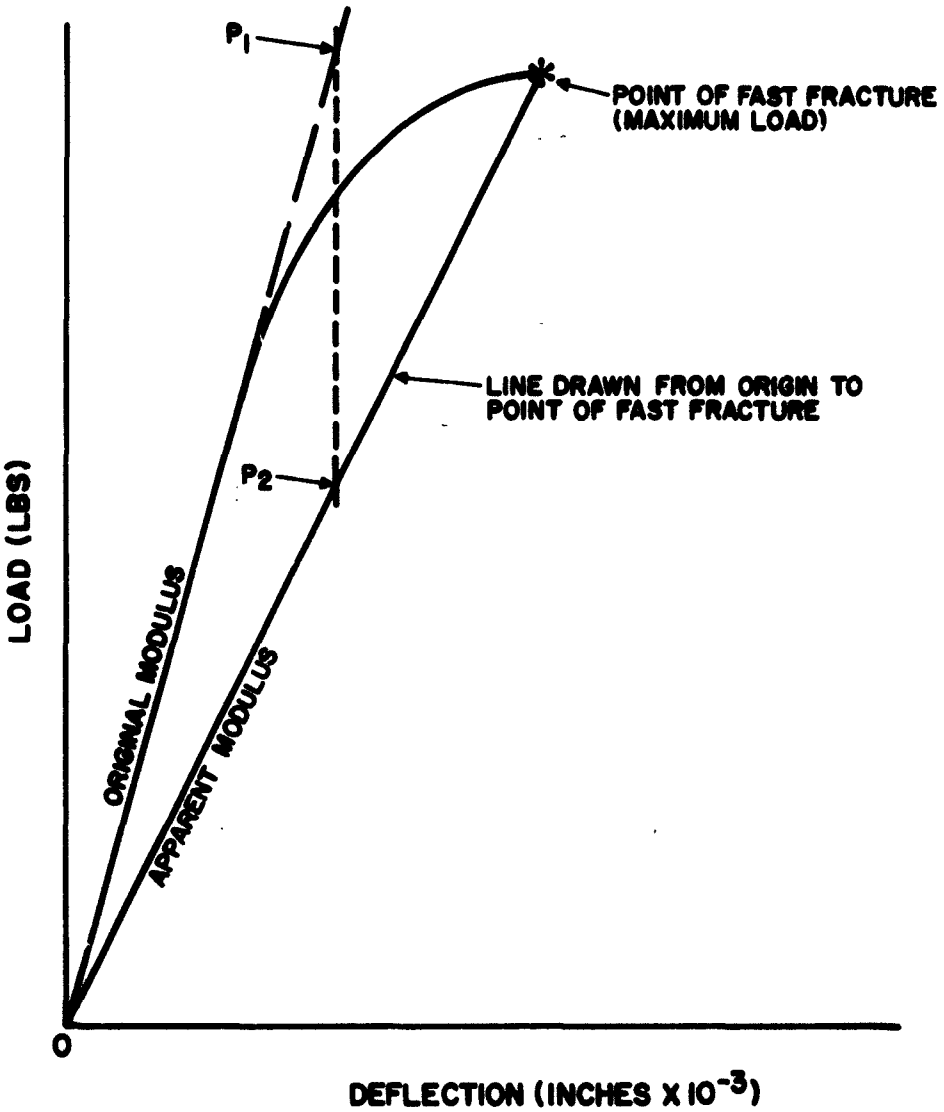

$$\text{PERCENT DECREASE IN MODULUS} = \frac{P_1 - P_2}{P_1} \times 100$$

(PERCENT DECREASE IN MODULUS) x (0.0185) = CRACK GROWTH IN INCHES

Figure 158 Method for Computing Slow Crack Growth

Aeronautical Systems Division, Dir/Materials & Processes, Metals & Ceramics Lab, Wright-Patterson AFB, Ohio.
Rpt No. ASD-TDR-63-132. ELECTRON BEAM WELDING OF AEROSPACE MATERIALS. Final report, Feb 63, 177p., incl illus., tables, 28 refs.
Unclassified Report

High-voltage electron beam welding techniques were developed for B120VCA titanium, D6AC steel, molybdenum-0.5% titanium to tungsten, and beryllium. Welds were produced in material thicknesses of 0.125 inch for the B120VCA titanium; 0.290 inch and 0.090 inch for the D6AC steel; 0.100 inch, 0.050 inch, and 0.005 inch for the molybdenum-0.5% titanium welded to tungsten; and 0.040 inch

(over)

for the beryllium. The effects of thermal treatments (aging and heat treating) were investigated in the B120VCA and D6AC by welding and testing a variety of weld/thermal treatment combinations. Butt welds of each material thickness, joint combination, and thermal treatment (where applicable) were evaluated for mechanical properties by tensile testing at temperatures to 2200 F and bend testing at temperatures to 1000 F. Internal-notch tensile properties of B120VCA titanium and D6AC steel were determined at room temperature. Results of the metallographic and mechanical property investigations of the electron beam welds were compared with base-metal properties and with published data for other joining techniques.

1. Welds
2. Electron-Beam Welding
3. Metallurgy
4. Thermodynamics

I. AFSC Proj 7351, Task 735102
II. Contract No. AF 33(657)-7763
III. United Aircraft Corp, Windsor Locks, Conn.
IV. Kern, William I., Lubin, Lawrence E.
V. Aval fr OTS
VI. In ASTIA collection

Aeronautical Systems Division, Dir/Materials & Processes, Metals & Ceramics Lab, Wright-Patterson AFB, Ohio.
Rpt No. ASD-TDR-63-132. ELECTRON BEAM WELDING OF AEROSPACE MATERIALS. Final report, Feb 63, 177p., incl illus., tables, 28 refs.
Unclassified Report

High-voltage electron beam welding techniques were developed for B120VCA titanium, D6AC steel, molybdenum-0.5% titanium to tungsten, and beryllium. Welds were produced in material thicknesses of 0.125 inch for the B120VCA titanium; 0.290 inch and 0.090 inch for the D6AC steel; 0.100 inch, 0.050 inch, and 0.005 inch for the molybdenum-0.5% titanium welded to tungsten; and 0.040 inch

(over)

for the beryllium. The effects of thermal treatments (aging and heat treating) were investigated in the B120VCA and D6AC by welding and testing a variety of weld/thermal treatment combinations. Butt welds of each material thickness, joint combination, and thermal treatment (where applicable) were evaluated for mechanical properties by tensile testing at temperatures to 2200 F and bend testing at temperatures to 1000 F. Internal-notch tensile properties of B120VCA titanium and D6AC steel were determined at room temperature. Results of the metallographic and mechanical property investigations of the electron beam welds were compared with base-metal properties and with published data for other joining techniques.

1. Welds
2. Electron-Beam Welding
3. Metallurgy
4. Thermodynamics

I. AFSC Proj 7351, Task 735102
II. Contract No. AF 33(657)-7763
III. United Aircraft Corp, Windsor Locks, Conn.
IV. Kern, William I., Lubin, Lawrence E.
V. Aval fr OTS
VI. In ASTIA collection

Aeronautical Systems Division, Dir/Materials & Processes, Metals & Ceramics Lab, Wright-Patterson AFB, Ohio.
Rpt No. ASD-TDR-63-132. ELECTRON BEAM WELDING OF AEROSPACE MATERIALS. Final report, Feb 63, 177p., incl illus., tables, 28 refs.
Unclassified Report

High-voltage electron beam welding techniques were developed for B120VCA titanium, D6AC steel, molybdenum-0.5% titanium to tungsten, and beryllium. Welds were produced in material thicknesses of 0.125 inch for the B120VCA titanium; 0.290 inch and 0.090 inch for the D6AC steel; 0.100 inch, 0.050 inch, and 0.005 inch for the molybdenum-0.5% titanium welded to tungsten; and 0.040 inch

(over)

for the beryllium. The effects of thermal treatments (aging and heat treating) were investigated in the B120VCA and D6AC by welding and testing a variety of weld/thermal treatment combinations. Butt welds of each material thickness, joint combination, and thermal treatment (where applicable) were evaluated for mechanical properties by tensile testing at temperatures to 2200 F and bend testing at temperatures to 1000 F. Internal-notch tensile properties of B120VCA titanium and D6AC steel were determined at room temperature. Results of the metallographic and mechanical property investigations of the electron beam welds were compared with base-metal properties and with published data for other joining techniques.

1. Welds
2. Electron-Beam Welding
3. Metallurgy
4. Thermodynamics

I. AFSC Proj 7351, Task 735102
II. Contract No. AF 33(657)-7763
III. United Aircraft Corp, Windsor Locks, Conn.
IV. Kern, William I., Lubin, Lawrence E.
V. Aval fr OTS
VI. In ASTIA collection

Aeronautical Systems Division, Dir/Materials & Processes, Metals & Ceramics Lab, Wright-Patterson AFB, Ohio.
Rpt No. ASD-TDR-63-132. ELECTRON BEAM WELDING OF AEROSPACE MATERIALS. Final report, Feb 63, 177p., incl illus., tables, 28 refs.
Unclassified Report

High-voltage electron beam welding techniques were developed for B120VCA titanium, D6AC steel, molybdenum-0.5% titanium to tungsten, and beryllium. Welds were produced in material thicknesses of 0.125 inch for the B120VCA titanium; 0.290 inch and 0.090 inch for the D6AC steel; 0.100 inch, 0.050 inch, and 0.005 inch for the molybdenum-0.5% titanium welded to tungsten; and 0.040 inch

(over)

for the beryllium. The effects of thermal treatments (aging and heat treating) were investigated in the B120VCA and D6AC by welding and testing a variety of weld/thermal treatment combinations. Butt welds of each material thickness, joint combination, and thermal treatment (where applicable) were evaluated for mechanical properties by tensile testing at temperatures to 2200 F and bend testing at temperatures to 1000 F. Internal-notch tensile properties of B120VCA titanium and D6AC steel were determined at room temperature. Results of the metallographic and mechanical property investigations of the electron beam welds were compared with base-metal properties and with published data for other joining techniques.

1. Welds
2. Electron-Beam Welding
3. Metallurgy
4. Thermodynamics

I. AFSC Proj 7351, Task 735102
II. Contract No. AF 33(657)-7763
III. United Aircraft Corp, Windsor Locks, Conn.
IV. Kern, William I., Lubin, Lawrence E.
V. Aval fr OTS
VI. In ASTIA collection